To the Graduate Council:

I am submitting herewith a dissertation written by Camilo Montes entitled "Three-dimensional structure and kinematics of the Piedras-Girardot foldbelt in the northern Andes of Colombia". I have examined the final copy of this dissertation for form and content and recommend that it be accepted in partial fulfillment of the requirements for the degree of Doctor of Philosophy, with a major in Geology.

Robert D. Hatcher Jr., Major Professor

We have read this dissertation
and recommend its acceptance:

William M. Dunne

Steven G. Driese

Kenneth H. Orvis

Accepted for the Council:

Vice Provost and Dean of Graduate Studies

THREE DIMENSIONAL STRUCTURE AND KINEMATICS OF THE PIEDRAS-GIRARDOT FOLDBELT IN THE NORTHERN ANDES OF COLOMBIA

A Dissertation
Presented for the
Doctor of Philosophy
Degree
The University of Tennessee, Knoxville

Camilo Montes
December, 2001

DEDICATION

To my parents, Maria Luisa, and José Joaquin.

ACKNOWLEDGMENTS

Many friends, colleagues and institutions made this work possible. The *Corporación Geológica ARES*, *Colciencias*, *Ecopetrol*, The *Universidad Nacional de Colombia*, and *Ingeominas* in Colombia provided information, financial, scientific, and logistic support. The *Integrated Interpretation Center* of *Conoco Inc.*, the *Science Alliance Center for Excellence* of the *University of Tennessee*, and the *AAPG* provided additional financial resources and access to research facilities and hardware. *Nigel Press Satellite Mapping, Paradigm Geo*, *GeoLogic Systems*, and *Midland Valley Inc.* provided software, and digital information.

I would like to thank my advisor, Bob Hatcher, who graciously agreed to direct his first dissertation in the Andes. His patience, dedication, and trust are greatly appreciated. Discussions and thorough reviews by Bill Dunne helped clarify, organize, and improve this work. Classroom discussions and reviews by Steve Driese and Ken Orvis greatly contributed to this research. While fishing for typos, grammar, and spelling errors, Nancy Meadows is the only person who has read this dissertation more times than I have. Thanks for everything Nancy. Since my early days in Knoxville moral support from everyone in the Hatchery has been invaluable. Don Geddes, Mark Carter, Doug Curl, and Steve Martin from the old wave, and Scott Giorgis, and Brendan Bream, Scott Williams, and Dave Settles from the new wave have been good friends, and source of motivation. Climbing/smoking partner and good friend Sara Bier will be missed.

I would like to give special thanks to professors and mentors that throughout my career have helped me define my interests: Pedro A. Restrepo Pace, Fernando Etayo Serna, Fabio Colmenares, Fabio Chaparro, and Tomás Villamil. Friends and colleagues Jairo Roncancio, and Germán Bayona helped me during the field season.

Abstract

Detailed geologic mapping, strain analysis, and simple stratigraphic principles indicate that deformation in the Piedras-Girardot foldbelt in the northern Andes began in the early Campanian with incipient propagation of faults that uplifted gentle domes where the accumulation of some sandy units did not take place. Maastrichtian unroofing of a metamorphic terrane west of the Piedras-Girardot foldbelt is documented by a conglomerate that was deformed shortly after deposition developing a conspicuous intragranular fabric of microscopic veins that accommodate little extension (between 1 and 2 percent in a general northeast-southwest direction). This extensional fabric, distortion of fossil molds, and a moderate cleavage most likely developed concurrently, during and after incipient late Cretaceous folding, but before large scale Paleogene faulting and folding. Cleavage also seems to record small amounts of contraction in a general northwest-southeast direction. Paleogene folding and thrust sheet propagation is recorded by syntectonic strata, and records westward to southwestward propagation of faults. Mesoscopic fabric elements associated with continuous Paleogene deformation are nearly absent, and apparently were passively rotated and translated along thrust sheets. Neogene deformation took place only in the norhtwestern flank of this foldbelt. As a result of this history of deformation, a complex array of faults and folds exists: northwest- and west-verging thrust faults, north- and northeast-verging normal faults, and north- and northeast-trending strike-slip faults. Changes in the structural trend delineate a sigmoidal sinistral stepover in this dextral system, with faults verging outwardly in opposite directions defining a positive flower structure. A piercing point constrains dextral motion of the Cotomal fault to 8 km approximately parallel to the trace of the Ibagué fault. Palinspastic restoration of the fault blocks indicates that approximately 52% ENE contraction is recorded in this foldbelt. A three-dimensional model integrating, and honoring all available information is presented and tested using simple forward modeling.

Preface

This dissertation summarizes the results of the research I have conducted for the past five years about the tectonics of a small part of the northern Andes. The motivation for this work comes from my fascination with the Andean landscape, geology, and people. One of the most rewarding, and arduous parts of this work was the time spent in the field hiking the traverses, and getting to better know my contry and my people. This experience remained as the source of motivation throughout this research project.

This work is divided in three parts that attempt to cover all the conclusions derived from this study. Part one consists of an in-depth review and critical assessment of published work about the tectonics of the northern Andes with special emphasis in the influence of Caribbean tectonics. This part helped narrow down the focus of this research project to the Piedras-Girardot foldbelt. Parts two and three will be submitted for publication to scientific journals, and thus were written with this format in mind. Part two examines in detail the timing of deformation, using basic stratigraphic principles mapped in the field and derived from two-dimensional seismic lines. Mesoscopic and microscopic fabric elements, and their contribution to deformation is analyzed in light of the results of the timing of deformation, and its contribution to strain. The third and final part of this work analyzes the structure of the Piedras-Girardot foldbelt in two- and three-dimensions using the geologic map, kinematic markers, and syntectonic features to construct a three-dimensional model, and a palinspastic restoration. Although this entire project relied heavily on Geographic Information Systems (GIS), this work is mostly in the background and confined to the appendices.

Plate I presents the gelogic map at a 1:50,000 scale. Plate II contains uninterpreted migrated industry seismic data provided by Ecopetrol. Plate III presents a summarized methodology to construct a three-dimensional GIS database that can be used in conjunction with Geosec

2D, and 3D. Plate IV contains the location of the field stations, and Plate V contains cross sections at the same scale as the geologic map.

Appendix I contains commented C, Arc Macro Language, and other macros code I wrote or modified to perform various database construction, querying, maintenance. It also contains notes I took to try to remember complex sequences of steps followed to create and manipulate digital maps. Appendix II contains a photographic record of the field photographs used to measure the orientation of intraclastic veins in the La Tabla Formation conglomerate. Appendix III contains the field data separated by fabric type.

Table of Contents

Part I Regional review of Caribbean and north Andean tectonics. **1**
INTRODUCTION 2
TRANSPRESSION 2
GEOLOGY OF THE CORDILLERA ORIENTAL 3
Regional Setting 4
Stratigraphy 6
Structure 10
Kinematic Reconstructions 12
Strike-Slip Faults in the Northern Andes 16
PALEONTOLOGICAL EVIDENCE FOR A MIGRATING DEFORMATION FRONT 18
KINEMATIC PLATE TECTONIC RECONSTRUCTIONS 21
GEOPHYSICAL DATA 22
Gravity and geodesy 23
Earthquake focal mechanisms 24
CONCLUSIONS 28
REFERENCES 30
Part II Strain and timing of deformation in the Piedras-Girardot foldbelt. **35**
ABSTRACT 36
INTRODUCTION 37
Regional setting 38
PIEDRAS-GIRARDOT FOLDBELT 42
Timing of deformation from stratigraphic data 42
General stratigraphy of the Piedras-Girardot foldbelt 43
Basement 44
Cretaceous sequence 45
Cenozoic 46
Evidence for syntectonic sedimentation. 46
Late Cretaceous 46
Paleogene 48
Neogene 51
Paleogeographic interpretation 52
MICROSCOPIC AND MESOSCOPIC STRAIN 54
Deformed fossils 55
Cleavage 58
Shattered pebbles and veins 61
RESULTS 66
REFERENCES 68
Part III Three-dimensional structure of the Piedras-Girardot foldbelt. **70**
ABSTRACT 71
INTRODUCTION 71
Methods 72
Caribbean Plate Boundary 74
STRUCTURAL OBSERVATIONS 76
Structural Style 80
Positive flower structure and Camaito fault 80
Plateau and Cotomal fault 82
Dip slopes and Hondita fault 85
Normal faults 86
Tectonic transport, shortening, and piercing points 88

DISCUSSION 90
Two-dimensional interpretation and cross section construction 90
Hondita fault and depth to detachment 93
THREE-DIMENSIONAL MODEL 98
Palinspastic restoration 102
RESULTS 103
REFERENCES 106
Appendices 108
Appendix I Code 109
INTRODUCTION 110
TRANSLATOR 110
ROTATE 121
ARC MACRO LANGUAGE CODE 128
Mkcover.aml 128
Mkgrid.aml 131
Dip.aml 132
Idfmaker.aml 133
Tips 135
Georeferencing 135
Converting to VRML 135
Plotting strikes and dips in ArcView 136
Bringing three-dimensional data into Geosec2D 136
Generating topographic cross-sections from DEMs 137
Create a shotpointmap 138
Excel Macro 138
Appendix II Field Photographs of La Tabla Fm. 142
DATA BY STATION AND PHOTO NUMBER. 143
FIELD PHOTOGRAPHS 144
ADDITIONAL FIELD PHOTOGRAPHS 155
THIN SECTIONS IN STATION 345 163
Appendix III Field Data 166
VITA 201

List of Figures

Part I

Figure 1: Tectonic map of the Caribbean region. 5
Figure 2: Shaded digital elevation model of part of the Cordillera Oriental. 6
Figure 3: Mesozoic and Cenozoic stratigraphic summary of the Cordillera Oriental, Magdalena Valley and Eastern foothills at about 6°N latitude. 8
Figure 4: Schematic cross section of the Cordilleras Central and Oriental at about 5°N. 11
Figure 5: Cross sections of the Cordillera Oriental. 13
Figure 6: Modern cross sections of the Cordillera Oriental. 14
Figure 7: Tectonic map of the Caribbean region. 17
Figure 8: Geologic map of the Cordillera Oriental and parts of the Cordillera Central and Occidental. 19
Figure 9: Schematic paleogeographic reconstruction of the Caribbean region. 20
Figure 10: Tomographic images beneath northwestern South America (van der Hilst and Mann, 1994). .. 26
Figure 11: Three-dimensional visualization of earthquake hypocenter data under northwestern South America and Central America using Geosec 3D®. 27

Part II

Figure 1: Tectonic map of the Caribbean region 37
Figure 2: Tectonic map of part of the northern Andes modified after Schamel (1991) 39
Figure 3: Simplified geologic map of the area mapped 40
Figure 4: Generalized stratigraphic column of the Piedras-Girardot foldbelt. 41
Figure 5: Seismic section across the Gualanday syncline 49
Figure 6: Nonpalinspastic paleogeographic reconstruction of the Piedras-Girardot foldbelt. 52
Figure 7: Map of mesoscopic structures in the Piedras-Girardot foldbelt 57
Figure 9: Strong cleavage in fine-grained rocks of the Nivel de Lutitas y Arenas in the southwestern end of La Tabla Ridge. 59
Figure 8: Traces of cleavage exposed on a bedding plane in mudstone of the Nivel Intermedio of the Oliní Group. 59
Figure 10: Photomicrograph of cleavage domains taken parallel to bedding in a siliceous mudstone. 60
Figure 11: Map of mesoscopic structures in the Piedras-Girardot foldbelt. Traces of veins were interpolated from field measurements. 62
Figure 12: Shattered pebbles of La Tabla conglomerate. 63
Figure 13: Photomicrographs of La Tabla conglomerate looking onto bedding. 63
Figure 14: Microscopic intragranular veins in conglomerate of the La Tabla Formation. 65

Part III

Figure 1: Tectonic map of the Caribbean region. 72
Figure 2: Tectonic map of part of the northern Andes modified after Schamel, (1991). 76
Figure 3: Southern end of La Tabla Ridge. 77
Figure 4: Stratigraphy of the Piedras-Girardot foldbelt. 78
Figure 5: Simplified geologic map of the Piedras-Girardot foldbelt. 79
Figure 6: Detailed geologic map of the northern half of the Piedras-Girardot foldbelt. 81
Figure 7: Equal-area, lower-hemisphere Kamb contour diagrams of poles to bedding in the Piedras-Girardot foldbelt. 82
Figure 8: Camaito fault near the northern end of the La Tabla Ridge.83
Figure 9: Outcrop expression of the Camaito fault. 83
Figure 10: Nearly horizontal strata of the Oliní Group in the topographic domain of the plateau. Looking west. 84
Figure 11: Cotomal fault in the eastern edge of the plateau (to the right). 84
Figure 12: Gently southeast-dipping strata (to the left) in the western flank of the La Vega-Vindí synclines. 86
Figure 13: Normal faults in the Piedras-Girardot foldbelt. 87
Figure 14: Southern end of the northeast-trending Guaduas syncline. Looking northeast. 88
Figure 15: Serial cross sections of the Piedras-Girardot foldbelt. 91

Figure 16: Seismic lines across the southwestern part of the Piedras-Girardot foldbelt. 94
Figure 17: Seismic line across the southern part of the plateau. 98
Figure 18: Failed restoration attempt of three of the cross sections in the Piedras-Girardot foldbelt..... 99
Figure 19: Perspective views of the three-dimensional model constructed using Geosec 3D. 100
Figure 20: Perspective view of the three-dimensional model with the major faults of the Piedras-Girardot foldbelt. 101
Figure 21: Palinspastic reconstruction of the top of the Villeta Group (pattern) in the Piedras-Girardot foldbelt. 103
Figure 22: Simplified palinspastic geometry of the Piedras-Girardot foldbelt. 104

List of Plates

Plate I: Geologic map of the Piedras-Girardot foldbelt.....in pocket
Plate II: Seismic sections across the Piedras-Girardot foldbelt.....in pocket
Plate III:Creation of a fully digital, three-dimensional geologic map and GIS database.....in pocket
Plate IV: Station map.....in pocket
Plate V: Cross sections of the Piedras-Girardot foldbelt.....in pocket

Part I

Regional review of Caribbean and north Andean tectonics.

INTRODUCTION

This section presents a comprehensive review and critical assessment of the regional geology and geophysics of the southern Caribbean Plate and the northern Andes. This bibliographic review served the purpose of narrowing down the focus of this research to the Piedras-Girardot fold belt in the northern Andes of central Colombia.

Kinematic plate tectonic reconstructions predict that the Cordillera Oriental, along the northwestern margin of South America, experienced oblique convergence throughout the Cenozoic (Ladd, 1976). Despite this, a doubly vergent fold-thrust geometry has been suggested for the Cordillera Oriental, and about 100 km of NW-SE horizontal shortening has been estimated using standard two-dimensional reconstruction techniques. Because oblique convergence along plate boundaries is usually partitioned between transcurrent and contractional components of deformation, estimates of horizontal shortening for the Cordillera Oriental of Colombia are incomplete, and published two-dimensional reconstructions are thus flawed.

TRANSPRESSION

Transpression, as originally defined by Harland (1971), is the simultaneous action of wrench and pure shear, and it must occur in any orogenic belt with curvature greater than a great circle. Therefore, even rectangular plates moving along great circles cannot move extensively without some oblique relative motion. Axial elongation and strike-slip faulting were initially recognized (Harland, 1971) as diagnostics of transpression.

The original definition of transpression has been modified to include not only coeval wrench and pure shear (in two dimensions), but also vertical lengthening along the shear plane in three dimensions. Transpression produces flattening strain, folds and thrusts at small oblique angles to the shear zone, extension at high angles to the zone, steep cleavage and stretching

lineation, and vertical uplift. Factorization of the pure and simple shear components of deformation predicts that the strain ellipsoid in a shear zone undergoing transpression will have one principal strain axis always vertical, but the plane containing the axis of maximum shortening switches from vertical to horizontal, depending on the relative contributions to deformation along and across the shear zone (Sanderson and Marchini, 1984). In pure-shear-dominated transpression, the strain ellipse is sequentially rotated as deformation progresses by the noncoaxial strain imposed by the wrench component. In wrench-dominated transpression, the shape of the strain ellipsoid changes throughout deformation starting with maximum axis in the horizontal plane, and switching to the vertical plane as deformation progresses (Teyssier *et al.*, 1995).

The degree of transcurrent and shear components accommodated along zones of diffuse deformation or discrete strike-slip faults, defines the degree of partition in a transpressive system. Two end-members have been defined according to the degree of partition: the San Andreas fault system, and the South Island of New Zealand. The former accommodates much of the strike-slip predicted by plate motion (about 95%); the latter is not strike-slip partitioned at all, because even though a major strike-slip fault is present (Alpine fault), the kinematics of the fault matches the kinematics of a wide zone (100 km) of deformation east of the fault. The degree of partition fundamentally depends on the angle of convergence, and dictates the orientation of the instantaneous strain axis, and the behavior of faults in the borderland (Teyssier *et al.*, 1995).

GEOLOGY OF THE CORDILLERA ORIENTAL

The review of structural, paleontological, and geophysical studies presented here reveals that the general assumption of a SE-dipping subduction regime driving deformation in the northern Andes is inadequate. Coeval transcurrent and thrust faulting arising from eastward

movement of the Caribbean Plate with respect to South America better explains available data. The surface expression of transpression in the Cordillera Oriental, nonetheless, is difficult to assess due to the lack of comprehensive field databases. Detailed field and geophysical studies have been concentrated on active oil exploration regions (eastern Foothills, and Magdalena Valley), whereas the axial zone of the Cordillera has remained relatively untouched. The opening of exploration in the Cordillera Oriental has renewed interest in studying its structural evolution, but kinematic reconstructions have been limited to comparisons with other orogens.

Regional Setting

The NE-trending Cordillera Oriental is located between the stable Guyana craton to the east, and the accreted terranes of the Cordillera Occidental (Etayo-Serna *et al.,* 1986) and Cordillera Central (Restrepo-Pace, 1992) to the west. Its basement, although showing affinity to the adjacent Guyana craton (Priem *et al.*, 1989), may have docked during the Early Devonian (Forero, 1990). Its thick Cretaceous sedimentary cover accumulated in a passive margin (Pindell and Dewey, 1982), as a result of early separation of the Americas. The Cordillera Oriental marks the eastern boundary of what Pennington (1981) called the "Andean block" (Fig. 1), a roughly triangular piece of crust extending from the Gulf of Guayaquil in Ecuador to the Mérida Andes in Venezuela, which contains the diffuse southern Caribbean Plate boundary (Mann *et al.,* 1990). Qualitative and semiquantitative kinematic block reconstructions (Laubscher, 1987; Ross and Scotese, 1988; Pindell *et al.*, 1988; Pindell and Barrett, 1990; Pindell, 1993) indicate that the Cordillera Oriental is the easternmost block of the southern Caribbean Plate boundary zone.

The Cordillera Oriental from 4°N to 6°N consists of a nearly flat, NE-trending, high plateau (about 2,600 m) rimmed to the east and west by 600 to 1,000 m high ridges that plunge

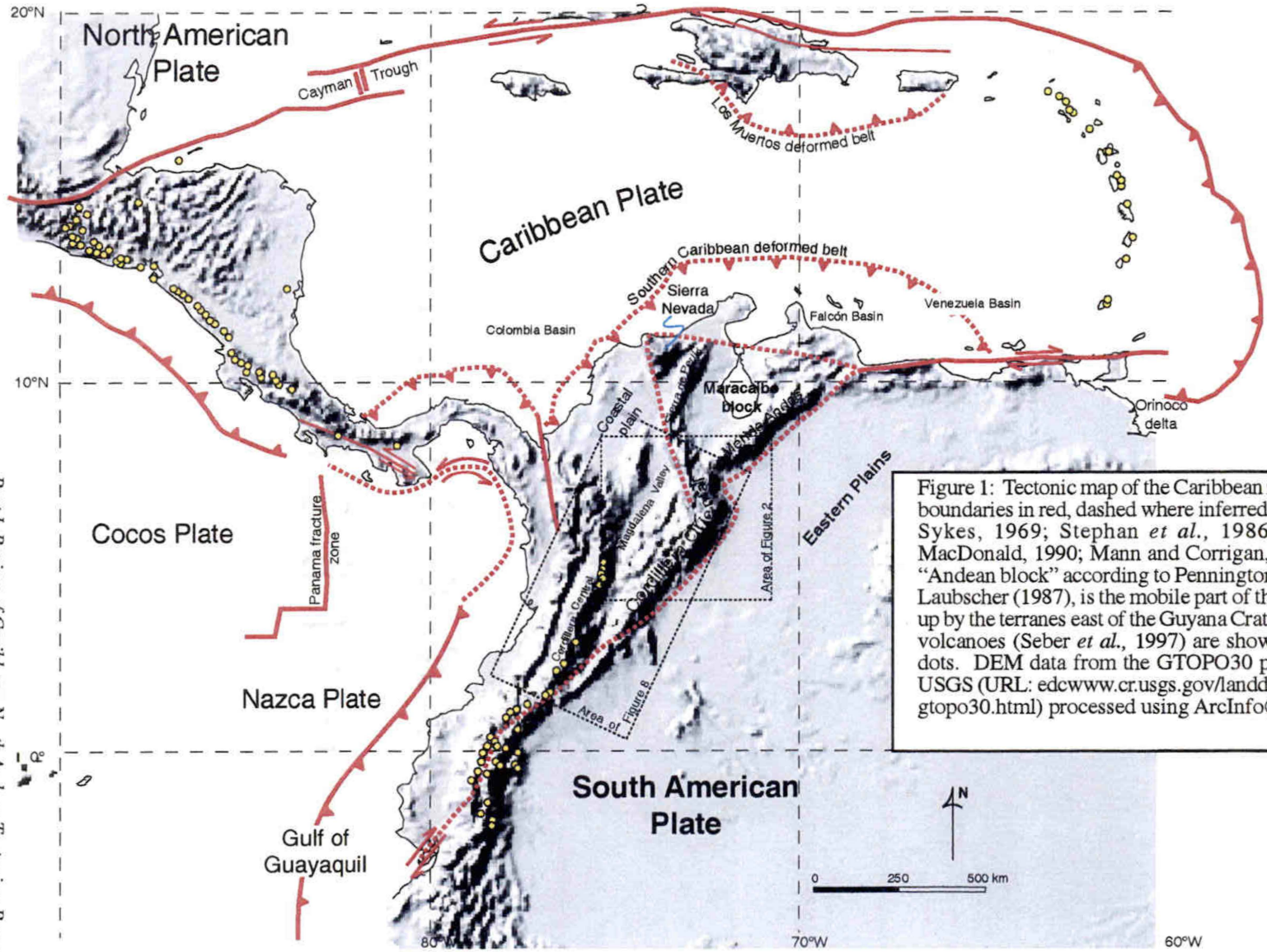


Figure 1: Tectonic map of the Caribbean region. Plate boundaries in red, dashed where inferred (Molnar and Sykes, 1969; Stephan *et al.*, 1986; Case and MacDonald, 1990; Mann and Corrigan, 1990). The "Andean block" according to Pennington (1981), and Laubscher (1987), is the mobile part of the crust made up by the terranes east of the Guyana Craton. Neogene volcanoes (Seber *et al.*, 1997) are shown by yellow dots. DEM data from the GTOPO30 project of the USGS (URL: edcwww.cr.usgs.gov/landdaac/gtopo30/gtopo30.html) processed using ArcInfo®.

steeply eastward into the plains of the Guyana craton, and to the west into the Magdalena Valley (Fig. 2). This plateau contains thick (400 m) lacustrine Neogene deposits within internally drained basins that follow the axis of the Cordillera (van der Hammen and González, 1963). The NE-trending Cordillera is most commonly less than 4,000 m elevation, but not uncommonly is more than 5,000 m in the Sierra Nevada del Cocuy, where the trend of the Cordillera changes from NE to NW.

Stratigraphy

Previously deformed and metamorphosed rocks that served as mechanical basement for the Andean orogenic cycle are considered basement in this compilation. Because the Andean orogenic cycle started with the rupture of Pangea during the Early Mesozoic, all Paleozoic and Precambrian rocks have traditionally been considered basement, even though mildly

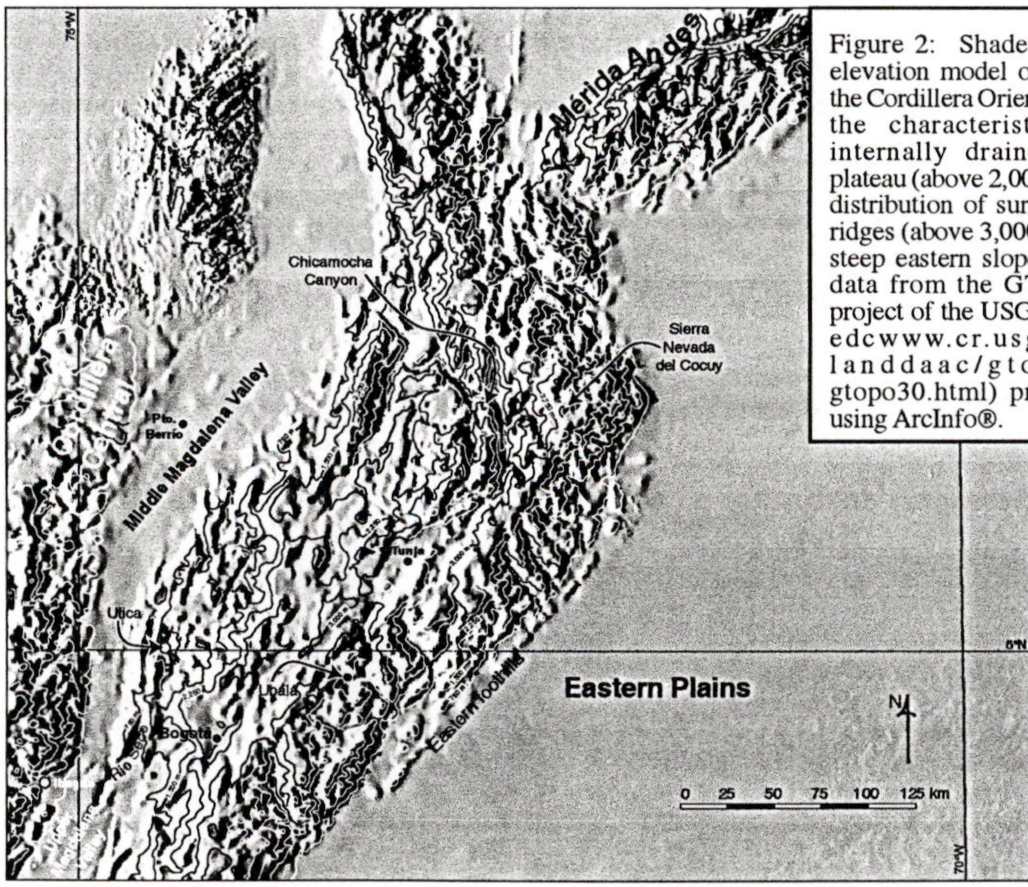


Figure 2: Shaded digital elevation model of part of the Cordillera Oriental. Note the characteristic flat, internally drained high plateau (above 2,000 m), the distribution of surrounding ridges (above 3,000 m), and steep eastern slope. DEM data from the GTOPO30 project of the USGS (URL: edcwww.cr.usgs.gov/landdaac/gtopo30/gtopo30.html) processed using ArcInfo®.

deformed Paleozoic sedimentary rocks are locally involved in Andean deformation along with cover rocks of Mesozoic and Cenozoic age.

Pre-Mesozoic rocks in the northern Andes have been divided into two major provinces: the Guyana craton, and the Garzón-Santa Marta belt (Kroonenberg, 1982). Granites, gneisses, and migmatites from the western Guyana craton yield ages of 1.45-1.56 Ga, with partial isotopic resetting at 1.3 Ga; younger, 900-1200 Ma dates have been obtained from volcanic rocks in the same region (Priem *et al.*, 1982). Granulites of the Garzón-Santa Marta belt yield ages between 1.9 and 1.45 Ga, metamorphosed at 1.0 Ga, and intruded by pegmatite dikes 850 Ma ago (Priem *et al.*, 1989; Restrepo-Pace *et al.*, 1997). The distribution of these radiometric dates in the Andes has been interpreted as the result of a Grenville-Orinoquense metamorphic event that affected the periphery of the Guyana craton, was later fragmented and remobilized during the Andean orogenic cycle, and is now exposed along the Andes from Argentina to Venezuela. The sporadic outcrops of Proterozoic rocks in the Cordillera Oriental are covered by Cambrian to Ordovician low-grade metamorphic assemblages metamorphosed during the Ordovician (Restrepo-Pace *et al.*, 1995), and by a younger clastic and carbonate sequence of Early Devonian to Carboniferous age deformed during the Permian. The fossil content of this clastic and carbonate sequence raises questions (Forero, 1990) about the autochthonous character of the basement of the Cordillera Oriental because of its faunal similarity to Laurentia. In summary, Paleozoic and Precambrian rocks along the western margin of Pangea were subject to polyphase deformation during the Paleozoic, and make up the basement for the Andean tectonic cycle.

Post-Paleozoic stratigraphic evolution of the Cordillera Oriental can be roughly summarized (Fig. 3) in three sedimentary stages that took place on a complex basement surface made up of mostly of Paleozoic sedimentary and metamorphic rocks: 1) Triassic-Jurassic clastic and volcanoclastic sediment accumulation in rift depressions resulting from the separation

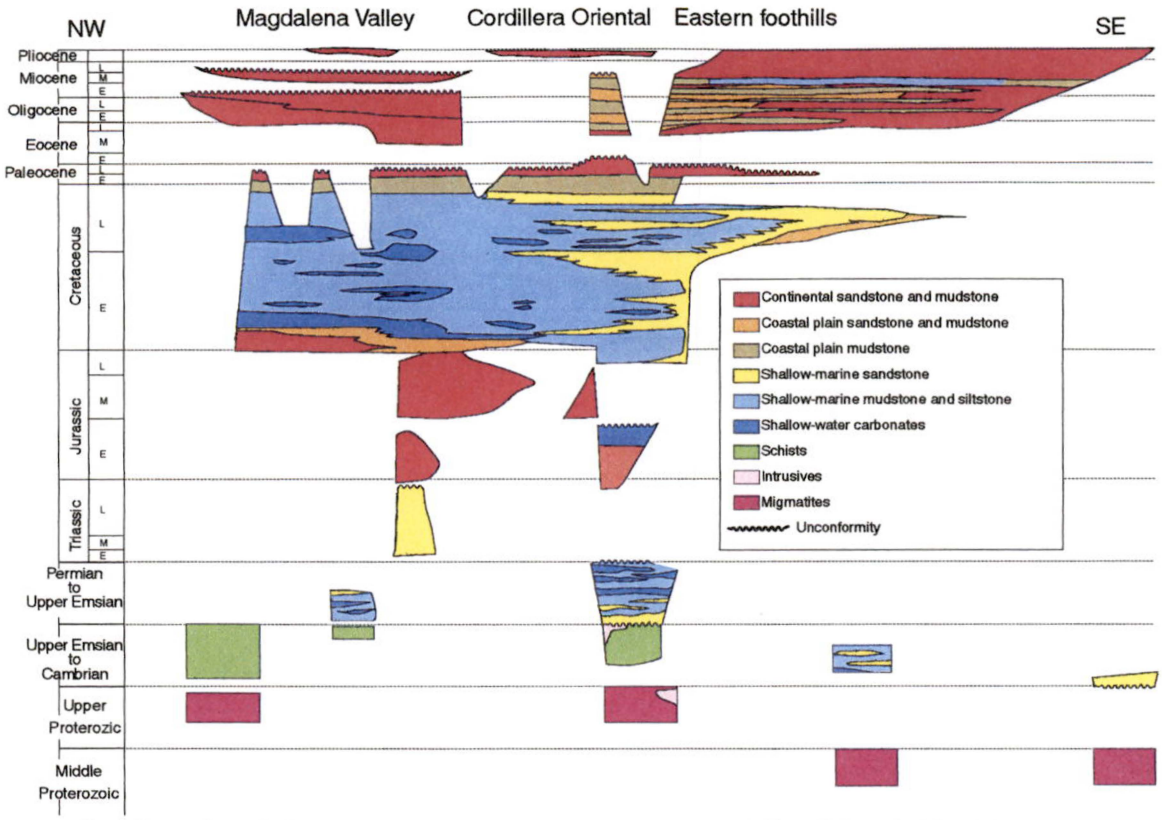


Figure 3: Mesozoic and Cenozoic stratigraphic summary of the Cordillera Oriental, Magdalena Valley and Eastern foothills at about 6°N latitude. Distribution of rocks deformed or metamorphosed previous to Early Mesozoic rifting (basement) is summarized into four main age groups, as detailed resolution is lacking. Lithostratigraphic names have been omitted for simplicity. Modified from Villarroel and Mojica (1988); Forero (1990); Restrepo-Pace (1992); and Cooper *et al.*, (1995).

between North and South America; 2) widespread Cretaceous shallow-marine sediment accumulation on a thermally subsiding continental margin; and 3) Tertiary shallow-marine and continental clastic accumulation on depressions resulting from advancing deformation fronts. Maximum thickness of the entire Mesozoic-Cenozoic sedimentary package has been estimated at between 10 and 15 km (Campbell and Bürgl, 1965; Roeder and Chamberlain, 1995).

Discontinuous lithostratigraphic units with limited exposures in the Magdalena Valley and Cordillera Oriental record the Early Triassic continental sediment accumulation, Late Triassic (Norian) marine incursion and carbonate accumulation, and Late Triassic-Jurassic felsic and intermediate volcanism and volcanoclastic sedimentation (Cediel, 1969; Cediel *et al.*,

1981). This period of sedimentation has been interpreted as early extension and marine incursion, followed by back-arc volcanism developed by subduction of the Farallon Plate under western Pangea (Pindell and Dewey, 1982).

Early Cretaceous (Berriasian-Valanginian) shallow-marine sedimentation took place within two main depocenters in the northern Cordillera Oriental: the Cocuy basin, and the Tablazo-Magdalena Basin, separated by the Santander massif. Hauterivian-Aptian marine sedimentation extended northeastward, covering the Santander massif by the Barremian, and the Maracaibo Basin by the Aptian. Maximum marine transgression took place during the Albian, extending southeastward along the Upper Magdalena Valley and southern Cordillera Oriental (Etayo-Serna *et al.*, 1969), and continued during the Campanian when sands onlapped the Cordillera Oriental foothills into the Guyana craton. Early Cretaceous depocenters contain a thick Cretaceous succession characterized by intercalation of thick black shale and sandstone units that result from shallow-marine sandstone (mostly from the Guyana craton) sporadically reaching interior, anoxic parts of the basin. The Upper Magdalena Valley and southern Cordillera Oriental typically contain thinner successions of Cretaceous marine black shale showing the same intercalation of sandstone, both from the Guyana craton, and from the west. Marine conditions remained stable in the Cordillera Oriental and Magdalena Valley until the end of the Cretaceous, when the sea regressed, and shallow-marine sequences prograded westward from the Guyana craton (Fabre, 1985; Cooper *et al.*, 1995).

Regional unconformities divide the Tertiary record into three main sequences: 1) a Paleocene coal-bearing, coastal and alluvial-plain sequence accumulated in the same domain (Cordillera Oriental and Magdalena Valley) as the Cretaceous marine sequences with breaks in sedimentation occurring in the eastern foothills of the Cordillera Oriental; 2) a Middle Eocene to Early Miocene sequence composed of coarse conglomerates, becoming sandstone-rich

fluvial and shallow-marine deposits to the east which accumulated on the eastern foothills of the Cordillera Oriental and on the Magdalena Valley; and 3) a Miocene and younger, mostly continental sequence that accumulated not only in the Cordillera Oriental foothills, but also on top of the Cordillera Oriental (van der Hammen, 1961; Cooper *et al.*, 1995). Paleoflora collected on the crest of the Cordillera record Pleistocene uplift from about 500 m to about 3,000 m (van der Hammen *et al.*, 1973). New data from the Middle Magdalena Valley also indicate that the Cordillera Oriental was tectonically active as early as the early Paleogene (Gómez and Jordan, in press). Middle to Late Pliocene upheaval of the axis of the Cordillera Oriental to about 2,500 m took place at an estimated rate of 1 to 5 mm/yr. Uplift rates for the Cocuy region, where Lower Cretaceous quartzite is exposed at 5,000 m, may have been as high as 5 to 10 mm/yr (van der Hammen *et al.*, 1973).

Structure

Geologic mapping has been the principal source of structural data to quantify deformation in the Cordillera Oriental. Few seismic reflection lines have been acquired beyond active oil exploration basins, and only a handful of wells have penetrated the sedimentary cover. It is clear, nonetheless, that the Cordillera Oriental is a doubly vergent orogen (Fig. 4). A mildly deformed, thick shell of Upper Cretaceous and Tertiary marine sedimentary strata comprises most of the high plateau, whereas highly deformed belts of older strata (Lower Cretaceous and occasional basement rocks) are symmetrically exposed along its flanks, verging in opposite directions, away from the axis of the Cordillera. Low-angle faults on the east flank of the Cordillera verge east, and low-angle faults on its west flank verge west (Hubach, 1945). Shortening along the flanks of the Cordillera (Restrepo-Pace, 1989; Namson *et al.*, 1994), and on the intramontane Magdalena Valley (Amézquita and Montes, 1994) has locally been estimated between 30 and 70 percent. North of 6°N, the Cordillera changes trend to northwest, and loses its symmetry as erosion along the Santa Marta-Bucaramanga

fault has excavated a deep canyon along its axis. South of 4°N only the west-verging deformed belt has been mapped (Gerth, 1955).

More subtle structural style elements may be deduced from mapped surface exposures. The thick cover of Upper Cretaceous and Tertiary rocks in the high plateau is nowhere broken by faults exposing Lower Cretaceous rocks (McLaughlin and Arce, 1975; Cediel and Cáceres, 1988), instead, most faults in the plateau simply repeat or disrupt the same sequences (Fig. 4). Similarly, deformation along the flanks of the Cordillera appears confined to Lower Cretaceous shaly sequences, stepping up into younger units only in the foothills. The significance of this apparent deformation layering in the Cordillera Oriental has not been addressed by any study. Older rocks in the core of the Cordillera Oriental, in any case, have been thrust on top of younger deposits of the intramontane Magdalena Valley to the west, and the plains of the Guyana craton to the southeast, while the crest remained only broadly folded, and passively uplifted.

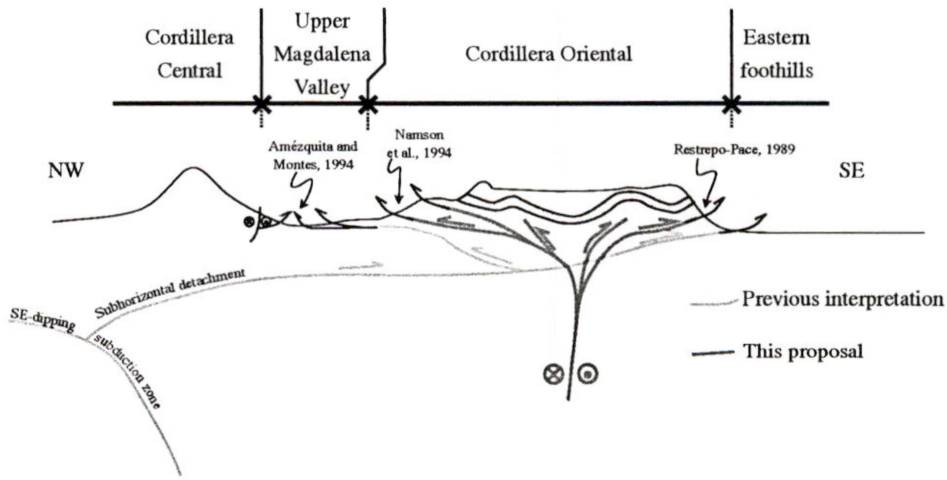


Figure 4: Schematic cross section of the Cordilleras Central and Oriental at about 5°N. Not to scale. Blue lines and arrows represent the basic geometry, and assumptions behind modern cross section reconstructions. Red lines represent the hypothesis put forward in this proposal: A right-lateral "palm tree" structure (Lowell, 1972; Sylvester, 1988) where thrusts along the flanks of the Cordillera Oriental accommodate fold-perpendicular contraction, and the fundamental strike-slip faults are concealed beneath a thick Upper Cretaceous and Tertiary shell. Yellow band represents the mildly deformed thick shell of Upper Cretaceous and Tertiary strata in the Cordillera Oriental. Vergence of structures is indicated by thin black arrows. References indicate field observations supporting vergence of structures and estimates of shortening: 49%: Amézquita and Montes (1994); 30 to 70%: Namson *et al.*, (1994); 42%: Restrepo-Pace, (1989).

Kinematic Reconstructions

The structure of the northern Andes has traditionally been explained in terms of a very unusual, doubly vergent retroarc thrust belt/basin formed on the distal edge of the high-angle convergent Nazca-South American Plate boundary (Paris and Marín, 1979; Toussaint and Restrepo, 1988; Restrepo and Toussaint, 1988). Extrapolation of structures mapped on the surface in the Cordillera Oriental into the middle crust has changed throughout the decades from vertical block tectonics to subhorizontal crustal detachments. Vertical block tectonic interpretations of the style of the Cordillera reflect early European influence (Fig. 5), whereas subhorizontal detachments across the entire width of the Cordillera reflect the influence of North American schools and the petroleum industry during the last 20 years (Fig. 6). Other speculative models of the Cordillera Oriental include gravity sliding (Jones, 1995), and only demonstrate the lack of solid field observations.

Modern cross sections reconstructing the predeformational geometry have in common the assumption that no mass was transported along the trend of the Cordillera. These studies (Colleta *et al.*, 1990; Dengo and Covey, 1989; Dengo and Covey, 1993; Cooper *et al.*, 1995; Roeder and Chamberlain, 1995) have neither evaluated the map expression of the faults assumed to be responsible for NW-SE shortening, nor have they presented subsurface geophysical evidence for large subhorizontal detachments. These reconstructions have also assumed that west-verging thrusts are backthrusts with relatively minor displacements ramping off a large, east-verging master detachment rooted beneath the Cordillera Central. Such large composite thrust sheets (>300 km wide) would have transported the entire basement-involved Magdalena Valley and Cordillera Oriental sequences 100 km eastward to rest atop the Guyana craton.

Two-dimensional restoration attempts of the Cordillera Oriental find it necessary to suggest the existence of a large detachment rooted beneath the Cordillera Central. Because of its

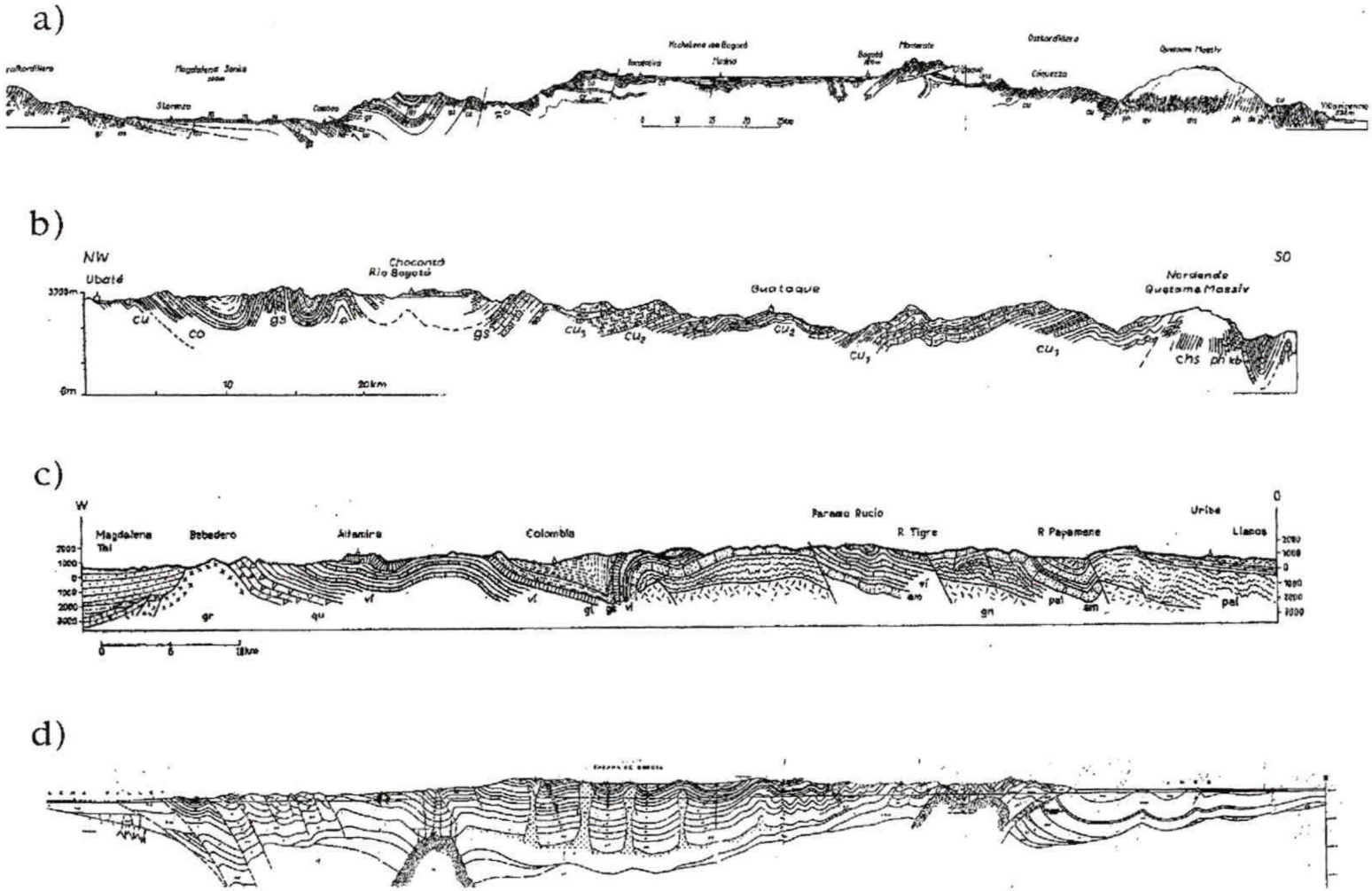


Figure 5: Cross sections of the Cordillera Oriental. a) Hubach (1945); b) Hubach *in* Gerth (1955); c) Renz *in* Gerth (1955); and d) Campbell and Bürgl (1965). Vertical block tectonics, and very little horizontal shortening was suggested to explain deformation in the Cordillera. Note that sections a), b), and c) have vertical exaggeration. See Fig. 7 for location of these cross sections.

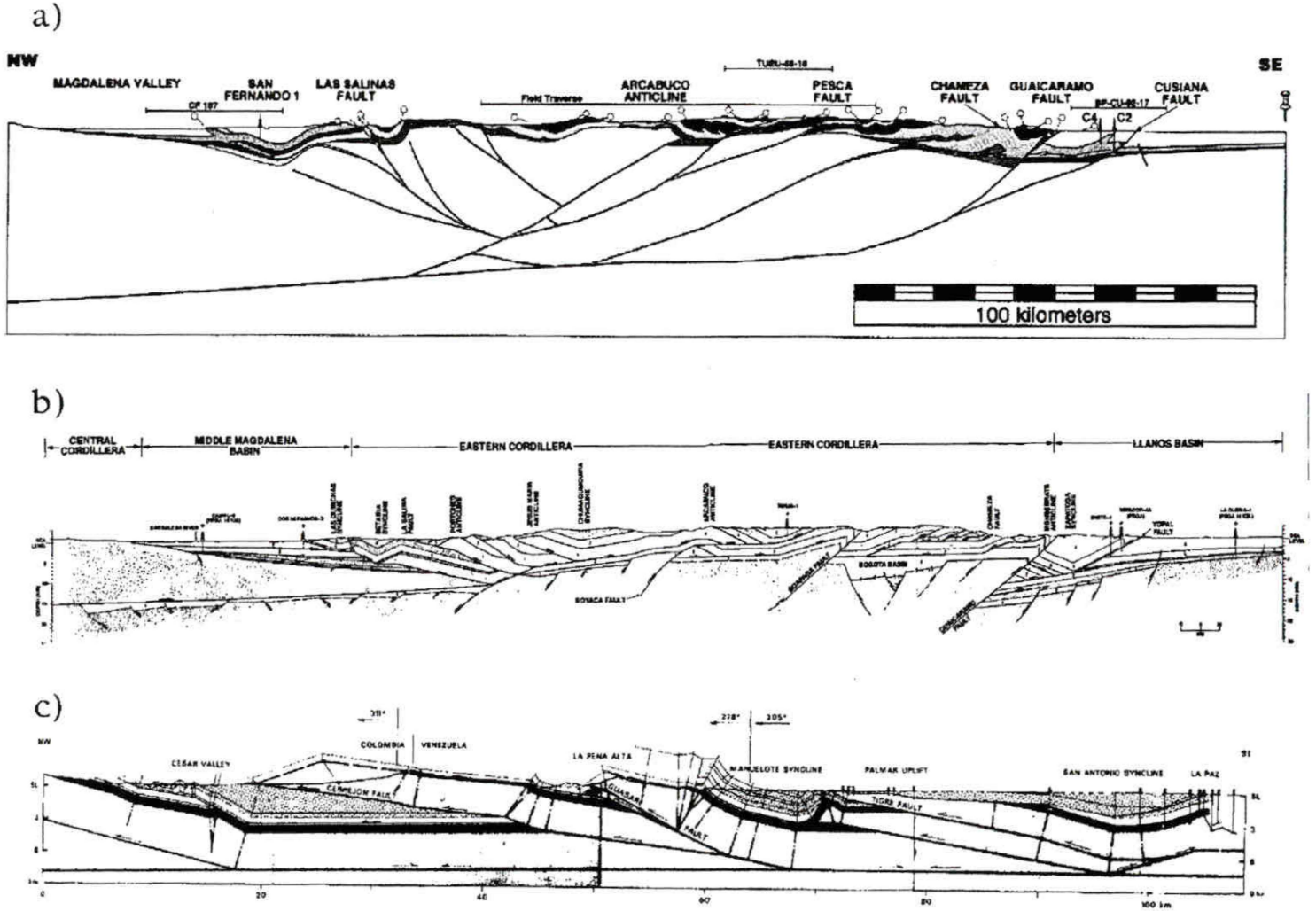


Figure 6: Modern cross sections of the Cordillera Oriental. a) Cooper *et al.* (1995); and b) Dengo and Covey (1989); c) a similar interpretation for the Sierra de Perijá after Kellog and Bonini (1982). See Fig. 7 for location of these cross sections.

doubly vergent structure, deformation on both flanks of the Cordillera Oriental (between 30 and 70 percent, Restrepo-Pace, 1989; Namson *et al.*, 1994) cannot be displaced towards a hinterland, as it would be in a foreland fold-thrust belt, because there is simply not enough room beneath the axis of the Cordillera Oriental to accommodate shortening along the flanks. Therefore, either the SE-vergent or the NW-vergent thrust faults and folds must be considered backthrusting. All reconstructions have chosen to model the NW-vergent deformation as backthrusting (Figs. 4 and 6); thus, the Cordillera Oriental is interpreted as a SE-vergent foreland fold-thrust belt with its internal part to the west (Cordillera Central) overlying a mid-crustal basal detachment.

The first objection to this model is that restoration of foreland deformation would place the internal parts of the orogen (Cordillera Central) beyond the edge of the continental crust in the northern Andes. As noted by Oldow *et al.* (1990), restoration of foreland fold-thrust belts also requires displacing the metamorphic assemblages and basement overlying the internal parts of the basal detachment. If the basement overlying the basal detachment (Cordillera Central) is also displaced, no mass balance can be reached because subdetachment mass would be missing as the Cordillera Central is the westernmost terrane in the northern Andes containing continental crust (Case *et al.*, 1973; Etayo-Serna *et al.*, 1986). The low metamorphic grade (greenschist) of the Cordillera Central (Restrepo-Pace, 1992) prevents it from having been brought from deep crustal levels to solve the room problem.

Second, regional isostatic adjustment of the lithosphere predicts that an advancing load on the lithosphere creates a basin and a forebulge in front of the load (Beaumont, 1981). Therefore, Pleistocene uplift (van der Hammen *et al.*, 1973), and southeastward advance of the Cordillera Oriental would have generated a Pleistocene or younger basin-forebulge in the plains east of the Cordillera. Even though a wedge-shaped basin is present in front of the Cordilleran foothills, it is filled with sediments as old as Cretaceous, and a topographic forebulge is absent (Pindell, 1993).

Strike-Slip Faults in the Northern Andes

Strike-slip faulting has long been recognized as a major component of deformation in the northern Andes (Dengo, 1953; Moody and Hill, 1956; Alberding, 1957). The northern Cordillera Central and the Mérida Andes (Fig. 1), trending parallel to the Cordillera Oriental, contain clear evidence of transcurrent faulting. In fact, dextral strike-slip faults are the dominant structural element (Barrero *et al.*, 1969; Schubert, 1981; Feininger *et al.*, 1970; Barrero and Vesga, 1976; Mosquera *et al.*, 1982). Piercing points (characteristic lithologic types, and older faults) have been used to reconstruct displacement on strike-slip faults in the Cordillera Central. Two major (800 and 300 km long) north- and NE-trending, apparently inactive, dextral strike-slip faults dominate the structure of the Cordillera Central: the Romeral fault of unknown displacement, and the Palestina fault (Fig. 7), with 27 km of dextral displacement since the Cretaceous (Feininger, 1970). The inactive nature of these faults, however, is challenged by their bold topographic expression, and more importantly, by the fact that the northernmost active volcanoes in South America are located along the trace of the Palestina fault (Fig. 7).

Kinematic reconstruction of extensional dextral pull-apart basins formed on right-stepping bends, indicates 60 to 100 km of Neogene displacement for the Boconó fault (Fig. 7) in the Mérida Andes (Schubert, 1983). To the NE, the Boconó fault connects with the Morón-Pilar fault system (Fig. 3) in northern Venezuela (Dengo, 1953), which undoubtedly is part of the Caribbean-South America plate boundary (Schubert, 1981), and has displacements of as much as 200 km during the last 8 m.y. (Robertson and Burke, 1989). This rate (25 km/ m.y.) is compatible with plate motion rates at the northern Caribbean Plate boundary (Rosencrantz *et al.*, 1988).

Only a few strike-slip faults have been recognized in the Cordillera Oriental, although the possibility that a number of faults previously interpreted as thrusts may have a major

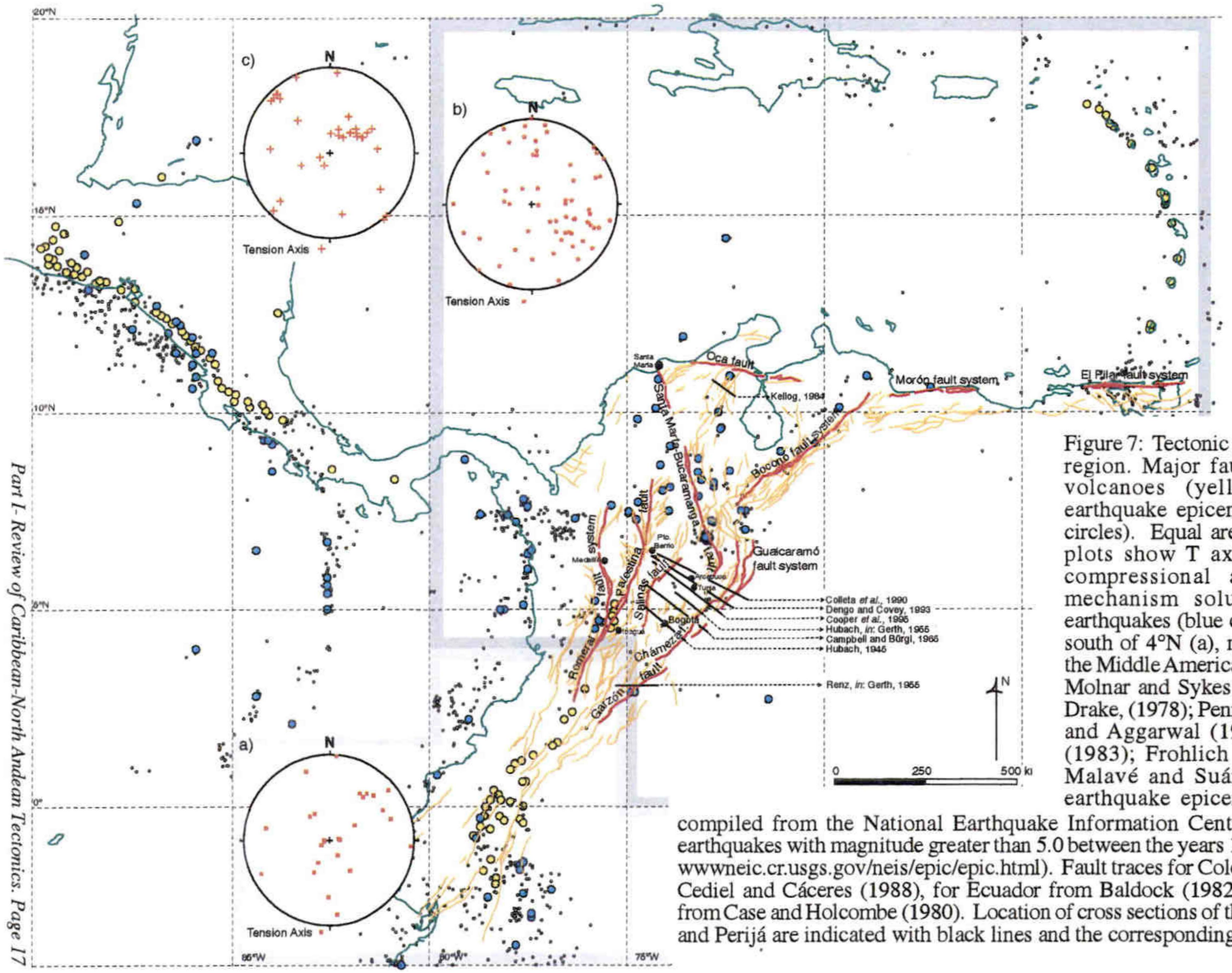


Figure 7: Tectonic map of the Caribbean region. Major faults (red), Neogene volcanoes (yellow circles), and earthquake epicenters (blue and gray circles). Equal area, lower hemisphere plots show T axes (recording first compressional arrivals) of focal mechanism solutions of selected earthquakes (blue circles) for the Andes south of 4°N (a), north of 4°N (b), and the Middle America arc (c) calculated by Molnar and Sykes (1969); Bradley and Drake, (1978); Pennington (1981); Pérez and Aggarwal (1981); Suárez *et al.*, (1983); Frohlich *et al.*, (1995); and Malavé and Suárez (1995). Other earthquake epicenters (gray circles) compiled from the National Earthquake Information Center of the USGS for earthquakes with magnitude greater than 5.0 between the years 1960 and 1996 (URL: wwwneic.cr.usgs.gov/neis/epic/epic.html). Fault traces for Colombia compiled from Cediel and Cáceres (1988), for Ecuador from Baldock (1982), and for Venezuela from Case and Holcombe (1980). Location of cross sections of the Cordillera Oriental and Perijá are indicated with black lines and the corresponding reference.

component of strike-slip motion has been explored (Galvis and de la Espriella, 1987). Reinterpretation of the Garzón fault (Chorowicz *et al.*, 1996) using remote sensing indicates that this fault is a dextral-strike slip fault with about 5 km of Holocene displacement. Rates calculated using these values (1.5 mm/year) indicate that this fault may play an important role as part of the diffuse plate boundary in this area. Other remarkably straight, relatively unknown (except for remote sensing data) faults in the Cordillera Oriental such as the Chámeza fault (Fig. 8) are candidates to have accommodated significant strike-slip displacements, although the true nature can only be evaluated in the field. Also, salt domes emplaced in the plateau probably broke through the thick sedimentary cover along the releasing bends of dextral strike-slip faults (Montes *et al.*, 1994). In the complex region of the northern Cordillera Oriental, the southern extension of the NE-trending Boconó fault is the NW-trending Chitagá-Pamplona (Fig. 8) thrust (Boinet *et al.*, 1985) that further south becomes the Sácama fault in the Cocuy Mountains. This sector of the Cordillera Oriental is dominated by the southern termination of the 550 km long, N15°W-trending, Santa Marta-Bucaramanga fault (Fig. 8). A well drilled in the Coastal Plain contains evidence for at least 100 km of sinistral displacement along this fault (Irving, 1975). The Upper Magdalena Valley is crossed by numerous dextral strike-slip faults that connect large faults of the Cordillera Central and Cordillera Oriental.

PALEONTOLOGICAL EVIDENCE FOR A MIGRATING DEFORMATION FRONT

The migrating Orinoco Delta provides independent evidence favoring an eastward advancing orogenic front along the northern coast of South America (Fig 9a). Endemic vertebrate faunas in sedimentary deposits along the coast of Venezuela can be used as fingerprints of the proto-Orinoco River deposits (Díaz de Gamero, 1996). The Maracaibo Basin (Fig. 1) was the site of a river delta draining the uplifted Cordillera Central and the Guyana craton

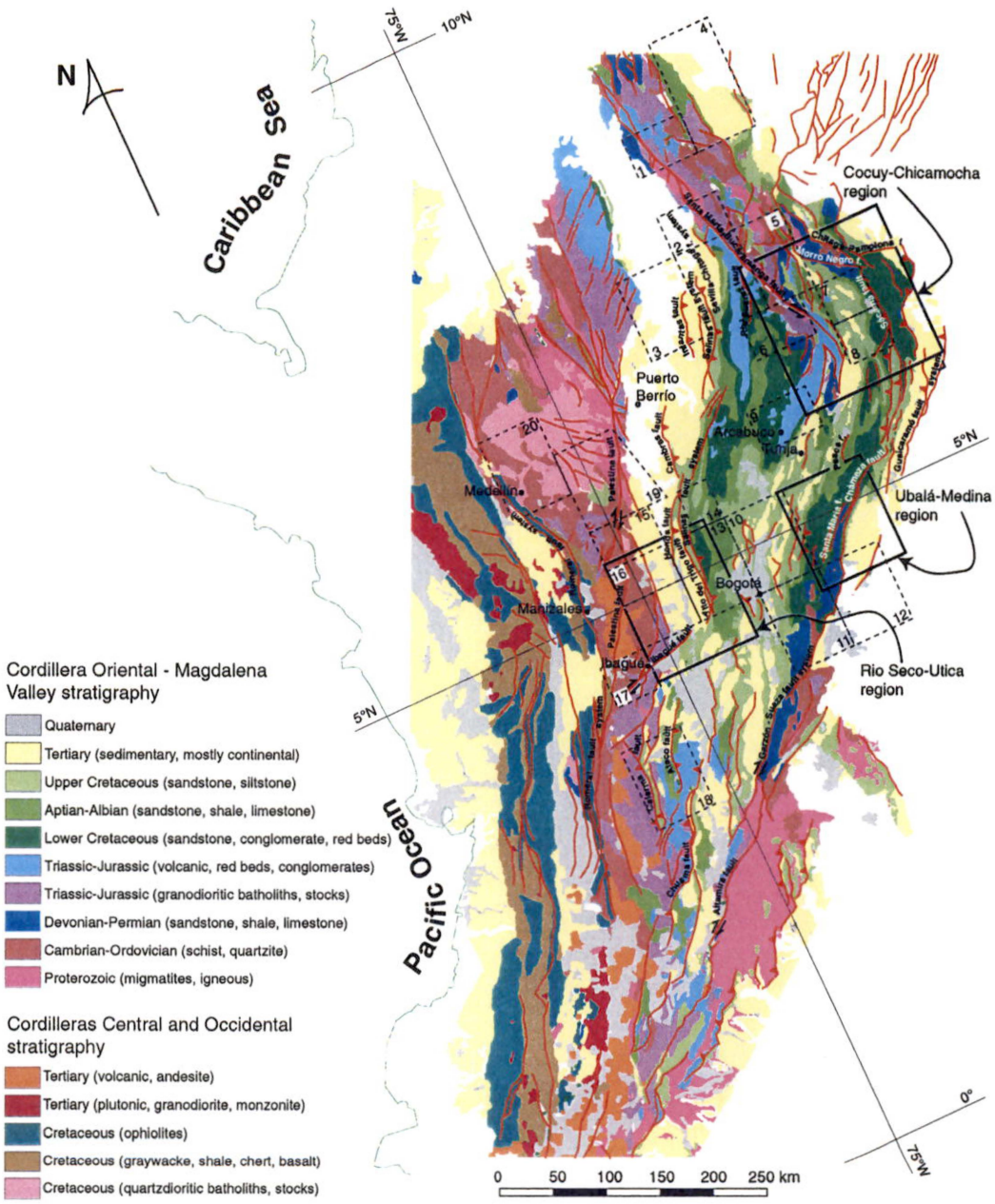
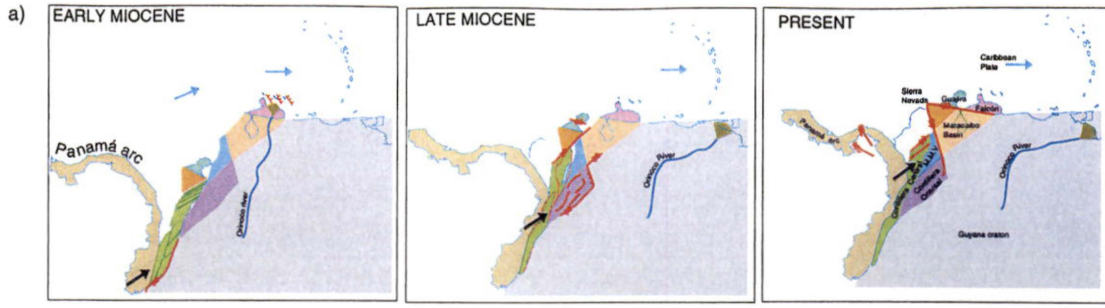


Figure 8: Geologic map of the Cordillera Oriental and parts of the Cordillera Central and Occidental. Fault traces shown with no teeth or arrows indicate unknown vergence. Modified from Cediel and Cáceres (1988). Rectangles indicate preliminary field areas, and are labeled accordingly. Solid rectangles indicate the location of preliminary field areas. Dashed rectangles indicate available geologic maps, and are labeled by authors: (1) Daconte and Salinas, 1980; (2) Vargas and Arias, 1981; (3) Ecopetrol, 1967; (4) Colpet and Geofoto, 1967; (5) Ward *et al.,* 1970; (6) Ward *et al.*, 1977; (7) Fabre *et al.*, 1984; (8) Fabre *et al.*, 1985; (9) Renzoni *et al.*, 1967; (10) McLaughlin and Arce, 1975; (11) Renzoni, 1965; (12) Segovia and Renzoni, 1965; (13) Champetier *et al.*, 1961; (14) Ingeominas, preliminary map; (15) Barrero and Vesga, 1976; (16) Raasveldt and Carvajal, 1957a; (17) Mosquera *et al.*, 1982; (18) Raasveldt and Carvajal, 1957b; (19) Feininger *et al.*, 1970; (20) Botero and Rico, 1965.



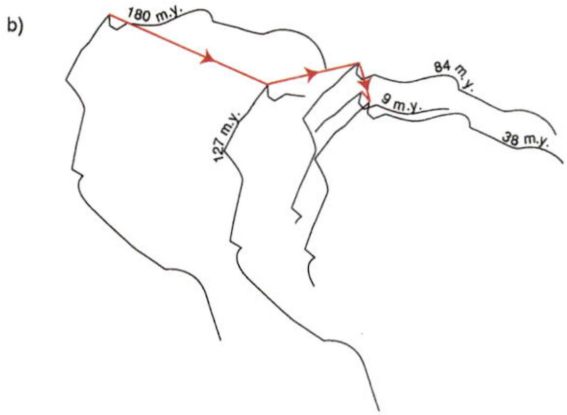


Figure 9: Schematic paleogeographic reconstruction of the Caribbean region. a) Modified from Pindell, (1993). M.M.V.: Middle Magdalena Valley. Migration of the Orinoco Delta after Díaz de Gamero (1996) and Robertson and Burke, (1989). The paleogeographic location of Andean terranes is uncertain and highly speculative. Migration of Caribbean orogenic front suggests that early deformation (Paleocene-Eocene) of the Cordillera Oriental may be related to the passage of the Antilles arc along NW South America, whereas Miocene-Pliocene uplift, and escape of the Santa Marta block (Kellog and Bonini, 1982) may be related to the oblique collision of the Panamá arc. b) Migration of South America keeping North America fixed since the Eary Jurassic (Ladd, 1976) suggests that Andean terranes may have been fragmented by and transported northeastward by dextral strike-slip faults. Note that, comparatively, the amount of N-S contraction is minimal.

during the middle Eocene. This depocenter shifted to the south during the late-middle Eocene, as the leading edge of the Caribbean Plate progressively advanced eastward destroying the passive margin established around the northwestern corner of South America following Triassic-Jurassic rifting. During the earliest Miocene the primary depocenter moved northeastward, to the transtensional Falcón basin, behind the east-moving Antilles arc. By the late Miocene, the initiation of the oblique collision of the Panamá arc uplifted the Mérida Andes and the Cordillera Oriental, causing the Orinoco Delta to shift to its present position in front of the Antilles arc.

Study of the migrating Orinoco Delta also highlights problems in the hypothesis of an eastward-migrating Caribbean Plate (Pindell and Dewey, 1982). First of all, if the eastward advancing Antilles arc progressively emplaced thrust sheets onto the margin of the Guyana

craton (Pindell and Barrett 1990), how did the Orinoco River find an opening to discharge behind an advancing arc? An analogy could be made to a snow plow cleaning a road, but blocking driveways. The most logical location for the Orinoco Delta is its present position, in front of the arc, being constantly pushed eastward by it (Robertson and Burke, 1989). Second, the age of metamorphism in the thrust sheets emplaced during the eastward migration of the Antilles arc is consistently younger eastward in northern Venezuela (Pindell, 1993). The age of metamorphism for the Cordillera Central, however, has not been satisfactorily dated partly because of the strong Triassic-Jurassic thermal overprint (Restrepo-Pace *et al.*, 1995; Restrepo-Pace *et al.*, 1997). Clearly, the Cordillera Central could not have been the product of thrust sheets emplaced by the advancing Antilles arc during the Cretaceous, as suggested by Pindell and Barrett (1990) and Pindell (1993), because the timing of metamorphism here is pre-Cretaceous. The fact that the Orinoco Delta has been located in the Maracaibo region since at least since the Eocene, nonetheless, indicates that a N-S topographic barrier existed along the western margin of South America. The Cordillera Central has been the logical choice, but an initial phase of uplift in the Cordillera Oriental may have also produced a topographic barrier.

KINEMATIC PLATE TECTONIC RECONSTRUCTIONS

The well-documented opening history of the Atlantic Ocean shows that the Caribbean Plate originated in the Pacific Ocean, and was not subducted thanks to the opening that the South American plate left as it drifted westward since the Aptian (Ladd, 1976; Pindell and Dewey, 1982). Even though the sequence of finite rotations developed using the mid-Atlantic magnetic anomalies (Ladd, 1976) provides a reliable framework to study the kinematic development of the Caribbean Plate (Fig 9b), reconstruction of small blocks (such as the blocks in the northern Andes) remains controversial and highly speculative.

The overall relative separation history of North and South America (Ladd, 1976) occurred in four steps: 1) Early Jurassic to Early Cretaceous rifting related to the opening of the North Atlantic recorded as ESE motion of South America relative to North America. 2) Early to Late Cretaceous separation of South America and Africa that produced a large E-W strike-slip component in the Caribbean region. 3) Late Cretaceous to Eocene relative motion switched to SSE extension; and 4) N-S contraction during the Oligocene to Miocene. Nowhere in this sequence of events is NW-SE-trending contraction required to validate reconstructions that assume more than 100 km of NW-SE horizontal shortening in the Cordillera Oriental (Colleta *et al.*, 1990; Dengo and Covey, 1989; Cooper *et al.*, 1995; Roeder and Chamberlain, 1995). In fact, most deformation in the Caribbean region seems to be accommodated by strike-slip faulting. The Cayman Trough pull-apart basin provides evidence for at least 1,100 km of left-lateral movement on the northern Caribbean Plate boundary since the Eocene (Rosencrantz *et al.* 1988), with an additional 300 km accommodated along the Barracuda fracture zone (Pindell and Barrett, 1990). At the diffuse southern boundary of this plate, however, no continuous strike-slip faults or other plate boundary features have been mapped between the Mérida Andes and the active arc systems of Central America (Mann *et al.*, 1990). Kafka and Weidner (1981) have suggested that, unlike its sharp transcurrent northern boundary, the southern Caribbean plate boundary is characterized by a broad zone of strike-slip deformation with the Cordillera Oriental forming its eastern border.

GEOPHYSICAL DATA

Even though geophysical data only provide information regarding the present-day nature of the boundary, earthquake focal mechanisms and tomographic imaging demonstrate that the northern Andes today are different from the rest of the Andes where right-angle convergence and subduction are taking place (Meissnar *et al.*, 1976; Jordan *et al.*, 1983).

Gravity and geodesy

Large gravity anomaly contrasts mapped in the boundary zone between the South American and Caribbean plates reveal the heterogeneity of the crust in this region (Zeil, 1979; Westbrook, 1990). Subduction of Caribbean crust under the northern Andes has been proposed as the mechanism responsible for the gravity signatures, and for the distribution of NW-SE trending compressional stresses driving deformation in the northern Andes during the Cenozoic (Kellog and Bonini, 1982; Freymueller *et al.*, 1993). A dramatic lack of isostatic equilibrium is present in the Sierra Nevada de Santa Marta: an isolated block of crystalline rocks rises 5,900 m above sea level that has a large (120 mgal) positive Bouger anomaly. This anomaly, the opposite of what should be expected over such a topographic high in continental crust, has been explained as very recent thrusting of the Santa Marta block toward the NW over Caribbean oceanic crust along the Santa Marta-Bucaramanga, and Oca faults (Case and MacDonald, 1973; Kellog and Bonini, 1982). Global Positioning System measurements between 1988-1991 support the hypothesis of the relative northwestward movement of the northern coast of Colombia onto the Caribbean Plate (Freymueller *et al.*, 1993). These results have been interpreted as evidence of active subduction of the Caribbean Plate beneath the northern Andes, postulating the southern Caribbean deformed zone (Fig. 1) as the plate boundary where Caribbean crust is subducted beneath the northern Andes (Kellog and Bonini, 1982; Freymueller *et al.*, 1993).

Geophysical and geomorphic features of the Caribbean crust are atypical of oceanic crust and may cause it to be particularly difficult to subduct. Caribbean ocean floor is 1-2 km shallower than predicted by its minimum age (Early Cretaceous), lacks magnetic anomaly and fracture zone patterns, and exhibits numerous seismic velocity contrasts and complex structural relief on its surface (Fox and Heezen, 1975; Burke *et al.*, 1978; Case and MacDonald, 1990). Early seismic refraction studies revealed an abnormally thick (12 to 15

km) crust (Edgar *et al.*, 1971), but more recent surveys indicate that anomalous depths to mantle can be explained by addition, on an otherwise normal oceanic crust, of 1 to 2.5 km of igneous overburden in the Venezuela Basin, and more than 3 km of sediment overburden in the Colombia Basin (Houtz and Ludwig, 1977). The unusually shallow Caribbean ocean floor may also be the result of a buoyant crust from the emplacement of basaltic and diabase sills, and underplating during the Late Cretaceous (Fox and Heezen, 1975; Burke *et al.*, 1978). Such crust may have been difficult to subduct, with internal deformation, rather than subduction, accommodating about 200 km of Oligocene-Miocene N-S convergence (Burke *et al.*, 1978). The complex structure of the Caribbean crust (Houtz and Ludwig, 1977) may also be the result of internal deformation as the Caribbean Plate moved eastward through a bottleneck between the Los Muertos and Southern Caribbean deformed belts (Burke *et al.*, 1978). Therefore, even though some N-S contraction may be recorded along the northern and southern Caribbean deformed zones, this can be explained by irregularities along the margin resisting the overall eastward motion of the plate (Stephan *et al.*, 1986), by northward escape of continental blocks related to the Panamá collision, or by the difficulty of subducting the Caribbean Plate (Burke *et al.*, 1978). A three-year, two station GPS survey (Freymueller *et al.*, 1993) only confirms that the most recent interaction between the independent blocks of the northern Andes and the Caribbean plate has been N-S convergence, but the overall kinematics of the Caribbean Plate has mostly been of eastward motion relative to South America (Ladd, 1976). Therefore, neither gravity nor geodesic measurements can confirm the hypothesis of present or past subduction of the Caribbean Plate underneath the northern Andes.

Earthquake focal mechanisms

Subduction of the buoyant Caribbean Plate underneath the northern Andes has also been proposed based on earthquake focal mechanism studies, and earthquake foci distribution

within the crust. The distribution of earthquake foci, and the nature of focal mechanisms, however, are not clear and does not conform to a typical subduction regime.

Nonvolcanic segments of the Andes where subduction is clearly taking place (Perú 5°S to 15°S, and Argentina 28°S to 33°S) have characteristically shallow, well-defined Wadati-Benioff zones with earthquake "P" compressional axes consistently oriented east-west, thick-skinned basement-involved foreland deformation (Jordan *et al.*, 1983; Jordan and Allmendinger, 1988), and extraordinary structural relief (Cordillera Blanca in Peru, and Aconcagua and Sierras Pampeanas in Argentina), with elevations over 6,000 m. Accurate plotting of earthquake hypocenters delineated subducted oceanic lithosphere in these and other segments of the Andes (Barazangi and Isacks, 1976). Evidence for active subduction north of 5°N, however, is less clear than in the rest of the Andes: Neogene volcanoes are absent in this region, and earthquake focal-mechanism solutions have contrasting styles and diffuse distribution within the crust. North of 5°N, earthquake hypocenters commonly have strike-slip solutions (Pennington, 1981), and do not delineate a clearcut Wadati-Benioff zone (Zeil, 1979; McCann and Pennington, 1990). Instead, seismicity is concentrated in "nests" (earthquake clusters) of unknown origin (the Bucaramanga nest, McCann and Pennington, 1990; Frohlich *et al.*, 1995), and earthquakes irregularly distributed within the crust. Despite this irregular distribution of hypocenters under the northern Andes, a SE-dipping Wadati-Benioff zone was delineated (Pennington, 1981; Frohlich *et al.*, 1995; Malavé and Suárez, 1995), and two subducted slabs were suggested by connecting distant earthquake hypocenters. Further to the east, in northern Venezuela, Pérez and Aggarwal (1981) concluded that present-day subduction is insignificant, and seismicity is only remnant.

Tomographic imaging (van der Hilst and Mann, 1994) has also been used to probe the lithosphere beneath northwestern South America. Travel time of direct and surface-reflected earthquake waves was compared with an assumed mantle model for seismic velocities.

Such a mantle model is an ideal distribution of concentric layers with different seismic velocities. Deviations of measured earthquake P-wave velocity from the model are interpreted as compositional and thermal anomalies resulting from subducted slabs. It is clear from the results (Fig. 10) that most shallow seismicity in the region is associated with known strike-slip fault zones (white arrows), and unrelated to the deep structure shown by the tomographic images. Two slabs, nonetheless, were defined using these results: the Bucaramanga slab, dipping 50° ESE, and the Maracaibo slab dipping 17° SW. There are several possible interpretations of these slabs: 1) aseismic subduction of the Caribbean and Nazca plates; and 2) these may be relics from ancient subduction now resting beneath northwestern South America, and unrelated to subduction along this margin, as previously suggested by Pérez and Aggarwal (1981) further to the east.

Simple, three-dimensional visualization of earthquake hypocenters (Fig. 11) reveals striking differences between segments where earthquake data can be explained by the simple model

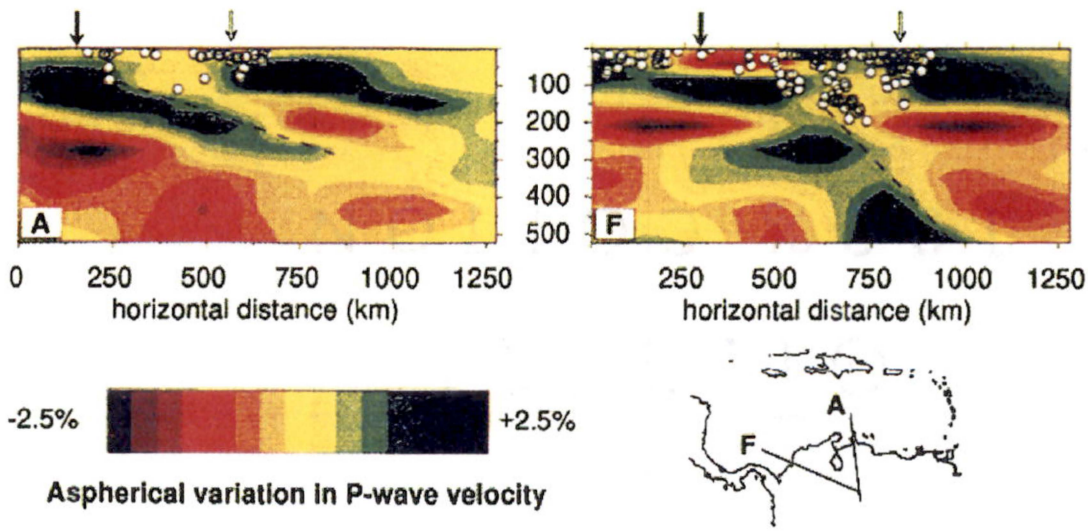


Figure 10: Tomographic images beneath northwestern South America (van der Hilst and Mann, 1994). Earthquake hypocenters are shown as light dots, light arrows indicate intersection with major strike-slip faults, and dark arrows indicate intersection with collision zones. Color scale indicates the variation in P-wave velocity with respect to a radially stratified mantle model. Note: 1) The disjunction between seismicity and mantle structure; 2) The amplitude of variation is only about 1%; 3) Most features are at or below the resolution limit (300 km horizontal, 100 km vertical); and 4) The correlation between seismicity and major strike-slip faults.

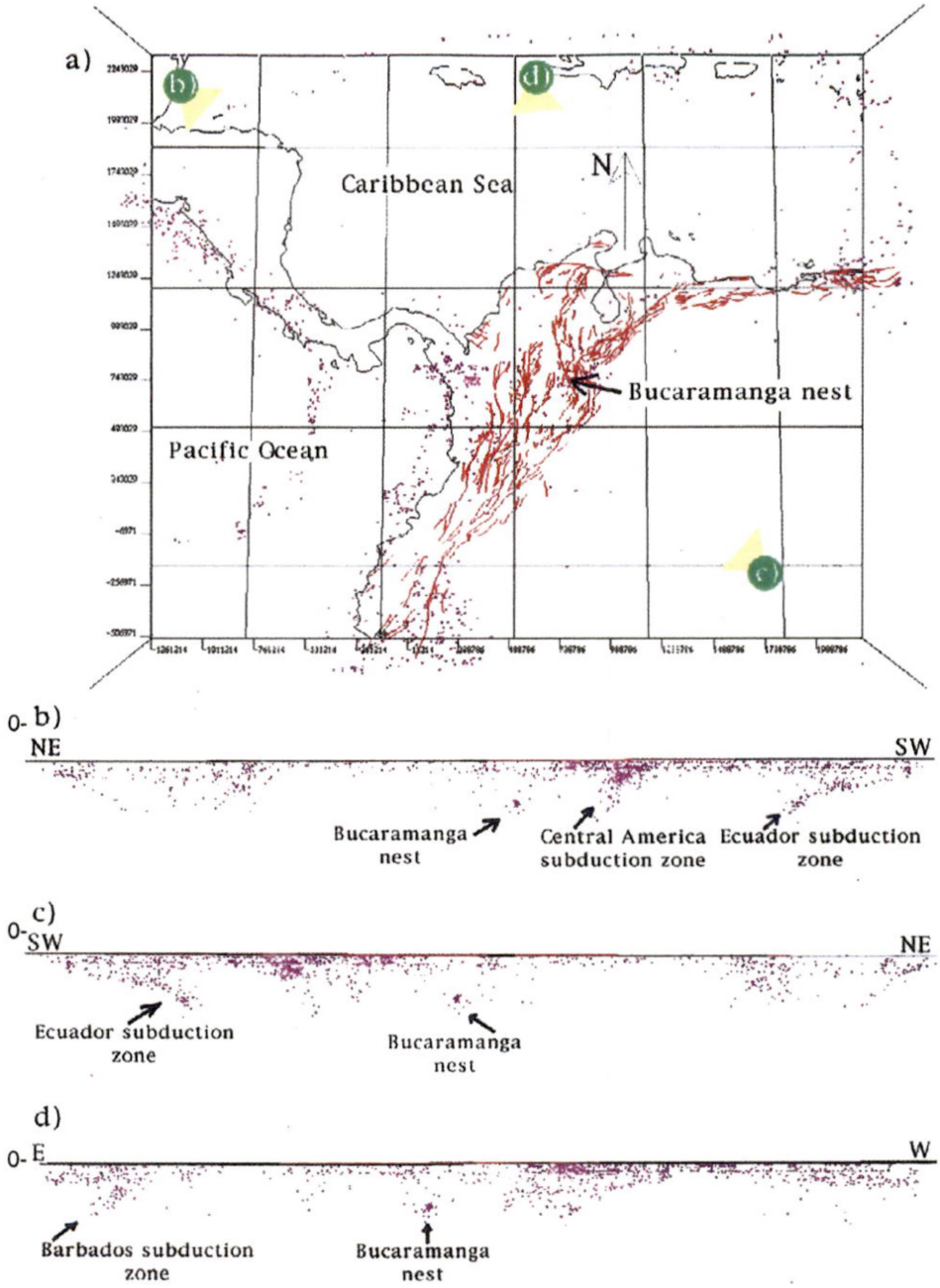


Figure 11: Three-dimensional visualization of earthquake hypocenter data under northwestern South America and Central America using Geosec 3D®. The three different lateral views reveal Wadati-Benioff zones under Central America, Ecuador, and the Antilles. Seismicity under northern Colombia is distinctively diffuse, and does not conform to the simple model of a descending oceanic slab. a) Map view of earthquake distribution, green dots represent viewpoints for each of the three profile views (b, c, and d). The Bucaramanga Nest is noted in each diagram for reference. Data compiled from the National Earthquake Information Center of the USGS for earthquakes with magnitude greater than 5.0 between the years 1960 to 1996 (URL: wwwneic.cr.usgs.gov/neis/epic/epic.html). b) View from the northwest looking southeast highlights the northeast dipping Central America and Ecuador subduction zones. c) View from the north looking south.

of a descending oceanic slab (Andes south of 5°N, and Central America), and regions where earthquake hypocenter distribution is irregular (northern Andes). From this database alone, it ought to be clear that a process other than active subduction is responsible for seismicity patterns under northern South America. Additionally, Neogene volcanoes are absent, and focal mechanisms indicate that strike-slip solutions are common in the same region. Tomographic images do show slab-like features beneath northern Colombia, but they do not seem connected to present-day seismic activity (Fig. 10). Geophysical data indicate that the simple model of a subducting slab as the mechanism driving deformation for the northern Andes during the Neogene is unlikely. The arched structures resembling accretionary prisms (southern Caribbean deformed belt, Fig. 1) and paired gravity anomalies along the southern boundary of the Caribbean Plate can be explained by bending, not subduction of the Caribbean Plate (Burke *et al.*, 1978) due to the irregular geometry of the continental margin, or escape of continental blocks related to the Panamá collision (Stephan *et al.*, 1986).

CONCLUSIONS

Deformation in the Cordillera Oriental must be related to transpression (*cf.* Harland, 1971) produced by oblique convergence (Ladd, 1976), and dextral motion of the Caribbean Plate along the NW corner of South America since the Eocene. The overall structure of the Cordillera Oriental might resemble a dextral "palm tree" structure (*cf.* Lowell, 1972; Sylvester, 1988) where the double vergence is the expression of a room problem created as two blocks obliquely converge, and the material in between is thrust up (Fig. 4). These upthrusts, however, flatten upwards and cause passive uplift, and mild deformation on the thick layer of Upper Cretaceous and Tertiary sediments along the axis of the Cordillera. Oblique convergence may have been accommodated by thrust sheets moving out of the NW-SE plane usually chosen to model the two dimensional structure, therefore, prominent

strike-slip faulting is not necessarily present. Extension along the axis of the Cordillera, expected to occur in transpressional systems (Harland, 1971; Jamison, 1991), may be recorded in the form of basins containing thick Pleistocene to Recent deposits (van der Hammen, 1961), and by the intrusion of salt domes (Montes *et al.*, 1994).

The presence of subhorizontal detachments beneath the Cordillera Oriental, and of back thrusting along its western flank, remains untested. Modern kinematic reconstructions (Colleta *et al.*, 1990; Dengo and Covey, 1989; Cooper *et al.*, 1995; Roeder and Chamberlain, 1995) have presented no field or subsurface evidence supporting either assumption. These features probably are geometric artifacts produced by attempts to restore a doubly vergent orogen using rules designed to describe other kinematic situations. Consequently, current models of the Cordilleran structure are flawed and cannot yield realistic estimates of magnitude and direction of shortening.

REFERENCES

Alberding, H., 1957, Application of principles of wrench-fault tectonics of Moody and Hill to northern South America: Geological Society of America Bulletin, v. 68, p. 785-790.

Amézquita, F., and Montes, C., 1994, Sección geológica El Maco-Buenavista: Estructura en el sector occidental del Valle Superior del Magdalena, *in* Etayo-Serna, F., ed., Estudios geológicos del Valle Superior del Magdalena: Bogotá, Ecopetrol, p. VI-1 to VI-36.

Baldock, J., 1982, National geological map of the Republic of Ecuador: Dirección General de Geología y Minas, scale: 1:1,000.000.

Barazangi, M., and Isacks, B. L., 1976, Spatial distribution of earthquakes and subduction of the Nazca plate beneath South America: Geology, v. 4, p. 686-692.

Barrero, D., Alvarez, J., and Kassem, T., 1969, Actividad Ignea y Tectónica en la Cordillera Central Durante el Meso - Cenozoico: Boletín Geológico del Ingeominas, v. XVII, p. 145-173.

Barrero, D., and Vesga, C., 1976, Mapa geológico del cuadrángulo K-9 Armero y parte sur del J-9 La Dorada, Bogotá, Ingeominas, scale 1:100,000.

Beaumont, C., 1981, Foreland basins: Geophysical Journal of the Royal Astronomical Society, v. 65, p. 291-329.

Boinet, T., Bourgois, J., Mendoza, H., and Vargas., R., 1985, Le poinçon de Pamplona (Colombie): un jalon de la frontiére méridionale de la plaque caraïbe: Bulletin of the Geological Society of France, v. 3, p. 403-413.

Botero, G., and Rico, H., 1965, Mapa geológico de la plancha I-8 Medellin, Bogotá, Inventario Minero Nacional, scale 1:200,000.

Bradley, W. D., and Drake, C. L., 1978, Focal mechanism solutions and tectonics of the middle America arc: Journal of Geology, v. 86, p. 111-128.

Burke, K., Fox, P. J., and Sengör, A. M. C., 1978, Buoyant ocean floor and the evolution of the Caribbean: Journal of Geophysical Research, v. 83, p. 3949-3954.

Campbell, C.J., and Bürgl, H., 1965, Section through the Eastern Cordillera of Colombia, South America: Geological Society of America Bulletin, v. 76, p. 567-590.

Case, J. E., Barnes, J., Paris, G., Gonzalez, H., and Vina, A., 1973, Trans-Andean geophysical profile, southern Colombia: Geological Society of America Bulletin, v. 84, p. 2895-2904.

Case, J. E., and Holcombe, T. L., 1980, Geologic-tectonic map of the Caribbean region: Miscellaneous Investigations Series Map I-1100, U.S. Naval Oceanographic Office, and U.S. Ocean Research and Development Activity, scale: 1:2,500.000.

Case, J. E., and MacDonald, W. D., 1973, Regional gravity anomalies and crustal structure in northern Colombia: Geological Society of America Bulletin, v. 84, p. 2905-2916.

Case, J. E., and MacDonald, W. D., 1990, Crustal structure of the Caribbean Region, Plate 3, *in* Dengo, G., and Case, J. E., eds., The Caribbean region: Boulder, Colorado, Geological Society of America, The Geology of North America, vol. H., scale 1:10,000.000.

Cediel, F., 1969, Geología del Macizo de Floresta: Memorias del primer congreso Colombiano de geología, p.17-30.

Cediel, F., and Cáceres, C., 1988, Geologic map of Colombia: Bogotá, Geotec Editions, scale 1:1,200.000.

Cediel, F., Mojica, J., and Macia, C., 1981, Las Formaciones Luisa, Payandé, and Saldaña sus columnas estratigraficas características: Geología Norandina, v. 3, p.11-19.

Champetier, G., Weecksteen, G., and Quintero, R., 1961, Mapa geológico de la plancha K-10 Villeta: Bogotá, Servicio Geológico Nacional, scale 1:200,000.

Chorowicz, J., Chotin, P., and Guillande, R., 1996, The Garzón fault: Active southwestern boundary of the Caribbean Plate in Colombia: Geologische Rundschau, v. 85, p. 172-179.

Colletta, B., Hebrard, F., Letouzey, J., Werner, P., and Rudkiewickz, J. L., 1990, Tectonic style and crustal structure of the Eastern Cordillera (Colombia) from a balanced cross-section, *in* Letouzey, J., ed., Petroleum and tectonics in mobile belts: Paris, Editions Technip, p. 81-100.

Colpet and Geofoto, 1967, Geología del cuadrángulo F-13 Tibú: Bogotá, Servicio Geológico Nacional, scale 1:200,000.

Cooper, M. A., and 11 others, 1995, Basin development and tectonic history of the Llanos basin, Eastern Cordillera, and middle Magdalena Valley, Colombia: American Association of Petroleum Geologists Bulletin, v.79, p. 1421-1443.

Daconte, R., and Salinas, R., 1980, Mapa geológico de la plancha 76-Ocaña: Bogotá, Ingeominas, scale 1:100,000.

Dengo, C. A., and Covey, M. C., 1989, Structure of the Eastern Cordillera of Colombia: A tectonic model of the Colombian Andes: Memoria del IV Simposio Bolivariano-exploración en las cuencas subandinas, p. 1-8.

Dengo, C. A., and Covey, M. C., 1993, Structure of the Eastern Cordillera of Colombia: implications for trap styles and regional tectonics: American Association of Petroleum Geologists Bulletin, v.77, p. 1315-1337.
Dengo, G., 1953, Geology of the Caracas region, Venezuela: Geological Society of America Bulletin, v. 64, p. 7-40.
Díaz de Gamero, M. L., 1996, The changing course of the Orinoco river during the Neogene: A review: Palaeontology, Palaeoclimatology, Palaeoecology, v. 123, p. 385-402.
Ecopetrol, 1967,Geología del cuadrángulo H-11 Barrancabermeja: Bogotá, Servicio Geológico Nacional, scale 1:200,000.
Edgar, T., Ewing, J., and Hennion, J., 1971, Seismic refraction and reflection in Caribbean Sea: American Association of Petroleum Geologists Bulletin, v. 55, p. 833-870.
Etayo-Serna F., and 24 others, 1986, Mapa de Terrenos Geológicos de Colombia: Publicaciones Geológicas Especiales del Ingeominas, v. 14-1, 235 p.
Etayo-Serna, F., Renzoni, G., and Barrero, D., 1969, Contornos sucesivos del mar Cretáceo en Colombia: Memorias del primer congreso Colombiano de geología, p. 217-252.
Fabre, A., 1985, Dinámica de la sedimentación Cretácica en la región de la Sierra Nevada del Cocuy (Cordillera Oriental de Colombia), *in* Etayo-Serna, F., and Laverde, F., eds., Proyecto Cretacico: Publicaciones geológicas especiales del Ingeominas, v. 16, p. XIX-1 XIX-20.
Fabre, A., Osorio, M., Vargas, R., and Etayo-Serna, F., 1984, Mapa geológico preliminar de la plancha 153, Chita: Bogotá, Ingeominas, scale 1:100,000.
Fabre, A., Osorio, M., Vargas, R., and Etayo-Serna, F., 1985, Mapa geológico preliminar de la plancha 137, El Cocuy: Bogotá, Ingeominas, scale 1:100,000.
Feininger, T., 1970, The Palestina fault, Colombia: Geological Society of America Bulletin, v. 81, p. 1201-1216.
Feininger, T., Barrero, D., Castro, N., Ramirez, O., Lozano, H., and Vesga, J., 1970, Mapa geológico del oriente del depto de Antioquia, Colombia, Hoja 2: Bogotá, Ingeominas, scale 1:100,000.
Forero, A., 1990, The basement of the Eastern Cordillera, Colombia: An allochthonous terrane in northwestern South America: Journal of South American Earth Sciences, v. 3, p. 141-151.
Fox, J., and Heezen, B., 1975, Geology of the Caribbean crust, *in* Narin, A., and Stehli, F., eds., The Ocean basins and margins, vol. 3, The Gulf of Mexico and the Caribbean: New York, Plenum Press, p. 421-466.
Freymueller, J. T., Kellog, J. N., and Vega, V., 1993, Plate motions in the North Andean region: Journal of Geophysical Research, v. 98, B12, p. 21,853-21,863.
Frohlich, C., Kadinsky-Cade, K., and Davis, S., 1995, A reexamination of the Bucaramanga, Colombia, earthquake nest: Bulletin of the Seismological Society of America, v. 85, No. 6, p. 1622-1634.
Galvis, J., and de la Espriella, R., 1987, La gran falla del borde llanero: Geología Colombiana, v. 16, p. 105-113.
Geiser, P., 1988, The role of kinematics in the construction and analysis of geological cross sections in deformed terranes, *in* Mitra, G., and Wojtal, S., eds., Geometries and mechanisms of thrusting, with special reference to the Appalachians: Geological Society of America Special Paper, v. 222, p. 47-76.
Gerth, H., 1955, Der geologische bau der Südamerikanischen kordillere: Berlin, Gebrüder Borntraeger-Berlin-Nikolassee, 264 p.
Gómez, E., and Jordan, T., in press, Relative timing of Cenozoic deformation of the Middle Magdalena Valley Basin and bounding mountain ranges, Colombia: American Association of Petroleum Geologists Annual Convention, Utah.
Harland, W. B., 1971, Tectonic transpression in Caledonian Spitsbergen: Geological Magazine, v. 108, p. 27-42.
Houtz, R. E., and Ludwig, W. J., 1977, Structure of Colombia basin, Caribbean Sea, from Profiler-Sonoubuoy measurements: Journal of Geophysical Research, v. 82, p. 4861-4867.
Hubach, E., 1945, La Formación Cáqueza, Región de Cáqueza (Oriente de Cundinamarca): Compilación de estudios geológicos oficiales en Colombia, Tomo VI, p. 25-27.
Irving, E., M., 1975, Structural evolution of the northernmost Andes, Colombia: U.S. Geological Survey Professional Paper 846, p. 1-47.
Jamison, W. R., 1991, Kinematics of compressional fold development in convergent wrench terranes: Tectonophysics, v. 190, p. 209-232.
Jones, P. B., 1995, Geodynamic evolution of the Eastern Andes, Colombia-An alternative hypothesis, *in* Tankard, R., Suárez, S., and Welsink, H. J., eds., Petroleum basins of South America: American Association of Petroleum Geologists Memoir 62, p. 647-658.
Jordan, T. E., and Allmendinger, R. W., 1988, The Sierras Pampeanas of Argentina: A modern analogue of Rocky Mountain foreland deformation: American Journal of Science, v. 286, p. 737-764.
Jordan, T. E., Isacks, B. L., Allmendinger, R. W., Brewer, J. A., Ramos, V. A., and Ando, C. J., 1983, Andean tectonics related to geometry of subducted Nazca plate: Geological Society of America Bulletin, v. 94, p. 341-361.

Julivert, M., 1970, Cover and basement tectonics in the Cordillera Oriental of Colombia, South America, and a comparison with some other folded chains: Geological Society of America Bulletin, v. 81, p. 3623-3646.
Kafka, A. L., and Weidner, D. J., 1981, Earthquake focal mechanisms and tectonic processes along the southern boundary of the Caribbean Plate: Journal of Geophysical Research, v. 86, p. 2877-2888.
Kammer, A., 1993, Steeply dipping basement faults and associated structures of the Santander Massif, Eastern Cordillera, Colombian Andes: Geología Colombiana, v. 18, p. 47-64.
Kellog, J., N., and Bonini, W. E., 1982, Subduction of the Caribbean Plate and basement uplifts in the overriding South American plate: Tectonics, v. 1, p. 251-276.
Kroonenberg, S. B., 1982, A Grenvillian granulite belt in the Colombian Andes and its relation to the Guiana Shield: Geologie en Mijnbouw, v. 61, p. 325-333.
Ladd, J. W., 1976, Relative motion of South America with respect to North America and Caribbean tectonics: Geological Society of America Bulletin, v. 87, p. 969-976.
Laubscher, H. P., 1987, The kinematic puzzle of the Neogene Northern Andes, *in* Schaer, J. P., and Rodgers, J., eds., The Anatomy of Mountain Ranges: Princeton, New Jersey, Princeton University Press, p. 211-227.
Lowell, J. D., 1972, Spitsbergen Tertiary orogenic belt and the Spitsbergen fracture zone: Geological Society of America Bulletin, v. 83, p. 3091-3101.
Malavé, G., and Suárez, G., 1995, Intermediate-depth seismicity in northern Colombia and western Venezuela and its relationship to Caribbean Plate subduction: Tectonics, v. 14, p. 617-628.
Mann, P., and Corrigan, J., 1990, Model for late Neogene deformation in Panamá: Geology, v. 18, p. 558-562.
Mann, P., Schubert, C., and Burke, K., 1990, Review of Caribbean neotectonics, *in* Dengo, G., and Case, J. E., eds., The Caribbean region: Boulder, Colorado, Geological Society of America, The Geology of North America, v. H, p. 307-338.
McCann, W. R., and Pennington, W. D., 1990, Seismicity, large earthquakes, and the margin of the Caribbean Plate, *in* Dengo, G., and Case, J. E., eds., The Caribbean region: Boulder, Colorado, Geological Society of America, The Geology of North America, v. H, p. 291-306.
McLaughlin, D. H., and Arce, M., 1975, Mapa Geológico del cuadrángulo Zipaquirá (K-11), Colombia: Bogotá, Colombia, Ministerio de Minas y Petroleos, scale 1:100,000.
Meissnar, R. O., Flueh, E. R., Stibane, F., and Berg, E., 1976, Dynamics of the active plate boundary in southwest Colombia according to recent geophysical measurements: Tectonophysics, v. 35, p. 115-136.
Molnar, P., and Sykes, L. R., 1969, Tectonics of the Caribbean and Middle America regions from focal mechanisms and seismicity: Geological Society of America Bulletin, v. 80, p. 1639-1684.
Montes C., Baquero M., Castillo, D., and Cortés, M., 1994, Salt-related structures postdating thrust tectonics: An example from the Cordillera Oriental, Colombia: Geological Society of America Abstracts with Programs, v. 26, p. 185.
Moody, J. D., and Hill, M. J., 1956, Wrench-fault tectonics: Geological Society of America Bulletin, v. 67, p. 1207-1246.
Mosquera, D., Nuñez, A., and Vesga, C. J., 1982, Mapa geológico preliminar de la plancha 244 Ibagué, Informe 1879: Bogotá, Ingeominas, scale 1:100,000.
Namson, J., Cunningham, R., and Woodcock, G., 1994, Structural geology and hydrocarbon potential of the Northern part of the Upper Magdalena Basin, Colombia: V Simposio Bolivariano Exporación Petrolera en las Cuencas Subandinas, Puerto de la Cruz, Venezuela, p. 356-364.
Norris, R. J., Koons, P. O., and Cooper, A. F., 1990, The obliquely-convergent plate boundary in the South Island of New Zealand: implications for ancient collision zones: Journal of Structural Geology, v. 12, p. 715-725.
Oldow, J. S., Bally, A. W., and Avé-Lallemant, H. G., 1990, Transpression, orogenic float, and lithospheric balance: Geological Society of America Geology, v. 18, p. 991-994.
Paris, G. Q., and Marín, P. A., 1979, Generalidades acerca de la Geología del Departamento del Cauca: Bogotá, Colombia, Boletín Geológico del Ingeominas, 38 p.
Pennington, W. D., 1981, Subduction of the eastern Panamá basin and seismotectonics of northwestern South America: Journal of Geophysical Research, v. 86, B11, p. 10,753-10,770.
Pérez, O. J., and Aggarwal, Y. P., 1981, Present-day tectonics of the southeastern Caribbean and northeastern Venezuela: Journal of Geophysical Research, v. 86, p. 10,791-10,804.
Pindell, J. L., 1993, Regional synopsis of Gulf of Mexico and Caribbean Evolution: Proceedings of the GCSSEPM Foundation 13th Annual Research Conference, p. 251-274.
Pindell, J. L., and Barrett, S. F., 1990, Geological evolution of the Caribbean region; A plate-tectonic perspective, *in* Dengo, G., and Case, J. E., eds., The Caribbean region: Boulder, Colorado, Geological Society of America, The Geology of North America, v. H, p. 405-432.
Pindell, J. L., and Dewey, J. F., 1982, Permo-Triassic reconstruction of western Pangea and the evolution of the Gulf of Mexico/Caribbean region: Tectonics, v. 1, p. 179-211.

Pindell, J. L., Cande, S. C., Pitman III, W. C., Rowley, D. B., Dewey, J. F., LaBrecque, J., and Haxby, W., 1988, A plate-kinematic framework for models of Caribbean evolution: Tectonophysics, v. 155, p. 121-138.

Priem, H. N. A., Andriessen, P. A . M., Boelrijk, A. I. M., De Boorder, H., Hebeda, E. H., Huguett, A., Verdurmen, E. A., and Verschure, R. H., 1982, Geochronology of the Precambrian in the Amazonas region of southeastern Colombia (western Guiana Shield): Geologie en Mijnbouw, v. 61, p. 229-242.

Priem, H. N. A., Kroonenberg, S B., Boelrijk, N. A. I. M., and Hebeda, E. H., 1989, Rb-Sr and K-Ar evidence for the presence of a 1.6 Ga basement underlying the 1.2 Ga Garzón-Santa Marta granulite belt in the Colombian Andes: Precambrian Research, v. 42, p. 315-324.

Raasveldt, H. C., and Carvajal, J. M., 1957a, Mapa geológico de la plancha K-9 Armero: Bogotá, Servicio Geológico Nacional, scale 1:200,000.

Raasveldt, H. C., and Carvajal, J. M., 1957b, Mapa geológico de la plancha M-8 Ataco: Bogotá, Servicio Geológico Nacional, scale 1:200,000.

Renzoni, G., 1965, Geología del cuadrángulo L-11 Villavicencio: Bogotá, Ingeominas, scale 1:200,000.

Renzoni, G., Rosas, H., and Etayo-Serna, F., 1967, Mapa geológico de la plancha 171-Duitama: Bogotá, Ingeominas, scale 1:100,000.

Restrepo, J. J., and Toussaint, J. F., 1988, Terranes and continental accretion in the Colombian Andes: Episodes, vol. 11, p. 189-192.

Restrepo-Pace, P. A., 1989, Restauración de la sección geológica Caqueza-Puente Quetame: Moderna interpretación estructural de la deformación del flanco este de la Cordillera Oriental: Universidad Nacional de Colombia (unpublished thesis), Bogotá, Colombia, 45 p.

Restrepo-Pace, P. A., 1992, Petrotectonic characterization of the Central Andean Terrane, Colombia: Journal of South American Earth Sciences, v. 5, p. 97-116.

Restrepo-Pace, P. A., Gehrels G., and Cosca M., and Ortega-Gutierrez, F., 1995, Geochronology and Nd isotopic geochemistry of the Proterozoic and Paleozoic rocks of the Oaxaca and Acatlán complexes, southern Mexico and the Santander Massif, Colombia: Geological Society of America Abstracts with Programs, v. 27, p. A-398.

Restrepo-Pace, P. A., Ruiz J., Gehrels G., and Cosca M., 1997, Geochronology and Nd isotopic data of Grenville-age rocks in the Colombian Andes: New constraints for late Proterozoic-early Paleozoic paleocontinental reconstructions of the Americas: Earth and Planetary Science Letters, v. 150, p. 427-441.

Robertson, P., and Burke, K., 1989, Evolution of southern Caribbean Plate boundary, vicinity of Trinidad and Tobago: American Association of Petroleum Geologists Bulletin, v. 73, p. 490-509.

Roeder, D., and Chamberlain, R. L., 1995, Eastern Cordillera of Colombia: Jurassic-Neogene Crustal evolution, *in* Tankard, R., Suárez, S., and Welsink, H. J., eds., Petroleum basins of South America: American Association of Petroleum Geologists Memoir 62, p. 633-645.

Rosencrantz, E., Ross, M., and Scatler, G., 1988, Age and spreading history of the Cayman Trough as determined from depth, heat flow, and magnetic anomalies: Journal of Geophysical Research, v. 93, p. 2141-2157.

Ross, M. I., and Scotese, C. R., 1988, A hierarchical tectonic model of the Gulf of Mexico and Caribbean region: Tectonophysics, v. 155, p. 139-168.

Sanderson D. J., and Marchini, W. D. R., 1984, Transpression: Journal of Structural Geology, v. 6, p. 449-458.

Schubert, C., 1981, Are the Venezuelan fault systems part of the southern Caribbean Plate boundary?: Geologische Rundschau, v. 70, p. 542-551.

Schubert, C., 1983, La Cuenca de Yaracuy: Una estructura neotectónica en la región Centro-Occidental de Venezuela: Geologia Norandina, v. 8, p. 3-11.

Seber, D., Vallvé, M., Sandvol, E., Steer, D., and Barazangi, M., 1997, Middle East tectonics: Applications of Geographic Information Systems (GIS): GSA Today, v. 7, p. 1-6.

Segovia, A., and Renzoni, G., 1965, Geología del cuadrángulo L-12 Medina: Bogotá, Servicio Geológico Nacional, scale 1:200,000.

Stephan, J. F., Blanchet, R., and Mercier de Lepinay, B., 1986, Northern and southern festoons (Panamá, Colombia-Venezuela, and Hispanola-Puerto Rico), interpreted as pseudo-subductions induced by the East-West shortening of the pericaribbean continental frame, *in* Wezel, F. C., ed., The origin of arcs: Developments in Geotectonics, Amsterdam, Elsevier, p. 401-422.

Suárez G., Molnar, P., and Burchfiel, B. C., 1983, Seismicity, fault plane solutions, depth of faulting and active tectonics of the Andes of Perú, Ecuador, and southern Colombia: Journal of Geophysical Research, v. 88, B12, p. 10403-10428.

Sylvester, A. G., 1988, Strike-slip faults: Geological Society of America Bulletin, v. 100, p. 1666-1703.

Teyssier, C., Tikoff, B., and Markley, M., 1995, Oblique plate motion and continental tectonics: Geology, v. 23, p. 447-450.

Toussaint, J. F., and Restrepo, J. J., 1988, ¿Son alóctonos los Andes Colombianos?: Revista del I.C.N.E., v. 1, p. 17-41.

Ulloa, C., and Rodríguez, E., 1979, Geología del cuadrángulo K-12, Guateque: Boletín Geológico del Ingeominas, v. XXII, p. 3-56.
van der Hammen, T., 1961, Late Cretaceous and Tertiary stratigraphy and tectogenesis of the Colombian Andes: Geologie en Mijnbouw, v. 40, p. 181-188.
van der Hammen, T., and González, E., 1963, Historia de clima y vegetación del Pleistoceno superior y del Holoceno de la Sabana de Bogotá: Boletín Geológico del Servicio Geológico Nacional, v. XI, p. 189- 266.
van der Hammen, T., Werner, J. H., and van Dommelen, H., 1973, Palynological record of the upheaval of the northern Andes: A study of the Pliocene and lower Quaternary of the Colombian eastern Cordillera and the early evolution of its high-Andean biota: Review of Paleobotany and Palynology, v. 16, p. 1-122.
van der Hilst, R. D., and Mann, P., 1994, Tectonic implications of tomographic images of subducted lithosphere beneath northwestern South America: Geology, v. 22, p. 451-454.
Vargas, R., and Arias, A., 1981, Mapa geológico de la plancha 97 Cáchira: Bogotá, Ingeominas, scale 1:100,000.
Verbyla, D. L., 1995, Satellite remote sensing of natural resources: Boca Ratón, Florida, CRC press, 196 p.
Villarroel, C., and Mojica, J., 1988, El Paleozoico Superior (Carbonifero-Pérmico) sedimentario de Colombia. Afloramientos conocidos y características generales: Geología Colombiana, v. 16, p. 81-87.
Walcott, R. I., 1978, Present tectonics and Late Cenozoic evolution of New Zealand: Royal Astronomical Society Geophysical Journal, v. 52, p. 137-164.
Ward, D. E., Goldsmith, R., Cruz, J., Tellez, N., and Jaramillo, L., 1977, Mapa geológico San Gil y Málaga (Parte de los cuadrángulos I-12 y I-13), Colombia: Bogotá, Ingeominas, scale 1:100,000.
Ward, D., Goldsmith, R., Cruz, J., Jaramillo, L., and Vargas, R., 1970, Mapa geológico del cuadrángulo H-13 Pamplona, Colombia: Bogotá, Ingeominas, scale 1:100,000.
Westbrook, G. K., 1990, Gravity anomaly map of the Caribbean region, *in* Dengo, G., and Case, J. E., eds., The Caribbean region: Boulder, Colorado, Geological Society of America, The Geology of North America, v. H, scale: 1:5,000,000.
Zeil, W., 1979, The Andes, A geological review: Berlin-Sttutgart, Gëbruder Borntraeger, 260 p.

Part II

Strain and timing of deformation in the Piedras-Girardot foldbelt.

ABSTRACT

Deformation of the Piedras-Girardot foldbelt in the northern Andes of Colombia is analyzed using detailed geologic mapping, strain analysis, and simple stratigraphic principles. This analysis indicatesthat deformation in the Piedras-Girardot foldbelt began in the early Campanian with incipient propagation of the northern, northeast-trending segments of the Camaito and Cotomal faults that uplifted gentle domes where the accumulation of the sandy member of the Nivel Intermedio of the Oliní Group did not take place. Maastrichtian unroofing of a metamorphic terrane west of the Piedras-Girardot foldbelt is documented by the conglomerate of the La Tabla Formation. This conglomerate was deformed shortly after deposition developing a conspicuous intragranular fabric of microscopic veins that accommodate little extension (between 1 and 2 percent in a general northeast-southwest direction). This extensional fabric, distortion of fossil molds, and a moderate cleavage most likely developed concurrently, during and after the incipient late Cretaceous folding, but before large scale Paleogene faulting and folding took place. Cleavage also seems to record small amounts of contraction in a general northwest-southeast direction. Paleogene folding and thrust sheet propagation is recorded by syntectonic strata in the Gualanday syncline, and records westward to southwestward propagation of the Hondita fault. Mesoscopic fabric elements associated with continuous Paleogene deformation are nearly absent, and apparently were passively rotated and translated along thrust sheets. Neogene deformation took place only in the western flank of this foldbelt.

INTRODUCTION

Reconstruction of deformed strata in two and three dimensions is a kinematic exercise commonly constrained by surface geology and/or subsurface seismic reflectors. Additional constraints such as strain markers, kinematic indicators, and timing of deformation can be derived from detailed geologic mapping, greatly improving the quality of these reconstructions. This paper presents field data regarding the strain state and timing of deformation of the Piedras-Girardot foldbelt in central Colombia that will aid the construction of two- and three-dimensional models of this foldbelt.

The Piedras-Girardot foldbelt is located in the only segment of the northern Andes where the Cordilleras Central and Oriental overlap, thus opening a unique window into an area key to understanding the interaction between the Caribbean, South American, and Nazca plates (Fig. 1). This work provides supporting evidence to two- and three-dimensional reconstructions of this foldbelt (Montes *et al.*, in preparation), that test the validiy of competing hypotheses regarding the nature of the southern Caribbean plate boundary and the tectonic evolution of the northern Andes. The pronounced curvature of structures, their geometric arrangement in a sigmoidal pattern, and the variety of structural styles within this foldbelt suggest significant amounts of transcurrent deformation that have not been reported, or accounted for in this part of the Andes.

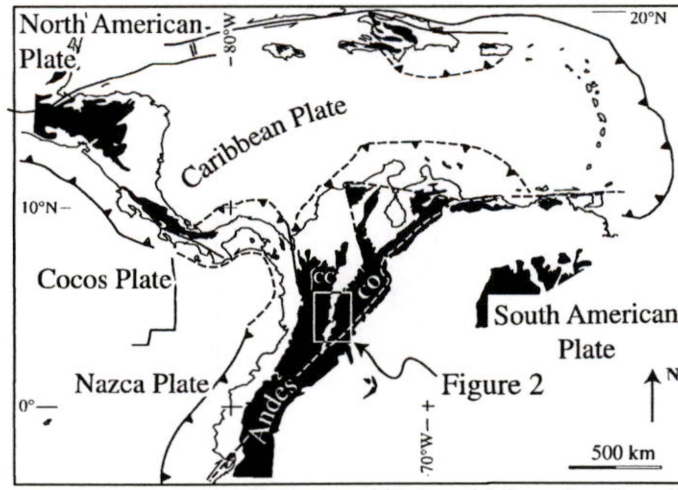


Figure 1: Tectonic map of the Caribbean region. Black indicates elevations higher than 500 m above sea level delineating the three branches of the northern Andes in Colombia. CC: Cordillera Central; CO: Cordillera Oriental.

Detailed geologic mapping and collection of fabric and stratigraphic data in the field constitute the core of this study. Field studies concentrated on collecting structural data and mapping lithologic contacts at 1:25,000 scale, and following strata along strike to map changes in thickness and stratigraphic pinchouts. Fabric element such as cleavage, veins, systematic joints, folds, fault surfaces, and slickenlines were measured in the field recording lithology, surface morphology, and a visual estimate of spacing, although discontinuities in fresh samples tend to be less evident than in weathered ones. Shattered pebbles in conglomerate and deformed ammonite molds in black shale were employed to obtain the orientation of the strain axes and their geometric relationship to more widespread fabric elements such as cleavage and veins. Image enhancing and digitizing of angles, lengths, and areas of fabric elements was done using the public domain NIH Image program (available at http:// rsb.info.nih.gov/nih-image/) and Adobe Photoshop™. Rotation of large sets of linear and planar fabric data was performed using a modified version of a computer algorithm (Appendix I) by Vissers and Bollegraaf (1989).

Regional setting

The rugged hills of the Piedras-Girardot foldbelt are located between two branches of the northern Andes (Cordilleras Oriental and Central), splitting the otherwise flat and wide topographic depression of the intramontane Magdalena Valley into two distinctive geomorphologic units: the Upper Magdalena Valley to the south, and the Middle Magdalena Valley to the north (Fig. 2). The topographic relief of this foldbelt locally exceeds 500 m, with maximum elevation reaching approximately 900 m above sea level, constituting the only barrier that the Magdalena River encounters in its northbound path to the Caribbean Sea. This anomalous geomorphic province exposes critical relationships between the Cordilleras Oriental and Central covered elsewhere by Neogene deposits.

The western foothills of the Cordillera Oriental constitute the eastern boundary of the Piedras-

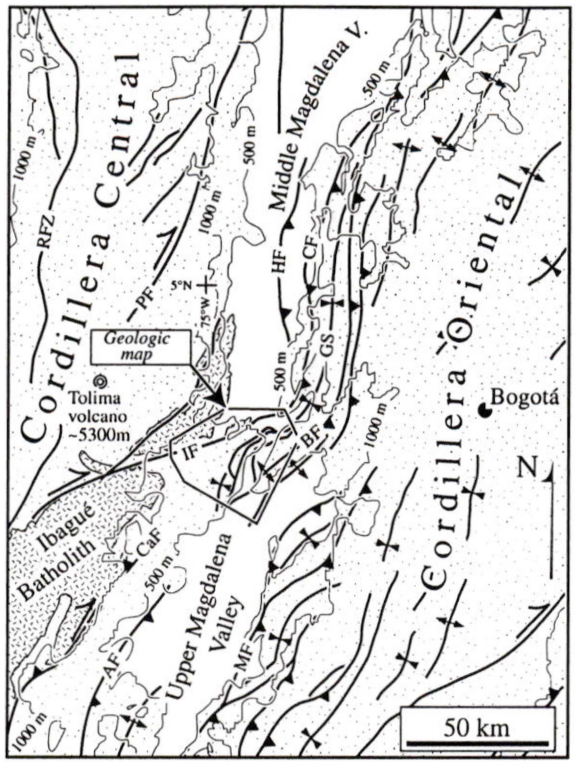


Figure 2: Tectonic map of part of the northern Andes modified after Schamel (1991). Stippled pattern indicates elevations greater than 500 m above sea level and delineates the topographic domain of the Magdalena Valley. Notice the narrowing of the Magdalena Valley in the Piedras-Girardot foldbelt, and termination of major structures of the Cordilleras Central and Oriental. IF: Ibagué fault, PF: Palestina fault; RFZ: Romeral fault zone; CaF: Calarma fault; BF: Bituima fault; GS: Guaduas syncline; CF: Cambao fault; HF: Honda fault; MF: Magdalena fault; AF: Ataco fault.

Girardot foldbelt where elevations commonly exceed 1000 m above sea level. Shortening in the western flank of the Cordillera Oriental ranges between 30 and 70 percent (Namson *et al.*, 1994; Restrepo Pace *et al.*, 1999), and is accommodated mostly by low-angle, northeast-trending, west-verging faults (Hubach, 1945) that terminate in this belt (Fig. 2). The ENE-trending Ibagué fault constitutes the northwestern boundary of the Piedras-Girardot foldbelt (Figs. 2 and 3). The trace of this fault, some 70 to 150 km long (Cediel and Cáceres, 1988; Ingeominas, 1988), traverses the Cordillera Central into the Magdalena Valley offsetting not only the northernmost exposures of the Ibagué batholith granodiorite at least 40 km to the east, but also the north-trending topographic front of the Cordillera Central (marked by the 1000 m contour in Fig. 2). The vertical component of this fault seems to be large as well; geologic maps (Raasveldt, 1956; Barrero and Vesga, 1976) and exploration wells (Schamel, 1991) show flat-lying Neogene strata overlapping granodioritic basement. A conservative estimate of the thickness of Cretaceous strata (Fig. 4b), and the assumption that the northern

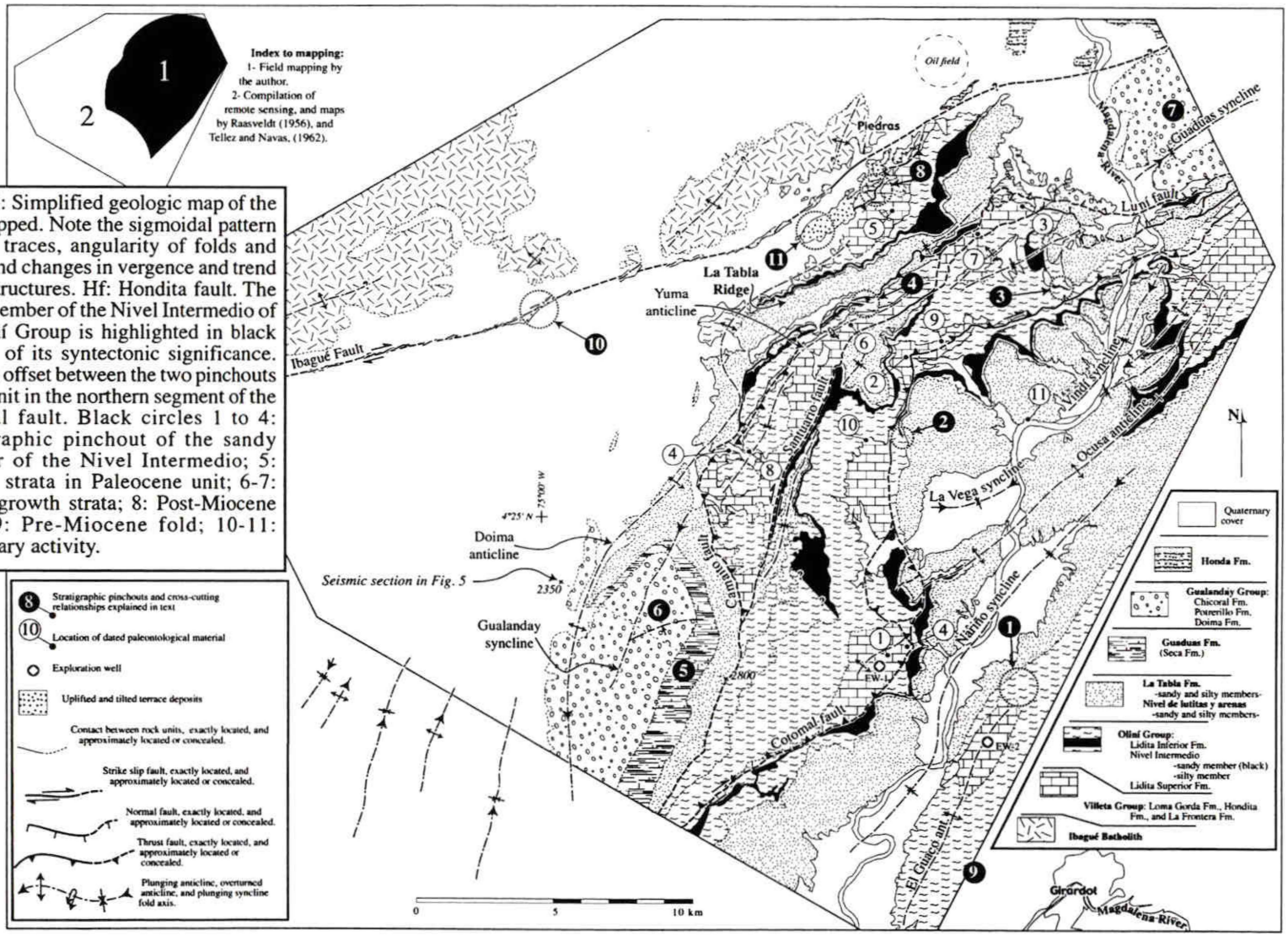
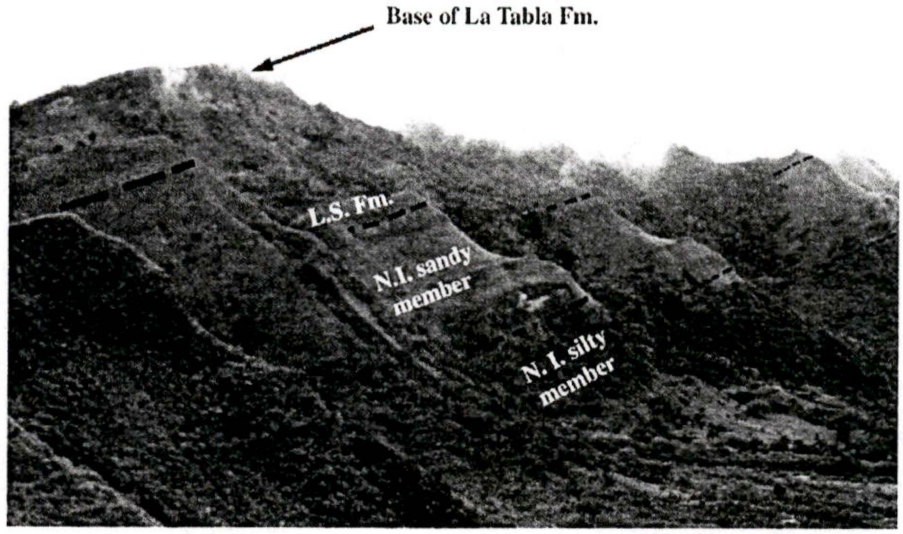


Figure 3: Simplified geologic map of the area mapped. Note the sigmoidal pattern of fault traces, angularity of folds and faults, and changes in vergence and trend of the structures. Hf: Hondita fault. The sandy member of the Nivel Intermedio of the Oliní Group is highlighted in black because of its syntectonic significance. Note the offset between the two pinchouts of this unit in the northern segment of the Cotomal fault. Black circles 1 to 4: Stratigraphic pinchout of the sandy member of the Nivel Intermedio; 5: Growth strata in Paleocene unit; 6-7: Folded growth strata; 8: Post-Miocene fault; 9: Pre-Miocene fold; 10-11: Quaternary activity.

a)



b)

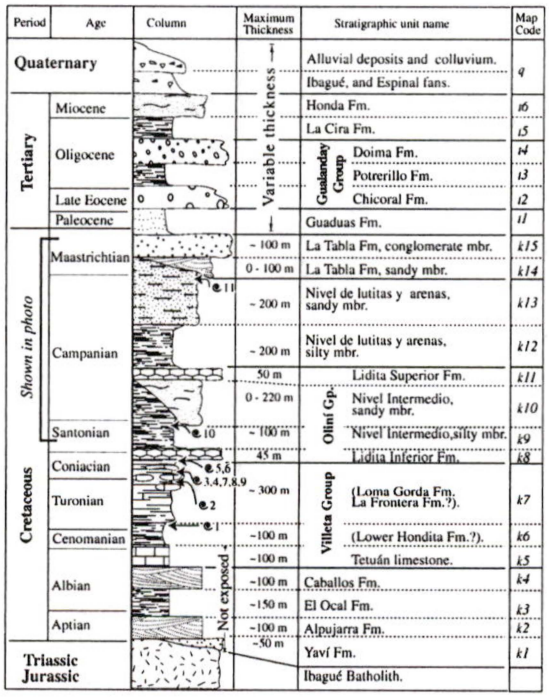


Figure 4: Generalized stratigraphic column of the Piedras-Girardot foldbelt. a) Field photo of northwestern flank of the La Tabla Ridge where most of the Cretaceous stratigraphic column is well exposed. L.S. Fm.: Lidita Superior Formation; N.I.: Nivel Intermedio. b) Stratigraphic column, numbers in column indicate the location of paleontologic material in the geologic map (Fig. 3) and column (Etayo Serna, pers. comm.). 1: *Wrightoceras ralphimlayi* (Etayo Serna); 2: *Coilopoceras sp.* ind.; 3: *Peroniceras correai* (Etayo Serna); 4: *Subprionotropis columbianus* (Basse); 5: *Prionocycloceras guayabanum* (Steinmann); 6: *Niceforoceras boyacaense* (Etayo Serna), *Peroniceras correai* (Etayo Serna); 7: *Barroisiceras loboi* (Etayo Serna), *Barroisiceras subtuberculatum* (Gerhardt), *Peroniceras guerrai* (Etayo Serna); 8: *Niceforoceras boyacaense* (Etayo Serna); 9: *Protexanites cucaitaense* (Etayo Serna); 10: *Reginaites sp* aff. leei (Reside); 11: *Exiteloceras* cf. jenneyi (Whitfield).

block was covered by a Mesozoic sedimentary sequence imply that the vertical component is 1000 m or more, since sedimentary Mesozoic strata are absent in the northern block (Raasveldt, 1956; Barrero and Vesga, 1976). Recent activity along this fault is also indicated by tilted and uplifted Holocene volcanoclastic deposits.

PIEDRAS-GIRARDOT FOLDBELT

Two manifestations of deformation are discussed in the following sections: first, the stratigraphic signature of deformation (onlaps, growth strata, pinchouts) is analyzed to establish the timing, and approximate locus of deformation along mapped faults or folds. Second, the structural signature of deformation (microscopic and mesoscopic strain markers) is analyzed to approximately define the orientation of finite strain axes, and the magnitude of strain recorded by mesoscopic fabric elements. Together, these stratigraphic and structural criteria are used to propose a history of deformation and sedimentation that will be geometrically and kinematically tested using two- and three-dimensional models (Montes *et al.*, in preparation).

Timing of deformation from stratigraphic data

Various stratigraphic relationships derived from the geologic map were analyzed to deduce the distribution of deformation in time and space. First, basic stratigraphic relationships helped decipher maximum and minimum age of deformation of specific structures. For instance, the age of the oldest unit fossilizing a given fault, or not affected by folding, brackets the time of deformation to sometime between the accumulation oldest undeformed strata, and the youngest offset, or folded strata. Second, thickness changes and depositional pinchouts record syntectonic accumulation directly dating the deformation age and duration around the locus of accumulation. These two criteria are fundamentally different in that while one provides minimum and/or maximum age of deformation along specific structures,

the other dates the time and duration of deformation without a direct link to a given structure. Third, the composition of coarse-grained syntectonic deposits record the stratigraphic level being eroded in the source area, and provide supporting evidence to interpret other stratigraphic criteria recording local or regional deformation. Fourth, growth folds contain information about both the time, and locus of deformation, and if accurate absolute ages are available within the growth strata, rates of faulting and folding can be derived (Suppe *et al.*, 1992).

A major caveat when trying to decipher absolute timing of Cenozoic deformation in the Piedras-Girardot foldbelt is the exceedingly complex chronostratigraphic framework of the Tertiary sedimentary sequence (Van Houten and Travis, 1968; Wellman, 1970; Van der Wiel and Van den Bergh, 1992; Van der Wiel *et al.*, 1992), and the absence of suitable material for age determinations. In contrast, abundant fossil material yields precise absolute ages within most of the Cretaceous sedimentary sequence (Fig. 4b) allowing accurate determinations for timing of late Mesozoic deformation.

General stratigraphy of the Piedras-Girardot foldbelt

The stratigraphic column presented here (Fig. 4) is a compilation of early studies by Bürgl and Dumit (1954) and DePorta (1965), and modern regional stratigraphic work by Etayo Serna (1994), Florez and Carrillo (1994), and Gómez and Pedraza (1994) modified only to include sandstone units and stratigraphic pinchouts encountered while mapping. A reference Cretaceous stratigraphic column was established along La Tabla Ridge (Fig. 4a), where good exposures and simple structure allowed better observation of the sequence and more accurate estimation of stratigraphic thicknesses. Stratigraphic thicknesses were calculated by correcting the width of the outcrop with measured dips on the map.

Two very distinctive stratigraphic packages are exposed in the Piedras-Girardot foldbelt: a

Late Cretaceous marine carbonate and siliciclastic sequence, and a Tertiary nonmarine, coarse grained, and mostly red siliciclastic sequence. These sequences rest on a volcanoclastic, and plutonic basement of Triassic-Jurassic age.

Basement

Volcanic, volcanoclastic, and sedimentary rocks recording Early Triassic continental extension, Late Triassic (Norian) marine incursion and Late Triassic-Jurassic felsic and intermediate back-arc volcanism, plutonism, and volcanoclastic sedimentation (Cediel, 1969; Cediel *et al.*, 1981; Bayona *et al.*, 1994) constitute the mechanical basement for the Late Cretaceous-Cenozoic deformation (Andean orogenic cycle). This partially layered basement was extensionally deformed during the rupture of Pangea in the Early Mesozoic and served as mechanical basement for the Andean orogenic cycle. Because of the presence of weak sedimentary layers within this sequence, this basement may be partially involved in the deformation.

These sequences developed in response to subduction of the Farallon Plate under western Pangea (Pindell and Dewey, 1982). In the study area, however, basement is only exposed in the northern block of the Ibagué fault and is only composed of Jurassic granodiorite (Fig. 2, Ibagué batholith), commonly sheared and frequently intruded by basaltic dikes up to 10 m thick. Older basement immediately outside the Piedras-Girardot foldbelt consists of sporadic outcrops of Proterozoic rocks covered by Cambrian to Ordovician low-grade assemblages metamorphosed during the Ordovician (Restrepo Pace *et al.*, 1997), and by a younger clastic and carbonate sequence of Early Devonian to Carboniferous age deformed during the Permian (Forero, 1990).

Cretaceous sequence

Well-exposed Cretaceous strata of the Piedras-Girardot foldbelt were the subject of detailed studies by Bürgl and Dumit (1954), and DePorta (1965). These efforts helped delineate the stratigraphic framework for the Upper Magdalena Valley and western Cordillera Oriental providing detailed, albeit local, lithologic and faunal descriptions. This work follows their nomenclature for the most part, and it is summarized in the stratigraphic column (Fig. 4b). The main contribution of our stratigraphic observations consists of mapping previously unrecognized stratigraphic pinchouts (Fig. 3).

Overall, the Cretaceous stratigraphic sequence (Fig 4b) in this part of the Magdalena Valley records a marine incursion on a complex Triassic-Jurassic basement. This sequence starts with a retrograding, fining-upward, Early Cretaceous fluvial system (Yaví Formation) that by the Aptian was onlapped by shallow marine deposits (El Ocal Formation). By the middle Albian, a combination of tectonic and eustatic sea-level drop allowed the accumulation of coarse, shallow marine to deltaic sandstone (Caballos Formation) that prograded from south to north. The more extensive and faster sea-level rise that followed, allowed the accumulation of a continuous blanket of fine-grained material in a relatively deep, and anoxic ocean floor. These conditions prevailed until the beginning of the Coniacian and are recorded by the shale, siltstone and limestone of the Villeta Group. Starting with the Oliní Group the proportion of siliciclastic material increases, so that from the late Coniacian until the Maastrichtian, the stratigraphic record can be considered a coarsening-upward sequence (Nivel de Lutitas y Arenas) with shallowing water conditions that culminate in the conglomerate of the La Tabla Formation (Etayo Serna, 1994). This unit consists of a coarsening-upward clastic sequence that near Piedras contains a basal medium-grained, well-sorted, and permeable quartz sandstone occurring in massive beds up to 10 m thick that grades upward into polymictic conglomerate with calcareous matrix, and distinctive

biomicritic lenses containing large oyster shells. This conglomerate contains mostly white quartzite pebbles, with minor amounts of black chert, siltstone, greenschist, and shell fragments. Grain size distribution is bimodal, with well-rounded pebbles within a coarse-grained, calcareous sandy matrix. This conglomerate marks the end of marine conditions in this part of the Magdalena Valley, and contains evidence of unroofing of western source areas (Cordillera Central).

Cenozoic

The Cenozoic deposits of the Madgalena Valley consist of a molassic sequence of alternating nonmarine conglomerate, lithic sandstone and mudstone characterized by marked discontinuities, unconformities, and abrupt thickness and facies changes. As the Late Cretaceous sea retreated, the Paleocene Guaduas Formation accumulated mud and silt on poorly drained low lands and swamps. Later, two distinctive molasses (Gualanday Group) consisting of massive, thick conglomerate and mudstone were accumulated in braided rivers, alluvial fans, and on flood plains (Anderson, 1972; Caicedo and Roncancio, 1994) starting in the Late Eocene and ending in the Early Miocene. The composition of clasts in the two conglomerate units of the Gualanday Group in the Piedras-Girardot foldbelt changes from mostly chert and milky quartz, with minor igneous and metamorphic clasts in the Chicoral Formation, to mostly tan and black chert in the Doima Formation (Van Houten and Travis, 1968). Continuous deformation, and marked volcanic activity are recorded in the arkosic sandstone of the Miocene Honda Formation (Van Houten and Travis, 1968; Wellman, 1970).

<u>Evidence for syntectonic sedimentation.</u>

Late Cretaceous

Stratigraphic pinchouts occur throughout the study area in Upper Cretaceous strata across and within fault blocks. Two prominent, cliff-forming, thick sandstone units of Campanian

age (Fig. 4a) are present south of Piedras: the sandy member of the Nivel de Lutitas y Arenas, originally reported by DePorta (1965), and the sandy member of the Nivel Intermedio. These units are absent to the south near Girardot (Bürgl and Dumit, 1954; Cortés, 1994) and disappear or thin most notably across the Camaito and Cotomal faults (Fig. 3). These two sandy units up to 200 m thick, consist of similar monotonous fine-grained, lithic sandstone commonly occurring in planar beds up to 50 cm thick, with abundant shelly material and calcareous cement. To the north, a third sandy member, present locally along La Tabla Ridge, is the sandy member of the La Tabla Formation of Maastrichtian age. Unlike the other two sandy members, this unit is a clean, medium-grained, well-sorted, permeable sandstone that occurs in massive beds up to 10 m thick immediately below the conglomerate of the La Tabla Formation.

The sandy member of the Nivel Intermedio in the Oliní Group (Fig. 4) disappears across the northeast-trending, northern segments of the Camaito and Cotomal faults, and along the El Guaco anticline (labeled 1 to 4 in Fig. 3). The most evident stratigraphic truncations of this unit occur within the hanging wall of the Camaito fault in the overturned flank of the Yuma anticline (labeled 2, 3, and 4 in Fig. 3). To the east, this unit thins to zero in the northernmost segment of the hanging wall of the Cotomal fault and in the footwall of the same fault approximately 8 km to the southwest. Published stratigraphic sections indicate that this unit is also missing in the core of the southern segment of the El Guaco anticline (labeled 1 in Fig. 3) immediately north of Girardot (Bürgl and Dumit, 1954; Cortés, 1994). Despite these stratigraphic truncations and hiatuses, the unit immediately above (Lidita Superior Formation) is present throughout this foldbelt, resting conformably with units below, and maintaining a constant thickness. The sandy member of the Nivel de Lutitas y Arenas also thins from approximately 200 m along La Tabla Ridge to zero along the southern segment of the El Guaco anticline near Girardot. Changes in thickness across the Cotomal

and Camaito faults cannot be evaluated because this unit has been eroded from these hanging walls.

These relationships were interpreted to record mild uplift during the early Campanian along the northern (northeast-trending) segments of two of the major faults of the Piedras-Girardot foldbelt (Cotomal and Camaito faults), and along the easternmost (also northeast-trending) structure of this foldbelt (El Guaco anticline). Although less well constrained, this mild uplift may have been rejuvenated during the late Campanian as the sandy member of the Nivel de Lutitas y Arenas is also missing in the El Guaco anticline. Altogether, these coarse-grained marine clastic units represent gentle deformation within the Piedras-Girardot foldbelt during the early and late Campanian (~84 and ~ 74 Ma) near the northeast-trending, northern segments of the Cotomal and Camaito faults. Although uplift clearly took place, no major unconformities were developed at this time, as overlying units rest apparently in conformity with syntectonic units below. Since bedding geometry remained mostly parallel, it is unlikely that the Cotomal and Camaito faults propagated to the surface at this time.

Paleogene

The massive mudstone and claystone of the Paleocene Guaduas Formation exhibits remarkable thickness changes within the Gualanday syncline. This unit is seldom exposed, thus most observations and interpretations are based on seismic reflection data (Fig. 5), and analysis of regional map patterns (Fig. 3).

In cross section view, the Gualanday syncline is an asymmetric fold with steeply dipping limbs, and a very wide, nearly horizontal hinge zone. Gualanday Group strata within this wide hinge zone gently dips to the west, while Cretaceous strata immediately below gently dips eastward (Fig. 5). This contrast occurs due to the pronounced thickness changes that take place within the intervening Guaduas Formation. Both the geologic map (Fig. 3), and

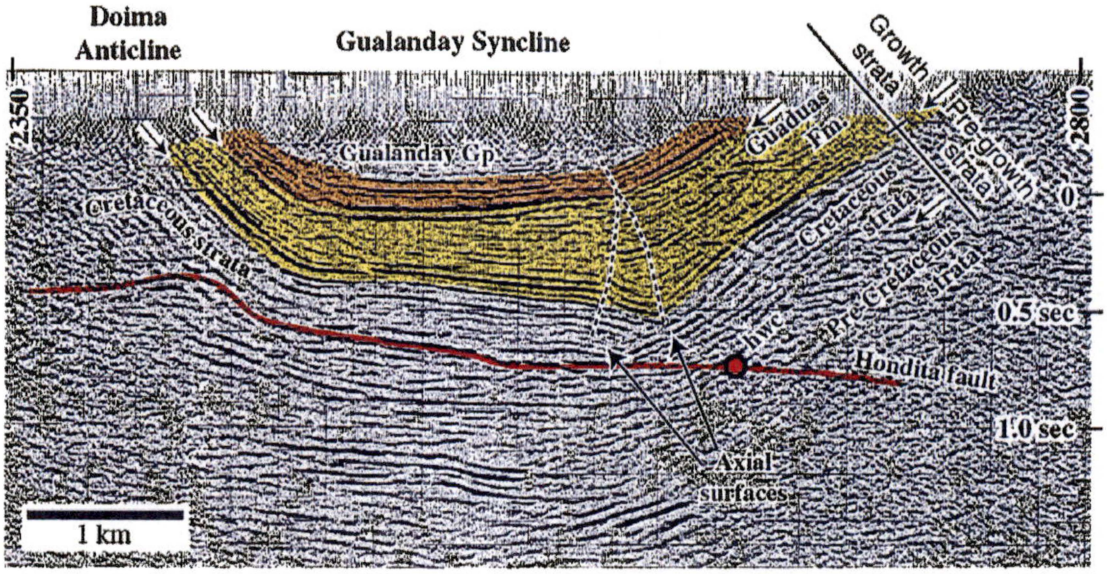


Figure 5: Seismic section across the Gualanday syncline. See Fig. 3 for location. Note thickening of folded Paleogene strata towards the axis of the Gualanday syncline, complex fold axial trace, and angularity between reflectors at the base of the Gualanday Group west of the eastern limb of the fold. Hwc: hanging wall cutoff.

a seismic section (Fig. 5) show that the Guaduas Formation significantly thickens eastward, from the axis of the Doima anticline toward the axis of the Gualanday syncline where it reaches its maximum thickness.

The Guaduas Formation apparently rests conformably on top of upper Cretaceous strata. In contrast, marked angularity exists between the bold reflectors at the base of the Gualanday Group and the faint reflectors at the top of the Guaduas Formation (Fig. 5). This angularity, however, disappears in the west-dipping, eastern limb of the Gualanday syncline where reflectors of the Guaduas Formation and the Gualanday Group become parallel. The fold axial trace of the Gualanday syncline in the time profile is complex because it diverges downward from the top of the Guaduas Formation (Fig. 5). A similar divergent pattern is inferred from the geologic map where the wide, south-plunging, northernmost part of the Gualanday syncline consists of three relatively uniform dip slopes: a NNE-trending, southeast-dipping western limb, and a NNE- and NNW-trending eastern limb that defines a converging axial trace (labeled 6 in Fig. 3).

Such complex fold axial geometries develop in growth strata as a result of the interplay between migrating or stationary fold axial surfaces and sedimentation. Fold axial surfaces develop as a thrust sheet propagates over a footwall ramp. If sedimentation takes place during propagation, the zone defined by the fold axial surfaces narrows upward to an intersection that marks the end of growth strata. If, for instance, a thrust sheet propagates over a footwall ramp, parallel fold axial surfaces will develop, keeping a constant width in pre-growth strata, and converging if syntectonic sedimentation takes place. Even though axial surfaces of a thrust sheet propagating over a footwall ramp remain stationary in space, they are considered active because they sweep through the rock as the thrust sheet moves. Fixed axial surfaces do not sweep through the rock, and may develop for instance along the leading edge of a thrust sheet that brings a hanging wall cutoff onto of a footwall flat. In this case the fixed axial surface develops from the hanging wall cutoff upward, and will remain fixed. Syntectonic sedimentation in both cases produces converging fold axial traces with slightly different patterns (Suppe *et al.*, 1992).

These simplified predictions can be directly applied to the interpretation of the growth strata in the Gualanday syncline where thickness variations define a complex fold axial trace morphology that splits in two with the axial trace delineating a roughly triangular zone that widens downward (Fig. 5). The apex of this triangular zone is at the base of the Gualanday Group, marking the end of growth strata. Thickness changes, and the morphology of the fold axial trace of the Gualanday syncline (both in map and cross section view), reveal a time of syntectonic sedimentation, fold growth and propagation (Paleocene Guaduas Formation), followed by a time of conglomerate accumulation and folding (Gualanday Group). Whether or not this later folding took place as the conglomerate of the Gualanday Group was accumulating, cannot be tested in the Piedras-Girardot foldbelt because erosion has removed higher stratigraphic levels.

Thicknening of the growth strata to the east, the location of the hanging wall cutoff (hwc in Fig. 5) east of the axis of the Gualanday syncline, and preservation of the eastern, but not of the western growth axial traces, indicate that the Hondita thrust sheet was moving westward to southwestward when growth strata accumulated.

Neogene

The distinctive volcanoclastic sandstone of the Late Oligocene to Miocene Honda Formation provides additional constraints to construct a timeline of deformation. This unit rests unconformably and overlaps upper Cretaceous folded strata near Girardot (Raasveldt, 1956). Near Piedras, in contrast, the same unit is folded, and in faulted contact with Cretaceous strata along the Hondita fault (labeled 8 and 9 in Fig. 3). These relationships simply indicate that while deformation took place along the Hondita fault after the Miocene, it did not take place to the south, near Girardot. In addition, this demonstrates that folding in the southern part of the Piedras-Girardot foldbelt is older than Miocene.

The Quaternary Ibagué fan covers the western half of the study area with a blanket between 50 to 300 m thick (Vergara, 1988) of volcanoclastic material derived from Pleistocene volcanic activity along the axis of the Cordillera Central (Thouret and Laforge, 1994; Thouret *et al.*, 1995). This fan, however, is tilted, uplifted, and offset near Piedras, and along the trace of the Ibagué fault in aligned en échelon domes with axes oriented obliquely to the main trace of the fault (labeled 10 and 11 in Fig. 3), constraining the latest activity of the Ibagué fault to the to the Holocene (Vergara, 1988). All other structures in the western side of the Piedras-Girardot foldbelt (Hondita and Camaito faults, Gualanday syncline and Doima anticline) are fossilized by these young deposits.

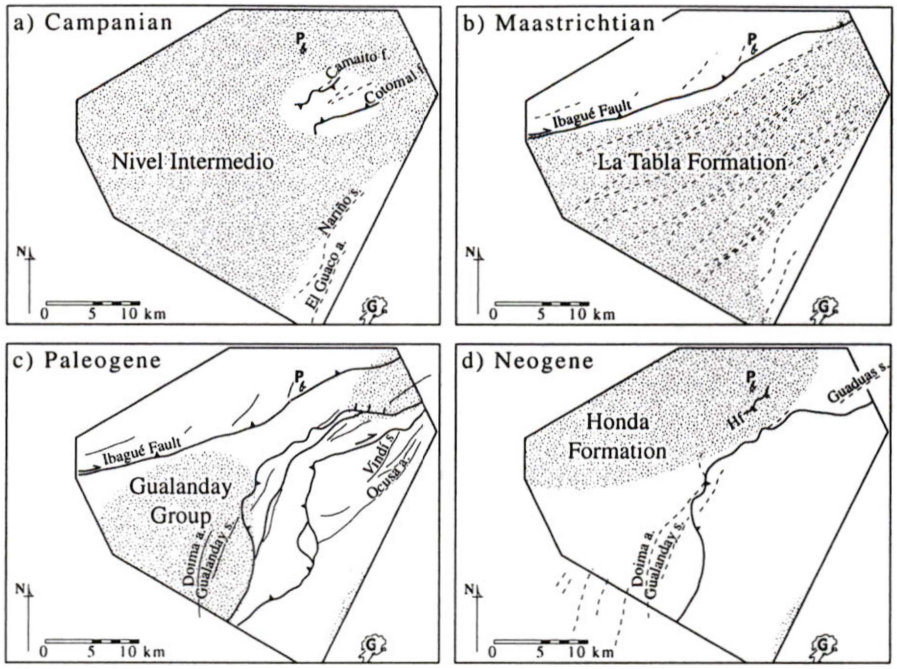


Figure 6: Nonpalinspastic paleogeographic reconstruction of the Piedras-Girardot foldbelt. Stippled pattern represents areas of active sedimentation and white areas indicate possible source areas, or regions of no accumulation. Solid lines represent fold axial traces, and dashed lines represent development of cleavage. Active structures shown for each time slice. Hf: Hondita fault; P: Piedras; G: Girardot; a: anticline; s: syncline.

Paleogeographic interpretation

Stratigraphic data indicate that a discontinuous and low topographic barrier began to develop during the Campanian, as fine-grained sandstone units accumulated around growing folds (Fig. 6a). These domes were probably related to incipient propagation of the northernmost, northeast-trending segments of the Camaito and Cotomal faults, although no evidence was found indicating that these faults breached the surface. During the Maastrichtian, a nearly continuous blanket of conglomerate and sand conformably covered underlying units, recording a time of local quiescence, and regional unroofing to the west (Fig. 6b). The white quartz and phyllite clasts in the La Tabla Formation is direct evidence for the unroofing of nearby highlands of the Cordillera Central where quartzite, phyllite from the metamorphic basement, and black chert, and mudstone from the Cretaceous sedimentary cover were exposed and eroded. The widespread distribution, lateral continuity, and overall uniformity

of this unit in the Piedras-Girardot foldbelt further indicate that Late Cretaceous uplift and deformation was minor with less than 400 m, as estimated from thicknesses of syntectonic units. Paleogeographic analysis of the uppermost Cretaceous Cimarrona Formation further north offers a model where a series of deltas dominated by braided rivers prograded from west to east as they drained the eastern flank of the Cordillera Central (Gómez and Pedraza, 1994). In contrast, regional tectono-stratigraphic models (Villamil, 1999) suggest that the present Cordillera Central was covered by Cretaceous strata that were not eroded until Eocene-Oligocene uplift (Anderson, 1972).

By the Paleogene, the depositional setting of the Piedras-Girardot foldbelt began to be partitioned by a rising north- and northeast-trending elongated plateau that prevented accumulation of sediments between the Camaito fault and El Guaco anticline (Figure 6c). As this plateau rose, sedimentation took place along its southwestern and northeastern flanks, in the Guaduas and Gualanday synclines. Growth strata in the Gualanday syncline record continuous movement of the Hondita thrust sheet to the west or southwest during the early Paleogene. Tertiary sedimentation took place only west of the Camaito fault, north of the Luní fault and east of the El Guaco anticline (Figs. 6c and 6d); because even in very low structural positions such as the hinge of the La Vega syncline, Tertiary sediments are absent.

The source of sediments for the molasse deposits accumulating in these basins during the Paleogene may have been both local and from the east of the Piedras-Girardot foldbelt. Changes in clast composition within the Gualanday Group (Van Houten and Travis, 1968) have been interpreted to result from changing source areas from a metamorphic source terrane (Chicoral Formation) to a sedimentary source area (Doima Formation). This interpretation is consistent with the observation that the Maastrichtian La Tabla Formation contains clasts like the metamorphic rocks of the Cordillera Central, so that by the time of accumulation of the Chicoral Formation, these clasts more likely indicates a western source.

In contrast, during the late Oligocene accumulation of the Doima Formation the source (eastern or local) was still covered by a veneer of Cretaceous sediments. An eastern source at this time, however, seems unlikely because pronounced uplift of the Cordillera Oriental to the east only took place during the Pliocene. Paleoflora collected on the crest of the Cordillera Oriental record uplift from about 500 m to about 3,000 m only until the Pleistocene (Van der Hammen *et al.*, 1973). Uplift rates during the Miocene (Gregory, 2000) are very low (0.03 - 0.05 mm/yr.), compared to rates for the Pliocene (0.6 - 3.0 mm/yr.). Therefore, the source for these clastic material may be local, with the Piedras-Girardot foldbelt providing at least part of the sediments for the Paleogene molasse deposits.

In summary, stratigraphic criteria indicate that the northernmost, northeast-trending segments of the Camaito and Cotomal faults, and the El Guaco anticline started moving and growing during the early to late Campanian. These gentle structures were later overlapped by the Maastrichtian conglomerate of the La Tabla Formation, that records unroofing to the west, most likely in the Cordillera Central. The early Paleogene marks a time of segmentation of accumulation environments due to the west- or southwestward propagation of the Hondita fault (and probably other faults in this foldbelt), and generation of accommodation space in the northeastern Guaduas syncline, and in the southwestern Gualanday syncline. The Piedras-Girardot foldbelt has been a positive area since then, shedding clastic material into these late Paleogene depocenters, that were being concurrently folded. Only the northern part of the study area contains evidence for post-Miocene, and Quaternary deformation, which is at least partially related to the latest movements along the Ibagué fault.

MICROSCOPIC AND MESOSCOPIC STRAIN

This section presents an analysis of mesoscopic and microscopic fabric elements of the Piedras-Girardot foldbelt to evaluate the amount, and directions of nonrigid deformation.

This information is valuable because two- and three-dimensional models and reconstructions of this foldbelt assume that only rigid body rotations and translations take place during deformation (Montes *et al.*, in preparation), therefore ignoring the contribution of internal deformation. If large amounts of internal deformation are recorded in these rocks, the validity of these models would be in question.

Three elements are investigated: 1) deformed fossils; 2) cleavage; and 3) microscopic and mesoscopic veins. Each element provides a partial, and sometimes local story. Deformed fossils record finite strain; but useful fossils are rare and restricted to a few stratigraphic horizons. Thus, they cannot be used alone to estimate the strain state of the Piedras-Girardot foldbelt. Cleavage is ubiquitous in some lithologic types, but its contribution to finite strain is difficult to assess. Microscopic intraclastic veins record amounts and direction of extension, but they are stratigraphically restricted to a small part of the column. Together, these elements are used to form a general picture of the contribution of nonrigid body deformation in the Piedras-Girardot foldbelt.

Deformed fossils

Deformed external molds of ammonite shells preserved in black shale of the lower part of the Villeta Group were used as strain markers. Fossilization completely eliminated the original shell, leaving behind only the shell imprint on a bedding surface. Thus, there is no ductility contrast between the rock and the strain marker. The fragility of the black shale where these molds are found prevented sample collection for lab study so only field measurements could be made. Although better preserved macro- and microfossils (ammonites, bivalves, forams, and gastropods) are present sometimes ubiquitously, either their plane of symmetry was not properly aligned with respect to bedding, or they were replaced shells that could not properly record finite strain due to a ductility contrast between the specimen and the matrix.

While determining the modification to the initial spiral angle for the ammonites would have been the prefered strain measurement technique (Tan, 1973), difficulty in measuring angles on frail imprints in weak shales precluded this approach. Instead, because most gastropod shells have typical spiral angles of more than 80° (Tan, 1973), which approaches a circle, they were treated as deformed circles for which long and short axial lengths were measured.

Field measurements of 16 deformed external molds of ammonite shells are presented in Table 1 and Fig. 7 (insets 1-4). Each station represents a number of measurements made along stratigraphic intervals of a few meters where molds were abundant. All four stations (insets 1 to 4 in Fig. 7) are located in black shale of the Villeta Group, except for one specimen measured within the lowermost part of the Oliní Group. The axial ratio measured in these localities ranges between 1.0 and 2.3, with an average of 1.5. Axial orientations were recorded in the field, and then later rotated to remove the tilt of bedding. This operation yields an ENE preferred orientation of the long axes of the ellipses (Fig 7a). Station 4 (inset 4 in Fig. 7) contains slightly deformed molds where the difference in axial length was very small, so that ellipses were treated as circles. Axial orientations for the deformed molds

Table 1: Field measurements of deformed impressions of ammonites. Hf: Hondita fault; Cfs: splay of Camaito fault; Cof: Cotomal fault.

Inset number (Fig. 7)	Fault	Approx. horizontal distance to fault (m)	Strat. unit (see codes in Fig.4)	Long axis trend	Long axis plunge	Dip azimuth of rotation axis	Rotation angle (dip)	Ellipse long axis (cm)	Ellipse short axis (cm)	Axial ratio	Long axis trend, rotated	Long axis plunge, rotated
1	Hf	100	k6	185	24	150	32	1.8	1.0	1.8	2	3
1	Hf	200	k6	197	15	140	28	5.0	3.5	1.4	14	1
1	Hf	200	k6	211	7	140	26	9.2	6.0	1.5	30	2
1	Hf	200	k6	183	20	135	35	1.9	0.8	2.4	359	5
1	Hf	200	k6	202	17	140	25	2.3	1.8	1.3	198	4
1	Hf	300	k6	202	3	309	13	1.9	0.9	2.1	203	7
1	Hf	400	k7	244	19	194	29	2.0	1.4	1.4	60	1
2	Cof	100	k7	61	2	132	35	6.3	5.0	1.3	239	9
2	Cof	100	k7	58	2	143	19	10.0	7.0	1.4	58	0
3	Cfs	200	k7	238	19	313	45	8.5	6.0	1.4	247	3
3	Cfs	200	k7	227	21	313	45	13.0	7.0	1.9	241	12
3	Cfs	200	k7	241	22	313	45	2.6	2.1	1.2	251	4
3	Cfs	200	k7	247	27	313	45	5.0	4.0	1.2	258	4
3	Cfs	200	k8	225	18	142	44	4.3	2.5	1.7	214	8
4	Cof	1000	k6	118	27	147	28	2.0	2.0	1.0	121	2
4	Cof	1000	k6	75	9	147	28	3.0	3.0	1.0	257	0

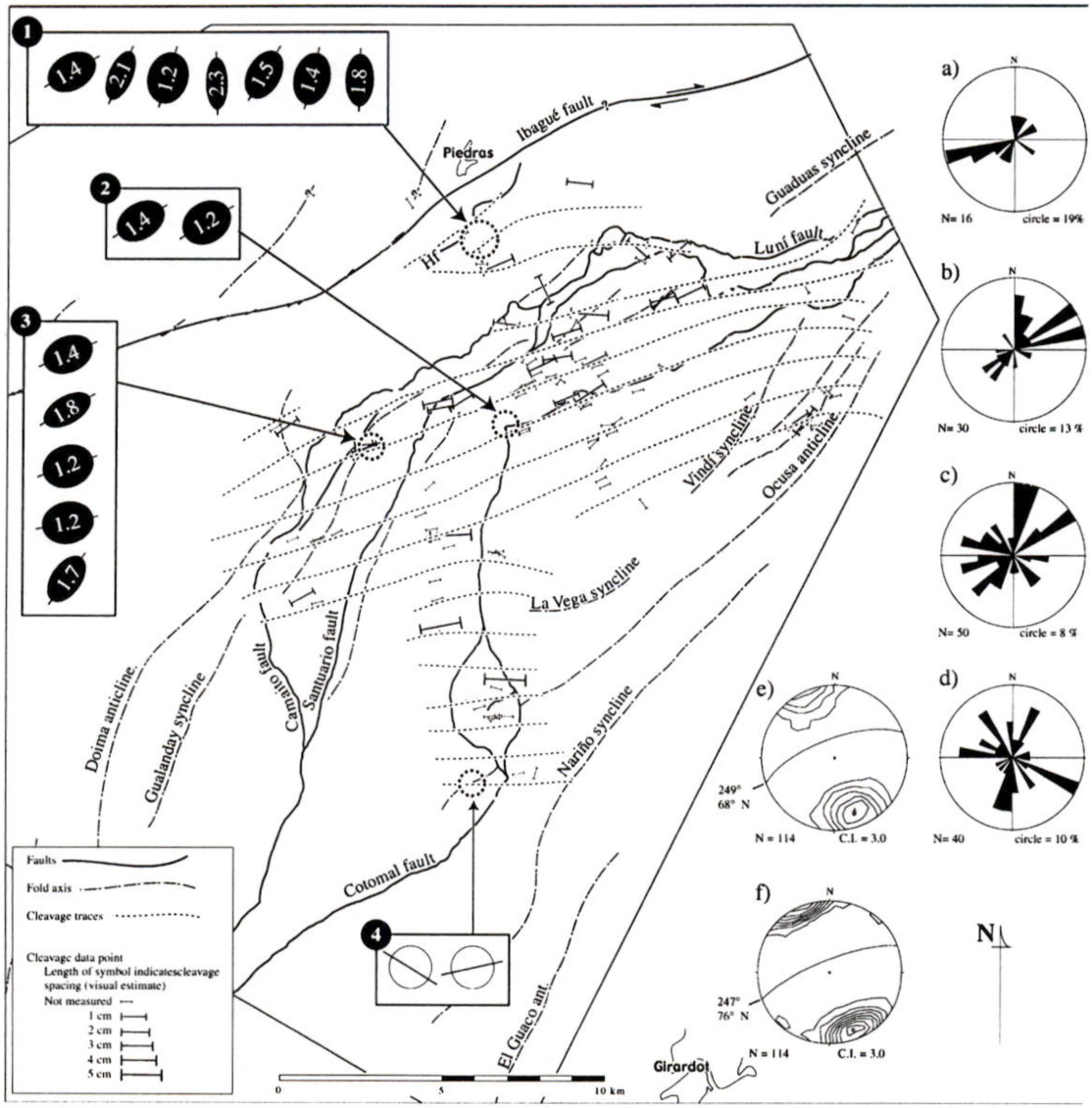


Fig. 7: Map of mesoscopic structures in the Piedras-Girardot foldbelt. Insets 1 to 4 contain two-dimensional strain ellipses estimated from deformed ammonite impressions in black shale (Table 1). Rose Diagrams of: a) Long axes of deformed ammonite molds after dip of bedding has been removed; b) Mesoscopic fold axes; c) Mesoscopic fault planes; d) Slickenlines. Lower hemisphere, equal-area Kamb contour diagram of: e) poles to cleavage; f) poles to cleavage after tilt of bedding has been removed.

indicate east- and southeast shortening directions. Although minor deviations exist, the orientations of the long axes are generally parallel to the trend of cleavage in the Piedras-Girardot foldbelt (Fig. 7).

Magnitude of axial ratios is related to distance to faults (Table 1). High ellipticity values are high less than 400 m from a fault, whereas low values to undeformed molds are found more than 1000 m from a fault. The true distance to the fault surface in all cases must be less than the horizontal distance reported in Table 1 because the station are in all cases located in the hanging wall of a fault. These observations indicate that greater strain occurs closer to faults, and therefore is not a strain pervasive to the entire stratigraphic column.

Cleavage

Cleavage is the most pervasive, uniform, and prominent outcrop-scale structure found in fine-grained Cretaceous strata of the Piedras-Girardot foldbelt. Cleavage is commonly anastomosing (e.g., Powell, 1979), bedding normal, and regularly spaced even in the hinges of map-scale and mesoscopic folds. Cleavage stands out in weathered exposures, where the intersection between wavy domains and lamination in shale commonly defines pencil structures. Cleavage domain surfaces are commonly smooth in hand sample, and microlithons show no detectable deformation structures.

Visual estimation of spacing between cleavage domains is independent of distance to faults or fold axial traces, but is dependent on lithology. Siliceous mudstone, siltstone, and calcareous shale have strong to moderate (e.g., Engelder and Marshak, 1985) non-sutured, wavy cleavage (Figs. 8 and 9). Fine-grained sandstone commonly develops a weak planar cleavage. Coarse-grained sandstone beds lack cleavage, but have widely spaced nonsystematic fractures. Chert, also, contains no cleavage.

Microscopic examination of cleavage domains in siliceous siltstone reveals surfaces with a



Figure 8: Traces of cleavage exposed on a bedding plane in mudstone of the Nivel Intermedio of the Oliní Group. Note that cleavage domains frequently intersect. Unfortunately, the fossil molds are not symmetrical across the hinge, rendering them useless for strain analysis.

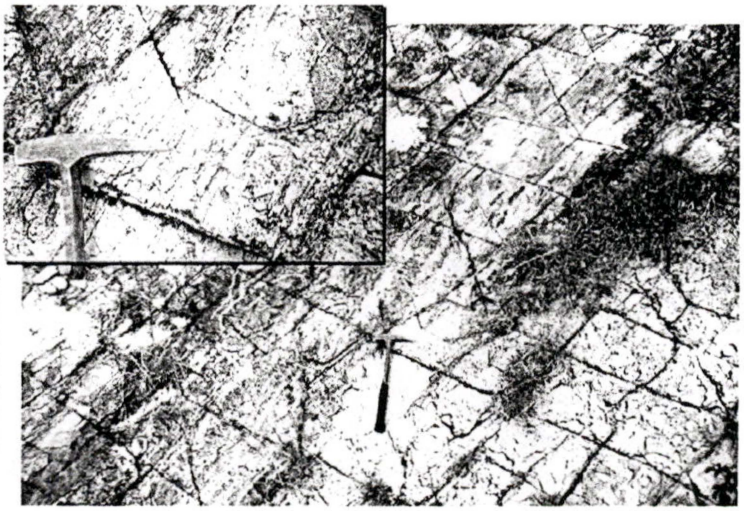


Figure 9: Strong cleavage in fine-grained rocks of the Nivel de Lutitas y Arenas in the southwestern end of La Tabla Ridge. Two sets of joints, one continuous, and the other discontinuous, are also present. Hammer is approximately 41 cm long.

sutured morphology (e.g., Engelder and Marshak, 1985) where thin films (approximately 0.1 mm) of insoluble material are concentrated indicating pressure solution (Fig. 10a). Each cleavage domain consists of a few (three or four) discontinuous overlapping, and osculating surfaces. Some microfossils are truncated, although cleavage surfaces are more often deflected around relatively large particles. The microlithons show no evidence of dissolution (Fig. 10b), and the rock is pristine. Assuming that each film of insoluble material accommodates a very large amount of shortening (for instance 50 percent), and that each cleavage domain consists of 5 overlapping selvages, each one 0.1 mm thick, the amount of

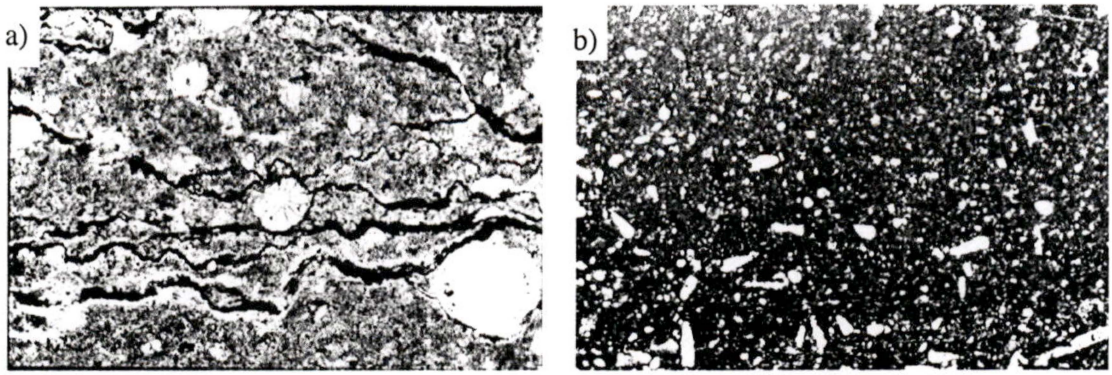


Figure 10: Photomicrograph of cleavage domains taken parallel to bedding in a siliceous mudstone: a) Note truncated microfossil. Width of photograph is 1.7 mm; b) Microlithon showing no evidence for dissolution. Note the cleavage domain at the bottom of the photograph. Width of photograph is 25 mm..

shortening accommodated by a rock with a 2 cm domain spacing is only 5 percent. Shortening values, however, are likely to be less since volume loss along each film each film is likely to represent less extreme values, and because truncated fossils observed do not support extreme shortening values.

Cleavage commonly trends ENE, almost parallel to the Ibagué fault, and to fault traces in the northern third of the study area (northern segments of Cotomal, Camaito and Santuario faults). Cleavage traces, on the other hand, are oblique to the southern, north- and NNE-trending segments of the Camaito and Santuario faults, and nearly perpendicular to the southern half of the north-trending segment of the Cotomal fault. Cleavage traces are also oblique to the traces of most folds in the study area. A Kamb equal-area stereographic plot shows a simple unimodal distribution of poles to cleavage (Fig. 7e) that coincides with the observation that cleavage traces are nearly independent from changes in trend of map-scale structures such as faults and folds.

Removing the dip of bedding due to folding and faulting from the attitude of cleavage surfaces results in an unimodal distribution of poles to cleavage, slightly tighter and with a steeper mean pole (Fig. 7f), that is still 14 degrees away from vertical. This agres well with field observations of cleavage almost always perpendicular, or very close to perpendicular

to bedding. If cleavage had developed entirely before folding, the resulting distribution of poles after removing the tilt of bedding would be closer to vertical, or vertical. An explanation for the failure of these poles to reach a vertical attitude after removal of the tilt of bedding may be that some gentle folding had already taken place by the time cleavage started to develop (Figs. 6a and 6b). This agrees well with stratigraphic observations that indicate that folds started to grow as early as the late Campanian. Upper Cretaceous rocks crossed by cleavage, however, constrain cleavage formation to at least the latest Cretaceous. Therefore, cleavage must have started to develop after the Campanian, when gentle folds started to grow, and continued to develop until before Paleogene tectonic activity.

Shattered pebbles and veins

The conglomeratic unit atop of the Cretaceous sequence of the Piedras-Girardot foldbelt (La Tabla Formation) shows a conspicuous deformation fabric of intragranular fractures (Fig. 11). Only clast-supported, quartzite-rich conglomerate mostly near the top of this unit shows systematic intragranular microveins perpendicular to bedding (Fig. 12). Matrix-supported conglomerate lacks this fabric. Microscopic analysis reveals that this fabric consists of calcite-filled microscopic veins (Fig. 13a) that become visible in outcrop exposures due to weathering. The trend of this microscopic intragranular fabric remains roughly constant from pebble to pebble defining a systematic mesoscopic deformation fabric. Microscopic pock marks where dissolution occured (Fig. 13b), are also common at grain-to-grain contacts, although the poor framework packing in this conglomerate precludes a high density of these contacts. Microscopic examination also revealed that the calcareous matrix is twinned.

The overall trend of intraclastic and mesoscopic veins changes significantly throughout the study area. Southeast of the Cotomal fault mesoscopic and intraclastic veins have nearly identical northwest trends at almost right angles to the axial traces of major folds and the

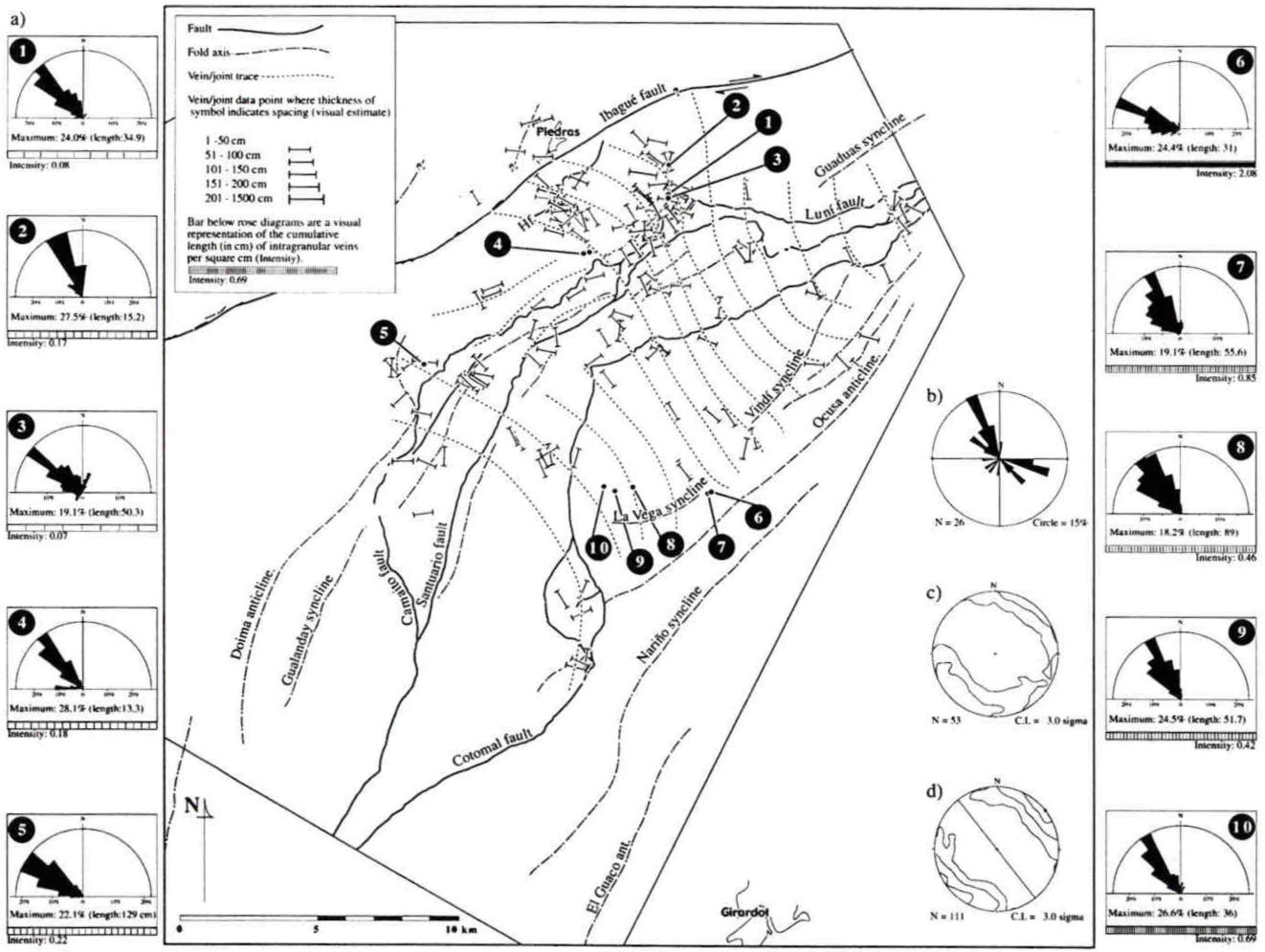


Figure 11: Map of mesoscopic structures in the Piedras-Girardot foldbelt. Traces of veins were interpolated from field measurements. a) Insets contain length-azimuth diagrams (after the dip of bedding was removed) of intraclastic veins on 23 field photographs from 10 field stations (Table 2). b) Rose diagram of field measurements of intraclastic veins in conglomerate of the La Tabla Formation (dip of bedding removed); c) Lower hemisphere, equal-area Kamb contour diagram of poles to veins, and d) poles to joints.

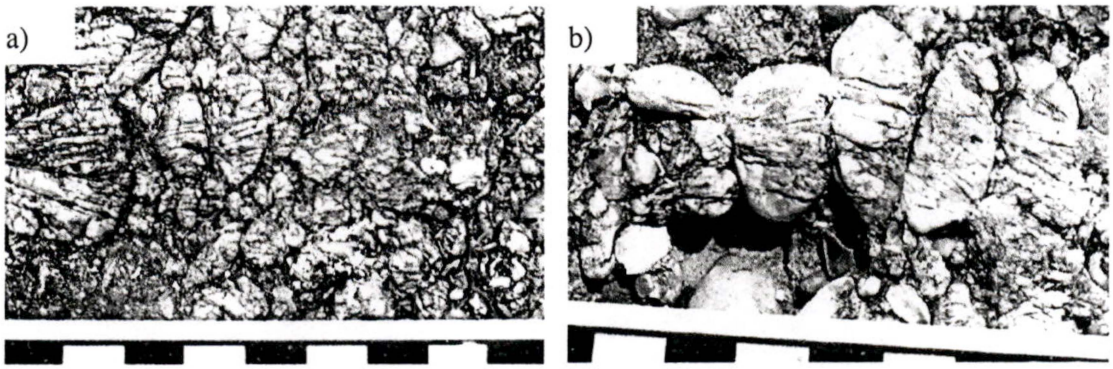


Figure 12: Shattered pebbles of La Tabla conglomerate. a) Shattered pebbles in a clast-supported conglomerate. b) Extreme case of intensely deformed pebbles displaying a brecciated texture. Scale for both photographs is in centimeters.

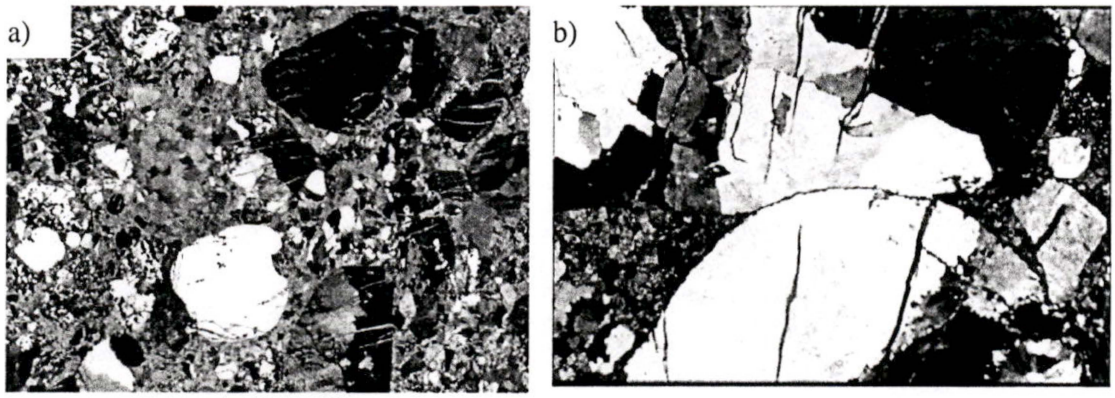


Figure 13: Photomicrographs of La Tabla conglomerate looking onto bedding. a) Calcite-filled microscopic veins transecting quartzite pebbles. Width of photograph is 16 mm. b) Sutured contact between two quartzite pebbles, note the coordination between calcite-filled veins and the sutured contact. Width of photograph is 4.2 mm.

northern, northeast-trending segment of the Cotomal fault (Fig. 11, insets 6 to 10). Intraclastic and mesoscopic veins also trend northwest although the variability is more pronounced, and change to WNW near Piedras. Northeast-trending mesoscopic veins were measured along both flanks of La Tabla Ridge parallel to the Camaito fault and west of the Santuario fault, which is a 90 degree change from veins trends to the south, north, and east (Fig. 11a , insets 4 and 5).

Because this microscopic intragranular fabric is conspicuous in outcrop exposures, field photographs looking onto bedding were used to measure the orientation and length of

intragranular veins, recording every visible vein tracelength in the photographs. Field photographs (Appendix II) at 10 different stations were analyzed to count the number, length, and orientation of all visible veins. In total, 3,463 intragranular veins were measured with a total length of 2,348 cm in a total surface area of 11,201 cm^2 (Table 2). The percentages of matrix versus grains in three thin sections (Appendix II) of a conglomerate from La Tabla Formation (station 5 in Table 2, and Fig. 11) was also measured, and the total area of intraclastic veins was calculated for the purpose of obtain total area change (Table 3, and Fig. 14).

Overall, the average vein length is 0.73 cm, which is indicative of the average grain dimension parallel to veins because most veins completely cross pebbles. A more meaningful number is the intensity or average length of intragranular veins per square centimeter (Wu and Pollard, 1995), and its variation across the area mapped. Exposures of the La Tabla conglomerate on the northwestern side of the Piedras-Girardot foldbelt have smaller length values per square centimeter (between 0.07 and 0.22), than exposures on the southeastern side (between 0.42 and 2.08). The southeastward increase in intensity is indicative of a

Table 2: Measurements of intragranular microveins in the La Tabla Formation conglomerate.

Station number (Fig. 11)	Number of veins measured	Total cumulative length (cm)	Area measured in photo (cm^2)	Number of veins per cm^2	Length of vein per cm^2	Average vein length
1	152	145.07	1847	0.08	0.08	0.95
2	60	55.41	326	0.18	0.17	0.92
3	322	263.87	3761	0.09	0.07	0.82
4	59	47.55	267	0.22	0.18	0.81
5	928	583.52	2643	0.35	0.22	0.63
6	278	127.02	61	4.56	2.08	0.46
7	340	290.5	532	0.64	0.55	0.85
8	656	489.49	1062	0.62	0.46	0.75
9	464	211.15	505	0.92	0.42	0.46
10	204	135.38	199	1.03	0.68	0.66
TOTAL	**3463**	**2348.96**	**11203**			
AVERAGE				**0.87**	**0.49**	**0.73**

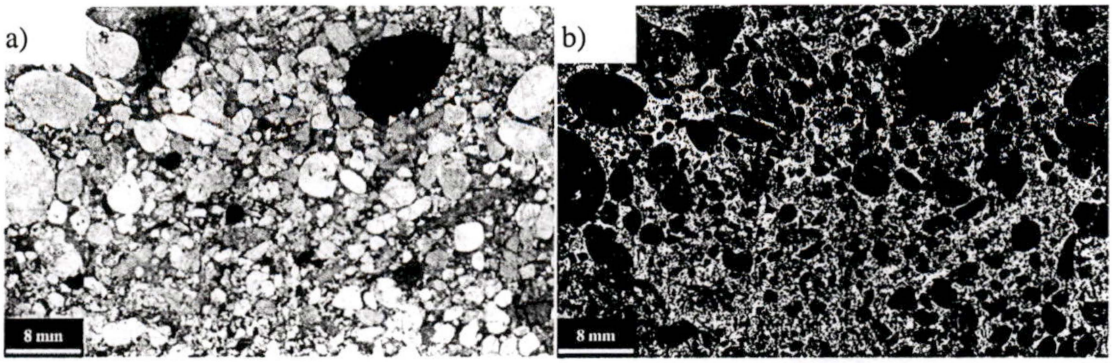


Figure 14: Microscopic intragranular veins in conglomerate of the La Tabla Formation. a) Thin section in under plane light. b) After image-enhancing allows quick estimation of the percentages of grains versus matrix taking advantage of the high birefringence contrast between calcite cement and quartz grains. Results shown in Table 2.

greater amount of extension by vein development. Despite the conspicuous appearance of this fabric, the total area change accommodated by intraclastic veins with average intensity on the northwestern side of the Piedras-Girardot foldbelt (inset 5 in Fig. 11a) is only between 1 and 2 percent (Table 3).

Previous studies in similarly deformed conglomerates indicate that the direction perpendicular to the intragranular veins or fractures is parallel to the maximum finite stretch axis of the finite strain ellipse (Tyler, 1975; Tanner, 1976; Wiltschko *et al.*, 1982; Jerzykiewicz, 1985; Calamita and Invernizzi, 1991; Lin and Huang, 1997). Similar fractured clasts have been reported on recent deposits adjacent to active faults (Tanner, 1976; Eidelman and Reches, 1992; Lin and Huang, 1997), and may develop under as little as 700 m of overburden, (Wiltschko *et al.*, 1982). Photomechanical and experimental studies indicate that extensional fractures in grains of stressed cemented aggregates where grains and matrix having similar

Table 3: Relative and absolute values of digitized matrix, grains, and intragranular veins in thin sections of La Tabla conglomerate in station 5 in Fig. 11, and Table 2.

Thin Section	Percentage black pixels (clasts)	Percentage white pixels (matrix)	Total area measured (mm^2)	Clasts and sand (mm^2)	Calcareous matrix (mm^2)	Total area of intraclastic veins (mm^2)	Percentage area of veins in clasts and sand
CM-LT-2	57.64	42.36	1893.62	1091.48	802.14	18.74	1.72
CM-LT-3	57.47	42.53	2021.26	1161.70	859.56	15.99	1.38
La Tabla 345	78.70	21.30	2159.62	1699.71	459.91	30.85	1.82

elastic modulii exhibit a higher degree of preferred orientation than uncemented aggregates (Gallagher *et al.*, 1974). These experiments indicate that microfractures tend to develop parallel to the greatest principal stress trajectory, with little influence of stress concentration at grain-to-grain contacts in cemented aggregates. Therefore, the deformation fabric in the La Tabla Formation conglomerate may have developed shortly after its accumulation, whith very little overburden, and it may be used to deduce the direction of maximum extension, as the direction perpendicular to the veins.

In summary, the intraclastic microscopic veins in the La Tabla conglomerate record small amounts of extension (between 1 and 2 percent) in the northwestern side of the Piedras-Girardot foldbelt. The trends of these microscopic veins is mostly to the northwest, defining a direction of the maximum finite stretch of the finite strain ellipse to the northeast. Such stretch is approximately perpendicular to the direction of minimum finite stretch independently deduced from cleavage and deformed fossils.

RESULTS

Microscopic and mesoscopic fabric elements in the Piedras-Girardot fold belt, albeit prominent and pervasive, record small contractions or extensions. Cleavage may accommodate less than 5 percent shortening in a mostly northwest direction, whereas microscopic veins accommodate between 1 and 2 percent extension in a northeast direction. Strain ellipses measured from deformed fossils have similar directions but greater strain ratios, which is incompatible with small contraction and extension values. This difference is interpreted to result from the geographic and stratigraphic locations of deformed fossil findings: geographically near faults, or stratigraphically near detachment levels in the lower part of the Villeta Group (Montes *et al.*, in preparation).

The orientation of most mesoscopic fabric elements supports stratigraphic evidence indicating

that the northern, northeast-trending segments of the Cotomal and Camaito faults were starting to propagate in the early Campanian (Figs. 6a and 6b). Cleavage must have developed sometime after initiation of mild Campanian folding, but before significant map-scale folding and faulting took place during the Paleogene. Microscopic intraclastic veins in conglomerate may have developed shortly after accumulation during the Maastrichtian, simultaneously with the later phase of cleavage development.

Therefore, Late Cretaceous initiation of deformation involved northwest-southeast contraction along the northeast-trending segments of the Cotomal and Camaito faults, that although did not breach the surface, were probably rooted along a basal detachment along the lower part of the Villeta Group were deformed fossils record high strain values. Paleogene deformation, although spectacularly recorded by thick, folded molasse deposits and map-scale faults, is missing a strong mesoscopic deformation fabric. Fabric elements associated with Late Cretaceous deformation were passively rotated and translated along thrust sheets. Neogene deformation took place only in the western flank of this foldbelt.

These results indicate that internal deformation can be ignored when performing two- and three-dimensional modeling of this foldbelt (Montes *et al.*, in preparation) because the amounts of extension or contraction are small. This fabric of deformation records Late Cretaceous contraction in a northwest-southeast direction, and extension in a northeast-southwest direction, and may be related to early movement along the northeast-trending, northern segments of the Cotomal and Camaito faults recorded by the pinchouts of the sandy member of the Nivel Intermedio of the Oliní Group (Figs. 6a and 6b).

REFERENCES

Anderson, T. A., 1972, Paleogene Nonmarine Gualanday Group, Neiva Basin, Colombia, and regional development of the Colombian Andes: Geological Society of America Bulletin, v. 83, p. 2423-2438.

Barrero, D., and Vesga, C., 1976, Mapa geológico del cuadrángulo K-9 Armero y parte sur del J-9 La Dorada: Ingeominas, scale 1:100,000.

Bayona, G., García, D. F., and Mora, G., 1994, La Formación Sandaña: Producto de la actividad de estratovolcanes continentales en un dominio de retroarco, in Etayo Serna, F., ed., Estudios Geológicos del Valle Superior del Magdalena: Bogotá, ECOPETROL, p. I.1-I.21.

Bürgl, H., and Dumit, Y., 1954, El Cretáceo Superior en la región de Girardot: Boletín Geológico del Ingeominas, v. II, p. 23-48.

Caicedo, J. C., and Roncancio, J. H., 1994, El Grupo Gualanday como ejemplo de acumulación sintectónica, en el Valle Superior del Magdalena, durante el Paleógeno, in Etayo Serna, F., ed., Estudios Geológicos del Valle Superior del Magdalena: Bogotá, ECOPETROL, p. X.1-X.19.

Calamita, F., and Invernizzi, C., 1991, Mesostructural analysis on the conglomerates of the outer Marchean area (between M. Ascensione and S. Bennedetto): Bollettino della Societa Geologica Italiana, v. 110, p. 667-673.

Cediel, F., 1969, Geología del Macizo de Floresta: Memorias del primer congreso colombiano de geología, v. 1, p. 17-30.

Cediel, F., and Cáceres, C., 1988, Geologic map of Colombia: Geotec Editions, scale 1:2,000.000.

Cediel, F., Mojica, J., and Macía, C., 1981, Las formaciones Luisa, Payandé y Saldaña sus columnas estratigraficas características: Geología Norandina, v. 3, p. 11-19.

Cortés, M., 1994, Análisis de la deformación estructural del Grupo Oliní en el Valle Superior del Magdalena, in Etayo Serna, F., ed., Estudios Geológicos del Valle Superior del Magdalena: Bogotá, ECOPETROL, p. IX.1-IX-16.

DePorta, J., 1965, La estratigrafía del Cretácico Superior y Terciario en el extremo S del Valle Medio del Magdalena: Boletín de Geología Universidad Industrial de Santander, v. 19, p. 5-50.

Eidelman, A., and Reches, Z. e., 1992, Fractured pebbles; a new stress indicator: Geology, v. 20, p. 307-310.

Engelder, T., and Marshak, S., 1985, Disjunctive cleavage formed at shallow depths in sedimentary rocks: Journal of Structural Geology, v. 7, p. 327-343.

Etayo Serna, F., 1994, Epílogo: A modo de historia geológica del Cretácico del Valle Superior del Magdalena, in Etayo Serna, F., ed., Estudios Geológicos del Valle Superior del Magdalena: Bogotá, Universidad Nacional, ECOPETROL, p. XX.1-XX-5.

Florez, M., and Carrillo, G. A., 1994, Estratigrafía de la sucesión litológica basal del Cretacico del valle superior del Magdalena, in Etayo Serna, F., ed., Estudios Geológicos del Valle Superior del Magdalena: Bogota, Colombia, ECOPETROL, p. II.1-II.26.

Forero, S. A., 1990, The basement of the Eastern Cordillera, Colombia; an allochthonous terrane in northwestern South America: Journal of South American Earth Sciences, v. 3, p. 141-151.

Gallagher, J. J., Jr., Friedman, M., Handin, J., and Sowers, G. M., 1974, Experimental studies relating to microfracture in sandstone: Tectonophysics, v. 21, p. 203-247.

Gómez, E., and Pedraza, P. E., 1994, El Maastrichtiano de la region Honda-Guaduas, limite N del valle superior del Magdalena; registro sedimentario de un delta dominado por rios trenzados, in Etayo Serna, F., ed., Estudios Geológicos del Valle Superior del Magdalena: Bogotá, ECOPETROL, p. III.1-III.20.

Gregory, W. K. M., 2000, Uplift history of the Central and Northern Andes; a review: Geological Society of America Bulletin, v. 112, p. 1091-1105.

Hubach, E., 1945, La formacion "Cáqueza," región de Cáqueza (oriente de Cundinamarca): Compilacion Estudios Geológicos Oficiales de Colombia, v. 6, p. 23-26.

Ingeominas, 1988, Mapa geológico de Colombia: Ingeominas, scale 1:1,500.000.

Jerzykiewicz, T., 1985, Tectonically deformed pebbles in the Brazeau and Paskapoo formations, central Alberta Foothills, Canada: Sedimentary Geology, v. 42, p. 159-180.

Lin, C. W., and Huang, M. L., 1997, The fractures and paleostress of deformed pebbles in the conglomerates of the Toukoshan Formation, Chiayi-Yunlin area: Journal of the Geological Society of China, v. 40, p. 281-297.

Montes, C., Restrepo-Pace, P. A., and Hatcher, R. D., Jr., in preparation, Kinematics of the Piedras-Girardot foldbelt: Implications for the Ibagué transfer zone and the southern Caribbean plate boundary, in Blickwede, J., ed., The circum-Gulf of Mexico and Caribbean region: Plate tectonics, basin formation and hydrocarbon habitats, American Association of Petroleum Geologists.

Namson, J., Cunningham, R., and Woodcock, G., 1994, Structural geology and hydrocarbon potential of the northern part of the upper Magdalena Basin, Colombia, in AAPG annual convention., Tulsa, OK, United States, p. 221.

Pindell, J., and Dewey, J. F., 1982, Permo-Triassic reconstruction of western Pangea and the evolution of the

Gulf of Mexico/ Caribbean region: Tectonics, v. 1, p. 179-211.
Powell, C. M., 1979, A morphological classification of rock cleavage: Tectonophysics, v. 58, p. 21-34.
Raasveldt, H. C., 1956, Mapa geológico de la plancha L-9 Girardot: Servicio Geológico Nacional, scale 1:200,000.
Restrepo Pace, P. A., Colmenares, F., Higuera, C., Mayorga, M., and Leal, J., 1999, Fold and thrust belt along the western flank of the Eastern Cordillera of Colombia; style, kinematics and timing constraints derived from seismic data and detailed surface mapping, in AAPG international conference and exhibition; abstracts., Tulsa, OK, United States, p. 1336.
Restrepo Pace, P. A., Ruiz, J., Gehrels, G., and Cosca, M., 1997, Geochronology and Nd isotopic data of Grenville-age rocks in the Colombian Andes; new constraints for late Proterozoic-early Paleozoic paleocontinental reconstructions of the Americas: Earth and Planetary Science Letters, v. 150, p. 427-441.
Schamel, S., 1991, Middle and upper Magdalena basins, Colombia, in Biddle, K. T., ed., Active margin basins: AAPG Memoir: Tulsa, OK, United States, American Association of Petroleum Geologists, p. 283-301.
Suppe, J., Chou, G. T., and Hook, S. C., 1992, Rates of folding and faulting determined from growth strata, in McClay, ed., Thrust tectonics.: London, United Kingdom, Chapman & Hall, p. 105-121.
Tan, B. K., 1973, Determination of strain ellipses from deformed ammonoids: Tectonophysics, v. 16, p. 89-101.
Tanner, W. F., 1976, Tectonically significant pebble types; sheared, pocked and second-cycle examples: Sedimentary Geology, v. 16, p. 69-83.
Thouret, J. C., Cantagrel, J. M., Robin, C., Murcia, A., Salinas, R., and Cepeda, H., 1995, Quaternary eruptive history and hazard-zone model at Nevado del Tolima and Cerro Machin volcanoes, Colombia: Journal of Volcanology and Geothermal Research, v. 66, p. 397-426.
Thouret, J. C., and Laforge, C., 1994, Hazard appraisal and hazard-zone mapping of flooding and debris flowage in the Rio Combeima Valley and Ibagué City, Tolima Department, Colombia: GeoJournal, v. 34, p. 407-413.
Tyler, J. H., 1975, Fracture and rotation of brittle clasts in a ductile matrix: Journal of Geology, v. 83, p. 501-510.
Van der Hammen, T., Werner, J. H., and Van Dommelen, H., 1973, Palynological record of the upheaval of the northern Andes; a study of the Pliocene and lower Quaternary of the Colombian Eastern Cordillera and the early evolution of its high-Andean biota: Review of Palaeobotany and Palynology, v. 16, p. 1-122.
Van der Wiel, A. M., and Van den Bergh, G. D., 1992, Uplift, subsidence, and volcanism in the southern Neiva Basin, Colombia; Part 1, Influence on fluvial deposition in the Miocene Honda Formation: Journal of South American Earth Sciences, v. 5, p. 153-173.
Van der Wiel, A. M., Van den Bergh, G. D., and Hebeda, E. H., 1992, Uplift, subsidence, and volcanism in the southern Neiva Basin, Colombia; Part 2, Influence on fluvial deposition in the Miocene Gigante Formation: Journal of South American Earth Sciences, v. 5, p. 175-196.
Van Houten, F. B., and Travis, R. B., 1968, Cenozoic deposits, Upper Magdalena valley, Colombia: American Association of Petroleum Geologists Bulletin, v. 52, p. 675-702.
Vergara, H., 1988, Actividad tectónica cuaternaria de la falla de Ibagué: edad y algunos aspectos sedimentológicos del abanico de Ibagué, in Ingeominas, ed., Microzonificación sísmica de Bogotá: Bogotá, Ingeominas.
Villamil, T., 1999, Campanian-Miocene tectonostratigraphy, depocenter evolution and basin development of Colombia and western Venezuela: Palaeogeography, Palaeoclimatology, Palaeoecology, v. 153, p. 239-275.
Vissers, R. L. M., and Bollegraaf, B., 1989, An algorithm for rotation of axial data: Computers and Geosciences, v. 15, p. 157-161.
Wellman, S. S., 1970, Stratigraphy and petrology of the nonmarine Honda Group (Miocene), Upper Magdalena Valley, Colombia: Geological Society of America Bulletin, v. 81, p. 2353-2374.
Wiltschko, D. V., Sutton, S. J., and Saltzer, S. D., 1982, Deformation by overburden of a coarse quartzite conglomerate: Journal of Geology, v. 90, p. 725-733.
Wu, H., and Pollard, D. D., 1995, An experimental study of the relationship between joint spacing and layer thickness: Journal of Structural Geology, v. 17, p. 887-905.

Part III

Three-dimensional structure of the Piedras-Girardot foldbelt.

ABSTRACT

Detailed geologic mapping of the Piedras-Girardot foldbelt reveals a dextral positive flower structure in the western border of the Cordillera Oriental of Colombia. The dextral, ENE trending strike-slip Ibagué fault serves as the northern boundary for a dextral shear zone approximately 30 km wide. South of the Ibagué fault, a complex array of faults and folds exists: northwest- and west-verging thrust faults, north- and northeast-verging normal faults, and north- and northeast-trending strike-slip faults. Changes in the structural trend delineate a sigmoidal sinistral stepover in this dextral system, with faults verging outwardly in opposite directions defining a positive flower structure. Syntectonic deposits of Campanian age constrain dextral motion of the Cotomal fault to 8 km approximately parallel to the trace of the Ibagué fault. Palinspastic restoration of the fault blocks indicates that approximately 52% ENE contraction is recorded in this foldbelt. A three-dimensional model integrating and honoring all available information is presented and tested using simple forward modeling

INTRODUCTION

Although agreement exists that oblique convergence has dominated the interaction between the Caribbean and South American Plates during most of the Cenozoic (Case *et al.*, 1971; Ladd, 1976; Pindell and Dewey, 1982; McCourt *et al.*, 1984; Laubscher, 1987), very little structural evidence exists supporting this observation on the ground. In fact, numerous two-dimensional models still ignore the contribution of strike-slip to deformation in the Cordillera Oriental and Magdalena Valley (Colletta *et al.*, 1990; Dengo and Covey, 1993; Cooper *et al.*, 1995; Roeder and Chamberlain, 1995), potentially making these reconstructions incomplete. Regional paleogeographic reconstructions are hindered by the lack of a better understanding of the kinematics of this margin (Villamil, 1999), particularly whether presently contiguous sedimentary facies have been telescoped perpendicular, oblique, parallel, or slid along major faults.

This paper presents the results of a detailed investigation regarding the three-dimensional structure and evolution of the Piedras-Girardot foldbelt in the northern Andes of Colombia (Fig. 1). This foldbelt is the only segment of the northern Andes where the Cordilleras Central and Oriental overlap, thus opening a unique window to understand the interaction between the Caribbean, South American, and Nazca plates. The Piedras-Girardot foldbelt also offers an excellent opportunity to study three-dimensional deformation because of its moderate size, adequate exposure, and availability of oil industry subsurface data.

Results include a detailed geologic map of this foldbelt, and two- and three-dimensional models of deformation. These results provide an anchor point to test competing hypotheses for the kinematic development of the northern Andes. They also contribute to the development of methodologies to study transpressional deformation in three dimensions.

Methods

Detailed geologic field mapping, collection of fabric and stratigraphic data, and exhaustive analysis of field relationships constitute the foundation of this study. The overall research strategy consisted of: 1) detailed geologic mapping and compilation of data from other

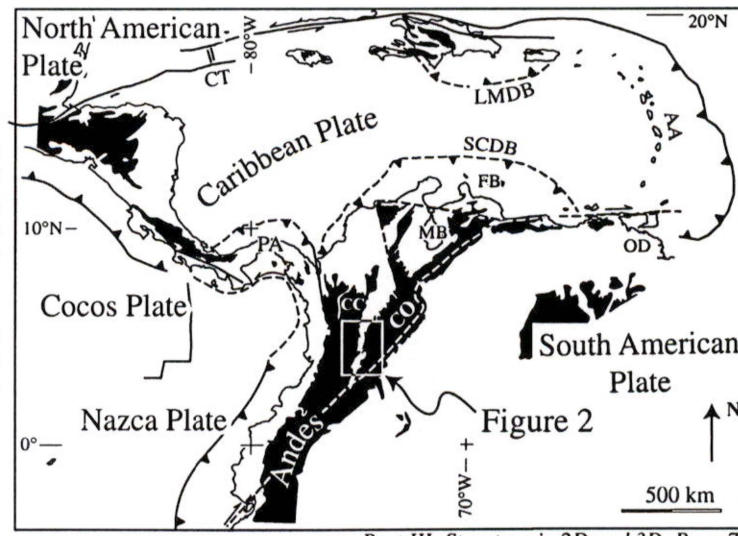


Figure 1: Tectonic map of the Caribbean region. Black indicates elevations higher than 500 m above sea level. LMDB: Los Muertos deformed belt; SCDB: Southern Caribbean deformed belt; OD: Orinoco delta; AA: Antilles arc; PA: Panamá arc; MB: Maracaibo basin; FB: Falcón basin; CT: Cayman trough; CC: Cordillera Central; CO: Cordillera Oriental.

sources (published maps, industry seismic data); 2) design of a three-dimensional digital database; 3) processing and projection of data into two- and three-dimensional workspaces; 4) inclusion of data about deformation from kinematic and strain markers (Montes *et al.*, in preparation); and 5) construction of two- and three-dimensional models to explain the deformation history in the Piedras-Girardot foldbelt.

Field mapping concentrated on fault traces and lithologic contacts at 1:25,000 scale and collection of structural data. Changes in cutoff geometry, kinematic markers, and, in some cases, dip of fault planes were documented by tracing structures along strike, using relief to study the vertical dimension, and occasionally examining neotectonic features such as tilted terrace deposits to map fault traces. Aerial photographs and satellite imagery were useful to extrapolate contacts beyond the area traversed during field seasons, to delineate fan and alluvial deposits, and to detect neotectonic features. With the exception of the Ibagué fault, and the Guaduas and Gualanday synclines, the nomenclature of faults and folds for the Piedras-Girardot foldbelt presented here is new. Correlation to regional faults of the Cordillera Oriental was not attempted because the lack of detailed geologic mapping elsewhere precludes defining the exact traces and styles of faults.

To facilitate data analysis, perform geometric and kinematic modeling in two and three dimensions, and export digital data to specialized computer software, all available data were compiled into a geologic database. This database contains all spatial and non-spatial information from the Piedras-Girardot foldbelt including field stations, stratigraphic and structural observations, geologic contacts, subsurface data, topographic data, and remote sensing data. The data are in a fully digital, georeferenced, three-dimensional geologic and geographic database that allows complex queries as well as construction and manipulation of surfaces. Manipulation of data (Appendix I) allowed us to export selected sets of data to specialized software for 2D and 3D analysis.

Caribbean Plate Boundary

Regional kinematic reconstructions indicate that the Caribbean Plate resisted subduction due to its origin as a thick buoyant oceanic plateau in the Pacific Plate (Malfait and Dinkelman, 1972; Pindell and Barrett, 1990), which drifted eastward into the opening that the American plates left as they separated (Case *et al.*, 1971; Ladd, 1976). Seismic refraction studies (Edgar *et al.*, 1971; Zeil, 1979; Westbrook, 1990) reveal that the Caribbean oceanic crust is abnormally thick (12 to 15 km) and 1-2 km shallower than predicted by its minimum age. This abnormally thick, shallow plate shows signs of internal deformation that may have resulted from its eastward insertion through a bottleneck (Fig. 1) between the Los Muertos and the Southern Caribbean deformed belts (Burke *et al.*, 1978).

The eastward drift of the buoyant Caribbean Plate with respect to the American plates requires large transcurrent components along the southern and northern Caribbean plate margins. The Cayman trough (Fig. 1) records at least 1100 km of left-lateral motion since the Eocene along the sharp northern Caribbean plate boundary (Rosencrantz *et al.*, 1988). In contrast, the southern Caribbean plate boundary is characterized by a broad and diffuse zone of oblique deformation (Kafka and Weidner, 1981; Audemard, 2001) with the Cordillera Oriental forming its eastern border (Mann *et al.*, 1990). Evidence for more than 1000 km of right-lateral transcurrent motions along this margin includes the spatial distribution of endemic vertebrate faunas of the Orinoco River delta as a function of host rock age (Diaz de Gamero, 1996). Their distribution shows that this delta migrated from the Maracaibo Basin in the middle Eocene, to the Falcón basin during the earliest Miocene, to its present position in the late Miocene (Fig. 1) as the leading edge of the Caribbean Plate progressively advanced eastward destroying the passive margin established in northwestern South America. The age of metamorphism is also consistently younger eastward in northern Venezuela (Pindell, 1993) again reflecting the eastward advance of a deformation front. Yet, structural evidence

supporting oblique convergence models in the northern Andes, whether partitioned between the Cordilleras Central (strike-slip) and Oriental (head-on convergence), or distributed in a transpressional zone, is missing.

The contrasting structural styles between the Cordilleras Central and Oriental in the northern Andes of Colombia suggest that oblique convergence predicted along the southern Caribbean plate boundary may be partitioned among these two orogens. Geologic maps show that large dextral strike-slip faults dominate the structure of the Cordillera Central (Barrero *et al.*, 1969; Feininger, 1970; Barrero and Vesga, 1976; Schubert, 1981; Mosquera *et al.*, 1982), whereas thrust faults and NW-SE contraction have been interpreted to dominate in the Cordillera Oriental. Models reconstructing the predeformational geometry of the Cordillera Oriental assume plane strain and large (> 300 km wide) composite thrust sheets riding along a crustal-scale, east-verging master detachment rooted beneath the Cordillera Central, with subduction of the Caribbean Plate (or another oceanic plate) driving deformation (Kellogg and Bonini, 1982; Dengo and Covey, 1993; Freymueller *et al.*, 1993). Restoration of foreland fold-thrust belts requires displacing the metamorphic assemblages and basement overlying the internal parts of the basal detachment (Oldow *et al.*, 1990). Normal restoration of these thrust sheets along a NW-SE trajectory, however, would displace the hinterland (metamorphic core of the Cordillera Central) beyond the edge of the continental crust in the northern Andes (Case and MacDonald, 1973; Etayo Serna *et al.*, 1986), and so subdetachment mass would be missing in these restoration attempts.

The Piedras-Girardot foldbelt, a small element in the complex north Andean tectonic puzzle, contains regional structures previously interpreted to accommodate NW-SE contraction (Namson *et al.*, 1994). The pronounced curvature of structures within this foldbelt, their geometric arrangement in a sigmoidal pattern, and the variety of structural styles (strike-slip, normal, and thrust faulting) suggest significant amounts of transcurrent deformation.

This foldbelt is stylistically similar to geometries produced by analog modeling of transpressional systems (Schreurs and Colletta, 1998; Casas *et al.*, 2001; McClay and Bonora, 2001). Being at the intersection of the Cordillera Central and Oriental, it is strategically situated for testing the role of strike-slip related deformation in a foreland system with possible oblique convergence, providing an anchor point to test regional tectonic models of the interaction between the southern Caribbean plate boundary and the northern Andes.

STRUCTURAL OBSERVATIONS

The rugged hills of the Piedras-Girardot foldbelt interrupt the otherwise flat and wide topographic depression of the Magdalena Valley in central Colombia (Fig. 2). Topographic

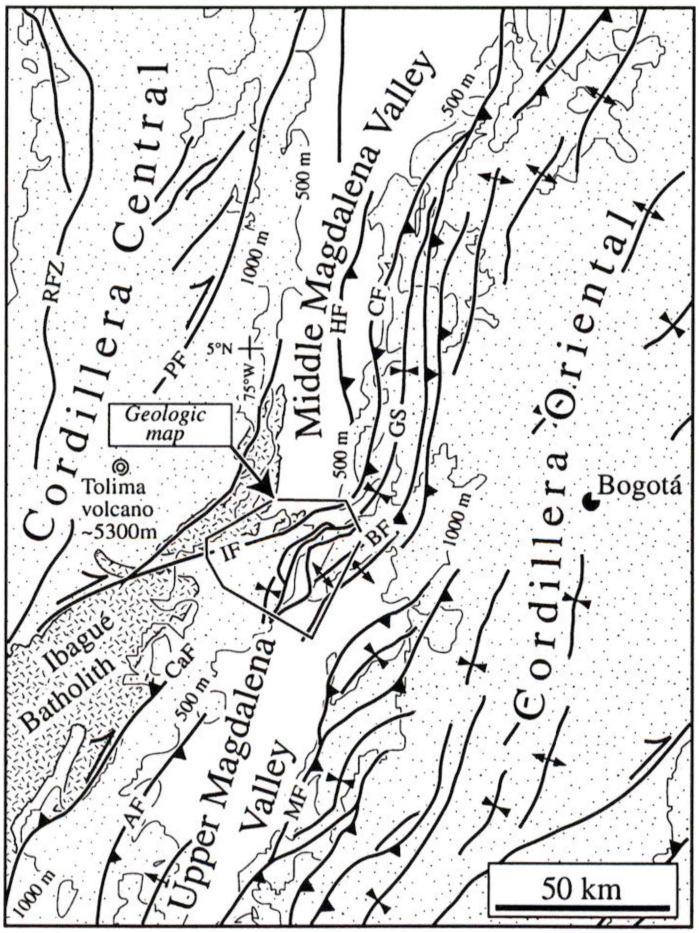


Figure 2: Tectonic map of part of the northern Andes modified after Schamel, (1991). Stippled pattern indicates elevations greater than 500 m above sea level. Notice the narrowing of the Magdalena Valley, and termination of major structures of the Cordilleras Central and Oriental. IF: Ibagué fault, PF: Palestina fault; RFZ: Romeral fault zone; CaF: Calarma fault; BF: Bituima fault; GS: Guaduas syncline; CF: Cambao fault; HF: Honda fault; MF: Magdalena fault; AF: Ataco fault.

relief locally exceeds 500 m with maximum elevations reaching approximately 900 m above sea level. This anomalous geomorphic province constitutes the only barrier that the Magdalena River encounters in its northward path to the Caribbean Sea and exposes critical relationships between the Cordilleras Oriental and Central which are covered elsewhere by Neogene deposits.

The study area has natural geographic boundaries to the east, in the western foothills of the Cordillera Oriental (where elevations commonly exceed 1000 m above sea level), and to the northwest, along the topographic front of the Cordillera Central. Quaternary volcanoclastic deposits mark the southern boundary of this foldbelt.

Shortening in the western flank of the Cordillera Oriental ranges between 30 and 70 percent (Namson *et al.*, 1994; Restrepo Pace *et al.*, 1999), and is accommodated mostly by low-angle, northeast-trending, west-verging faults (Hubach, 1945). These faults include the Cambao and Bituima faults, regional structures that parallel the eastern flank of the north-trending Guaduas syncline, and have their southern termination in this belt (Fig. 2).

The ENE-trending Ibagué fault (Figs. 2 and 3) constitutes the northwestern boundary of the

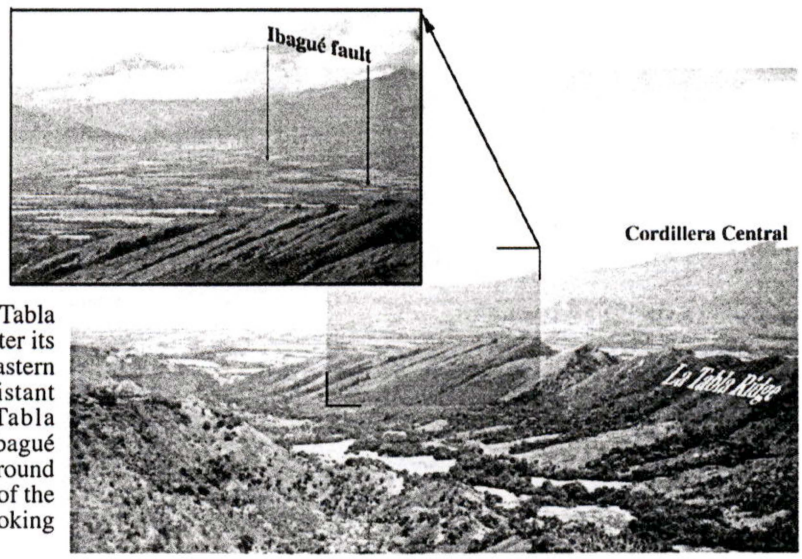
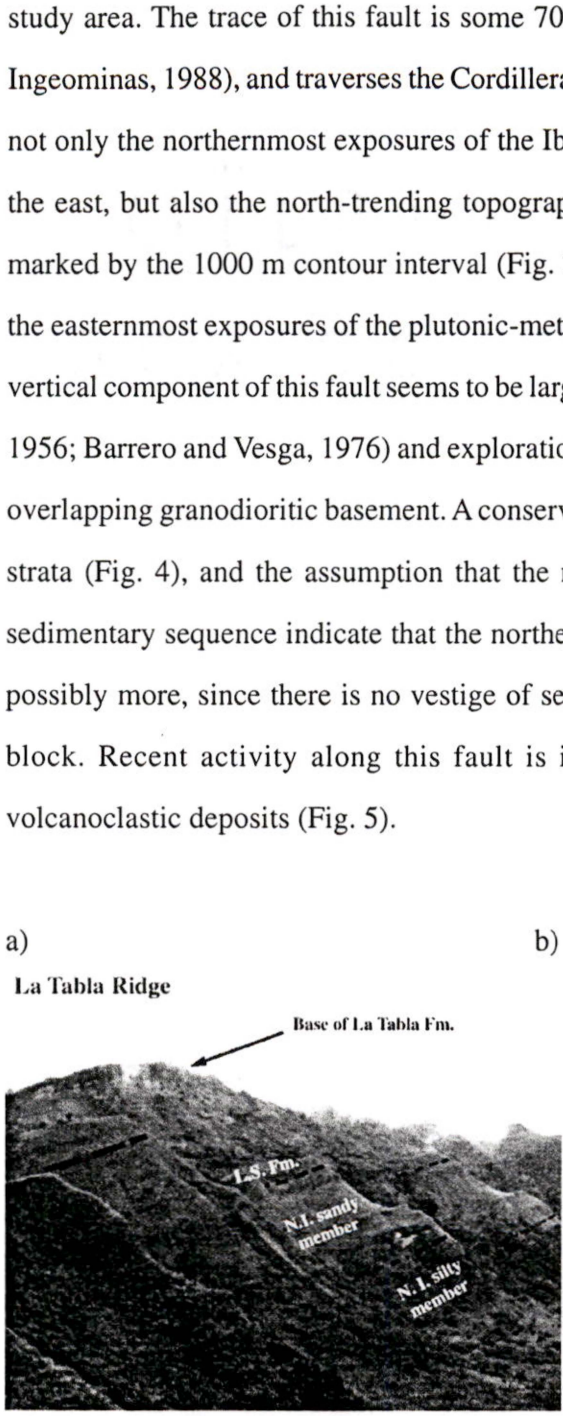


Figure 3: Southern end of La Tabla Ridge. This ridge is named after its characteristically flat southeastern slope which is held by resistant conglomerate of the La Tabla Formation. The trace of the Ibagué fault can be seen in the background offsetting the recent deposits of the volcanoclastic Ibagué fan. Looking southwest.

study area. The trace of this fault is some 70 to 150 km long (Cediel and Cáceres, 1988; Ingeominas, 1988), and traverses the Cordillera Central into the Magdalena Valley, offsetting not only the northernmost exposures of the Ibagué batholith granodiorite at least 40 km to the east, but also the north-trending topographic front of the Cordillera Central which is marked by the 1000 m contour interval (Fig. 2). This steep mountain front also represents the easternmost exposures of the plutonic-metamorphic front of the Cordillera Central. The vertical component of this fault seems to be large as well, because geologic maps (Raasveldt, 1956; Barrero and Vesga, 1976) and exploration wells (Schamel, 1991) show Tertiary strata overlapping granodioritic basement. A conservative estimate of the thickness of Cretaceous strata (Fig. 4), and the assumption that the northern block was covered by a Mesozoic sedimentary sequence indicate that the northern block was upthrown at least 1000 m, and possibly more, since there is no vestige of sedimentary Mesozoic strata anywhere in this block. Recent activity along this fault is indicated by tilted and uplifted Holocene volcanoclastic deposits (Fig. 5).

a)



b)

Period	Age	Column	Maximum Thickness	Stratigraphic unit name	Map Code
Quaternary			Variable thickness	Alluvial deposits and colluvium. Ibagué, and Espinal fans.	q
Tertiary	Miocene			Honda Fm.	t6
	Oligocene			La Cira Fm.	t5
				Guaduas Group: Doima Fm.	t4
				Guaduas Group: Potrerillo Fm.	t3
	Late Eocene			Guaduas Group: Chicoral Fm.	t2
	Paleocene			Guaduas Fm.	t1
Cretaceous (Shown in photo)	Maastrichtian		~ 100 m	La Tabla Fm, conglomerate mbr.	k15
			0 - 100 m	La Tabla Fm, sandy mbr.	k14
	Campanian		~ 200 m	Nivel de lutitas y arenas, sandy mbr.	k13
			~ 200 m	Nivel de lutitas y arenas, silty mbr.	k12
			50 m	Lidita Superior Fm.	k11
			0 - 220 m	Olini Gp.: Nivel Intermedio, sandy mbr.	k10
	Santonian		~ 100 m	Olini Gp.: Nivel Intermedio, silty mbr.	k9
			45 m	Lidita Inferior Fm.	k8
	Coniacian		~ 300 m	Villeta Group: (Loma Gorda Fm, La Frontera Fm.?).	k7
	Turonian				
	Cenomanian		~100 m	Villeta Group: (Lower Hondita Fm.?).	k6
			~100 m	Villeta Group: Tetuán limestone.	k5
	Albian	Not exposed	~100 m	Caballos Fm.	k4
			~150 m	El Ocal Fm.	k3
	Aptian		~100 m	Alpujarra Fm.	k2
Triassic Jurassic			~50 m	Yavi Fm.	k1
				Ibagué Batholith.	

Figure 4: Stratigraphy of the Piedras-Girardot foldbelt. a) Field photo of northwestern flank of the La Tabla Ridge where most of the Cretaceous stratigraphic column is well exposed. L.S. Fm.: Lidita Superior Formation; N.I.: Nivel Intermedio. b) Stratigraphic column.

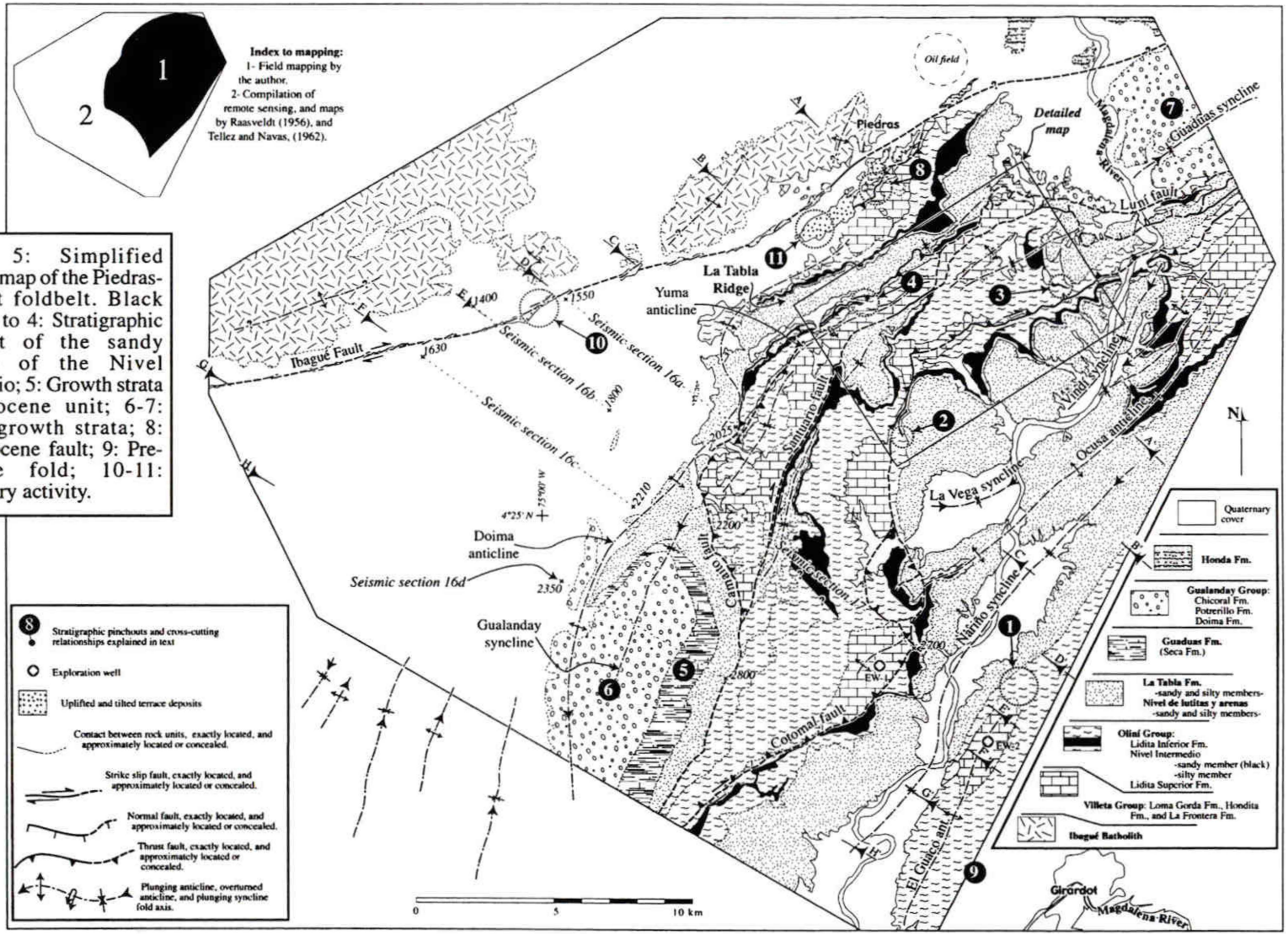


Figure 5: Simplified geologic map of the Piedras-Girardot foldbelt. Black circles 1 to 4: Stratigraphic pinchout of the sandy member of the Nivel Intermedio; 5: Growth strata in Paleocene unit; 6-7: Folded growth strata; 8: Post-Miocene fault; 9: Pre-Miocene fold; 10-11: Quaternary activity.

Structural Style

The Piedras-Girardot foldbelt exhibits a wide variety of structures, deformation styles, and trends, a hint of its complex structural evolution. This relatively small foldbelt (approximately 500 km^2), contains an array of dextral strike-slip faults, northwest and southeast-verging thrust faults, a positive doubly-vergent structure, northeast-trending tight folds, and north-dipping normal faults (Figs. 5 and 6). Structural trends swing from east-west to north-south in a sigmoidal array of folds and faults, which were previously explained as the result of fold interference patterns (Tellez and Navas, 1962) or gravity gliding tectonics (Kammer and Mojica, 1995).

From east to west, three provinces are defined by their distinctive structural styles and geomorphic signatures (Figs. 5, 6 and 7). Tight, northeast-trending folds along the eastern edge of the study area (east of the Cotomal fault, Figs. 5 and 6) give rise to a valley- and-ridge-type topography that climbs westward along a gentle dip slope (Fig. 7c) into a high, relatively flat plateau (between the Santuario and Cotomal faults, Figs. 5,6 and 7b) rimmed to the northwest by a narrow ridge that is defined by northwest- and southeast-verging thrust faults and an overturned anticline (Figs. 6 and 7a). Further west (west of the Camaito fault, Figs. 5 and 7c), the remarkably uniform La Tabla Ridge (Figs. 3 and 4) rises 600 m above the level of the Ibagué fan.

Positive flower structure and Camaito fault

The Piedras-Girardot foldbelt culminates in a narrow 2 km wide, structurally and topographically high, doubly vergent positive structure bounded to the west by the west-verging Camaito fault, and to the east by the east-verging Santuario fault (Figs. 5 and 6). The core of this structure exposes strata as old as Turonian (Villeta Group) in the tight,

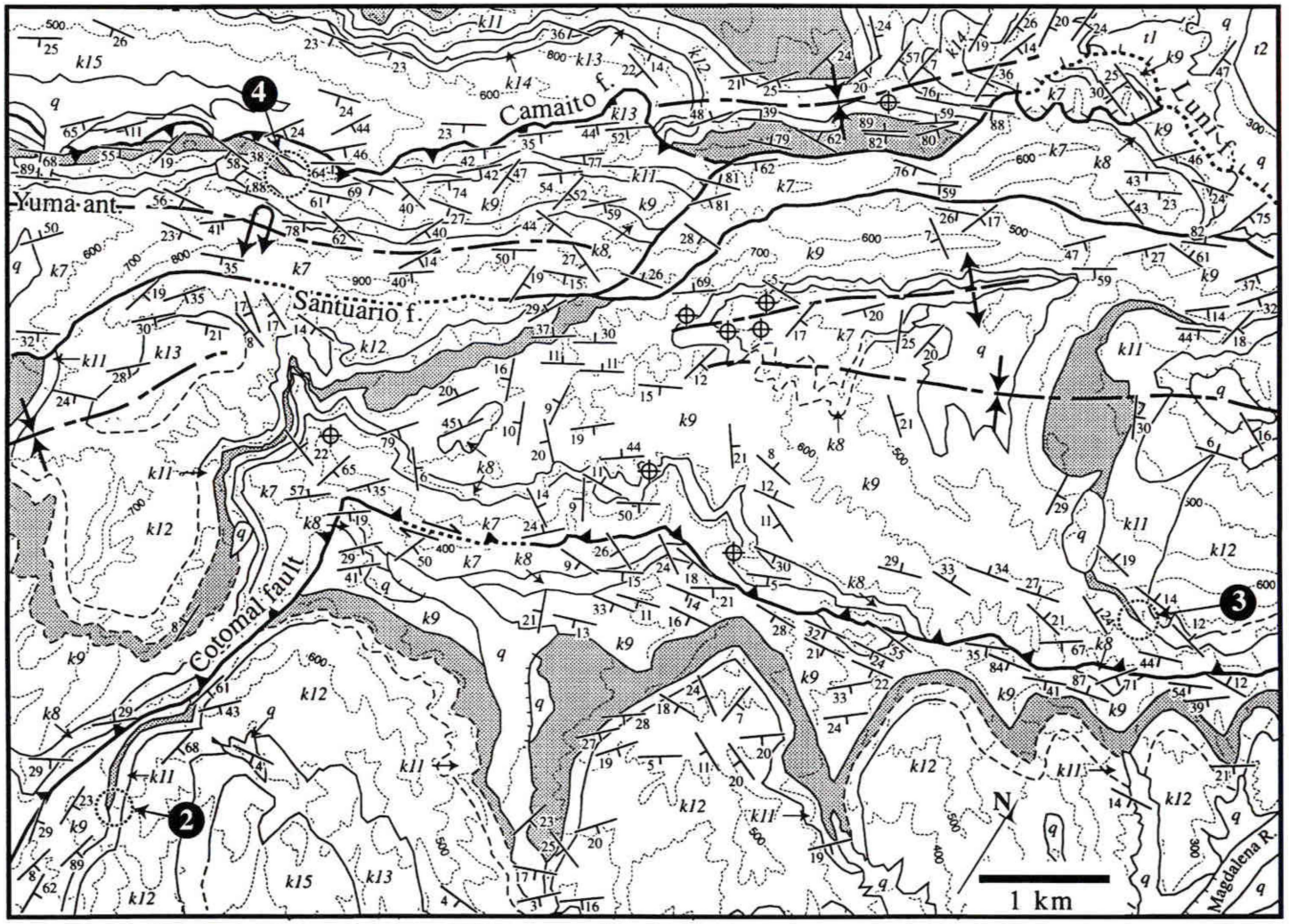


Figure 6: Detailed geologic map of the northern half of the Piedras-Girardot foldbelt. The sandy member of the Nivel Intermedio of the Oliní Group is patterned to highlight mapped pinchouts. Note the offset between the two pinchouts of this unit in this segment of the Cotomal fault. All symbols as in Figure 5.

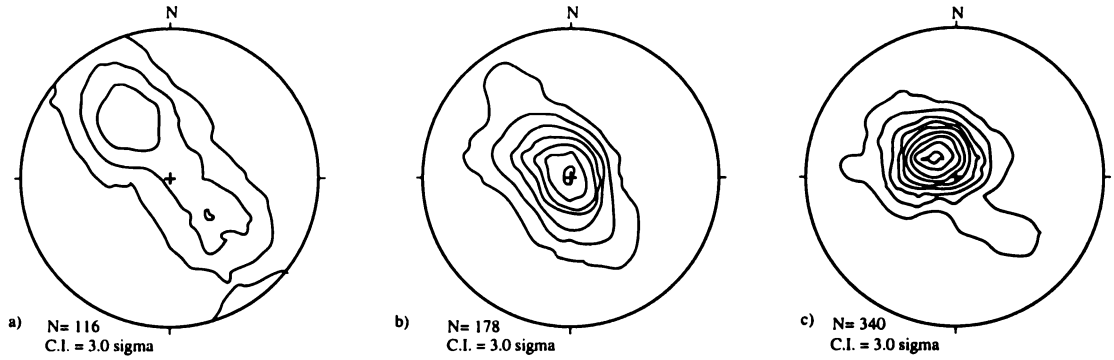


Figure 7: Equal-area, lower-hemisphere Kamb contour diagrams of poles to bedding in the Piedras-Girardot foldbelt. a) Between the Santuario and Camaito faults bimodal pattern defines a northeast-trending fold. b) Between the Santuario and Cotomal faults dip of bedding is very shallow. c) East of the Cotomal fault and west of the Camaito fault bedding shows the shallow southeast dipping monoclines that define ramps at depth.

northwest-verging, overturned, and locally faulted Yuma anticline (Figs. 6 and 8). The northwestern limb of this anticline is overturned and emplaced by the Camaito fault onto upright, gently dipping strata of the La Tabla Formation in a footwall flat, (Fig. 9). From south to north, the trace of the Camaito fault is arcuate with trends changing from NNW immediately east of the Gualanday syncline, to north-south, to northeast along La Tabla ridge. In the northern end of the study area, the trace turns east-west, merging with the north-dipping Luní normal fault. To the south, the trace merges with the Santuario fault as the trend changes to northeast. Observation of the dip angle of the Santuario fault was hindered by the lack of topographic relief along its trace in the plateau so this fault could only be mapped using truncation of stratigraphic units (mostly Oliní Group) against characteristic calcareous shale and micrite of the upper part of the Villeta Group. The arcuate fault trace for the Camaito fault, and the combination of two outward-verging thrust faults bounding an anticline are interpreted as a positive flower structure formed in a transpressive regime.

Plateau and Cotomal fault

Immediately east of the positive flower structure, a nearly flat and topographically high

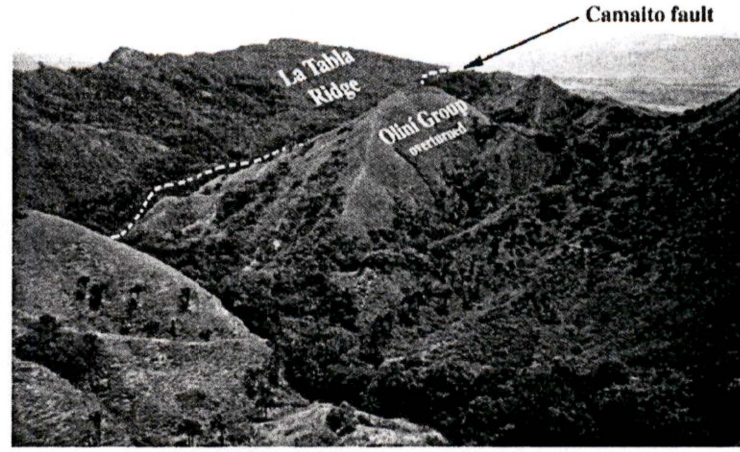


Figure 8: Camaito fault near the northern end of the La Tabla Ridge. This fault often places the overturned western limb of the Yuma anticline (hanging wall ramp) onto gently dipping strata of the La Tabla Formation (footwall flat). The valley in the foreground marks the approximate location of the anticlinal axis. Looking north.

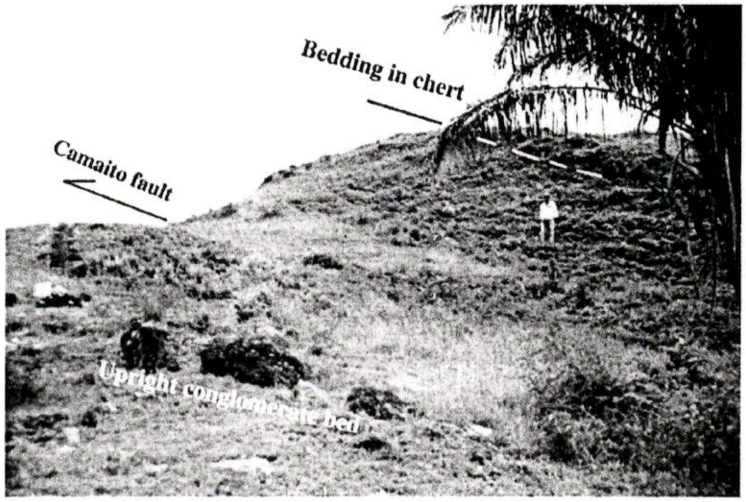


Figure 9: Outcrop expression of the Camaito fault. East dipping, upright conglomerate of the La Tabla Formation (footwall flat, on the left) is overthrust by overturned black chert of the Oliní Group. Looking north.

plateau (Figs. 6 and 10) exposes rocks mostly assigned to the Oliní Group. The structure of this plateau is simple with very shallow dips (Figs. 7b, and 10). Open, map-scale folding is only present near its northern end, apparently in continuity with the southern termination of the northeast-plunging Guaduas syncline.

This plateau is bounded to the southeast by the east-verging Cotomal fault (Fig. 11). From south to north, the trace of this fault shifts trend from northeast to north-south and again to northeast, merging at the northeast end of the study area with the Santuario, Luní, and Cotomal faults, along the southeastern flank of the Guaduas syncline (Figs. 2, 5 and 6).

Changes in trend are also accompanied by changes in style: unlike other faults in the Piedras-Girardot foldbelt, the northeast-trending segment of the Cotomal fault (Fig. 6) separates strata belonging to the same stratigraphic unit, commonly the Oliní Group. Detailed geologic mapping demonstrates that the vertical separation along the northern, northeast-trending segment of this fault is only a few tens of meters (Figs. 6 and 11). The north-trending segment of this fault, although less well constrained by geologic mapping, separates older strata of the lower Villeta Group in the hanging wall from strata of the Oliní Group in the footwall, thereby defining a larger stratigraphic gap of at least 600 m. Because the hanging wall cutoff was removed by erosion in the north-trending segment of this fault, the fault slip along this segment could be large.



Figure 10: Nearly horizontal strata of the Oliní Group in the topographic domain of the plateau. Looking west.

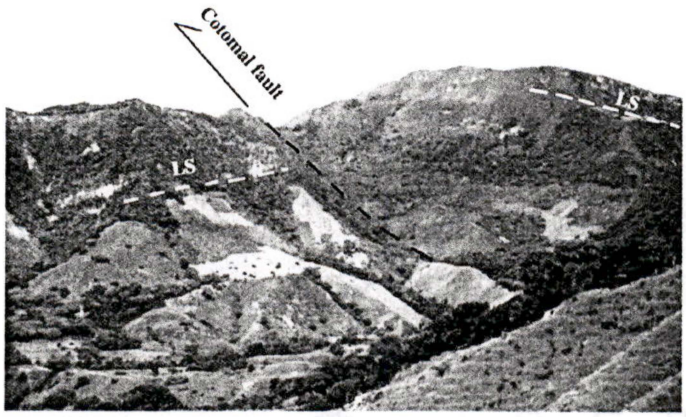


Figure 11: Cotomal fault in the eastern edge of the plateau (to the right). Deep canyons along the eastern side of the plateau expose the hanging wall and footwall cutoffs of this fault. Note that the cliff-forming unit (LS: Lidita Superior Formation) is offset against the fault in the footwall, and projections of the fault and same unit in the hanging wall intersect. Looking southwest.

Dip slopes and Hondita fault

Two southeast-dipping, remarkably uniform, map-scale dip slopes further characterize the Piedras-Girardot foldbelt. Strictly speaking, they are not monoclines, because they are in both cases demonstrably only one limb of a fold. Their surface expression, geometry, and location are remarkably different from other map-scale structures in the area mapped.

Northwest of the Camaito fault, a 10 km-long, 1 km wide dip slope gives rise to La Tabla Ridge (Figs. 3, 4a, 7c and 8), which is one of the most prominent topographic features of this foldbelt, exposing the entire Cretaceous stratigraphic sequence along its northwestern flank (Fig. 4). This southeast-dipping ridge is the southeastern flank of the open asymmetric Doima anticline, whose northwestern limb is poorly exposed as it is partially buried beneath younger volcanoclastic sediments of the Ibagué fan. Unfortunately, erosion of the Ibagué fan has opened only a small inlier through which the northwestern limb of this anticline and the Hondita fault can be studied (Fig. 5).

The northwest-verging Hondita fault constitutes the northwesternmost extension of thrusting in the Piedras-Girardot foldbelt, and has numerous and prolific oil seeps along its exposed length. This fault places the oldest exposed stratigraphic unit of the Piedras-Girardot foldbelt, the lower part of the Villeta Group, onto Miocene strata.

Immediately south of the southern termination of La Tabla Ridge, the hinge of the anticline in the hanging wall of the Hondita fault turns southeast, and then turns back to a northeastern trend over a distance of about 4 km. The southern segment of this anticline (Doima anticline), unlike its northern segment, is a tight upright fold with both limbs well exposed, and strata as old as the Oliní Group in its core (Fig. 5). Further south, this fold turns to a more northerly trend.

Southeast of the Cotomal fault, the northwestern flanks of the La Vega-Vindí (Fig. 12) and

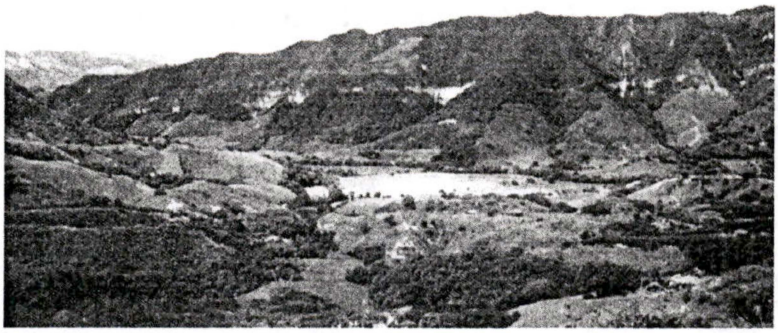


Figure 12: Gently southeast-dipping strata (to the left) in the western flank of the La Vega-Vindí synclines. Looking south.

Nariño synclines also stand out because of their uniformity, and similarity to the dip slope along La Tabla Ridge. These dip slopes, however, have gentler dips and more variable trends than in La Tabla Ridge. These gently dipping slopes are only present immediately southeast (footwall) of the northeast-trending segments of the Cotomal fault. East of the north-trending segment of the Cotomal fault this characteristic topographic expression is lost as strata dip more steeply.

Normal faults

The only east-west trending structures mapped in the entire area of the Piedras-Girardot foldbelt are north-dipping normal faults, separating upper Cretaceous strata in the footwall from poorly exposed Paleogene strata in the hanging wall. Alluvial fans and other recent deposits commonly conceal these structures, except along the north- and northwest-facing sides of the north-facing, topographic front in the northernmost part of the study area (Figs. 5 and 13a), and along streams draining the plateau to the north (Fig. 13b). A conspicuous fault breccia with up to brick-sized, angular fragments of mostly chert has developed along these faults (Fig 13 c). This breccia helped locate the fault trace not only along the east-west trending segment of the Luní fault, but also further east, as the Cotomal, Camaito and

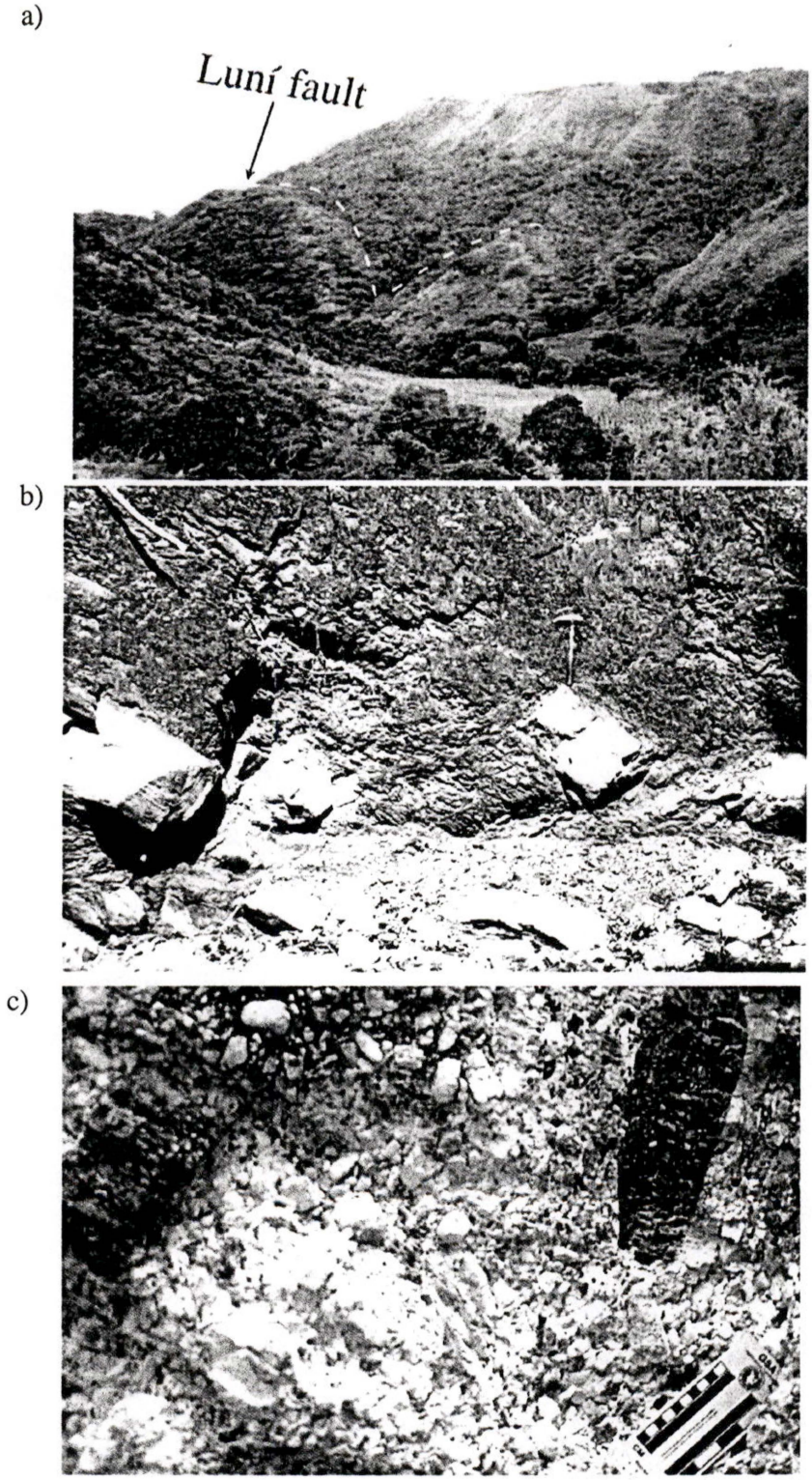


Figure 13: Normal faults in the Piedras-Girardot foldbelt. a) Map-scale expression of the Luní fault; b) Thick micrite layer offset by normal faults. Hammer is approximately 41 cm long; c) characteristic fault breccia developed along normal faults.

Santuario faults merge with the Luní fault, and turn to the northeast along the eastern limb of the Guaduas syncline.

These normal faults not only separate the Cretaceous from the Tertiary sequence, but also split the southernmost nose of the northeast-plunging Guaduas syncline into a northern block exposing only Paleogene strata (Fig. 14), and a southernmost tip exposing only Cretaceous strata (Figs. 5 and 6).

In summary, south of the Ibagué fault, a complex array of faults and folds exists: northwest- and west-verging thrust faults (Hondita and Camaito faults), north- and northeast-verging normal faults (Luní fault), and southeast-verging thrust faults (Cotomal fault), and northeast-trending tight folds. A positive flower structure is delineated by opposite-verging thrust faults (Camaito and Santuario faults) at the topographic culmination of this foldbelt. Changes in structural trends delineate a sigmoidal sinistral stepover, with faults verging outwardly in opposite directions.

Tectonic transport, shortening, and piercing points

The tectonic transport direction for structures of the Piedras-Girardot foldbelt cannot simply be assumed to be perpendicular to structural trends because of the dramatic changes in

Figure 14: Southern end of the northeast-trending Guaduas syncline. Looking northeast.



structural trends, and because of the concern about non-plane strain. A weak to moderate cleavage present within the Cretaceous sequence records only minor shortening and predates significant movement along the map-scale faults (Montes and Hatcher, in preparation), therefore it does not provide kinematic data to help decipher later thrusting.

Late Cretaceous syntectonic sedimentation, although only recording small amounts of fault movement, provides a crucial element for constraining the two- and three-dimensional reconstructions of this foldbelt. Mild deformation during the Campanian led to the development of gentle domes where the accumulation of some sandy units did not occur. These pinchouts constitute an excellent piercing point to determine the amount of strike-slip motion along faults because they define a mappable line in map-view. If this line is found on both sides of a fault, the horizontal separation along the fault can be measured.

The sandy member of the Nivel Intermedio of the Oliní Group (Fig. 4) pinches out across the Cotomal and Camaito faults providing one such kinematic marker. The two pinchouts mapped across the Cotomal fault (labeled 2 and 3 in Fig. 5 and 6) are equivalent because in both cases this unit thins out to the south. These pinchouts are offset 8 km across the fault, documenting a right-lateral separation that occurred since the accumulation of this unit (early Campanian).

Even though the distance measured between the two pinchouts provides the amount of horizontal separation, the direction and total amount of slip is not constrained because this piercing point is a line in a map. Independent evidence for the slip is derived from the observation that hanging wall and footwall cutoffs along the northern, northeast-trending segment of this fault record only small amounts of vertical separation (Figs. 6 and 11). Therefore, the direction of this 8 km of rigid-body motion must be laterally to the northeast, with very little contraction in a northwest-southeast direction.

An additional piercing point (labeled 4 in Fig. 5) helps determine the approximate extent of the area where no accumulation took place, because unlike the other two pinchouts, this one thins out to the north, thus defining a point along the southern boundary of the area where the accumulation of sand did not occur.

DISCUSSION

Two-dimensional interpretation and cross section construction

The structures described above were projected to depth in a suite of eight cross sections using Geosec 2D® (Fig. 15). Section locations coincide with industry seismic lines in the southern half of the study area (sections E-E' to H-H'), or cross parts of the map containing abundant field data in the northern half (sections A-A' to D-D'). Three basic assumptions guided the cross-section construction process: 1) a local detachment level runs along the weak Hondita Formation shale; 2) subsurface ramps are manifested in the surface as gently southeast-dipping monoclines, and 3) the stratigraphic column is a valid and uniform template with variations in thickness only in the case of syntectonic deposits.

Construction of the cross sections relied on the projection of strike and dip data and stratigraphic contacts from a three-dimensional space (defined in the geologic database) into a two-dimensional space defined by the vertical plane of the cross section. Wherever conflicting data were projected into a single point or area of the cross section, a hierarchy was established to consistently give priority to data types. In order of priority: 1) exactly located contacts in the geologic map; 2) thickness of stratigraphic unit; 3) dips projected from the map and wells; 4) seismic reflectors converted to depth; 5) approximately located or concealed geologic contacts. Additional constraints that were considered during cross section construction include the need to keep the geometry of folds and faults consistent between sections, and the need to honor kinematic data from the analysis of pinchouts

Figure 15: Serial cross sections of the Piedras-Girardot foldbelt. Caf: Camaito fault; Sf: Santuario fault; Cof: Cotomal fault; Ns: Nariño syncline; Da: Doima anticline; Gs: Gualanday syncline; Oa: Ocusa anticline; Vs: Vindí syncline; Hf: Hondita fault; IF: Ibagué fault. See Figure 5 for location.

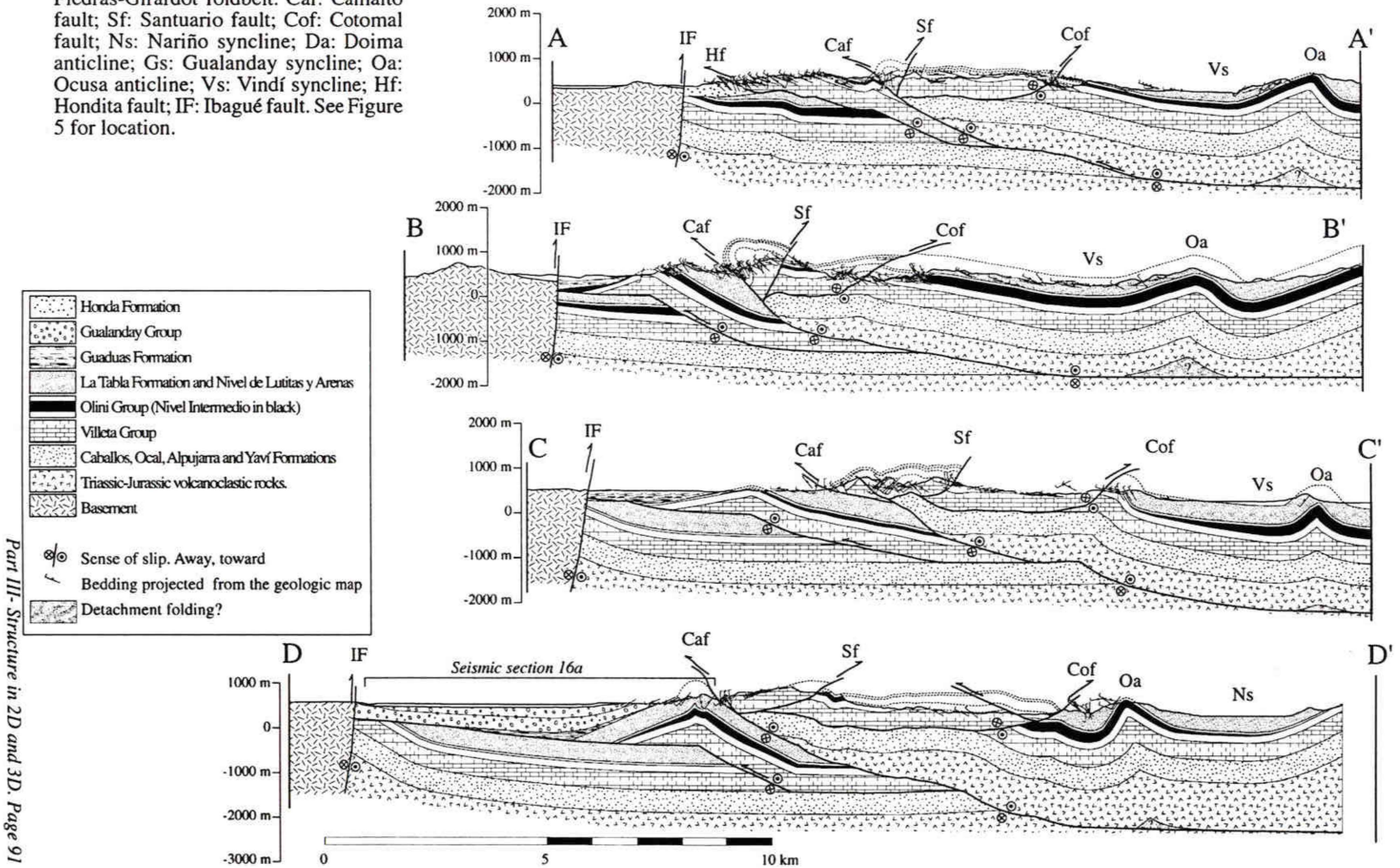
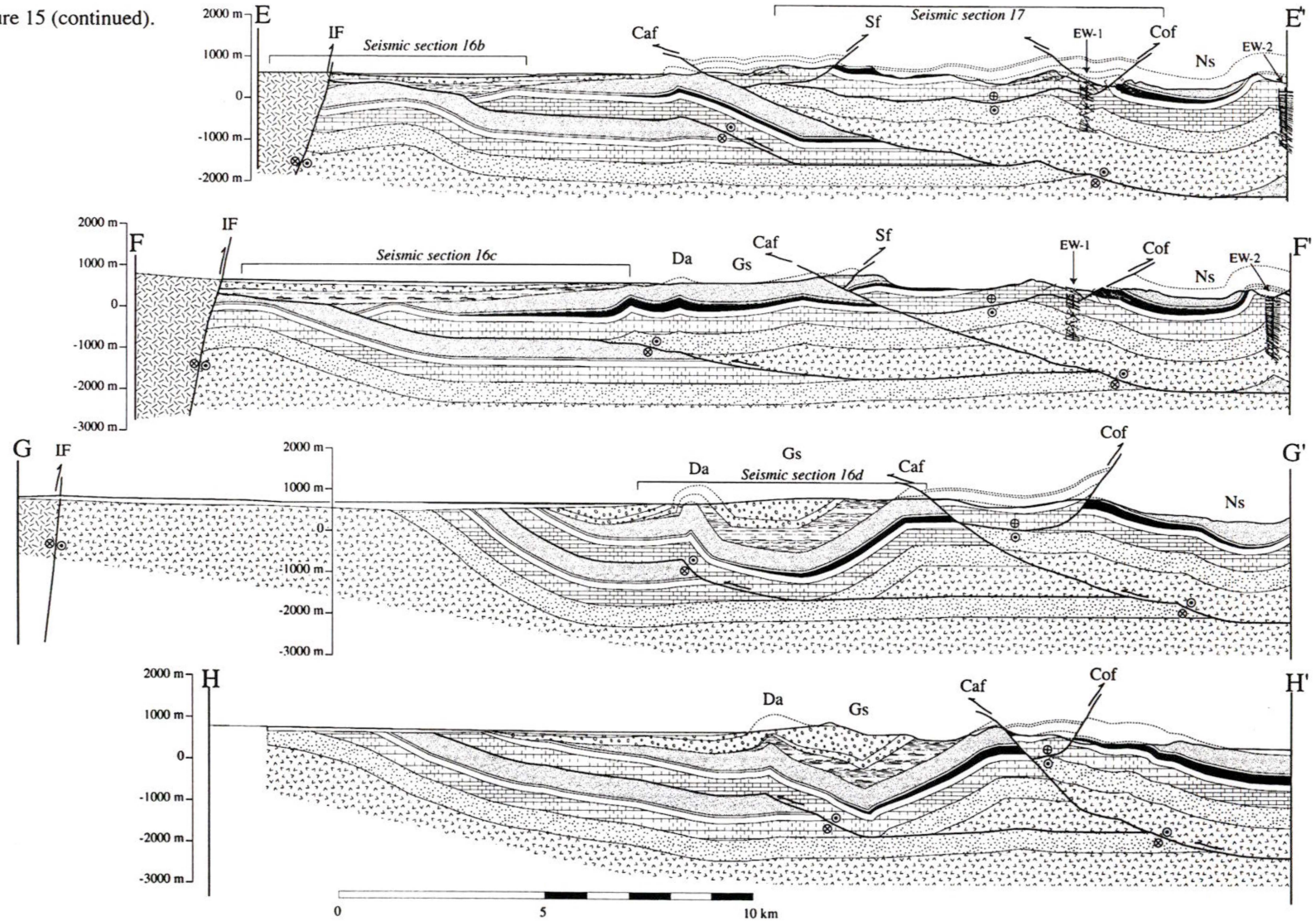


Figure 15 (continued).



regarding directions of tectonic transport, and syntectonic data regarding timing of deformation.

Seismic lines were converted to depth using migration velocity analysis checked against two exploration wells. These reflectors were then cross-referenced between lines using strike lines and exploration wells. Subsurface information was incorporated where it was supported by the geologic map (Fig. 16). Seismic acquisition in the mountainous regions of the Andes is notoriously difficult, often resulting in poorly imaged structures and noisy records. This problem is evident in the rugged terrain of the Piedras-Girardot foldbelt where seismic reflectors in some cases obviously contradict field mapping. Nonetheless, surface mapping in rolling hills (such as the plateau) agreed well with reflectors imaged in seismic lines. Thus, only the seismic reflectors acquired in the nearly flat Ibagué fan and in the plateau were projected into the cross sections or used to interpret deep structure.

Hondita fault and depth to detachment

The oldest stratigraphic unit exposed in the Piedras-Girardot foldbelt is the shaly lower part of the Villeta Group. This unit is also the lowermost stratigraphic unit exposed at the base of thrust sheets (Hondita fault near Piedras, Fig. 5, cross section A-A', Fig. 15). The unit immediately below the base of the Villeta Group is the Caballos Formation, a thick, massive quartz sandstone that is exposed south of the Piedras-Girardot foldbelt (Raasveldt, 1956) resting in angular unconformity on Triassic-Jurassic volcanoclastic rocks. The absence of this sandy unit in the study area has been previously interpreted to reflect the northernmost progradation of this sandstone during the Albian relative sea-level drop (Schamel, 1991; Etayo Serna, 1994).

It is more likely, however, that a detachment level utilizes the shale along the base of the Villeta Group (Lower Hondita Fm., Fig. 4b). If the only reason for the absence of the Caballos

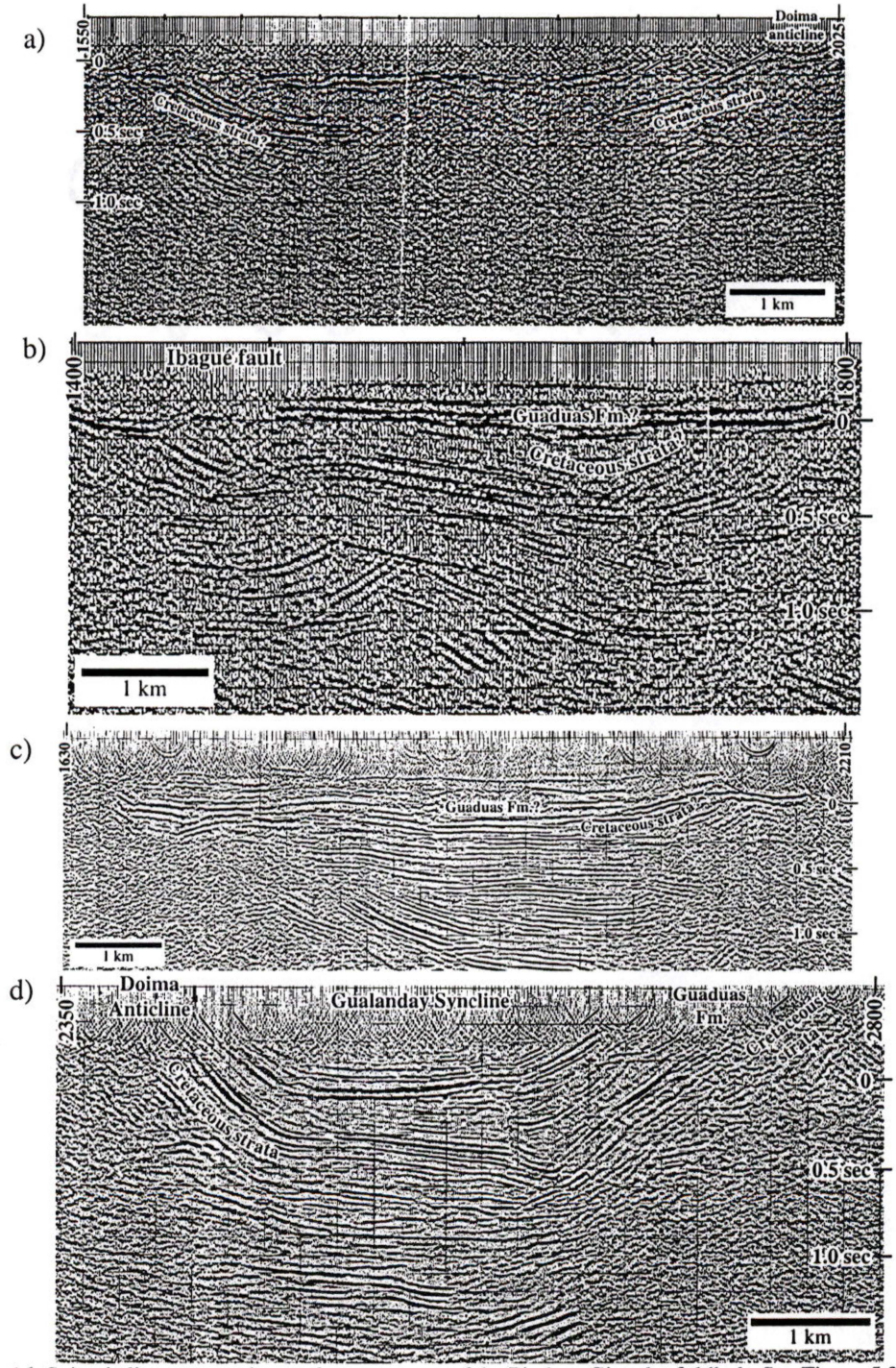


Figure 16: Seismic lines across the southwestern part of the Piedras-Girardot foldbelt. See Figure 5 for location. a) Cretaceous strata offset by Paleogene deposits. Compare with section D-D'. b) Cretaceous strata offset along the base of the Guaduas Formation Note that even though this line crosses the trace of the Ibagué fault, very little contrast exists on both sides of this steep fault. Compare with cross section E-E'. c) Cretaceous strata offset along the base of the Guaduas Formation. Compare with the western half of cross section F-F'; also note the deep reflectors imaged in this section probably corresponding to a repetition of the Cretaceous sequence below the Hondita fault. d) Spectacular growth strata in the core of the Gualanday syncline. Note the dramatic thickness changes in the Guaduas Formation. Compare with cross section G-G'.

Formation in the study area is stratigraphic, lower units, or even basement, would be exposed in the hanging wall of faults. They are not; thus Cretaceous and Tertiary strata are detached at this level. The black shale of the Hondita Formation, and equivalent units of the lower part of the Villeta Group, constitute the lowest continuous weak unit in the stratigraphic sequence of this part of the northern Andes. These units are commonly composed of black shale that accumulated as a result of the first widespread relative sea-level rise during the Turonian (Etayo Serna, 1994). Weak units stratigraphically below the Hondita Formation (Fig. 4b) such as the Ocal Formation (Florez and Carrillo, 1994), are characteristically discontinuous, and probably would not constitute an efficient detachment level.

The thickness of the Hondita thrust sheet above the Hondita detachment could only be measured where the Hondita fault reaches the surface near Piedras (Fig. 5, and cross section A-A' in Fig. 15). If the detachment remains at the same stratigraphic level to the south, the thickness of the thrust sheet can be calculated, along with the dip, and location of the footwall ramp in cross sections B-B' to D-D' (Fig. 15). Although the surface expression of the footwall ramp of the Hondita fault, which is La Tabla Ridge, is lost in the southern half of the study area, the eastern limb of the Doima anticline was still used to extrapolate the location of the footwall ramp (sections G-G' and H-H' in Fig. 15), while including the stratigraphic thickness changes of the Guaduas Formation and Gualanday Group (Fig. 16d). The presence of deep seismic reflectors (> 1 sec., approximately 3000 m, Fig. 16) in the western halves of sections E-E' to H-H', suggests that repetition of Cretaceous strata occurs in continuity with the Hondita fault to the north. So, even though this fault is not exposed, its presence in the subsurface of the Piedras-Girardot foldbelt is confirmed by deep seismic reflectors, and by syntectonic strata (Gualanday syncline), folded and transported by an intra-Cretaceous detachment, most likely the Hondita fault.

This interpretation indicates that the Hondita thrust sheet consists exclusively of Cretaceous

cover rocks in the northern and middle parts of the foldbelt (cross sections A-A' to E-E' in Fig. 15), whereas it involves lower parts of the stratigraphic sequence (possibly Triassic-Jurassic volcanoclastic rocks) in the southern end of the foldbelt (cross sections F-F' to H-H' in Fig. 15). Involvement of older stratigraphic units in the southernmost sections was included because seismic lines (Fig. 16d and easternmost part of 16c) show a relatively silent zone at shallow levels (approximately 0.5 secs) below the Cretaceous strata in the eastern limb of the Gualanday syncline. This zone was interpreted to correspond to Triassic-Jurassic volcanoclastic rocks in the hanging wall of the Hondita fault because Cretaceous and Tertiary reflectors are characteristically strong.

Although the Triassic-Jurassic volcanoclastic sequence may contain sporadic shale layers (Cediel *et al.*, 1981; Bayona *et al.*, 1994), it is a relatively strong sequence that has been interpreted to be part of the mechanical basement for the Cenozoic deformation (Andean phase of deformation). Nonetheless, the presence of basement-cored detached folds indicate that this part of the upper mechanical basement of Triassic-Jurassic volcanoclastic rocks is detached. A similar behavior was proposed further south, to explain asymmetric paired synclines and basement-cored anticlines (Schamel, 1991), although the depth to detachment proposed in his model was much deeper (middle crustal levels).

In the Piedras-Girardot foldbelt, not only the Hondita thrust sheet contains the upper part (approximately 1000 m) of the mechanical basement, but also the Camaito thrust sheet carries this part of the sequence as (e.g. wells EW1 and EW2 in cross sections E-E', and F-F' in Fig, 15). The thickness of the Camaito thrust sheet was calculated by projecting to depth the western limbs of the La Vega-Vindí and Nariño synclines until they intersected the Hondita fault. The projection of this thrust sheet underneath the axis of the synclines defines the depth to this detachment that cuts across the remaining Cretaceous sedimentary sequence (Caballos Formation) into the upper part of the Triassic-Jurassic volcanoclastic

sequence. Thus, the footwall of the Hondita fault defines a ramp-flat-ramp geometry that cuts across the upper part of the Cretaceous sequence, remains parallel to the base of the Hondita Formation along the detachment, and dips across the remaining Cretaceous sequence into a flat in Triassic-Jurassic basement.

A piercing point along the northern, northeast-trending segment of the Cotomal fault documents 8 km of right-lateral northeast-southwest displacement, with a small vertical component. The middle segment of this fault, however, trends to the north, and would be expected to have a much larger dip-slip displacement for the same northeast-trending slip vector. This north-trending segment would accommodate 8 km of NE-SW convergence, but only exposes the lower part of the Villeta Group in the hanging wall (cross sections C-C', D-D', E-E' in Fig. 15). If the Cotomal fault did not root at the weak shale of the base of the Villeta Group, the 8 km of northeast-southwest contraction should bring the basement to the surface. The geologic map (Fig. 5) shows that this is not the case. Therefore, the Cotomal fault is interpreted to root at the base of the Villeta Group separating the Villeta Group and younger units in the hanging wall from the Caballos Formation and older units in the footwall. The Cretaceous sequence below the Caballos Formation and the upper part of the mechanical basement thus define a tectonic wedge bounded above and below by thrust faults of opposite vergence (tectonic delamination, Price 1986). Delamination is also supported by seismic reflectors that allow tracing of the Cotomal fault beneath the plateau along the base of the Villeta Group (Fig. 17).

Given the interpretation of the Cotomal fault as a roof to the tectonic wedge above the Camaito fault, and the fact that the Cotomal fault has significant dextral offset, it seems appropriate to test whether restoration of the cross sections by removing simple convergence is viable (e.g. Elliot, 1983). Three cross sections were selected to attempt this plane-strain restoration (Figs. 15 and 18). Examining the equal-area restorations, large area deficiencies

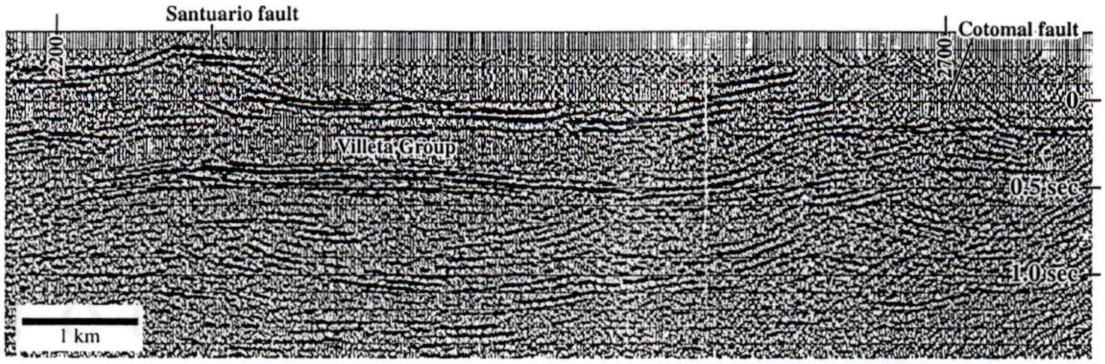


Figure 17: Seismic line across the southern part of the plateau. Note how the base of the Villeta Group is apparently detached along the east-verging Cotomal fault. See Figure 5 for location.

below the lower part of the Villeta Group are evident and cannot be solved while honoring available data and performing a plane-strain restoration. This exercise, in addition to identifying non-plane strain by map-scale structures in the Piedras-Girardot foldbelt, sets the foundation of the technique developed to attempt a three-dimensional reconstruction of the Piedras-Girardot foldbelt.

In summary, the Camaito thrust sheet obliquely transported the entire Cretaceous sequence and a portion of basement to the southwest over an irregularly shaped ramp-flat-ramp surface of the Hondita fault (Fig 19a). The emplacement of the Camaito thrust sheet was accommodated by two elements (Figs. 15, 19 and 20): tectonic wedging with the Cotomal fault as a root that has significant dextral offset (Figs. 15 and 19b); and development of a positive flower structure betweeen the Camaito and Santuario faults at the tip of the wedge (Figs. 15, 19b and 19c).

THREE-DIMENSIONAL MODEL

One goal of this investigation is to build a three-dimensional model of a set of deformed strata in a foldbelt characterized by non-plane strain (Fig 20). Following the example of the two-dimensional approach (Dahlstrom, 1969; Elliot, 1983), the model must contain the

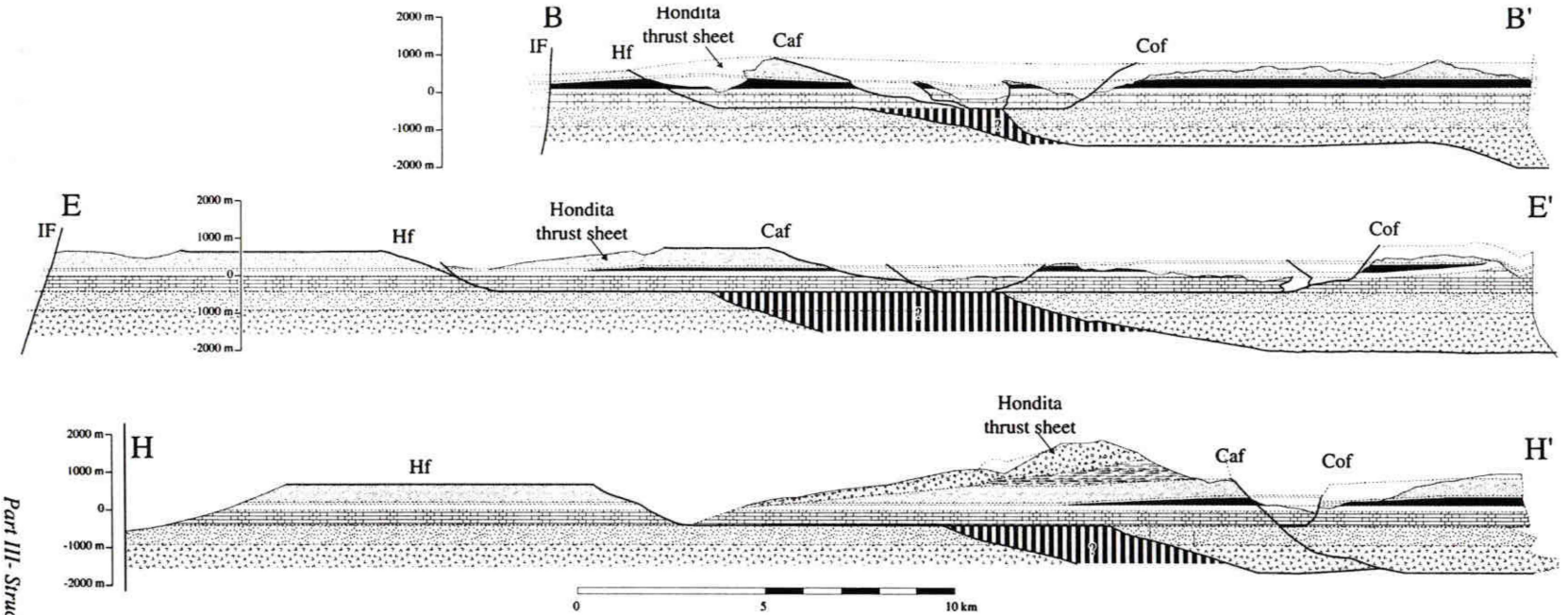


Figure 18: Failed restoration attempt of three of the cross sections in the Piedras-Girardot foldbelt. Note the significant deficiency of subdetachment area in all cross sections (vertical pattern). All symbols and patterns as in Figure 15.

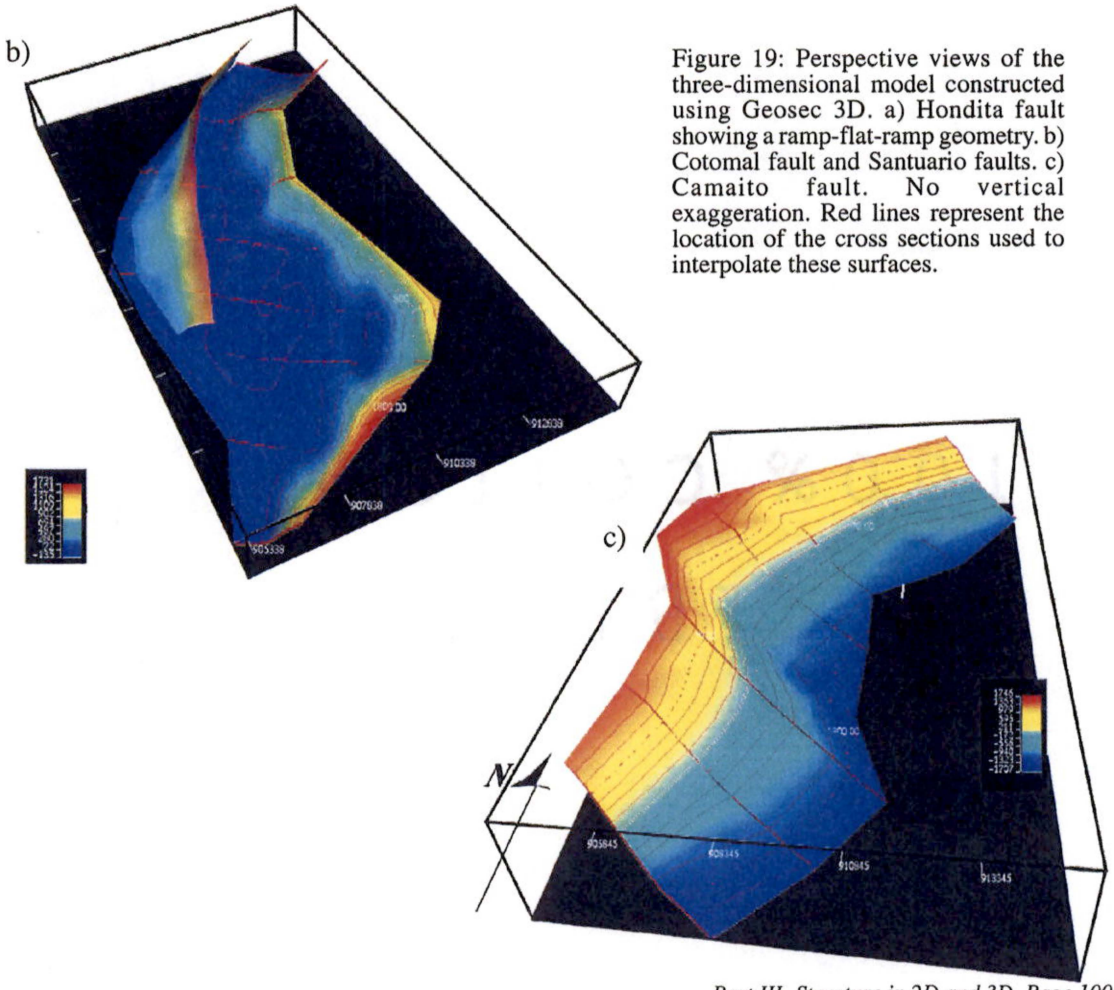


Figure 19: Perspective views of the three-dimensional model constructed using Geosec 3D. a) Hondita fault showing a ramp-flat-ramp geometry. b) Cotomal fault and Santuario faults. c) Camaito fault. No vertical exaggeration. Red lines represent the location of the cross sections used to interpolate these surfaces.

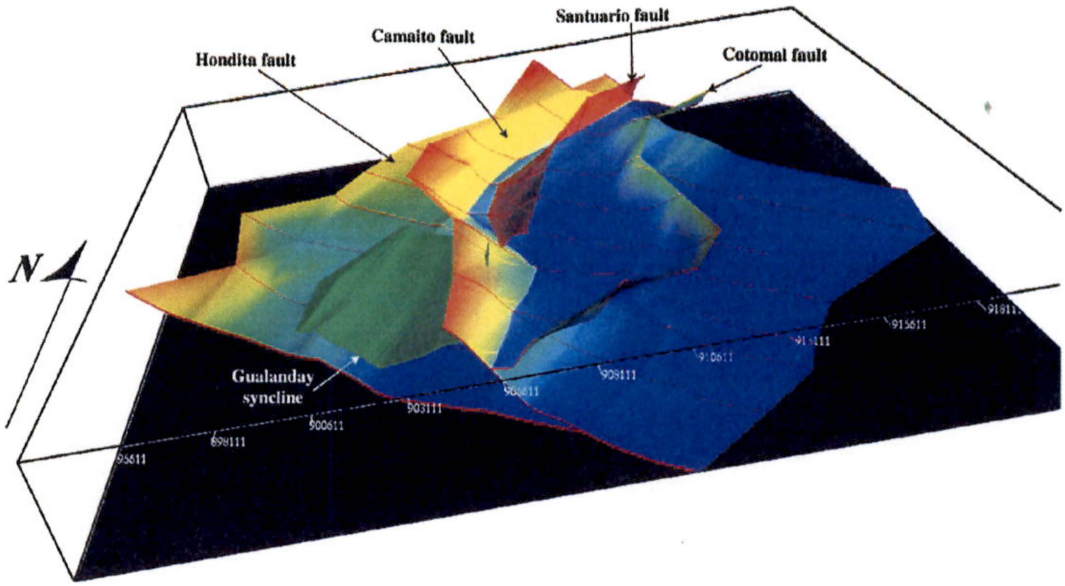


Figure 20: Perspective view of the three-dimensional model with the major faults of the Piedras-Girardot foldbelt. Color shading is different for each surface, and it was added only for clarity.

same amount of mass before and after deformation. While such a model is not necessarily uniquely correct, it is viable and has a better chance of being correct. Verification of the admissibility of the model, however, is obtained if the structural style portrayed in the model resembles natural structures in the geologic map. This type of verification is subjective, and laden with inferences. Because it is impossible to completely define an open natural system, it is equally impossible to quantitatively verify the admissibility or degree or correlation of a model (Oreskes *et al.*, 1994). Therefore, the value of a model does not lie in its numerical accuracy or degree of success at reproducing a given geometry or process, but in its ability to offer additional evidence to corroborate or challenge existing ideas. Geometric verification of viability using constant volume only demonstrates that the model is internally consistent.

Following this approach, the two- and three-dimensional models presented in the following sections simply attempt to demonstrate the viability of transpressional deformation in the northern Andes, a region where the contribution of strike-slip has been traditionally ignored.

Palinspastic restoration

Cross sections can be balanced where plane strain can be safely assumed and the lengths of hanging wall and footwall blocks match before and after deformation. In the Piedras-Girardot foldbelt, however, material moves in and out of the plane of the section as a result of displacements oblique or parallel to the structural trend (Fig 18). Nonetheless, the cross sections presented in this paper (Fig. 15) contain valuable information regarding the three-dimensional structure of this foldbelt; particularly the location of hanging wall and footwall cutoffs. These cutoffs were used to quantify the original shapes of individual thrust sheets by restoring the top of the Villeta Group to a horizontal position in all cross sections using local pin lines fixed in space for each thrust sheet.

Restoration of the top of the Villeta Group for each thrust sheet (Figs. 21a to 21d) reveals the initial geometric configuration of each thrust sheet assuming little internal distortion during transport. This restoration does not assume that the blocks restore along the cross section lines, instead they can be transported along the strike to achieve a better fit, like the pieces of a puzzle. Two of the pieces of this puzzle, however, contain a piercing point that constrains their initial positions relative to each other (blocks III and IV in Fig. 21e).

The direction and amount of displacement documented by the piercing point was used to propose a kinematic scheme where individual thrust sheets can be displaced along ENE trends, nearly parallel to the Ibagué fault until the restored top of the Villeta Group achieves a geometric fit with neighboring blocks. The resulting palinspastic restoration requires approximately 52% ENE contraction, not including the Ibagué fault. The best geometric fit is obtained if blocks III and IV are rotated clockwise 7 and 13 degrees respectively. Approximately 17 km of ENE contraction are telescoped to the ENE in the Hondita fault, approximately 7 km in the Camaito fault, and approximately 8 in the Cotomal fault.

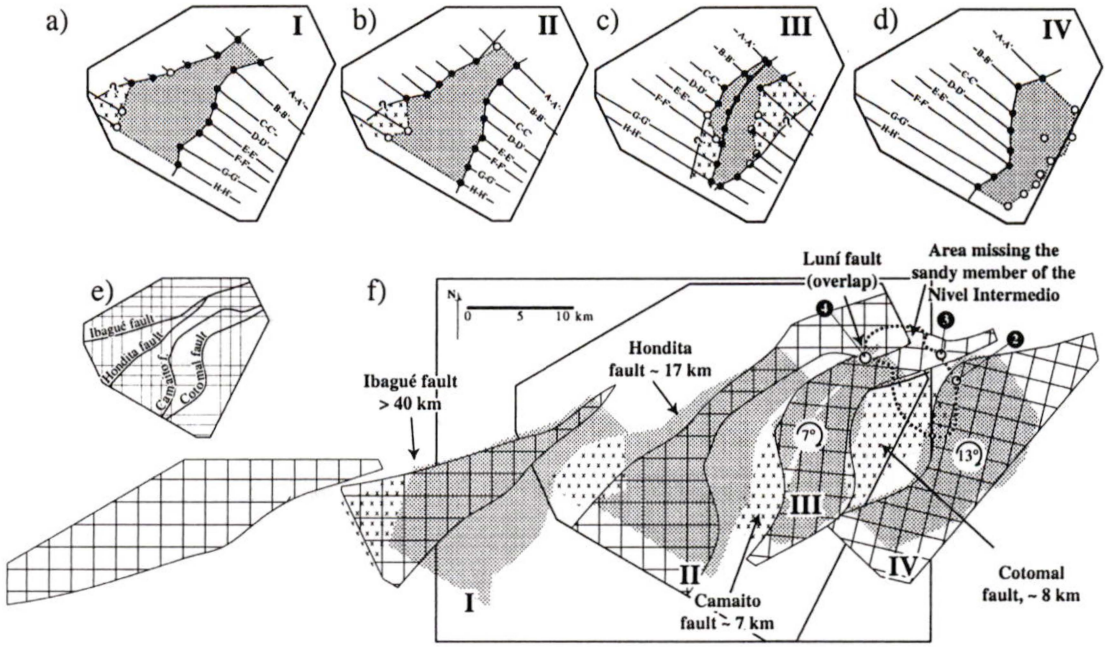


Figure 21: Palinspastic reconstruction of the top of the Villeta Group (pattern) in the Piedras-Girardot foldbelt. Black dots along cross section lines represent mapped or inferred hanging wall cutoff. White dot or half-white dot represents a cutoff either removed by erosion, or uncertain. Areas filled with a pattern of crosses indicates probable extension of top of the Villeta. a) Restored lengths in the footwall of the Hondita fault. Ibagué fault was used as pin line; b) restored lengths in the Hondita thrust sheet. An arbitrary pin line was chosen; c) restored lengths in the plateau (Camaito and Cotomal hanging walls); d) restored lengths in the footwall of the Cotomal fault. Hinge of the la Vega-Vindí and Nariño synclines used as pin lines; e) present-day configuration of the Piedras-Girardot foldbelt showing only first-order map structures; f) geometrically acceptable fit of the thrust sheets in the Piedras-Girardot foldbelt based on the piercing point.

RESULTS

Altogether, the Hondita, Cotomal, Camaito and Luní faults form a classic example of a dextral strike-slip system with a step-over to the left (Fig. 22), where contraction is accommodated along north- and northwest-trending segments of the Cotomal and Camaito faults, dextral strike-slip along their northeast-trending segments, and extension along the north-trending Luní fault. The Hondita fault represents the master fault in this foldbelt transporting the entire Mesozoic sequence and basement along a winding ramp-flat-ramp geometry. The direction of tectonic transport is demonstrably ENE-WSW, approximately parallel to the trace of the Ibagué fault. A palinspastic restoration of this foldbelt requires approximately 52% ENE contraction (about 40 km), not including the Ibagué fault. A

geometric fit constrained with a stratigraphic piercing point also requires clockwise rotation of the easternmost two thrust sheets 7 and 13 degrees. Approximately 17 km of contraction are telescoped to the ENE in the Hondita fault, approximately 7 km in the Camaito fault, and approximately 8 in the Cotomal fault. Syntectonic sedimentation dates these map-scale movements to the Early Paleogene, during the accummulation of the Guaduas Formation and part of the Gualanday Group.

The total amount of contraction calculated from the palinspastic restoration in the Piedras-Girardot, about 40 km, is similar to the minimum slip inferred along the Ibagué fault. The Ibagué fault has not been mapped east of Piedras, and it must transfer its slip to another fault system. Since the amounts and direction of contraction are compatible, it is proposed here that the Ibagué fault transfers its slip to the Piedras-Girardot foldbelt where it is solved in a transpressional system. The mechanisms for this transfer zone, however, cannot be defined at this time and require further study.

The northeastern projection of the dextral shear couple defined in this paper (Fig. 22) directly contradicts previous interpretations of the local and regional structures. This projection

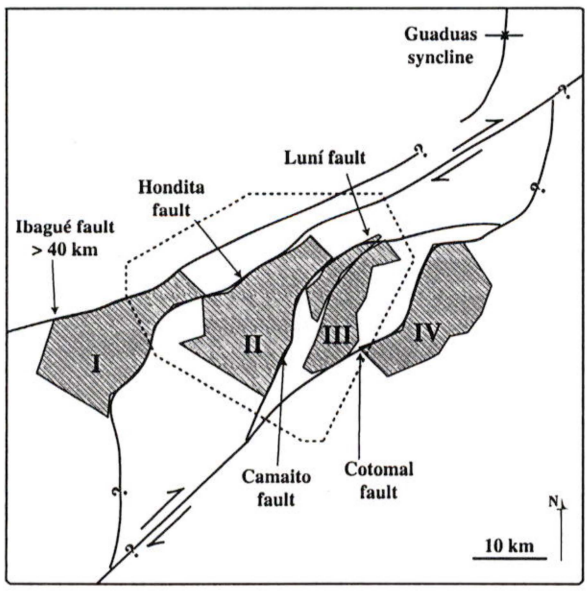


Figure 22: Simplified palinspastic geometry of the Piedras-Girardot foldbelt. Map view of this dextral strike-slip shear zone stepping over to the left defining a zone of transpressional deformation that projects northeast into the southern extension of the Guaduas syncline where only contractional had been interpreted.

intersects the southern axial trace of the Guaduas syncline immediately northeast of the Piedrass-Girardot foldbelt. The Bituima fault system bounds Guaduas syncline to the east (Fig. 2), and has been interpreted to accommodate only contractional deformation perpendicular to the structural trend (Namson *et al.*, 1994). Similarly, regional reconstructions of the Cordillera Oriental (Colleta *et al.*, 1990; Dengo and Covey, 1993; Cooper *et al.*, 1995; Roeder and Chamberlain, 1995) propose that this fault system, or equivalent west- or northwest-verging faults, accommodate large amounts of contractional deformation. A more comprehensive study of the effects of transpressional deformation are necessary for thrust structures in the Cordillera Oriental. The role of strike-slip related deformation in this thrust system is at least locally significant and must be incorporated in regional models of deformation in the northern Andes.

REFERENCES

Audemard, M. F. A., 2001, Quaternary tectonics and present stress tensor of the inverted northern Falcon Basin, northwestern Venezuela: Journal of Structural Geology, v. 23, p. 431-453.

Barrero, D., Alvarez, J., and Kassem, T., 1969, Actividad ígnea y tectónica en la Cordillera Central durante el Meso-Cenozoico: Boletín Geológico del Ingeominas, v. XVII, p. 145-173.

Barrero, D., and Vesga, C., 1976, Mapa geológico del cuadrángulo K-9 Armero y parte sur del J-9 La Dorada: Ingeominas, scale 1:100,000.

Bayona, G., García, D. F., and Mora, G., 1994, La Formación Sandaña: Producto de la actividad de estratovolcanes continentales en un dominio de retroarco, in Etayo Serna, F., ed., Estudios Geológicos del Valle Superior del Magdalena: Bogotá, ECOPETROL, p. I.1-I.21.

Burke, K., Fox, P. J., and Sengör, A. M. C., 1978, Buoyant ocean floor and the evolution of the Caribbean: Journal of Geophysical Research, v. 83, p. 3949-3954.

Casas, A. M., Gapais, D., Nalpas, T., Besnard, K., and Roman, B. T., 2001, Analogue models of transpressive systems: Journal of Structural Geology, v. 23, p. 733-743.

Case, J. E., Duran, S. L. G., Lopez, R. A., and Moore, W. R., 1971, Tectonic investigations in western Colombia and eastern Panama: Geological Society of America Bulletin, v. 82, p. 2685-2712.

Case, J. E., and MacDonald, W. D., 1973, Regional gravity anomalies and crustal structure in Northern Colombia: Geological Society of America Bulletin, v. 84, p. 2905-2916.

Cediel, F., and Cáceres, C., 1988, Geologic map of Colombia: Geotec Editions, scale 1:2,000.000.

Cediel, F., Mojica, J., and Macía, C., 1981, Las formaciones Luisa, Payandé y Saldaña sus columnas estratigraficas características: Geología Norandina, v. 3, p. 11-19.

Colletta, B., Hebrard, F., Letouzey, J., Werner, P., and Rudkiewicz, J. L., 1990, Tectonic style and crustal structure of the Eastern Cordillera (Colombia) from a balanced cross-section, in Letouzey, and Jean, eds., Petroleum and tectonics in mobile belts: Paris, France, Ed. Technip, p. 81-100.

Cooper, M. A., Addison, F. T., Alvarez, R., Coral, M., Graham, R. H., Hayward, A. B., Howe, S., Martinez, J., Naar, J., Penas, R., Pulham, A. J., and Taborda, A., 1995, Basin development and tectonic history of the Llanos Basin, Eastern Cordillera, and middle Magdalena Valley, Colombia: AAPG Bulletin, v. 79, p. 1421-1443.

Dahlstrom, C. D. A., 1969, Balanced cross sections: Canadian Journal of Earth Sciences, v. 6, p. 743-757.

Dengo, C. A., and Covey, M. C., 1993, Structure of the Eastern Cordillera of Colombia: A tectonic model of the Colombian Andes: American Association of Petroleum Geologists Bulletin, v. 77, p. 1315-1337.

Diaz de Gamero, M. L., 1996, The changing course of the Orinoco River during the Neogene: a review: Palaeogeography, Palaeoclimatology, Palaeoecology, v. 123, p. 385-402.

Edgar, N. T., Ewing, J. I., and Hennion, J., 1971, Seismic refraction and reflection in Caribbean sea: The American Association of Petroleum Geologists Bulletin, v. 55, p. 833-870.

Elliot, D., 1983, The construction of balanced cross-sections: Journal of Structural Geology, v. 5, p. 101.

Etayo Serna, F., 1994, Epílogo: A modo de historia geológica del Cretácico del Valle Superior del Magdalena, in Etayo Serna, F., ed., Estudios Geológicos del Valle Superior del Magdalena: Bogotá, Universidad Nacional, ECOPETROL, p. XX.1-XX-5.

Etayo Serna, F., and 24 others, 1986, Mapa de terrenos geológicos de Colombia: Publicaciones Geológicas Especiales del Ingeominas, v. 14, p. 235.

Feininger, T., 1970, The Palestina fault, Colombia: Geological Society of America Bulletin, v. 81, p. 1201-1216.

Florez, M., and Carrillo, G. A., 1994, Estratigrafía de la sucesión litológica basal del Cretacico del valle superior del Magdalena, in Etayo Serna, F., ed., Estudios Geológicos del Valle Superior del Magdalena: Bogota, Colombia, ECOPETROL, p. II.1-II.26.

Freymueller, J. T., Kellogg, J. N., and Vega, V., 1993, Plate motions in the North Andean region: Journal of Geophysical Research, v. 98, p. 21,853-21,863.

Hubach, E., 1945, La formacion "Cáqueza," región de Cáqueza (oriente de Cundinamarca): Compilacion Estudios Geológicos Oficiales de Colombia, v. 6, p. 23-26.

Ingeominas, 1988, Mapa geológico de Colombia: Ingeominas, scale 1:1,500.000.

Kafka, A. L., and Weidner, D. J., 1981, Earthquake focal mechanisms and tectonic processes along the southern boundary of the Caribbean Plate: Journal of Geophysical Research, v. 86, p. 2877-2888.

Kammer, A., and Mojica, J., 1995, Los pliegues de la barrera Guataquí-Girardot: ¿Producto de un despegue de la cobertera Cretácica de la Cordillera Oriental?: Geologia Colombiana, v. 19, p. 33-43.

Kellogg, J., and Bonini, W. E., 1982, Subduction of the Caribbean Plate and basement uplifts in the overriding South American Plate: Tectonics, v. 1, p. 251-276.

Ladd, J. W., 1976, Relative motion of South America with respect to North America and Caribbean tectonics: Geological Society of America Bulletin, v. 87, p. 969-976.

Laubscher, H. P., 1987, The kinematic puzzle of the Neogene Northern Andes, in Schaer, J. P., and Rodgers, J., eds., The anatomy of mountain ranges.: Princeton, NJ, Princeton Univ. Press, p. 211-227.

Malfait, B. T., and Dinkelman, M. G., 1972, Circum-Caribbean Tectonic and Igneous Activity and the Evolution of the Caribbean Plate: Geological Society of America Bulletin, v. 83, p. 251-271.

Mann, P., Schubert, C., and Burke, K., 1990, Review of Caribbean neotectonics, in Dengo, G., and Case , J. E., eds., The Caribbean region.: Boulder, CO, United States, Geological Society of America, p. 307-338.
McClay, K., and Bonora, M., 2001, Analog models of restraining stepovers in strike-slip fault systems: AAPG Bulletin, v. 85, p. 233-260.
McCourt, W. J., Aspden, J. A., and Brook, M., 1984, New geological and geochronological data from the Colombian Andes; continental growth by multiple accretion: Journal of the Geological Society of London, v. 141, p. 831-845.
Montes, C., and Hatcher, R. D., Jr., in preparation, Migration of deformation in time and space in the Piedras-Girardot foldbelt, northern Andes.
Montes, C., Restrepo-Pace, P. A., and Hatcher, R. D., Jr., in preparation, Kinematics of the Piedras-Girardot foldbelt: Implications for the Ibagué transfer zone and the southern Caribbean plate boundary, in Blickwede, J., ed., The circum-Gulf of Mexico and Caribbean region: Plate tectonics, basin formation and hydrocarbon habitats, American Association of Petroleum Geologists.
Mosquera, D., Nuñez, A., and Vesga, C., 1982, Mapa geológico preliminar de la plancha 244 Ibagué: Ingeominas, scale 1:100,000.
Namson, J., Cunningham, R., and Woodcock, G., 1994, Structural geology and hydrocarbon potential of the northern part of the upper Magdalena Basin, Colombia, in AAPG annual convention., Tulsa, OK, United States, p. 221.
Oldow, J. S., Bally, A. W., and Ave, L. H. G., 1990, Transpression, orogenic float, and lithospheric balance: Geology, v. 18, p. 991-994.
Oreskes, N., Shrader-Frechette, K., and Belitz, K., 1994, Verification, validation, and confirmation of numerical models in the Earth Sciences: Science, v. 263, p. 641-646.
Pindell, J., and Dewey, J. F., 1982, Permo-Triassic reconstruction of western Pangea and the evolution of the Gulf of Mexico/ Caribbean region: Tectonics, v. 1, p. 179-211.
Pindell, J., L., 1993, Regional synopsis of Gulf of Mexico and Caribbean evolution: Proceedings of the GCSSEPM Foundation 13th Annual Research Conference, p. 251-274.
Pindell, J., L., and Barrett, S., F., 1990, Geological evolution of the Caribbean region; a plate tectonic perspective, in Dengo, G., and Case, J. E., eds., The Caribbean region.: Boulder, CO, United States, Geol. Soc. Am., p. 405-432.
Price, R. A., 1986, The southeastern Canadian Cordillera; thrust faulting, tectonic wedging, and delamination of the lithosphere: Journal of Structural Geology, v. 8, p. 239-254.
Raasveldt, H. C., 1956, Mapa geológico de la plancha L-9 Girardot: Servicio Geológico Nacional, scale 1:200,000.
Restrepo Pace, P. A., Colmenares, F., Higuera, C., Mayorga, M., and Leal, J., 1999, Fold and thrust belt along the western flank of the Eastern Cordillera of Colombia; style, kinematics and timing constraints derived from seismic data and detailed surface mapping, in AAPG international conference and exhibition; abstracts., Tulsa, OK, United States, p. 1336.
Roeder, D., and Chamberlain, R. L., 1995, Eastern Cordillera of Colombia; Jurassic-Neogene crustal evolution, in Tankard, A., J, Suárez Soruco, R., and Welsink, H., J., eds., Petroleum basins of South America.: AAPG Memoir: Tulsa, OK, United States, American Association of Petroleum Geologists, p. 633-645.
Rosencrantz, E., Ross, M. I., and Sclater, J. G., 1988, Age and spreading history of the Cayman Trough as determined from depth, heat flow, and magnetic anomalies: Journal of Geophysical Research, v. 93, p. 2141-2157.
Schamel, S., 1991, Middle and upper Magdalena basins, Colombia, in Biddle, K. T., ed., Active margin basins: AAPG Memoir: Tulsa, OK, United States, American Association of Petroleum Geologists, p. 283-301.
Schreurs, G., and Colletta, B., 1998, Analogue modelling of faulting in zones of continental transpression and transtension, in Holdsworth, E ; Strachan, and A ; Dewey, eds., Continental transpressional and transtensional tectonics.: Geological Society Special Publications: London, United Kingdom, Geological Society of London, p. 59-79.
Schubert, C., 1981, Are the Venezuelan fault systems part of the southern Caribbean plate boundary?: Geologische Rundschau, v. 70, p. 542-551.
Tellez, N. I., and Navas, G. J., 1962, Interferencia de direcciones en los pliegues cretacico-terciarios entre Coello y Gualanday: Boletin de Geologia (Bucaramanga), v. 9, p. 45-61.
Villamil, T., 1999, Campanian-Miocene tectonostratigraphy, depocenter evolution and basin development of Colombia and western Venezuela: Palaeogeography, Palaeoclimatology, Palaeoecology, v. 153, p. 239-275.
Westbrook, G. K., 1990, Gravity anomaly map of the Caribbean region, in Dengo, G., and Case , J. E., eds., The Caribbean region: Boulder, Colorado, Geological Society of America.
Zeil, W., 1979, The Andes, A geological review: Berlin-Sttutgart, Gëbruder Borntraeger, 260 p.

Appendices

Appendix I

Code

INTRODUCTION

This appendix contains the computer code written to manipulate digital data in the geologic database included in this dissertation. The code presented here constitutes a contribution to methodology to design georeferenced, two- and three-dimensional, geologic databases. The code mostly consists of highly customized solutions to very specific problems of data input into geosec 2D and 3D, and into ArcInfo. Computer code is also included to rotate fabric data (lines and planes), and ArcInfo macros designed to speed up time-consuming processing of data in the geologic database.

In some cases the solutions presented here are "hard coded", but abundant comments are provided so that changes can be easily made. This appendix is divided in three sections: C code (programs translator), Arc Macro Language (AML) code, and finally, detailed instructions to use the program Translator, as well as general instructions to perform complex tasks in ArcInfo and Imagine.

TRANSLATOR

This program was designed to facilitate transfer of information between Adobe Illustrator (versions 5.5 to 8.01) to Geosec 2D, Geosec 3D, and ArcInfo. This program is a simple command-line utility that extracts information from ascii Illustrator files (lines and text blocks), and writes the data in formats compatible with ArcInfo and Geosec. The main problem this program addresses is the difficulty to input data into Geosec and ArcInfo. Since the graphic interface of Illustrator is better suited for digitizing geologic maps, this program allows the user to compile a geologic map in Illustrator, and then transfer it to Geosec and ArcInfo.

This program has been successfully compiled for IRIX, Sun, Macintosh, and Linux systems. There are no limitations as to the size of the files to be converted, however, there are instances

when the Illustrator file format contains characters unrecognized by Translator. In such cases it is advisable to copy the information to be translated into a new file.

```
/*********************************************************/
/*
/*        TRANSLATOR MAIN PROGRAM
/*           Camilo Montes
/*         May/10/199
/*********************************************************/

#include <stdio.h>
#include <string.h>
#include <ctype.h>
#include <stdlib.h>

#define EOH 9999          /*data termination value*/
#define LINE 160          /* # of chars on a line   */

/* function  prototypes */
void print_intro();
void print_main_help();
void print_main_menu();
void print_settings (float, float, float, float, int, int, int, char);
void print_units (void);
void print_kind (void);
void unit_reader (int, char[]);
int kind_reader (char);
char char_user();
int names (char);
void avance (FILE *);
int reader (FILE *, FILE *, int, float, float, float, float, char);
char cleanup (char [], float *, float *, int *, float *, char);
void quit_cds();
void geosec_header_map (FILE *, int, int);
void geosec_header_cross (FILE *, int, int);

main()
{
int obj = 0;
char c = 'z';     /*this variable holds user's choice throughout the program*/

print_intro();                    /* gives user an introduction first time around*/
print_main_menu();
printf("\n\n your selection: ");
c = char_user();

while (c != 'q')
  {
        if  ((c == 'x') || (c == 'm') || (c == 't') || (c == 'g') || (c == 'b') || (c == 'h') || (c == 'j') || (c == 'l'))
        {
          obj = names (c); /*File opening, settings update.*/
    printf ("\n%d objects were detected and written to output file\n", obj);
    print_main_menu();/*again*/
          printf("\n\n your selection: ");
          c = char_user();
    }
  else
        {
        printf("%c is not a valid request.\n", c);
```

```
                printf("\n\n your selection: ");
                c = char_user();
        }

        }
if (c == 'q')
        quit_cds();

return;

}  /*End of main

/*-------------------------------------------------------------------/
/* Get a line but only return the first character entered*/
/* This makes the program more robust and removes the   */
/* need to call getchar twice (once for the desired     */
/* character and once to remove the newline             */
/*-------------------------------------------------------------------*/

char char_user()
{
 char tmp[LINE];
 gets(tmp);
 return(tmp[0]);  /* return first character entered */
}
/*-------------------------------------------------------------------*/
void print_main_menu()
{
 puts("\n");
 puts("                    TRANSLATE:");
 puts("");
 puts("   x => CROSS-SECTION from lines ----------> Geosec 2D");
 puts("   m => MAP from lines ----------> Geosec 2D or 3D");
 puts("   g => Polys or arcs from lines ----------> ArcInfo Generate");
 puts("   t => X Y Z file from text blocks ----------> Geosec 3D");
 puts("   b => X Y Z file from lines ----------> Geosec3D");
 puts("   h => Pts (x,y,z) from text blocks ----------> ArcInfo TIN");
 puts("   j => Pts (x,y,z) from lines ----------> ArcInfo TIN");
 puts("   l => Lines (x,y,z) from lines ----------> ArcInfo TIN");
 puts("   q => QUIT, or choose Quit from File menu on Macs\n");
return;
}

/*********************************************************
*                    Funcion Names.
* RECEIVES: only the user choice (c)
* READS: from preferences file, and updates it, if needed
* SENDS:  appropriate variables to reader function
* RETURNS: number of objects
*********************************************************/


int names (char c) /* file handling, and settings update*/
{
/*-------------------------------------------------------------FILES*/
FILE *prefile;                  /*preferences file */
FILE *filein;                   /*Adobe illustrator 5.5. file*/
FILE *fileout;                  /*IHF, or generate file*/
/*-----------------------------------------------------------VARIABLES*/
float scale = 1;
float altitude = 0, xorigin = 0, yorigin = 0;
char v = 'y';                   /*used by print-settings*/
char tmp[LINE];                 /*used load data from preferences*/
```

```
char extension[] = ".ihf";
char extensiontxt[] = ".txt";
char unidades[] = "undefined ";
char adobe[12], geosec[16];
char choice[] = "q";
int obj = 0, hunits = 3, vunits = 3, kind = 0;

/*-------------------------------------------------------------OPENING FILES*/
if ((prefile = fopen("preferences", "r")) == NULL)    /*open preferences file*/
        {
        prefile = fopen("preferences", "w");/*create preferences file*/
        fprintf (prefile, "1 0 0 0 3 3 0");
        }
/*-------------------------------------------------------------------------*/
printf ("\n\nEnter the name of the Illustrator file to be hacked:\n");
printf ("or enter q to return (on Unix)");
printf ("\n—maximum 12 characters long—\n");

gets (adobe);

if (!(strcmp (adobe, choice)))
    quit_cds();             /*get outta here!*/

strcpy (geosec, adobe);

if ((c == 't') || (c == 'g') || (c == 'b') || (c == 'h') || (c == 'j') || (c == 'l'))
   strcat (geosec, extensiontxt);     /*Adds .txt to the file name*/
else
   strcat (geosec, extension);        /*Adds .ihf  to the file name*/


/*-------------------------------------------------------------*/
if ((filein = fopen(adobe, "r")) == NULL)  /*open illustrator file*/
        {
        puts ("Could not open Adobe Illustrator file.");
        puts ("Did you type the file name correctly?");
        puts ("Is the file in the same directory as this program?");
        quit_cds();
        }

if ((fileout = fopen(geosec, "w")) == NULL)/*open out_file*/
        {
        puts ("Could not create .ihf output file.");
        quit_cds();
        }
/*-------------------------------------------------------------*/
fgets(tmp, LINE, prefile);
sscanf (tmp, "%f %f %f %f %d %d %d", &scale, &altitude, &xorigin, &yorigin, &hunits, &vunits, &kind);
fclose (prefile);
/*-------------------------------------------------------------*/

while (v != 'n')
{
print_settings(scale, altitude, xorigin, yorigin, hunits, vunits, kind, c);
printf("\n\n Your choice: ");          /* ask user to make a choice */
v = char_user();
        {
        if (v == 's')
                {
                unit_reader(hunits, unidades);
                printf ("\nHow many Adobe points are equal to ten units?.<%5.12f>\n", 10/scale);
                scanf ("%f", &scale);
                scale = (10 / scale);
```

```
                }
        if (v == 'o')
                {
                printf ("\nEnter coords x y of origin in Adobe file <%f %f>\n", xorigin, yorigin);
                scanf ("%f %f", &xorigin, &yorigin);
                }
        if (v == 'a')
                {
                printf ("\nLayer name will be used for altitude value\n");
                }
        if (v == 'k')
                {
                print_kind();
                puts ("\nyour choice:");
                v = char_user();
                kind = kind_reader(v);
                }
        if (v == 'h')
                {
                print_units();
                printf("\n horizontal units: (select digit from the list) ");/* ask user to make a choice */
                v = char_user();
                hunits = kind_reader (v);
                }
        if (v == 'v')
                {
                print_units();
                printf("\n vertical units: (select digit from the list) ");/* ask user to make a choice */
                v = char_user();
                vunits = kind_reader (v);
                }

        if ((prefile = fopen("preferences", "w")) == NULL)   /*updating preferences file*/
                {
                printf ("Could not update preferences file");
                return;
                }
        rewind(prefile);                /* make sure you're at beginning  */
        fprintf (prefile, "%5.12f %f %f %f %d %d %d\n", scale, altitude, xorigin, yorigin, hunits, vunits,
kind);
        fclose (prefile);
        }
}

/*-------------------------------------------------CALLING DATA HANDLING FUNCTIONS*/
avance (filein); /*scans until beginning of A.I. layer*/
/*-------------------------------------------------CALLING FUNCTIONS*/

if (c == 'x')
        {
        geosec_header_cross (fileout, hunits, vunits);
        }

if (c == 'm')
        {
        geosec_header_map (fileout, hunits, vunits);

        }
obj = reader (filein, fileout, kind, scale, altitude, xorigin, yorigin, c);

return (obj);

}       /*-------------------------------------END OF FUNCTION NAMES*/
```

```
/*-------------------------------------------------------------*/
/*  Scans for beginning of layer on Adobe 5.5 file*/
/*-------------------------------------------------------------*/

void avance (FILE *filein)

{
char flag[] = "%%EndSetup";  /*compatible with illustrator 7.0 for Win*/
char guide [11];
do
        {
        fgets(guide, 11, filein);
        }
while (( strcmp (guide, flag) != 0));/*stops at start of AI-5.5 layer*/

printf ("Start of layers detected\n");
printf ("Reading coordinates...\n");
return;
}       /*END OF AVANCE FUNCTION*/


/*-------------------------------------------------------------*/
/*FUNCTION READER*/
/*RECEIVES: Settings (origin, scale, alt), choices (c)*/
/*SENDS: Buffer to cleanup, and writes to file*/
/*RETURNS: number of objects written to file*/
/*-------------------------------------------------------------*/

int reader (FILE *filein, FILE *fileout, int kind, float scl, float alt, float xcoord, float ycoord, char c)
    /*scl stands for scale, alt for altitude, xcoord for xorigin*/

{
char tester[] = "%%PageTrailer";
char head2[] = "SURFACE", guide [14], buf[80];
char wrte = 'n',eoh = 'n';
int objects = 0, count = 0, i = 0, length = 0, slower = 0;
float x = 0, z = 0, elev = 0;
int numpoints = 2;

do
  {
  length = (strlen (buf));
  numpoints++;

  if (numpoints == 2)       /*Writes the end-of-block line*/
        {
      if ((c == 'm') || (c == 'x'))   /*for cross-sections and maps*/
              fprintf (fileout, "%d %d %d", EOH, EOH, EOH);

      if ((c == 'g') || (c == 'l'))             /*for generate files*/
        fprintf (fileout, "END\n");
      count = 0;              /*Resets the point counter*/
      printf ("+");           /*slows down process*/
      slower++;
        }

  if ((buf[length-2] == 'm') && (buf[length-3] == ' '))    /*write surface headers*/
        {
    if ((c == 'm') || (c == 'x'))               /*for cross-sections and maps*/
      fprintf (fileout, "\n\n%s\n****\n%d 0\n", head2, kind);
```

```
    if (c == 'g')                    /*for generate files*/
            fprintf (fileout, "%d\n", objects);
        if (c == 'l')
            fprintf (fileout, "1\n");
          objects++;
          printf ("-");                          /*slows down process*/
          slower++;
         }

  if (wrte == 'y')       /*start of file writing block*/
        {
    if (c == 'm')     /*for maps*/
          fprintf (fileout, "%f %f %f\n", ((x * scl) + xcoord), ((z * scl) + ycoord), elev);

    if (c == 'x')     /*for cross-sections*/
      fprintf (fileout, "%f %f\n", x * scl, z * scl);

    if (c == 'g')     /*for generate files*/
          fprintf (fileout, "%f, %f\n", ((x * scl) + xcoord), ((z * scl) + ycoord));

        if (c == 'b')      /*for xyz files to geosec3D*/
          fprintf (fileout, "%f %f %f\n", ((x * scl) + xcoord), ((z * scl) + ycoord), elev);

        if ((c == 'h') || (c == 'j'))     /*for text blocks or xyz lines to GenerateTIN*/
          {
          fprintf (fileout, "1, %f, %f, %f\n", ((x * scl) + xcoord), ((z * scl) + ycoord), elev);
          if (c == 'h')
                objects++;
          }
        if (c == 't')      /*for text blocks to geosec*/
          {
          fprintf (fileout, "%f %f %f\n", ((x * scl) + xcoord), ((z * scl) + ycoord), elev);
          objects++;
          }
    if (c == 'l')
       fprintf (fileout, "%f, %f, %f\n", ((x * scl) + xcoord), ((z * scl) + ycoord), elev);


    count++;                    /*Increases the point counter each pass*/
    slower++;
    if (slower > 60)
        {
        printf ("\n");
        slower = 0;
        }
      printf (".");
        }

wrte = cleanup (buf, &x, &z, &numpoints, &elev, c);  /*GET LINE FROM FILE AND CLEAN IT UP*/

fgets (buf, 80, filein);
  for (i = 0; i < 14; i++)
    {
    guide [i] = buf [i];
    }
  guide [13] = '\0';

  }
while (( strcmp (guide, tester) != 0));

if ((c == 'g') || (c == 'l') || (c == 'h') || (c == 'j'))
 fprintf (fileout, "END\n");
```

```
if ((c == 't') || (c == 'b'))
  fprintf (fileout, "\n");

fclose (filein);
fclose (fileout);
return (objects);

}

/*-------------------------------------------------------*/
/*  FUNCTION CLEANUP*/
/*  CLEANS UP THE STRING*/
/*  takes the buffer read from the input file and:*/
/*  -gets rid of the A.I.'s character commands*/
/*  -reads floats (x,z) into pointers */
/*  -decides whether to write to file or not*/
/*  -decides whether to write block delimiter signatures*/
/*-------------------------------------------------------*/

char cleanup (char temp[], float *p, float *q, int *num, float *r, char c)
  /*p stands for x, q for z, temp for buf, num for numpoints, r for elev*/
{
int length = 0;
char wrte;
char lastchar = 'a';
char nextlastchar = 'a';

wrte = 'n';

length = (strlen (temp));

if (length > 5)       /*any object will hopefully be longer than 5*/
 {
 if ((( c == 't') || ( c == 'h')) && ((temp[length-3] == 'T') && (temp[length-2] == 'p')))
   {                    /*looks for location of text blocks*/
   wrte = 'n';
   temp[length-2] = ' ';
   sscanf (temp, "%f %f %f %f %f %f", p, p, p, p, p, q);
   }
 if ((( c == 't') || ( c == 'h')) && ((temp[length-4] == 'T') && (temp[length-3] == 'x')))
   {                      /*looks for elevation value in text block*/
   wrte = 'y';              /*AI places an additional space at the end of each txt block*/
   temp[length-2] = ' ';
   temp[length-3] = ' ';
   temp[length-5] = ' ';
   temp[0] = ' ';
   sscanf (temp, "%f", r);     /*scanfs from stream, a string, this time.*/
   }
 lastchar = toupper (temp[length-2]);
 nextlastchar = toupper (temp[length-3]);
 if ((nextlastchar == ' ') && ( c != 't'))  /*makes sure we are not reading patterns or gradients*/
   {

   if ((lastchar == 'M') || (lastchar == 'L'))
     {                            /*looks for objects*/
     wrte = 'y';                    /*without handles*/
     temp[length-2] = ' ';
     sscanf (temp, "%f %f", p, q);
     *num = 0;
     }
   if ((lastchar == 'Y') || (lastchar == 'V'))
     {                            /*looks for objects with*/
     wrte = 'y';                    /*one handle*/
```

```
    temp[length-2] = ' ';
    sscanf (temp, "%f %f %f %f", p, p, p, q);
    *num = 0;
    }
   if (lastchar == 'C')       /*looks for objects with*/
    {                  /*two handles*/
    wrte = 'y';
    temp[length-2] = ' ';
    sscanf (temp, "%f %f %f %f %f %f", p, p, p, p, p, q);
    *num = 0;
    }
  }
 }
if ((c == 'm') || (c == 'b') || (c == 'j') || (c == 'l'))
 {
 if ((lastchar == 'N') && (nextlastchar == 'L'))  /* set altitude variable to layer name*/
  {
          temp[0] = ' ';
          temp[length-2] = ' ';
          temp[length-3] = ' ';
          temp[length-4] = ' ';
          temp[length-5] = ' ';
          sscanf (temp, "%f", r);     /*scanfs from stream, a string, this time.*/
          printf ("\nStart of Layer %s detected\n", temp);
  }
 }
return (wrte);
}           /*END OF CLEAN UP FUNCTION*/

/*_____________________________________________*/
/* Function Name: quit_cds*/
void quit_cds()
{
int temp = 'n';
 printf("Exiting the App. Confirm exit (y or n) ");
          temp = char_user ();
          if (temp == 'y')
                  {
                  puts ("You can now choose Quit under the File menu (on Macs)");
                  puts ("Program normally terminated");
                  exit (0);
                  }
          else
                  return;
}
/*_____________________________________________________________________________*/
void print_intro()
{
 puts("          Welcome to Translator version 2.09");
 puts("   Author Camilo Montes, cmontes@megatectonics.gg.utk.edu");
 print_main_help();
 return;
}
/*_____________________________________________________________________________*/
void print_main_help()
{

 puts ("          THIS PROGRAM ASSUMES TWO THINGS:");
 puts ("A- ...no responsibility, and");
 puts ("B- that your Adobe Illustrator file:");
 puts ("   - uses dense Bezier lines, or no Bezier lines at all");
 puts ("   - is located in the same directory as this program (for Macs)");
 puts ("   - uses Layer's names for altitude values");
```

```
 return;
}
/*_____________________________________________________________________*/
void print_settings (float scale, float altitude, float xorigin, float yorigin, int hunits, int vunits, int kind, char c)
{

char unidades[] = "units-undefined";
puts("");
puts("            SETTINGS MENU");
puts("        Select an item to update");
puts("");
printf("      s - Scale factor: 10 units = %5.7f points\n", 10/scale);
  if (c == 'm')
    printf("      Altitude will be read from Layer name\n");
  if (c != 'x')
    printf("      o - Origin: x = <%f>, y = <%f>\n", xorigin, yorigin);
  if ((c == 'x') || (c == 'm'))
          {
          unit_reader(hunits, unidades);
          printf("      h - Horizontal units are: <%s>\n", unidades);
          unit_reader(vunits, unidades);
          printf("      v - Vertical units are: <%s>\n", unidades);
          unit_reader(kind, unidades);
          if (!(strcmp (unidades, "meters")))
                  strcpy (unidades, "undefined"); /*ugly fix*/
          printf("      k - Geological kind is: <%s>\n", unidades);
          }
puts("      n - None, everything is OK");
return;
}
/*_____________________________________________________________________*/
void print_units (void)
{
 puts("");
 puts("      UNITS MENU");
 puts("      Choose units");
 puts(" ");
 puts ("      1- meters");
 puts ("      2- kilometers");
 puts ("      3- feet");
 puts ("      4- seconds");
return;
}
/*_____________________________________________________________________*/
void print_kind (void)
{
 puts("");
 puts("          GEOLOGICAL KIND MENU");
 puts("      Choose kind of feature to be created");
 puts(" ");
 puts ("      o -Top");
 puts ("      c -Contour");
 puts ("      i -Intraformational");
 puts ("      f -Fault");
 puts ("      u -Unconformity");
 puts ("      t -Topography");
 puts ("      s -Sea level");
 puts ("      m -Marker");
 puts ("      b -Boundary");
 return;
}
/*_____________________________________________________________*/
/*    Reads input in a numeric form, and translates it  */
```

```
/*    to characters corresponding to the units          */
/*-------------------------------------------------------*/
void unit_reader (int units, char unidades[])
{
char tmp [20];
if (units == 0)
strcpy (tmp, "meters"); /*meters or undefined, depends who's asking*/
else if (units == 3)
strcpy (tmp, "kilometers");
else if (units == 10)
strcpy (tmp, "feet");
else if (units == 30)
strcpy (tmp, "seconds");
else if (units == 900)
strcpy (tmp, "top");
else if (units == 840)
strcpy (tmp, "contour");
else if (units == 800)
strcpy (tmp, "intraformational");
else if (units == 700)
strcpy (tmp, "fault");
else if (units == 600)
strcpy (tmp, "unconformity");
else if (units == 500)
strcpy (tmp, "topography");
else if (units == 400)
strcpy (tmp, "sea level");
else if (units == 90)
strcpy (tmp, "marker");
else if (units == 7)
strcpy (tmp, "boundary");
else
strcpy (tmp, "Not valid type");
strcpy (unidades, tmp);
return;
}
/*-------------------------------------------------------*/
/*    Reads input in a text form, and translates it      */
/*    to numeric values corresponding to surface types   */
/*-------------------------------------------------------*/
int kind_reader (char kind)
{
int tmp = 0;

if (kind == 'o')
tmp = 900;
else if (kind == 'c')
tmp = 840;
else if (kind == 'i')
tmp = 800;
else if (kind == 'f')
tmp = 700;
else if (kind == 'u')
tmp = 600;
else if (kind == 't')
tmp = 500;
else if (kind == 's')
tmp = 400;
else if (kind == 'm')
tmp = 90;
else if (kind == 'b')
tmp = 7;
else if (kind == 'l')
```

```
tmp = 0;
else if (kind == '2')
tmp = 3;
else if (kind == '3')
tmp = 10;
else if (kind == '4')
tmp = 30;
else
tmp = 0;/*undefined*/
return (tmp);
}
/*-------------------------------------------------------------------*/
/*  FUNCTION*/
/*  CREATES THE STANDARD GEOSEC HEADER FOR MAPS*/
/*-------------------------------------------------------------------*/

void geosec_header_map (FILE *fileout, int hunits, int vunits)

{
fprintf (fileout, "IMPORT_HORIZON_HEADER\n%d\n%d %d\n\nSURFACE_DATA_FORMAT\nMXYZ",
EOH, hunits, vunits);
return;
}          /*END OF FUNCTION GEOSEC_HEADER_MAP*/


/*-------------------------------------------------------------------*/
/*  FUNCTION*/
/*  CREATES THE STANDARD GEOSEC HEADER */
/*  FOR CROSS SECTIONS*/
/*-------------------------------------------------------------------*/

void geosec_header_cross (FILE *fileout, int hunits, int vunits)

{
fprintf (fileout, "IMPORT_HORIZON_HEADER\n%d\n%d %d\n\nSURFACE_DATA_FORMAT\nXZ",
EOH, hunits, vunits);
return;
}          /*END OF FUNCTION GEOSEC_HEADER_CROSS*/

/*END OF PROGRAM*/
```

ROTATE

This program is an adaptation of a BASIC code published by Vissers and Bollegraaf (1989), compiled in C, and enhanced to allow file manipulation.

```
/*-------------------------------------------------------------------
This is the C implementation of:
Vissers R. L. M., and Bollegraaf, B., 1989, An Algorithm for rotation of
     axial data: Computers & Geosciences, vol. 15, pp 157-161.
The original code was BASIC, I changed it by translating it to C,
implementing functions, and adding file handling capabilities.
          Camilo Montes Jun. 2001.
-------------------------------------------------------------------*/
#include <stdio.h>
#include <string.h>
```

```
#include <ctype.h>
#include <stdlib.h>
#include <Types.h>
#include <Memory.h>
#include <TextEdit.h>
#include <OSUtils.h>
#include <ToolUtils.h>
#include <SegLoad.h>
#include <math.h>
#include <time.h>
#include <MacTypes.h>

#define LINE 100        /* number of chars on a line  */

/*-------------------------------------------------------------------------------*/
void multiply_matrix (float MA[ ][ ], float MB[][], float MC[ ][ ]);
void rotate_function (float *, float *, float, float, float);
char char_user();
/*-------------------------------------------------------------------------------*/

main()
{

float az = 0;       /*dip azimuth of plane to be rotated  WARNING: POLES TO PLANES OR LINES*/
float dip = 0;      /*dip of plane to be rotated    WARNING: POLES TO PLANES OR LINES*/
float rotaz = 0;    /*azimuth of rotation axis*/
float rotdip = 0;   /*dip of rotation axis*/
float ran = 0;      /*angle of right-handed (??) rotation*/

/*----FILE DEF-----------------------*/
FILE *filein;                       /*INPUT FILE */
FILE *fileout;                  /*ROTATED OUTPUT FILE*/
FILE *original_fileout;             /*ORIGINAL OUTPUT FILE*/

/*-------------------------------------*/

char tmp[LINE];             /*used to load data from in_file*/
char sufix[] = "_rot";
char sufix_or[] = "_or";
char rawdata[20], rotatedata[20], ordata[20];  /*File names*/
int endoffile = 0;
int num_rec = 0;    /*number of lines in in_file*/
int i = 0;
int j = 0;
char c = 'z';    /*this variable holds user's choice for output format*/
char a = 'p';    /*this variable tells the program whether the input is lines or planes*/

/*-----------------------------------------------------GET THE FILE NAME FROM USER*/


printf ("\n----------------This is the C implementation of:----version 1.1--- \n");
printf ("Vissers R. L. M., and Bollegraaf, B., 1989, An Algorithm for rotation\n");
printf ("      of axial data: Computers & Geosciences, vol. 15, pp 157-161.\n");
printf ("----The comma-separated input file format is:\n");
printf ("First column: Dip azimuth of in_plane, or trend of in_line\n");/*plus 180 or minus 180*/
printf ("Second column: Dip of in_plane, or plunge of in_line\n");/*90 minus dip*/
printf ("Third column: Bedding dip azimuth (Rotation axis dip azimuth),\n");/*plus 90 or minus 270*/
printf ("Fouth column: Rotation axis plunge,(usually zero)\n");
printf ("Fifth column: Bedding dip (Rotation angle)\n");
printf ("OUTPUT FILE FORMAT WILL BE: dip azimuth, dip; or: trend, plunge\n");
printf ("----------Please enter the name of the file containing raw data-------:\n");
printf ("----maximum 20 characters long----\n");
gets (rawdata);
```

```
printf("\n Do you want both data sets to be formated");
printf("\n -dip azimuth, dip- for Allmendinger's? (y/n): ");
c = char_user();

printf("\n Do you want to rotate planes or lines? (p/l)");
a = char_user();


/*-------------------------------------------------START FILE HANDLING*/

strcpy (rotatedata, rawdata);
strcpy (ordata, rawdata);
strcat (rotatedata, sufix);
strcat (ordata, sufix_or);

if ((filein = fopen(rawdata, "r")) == NULL)  /*open in_file*/
        {
        puts ("Could not open input file.");
        puts ("Did you type the file name correctly?");
        puts ("Is the file in the same directory as this program?");
        return 0;
        }

if ((fileout = fopen(rotatedata, "w")) == NULL)        /*open out_file*/
        {
        puts ("Could not create output file.");
        return 0;
        }


if ((original_fileout = fopen(ordata, "w")) == NULL) /*open original out_file*/
        {
        puts ("Could not create original output file.");
        return 0;
        }



/*reads the whole in_file to keep track of the number of records*/
while (endoffile < 1)
        {
        fgets(tmp, LINE, filein);
                /*THERE SHOULD BE AN ERROR_CHECKING FUNCTION CALL HERE--------
*/
        if (feof (filein) )
                endoffile = 2;
        num_rec++;
        }
printf( "Total number of lines in file: %d\n", num_rec);

rewind (filein);
if (c == 'n')
        fprintf(fileout, "Dip_Az, Dip, Rot_ax, Rot_ax_plunge, Rot_angle, Dip_azROT, DipROT\n");

for (i = 0; i < num_rec; i++)  /*-------------------------------------MAIN LOOP*/
        {
        /*-------------------------------------READS ONE LINE OF DATA FROM THE RAW
FILE*/
        fgets(tmp, LINE, filein);
        puts (tmp);
        sscanf (tmp, "%f, %f, %f, %f, %f", &az, &dip, &rotaz, &rotdip, &ran);
```

```
        if (c == 'n')
                fprintf(fileout, "%7.3f, %7.3f, %7.3f, %7.3f, %7.3f, ", az, dip, rotaz, rotdip, ran);

        if (c == 'y')
                fprintf(original_fileout, "%7.3f, %7.3f\n", az, dip);

        if (a == 'p')           /*perform these conversion only if user chose planes*/
                {
                if ( (az + 180) > 360)  /*converting dip azimuth to pole to bedding*/
                        az = az - 180;
                else
                        az = az + 180;

                dip = 90 - dip;     /*converting dip to pole to bedding*/
                }

        if ( (rotaz + 90) > 360) /*converting bedding dip azimuth to trend of rotation axis*/
                rotaz = rotaz - 270;
        else
                rotaz = rotaz + 90;

/*-------------------------------------------------------------------------------
---------*/
        rotate_function (&az, &dip, rotaz, rotdip, ran); /*sending memory addresses for az and dip*/

        if (a == 'p')           /*perform these conversion only if user chose planes*/
                {
                if ( (az + 180) > 360)  /*converting pole to bedding to dip azimuth*/
                        az = az - 180;
                else
                        az = az + 180;

                dip = 90 - dip;     /*converting pole to bedding to dip*/
                }

        fprintf(fileout, "%7.3f, %7.3f\n", az, dip);
        }
fclose (filein);
fclose (fileout);
fclose (original_fileout);
printf( "Results written to file: %s\n", rotatedata);

return 0;
}

/*=======================================*/
/*=======================================*/
/*=======================================*/


void rotate_function (float *azPtr, float *dipPtr, float rotaz, float rotdip, float ran)

{
int i = 0;
int j = 0;

float pi = 3.141592654;

float MA [ 3 ] [ 3 ];
float MB [ 3 ] [ 3 ];
float MC [ 3 ] [ 3 ];

float LL [ 3 ];
```

```
float azr = 0;      /*azimuth converted to radians*/
float thetr = 0;    /*90-dip converted to radians*/
float razr = 0;     /*rotated azimuth in radians*/
float rthetr = 0;   /*rotated 90-dip in radians*/
float raz = 0;      /*rotated azimuth of axial data in degrees*/
float rdip = 0;     /*rotated dip of axial data in degrees*/
float a = 0;        /*azimuth of rotation axis in radians*/
float d = 0;        /*dip of rotation axis in radians*/
float h = 0;        /*angle of right-handed rotation in radians*/

float l = 0;                    /*direction cosines*/
float m = 0;
float n = 0;

float temp = 0;

/*——initialize matrices————————————————*/

for ( i = 0; i < 3; i++ )
        {
        LL [ i ] = 0;
        for ( j = 0; j < 3; j++ )
                {
                MA [ j ] [ i ] = 0;
                MB [ j ] [ i ] = 0;
                MC [ j ] [ i ] = 0;
                }
        }
/*————————————————————————————————————*/


/*————————convert to radians————————————*/
        azr = ( ( *azPtr *  pi ) / 180 );
        thetr =  ( ( pi / 2 )  -  ( ( *dipPtr * pi ) / 180 ) );  /* 90 - dip in radians*/

        /*————convert axis/angle to radians——*/
        a = ( ( rotaz *  pi ) / 180 );
        d = ( ( pi / 2 ) - ( ( rotdip * pi ) / 180 ) );   /*90 - rotdip in radians*/
        h = ( ( ran * pi ) / 180 );

        /*—Calculate rotation matrix——*/
        /*—Rotate about Z over -A (-azimuth)—*/

        MA[0][0] = cos ( a );
        MA[0][1] = sin ( a );
        MA[0][2] = 0;

        MA[1][0] = -sin ( a );
        MA[1][1] = cos ( a );
        MA[1][2] = 0;

        MA[2][0] = 0;
        MA[2][1] = 0;
        MA[2][2] = 1;

        /*—Rotate about -Y over D (90-theta)—*/

        MB[0][0] = cos ( d );
        MB[0][1] = 0;
        MB[0][2] = -sin ( d );

        MB[1][0] = 0;
        MB[1][1] = 1;
```

```
MB[1][2] = 0;

MB[2][0] = sin ( d );
MB[2][1] = 0;
MB[2][2] = cos ( d );

multiply_matrix (&MA[0], &MB[0], &MC[0]);

/*—Rotate about Z over H (rotation angle)—*/

MB[0][0] = cos ( h );
MB[0][1]= -sin ( h );
MB[0][2] = 0;

MB[1][0] = sin ( h );
MB[1][1] = cos ( h );
MB[1][2] = 0;

MB[2][0] = 0;
MB[2][1] = 0;
MB[2][2] = 1;

multiply_matrix (&MA[0], &MB[0], &MC[0]);

/*—Rotate back about -Y over -D (theta-90)—*/

MB[0][0] = cos ( d );
MB[0][1] = 0;
MB[0][2] = sin ( d );

MB[1][0] = 0;
MB[1][1] = 1;
MB[1][2] = 0;

MB[2][0] = -sin ( d );
MB[2][1] = 0;
MB[2][2] = cos ( d );

multiply_matrix (&MA[0], &MB[0], &MC[0]);

/*—Rotate back aboutZ over A (azimuth)—*/

MB[0][0] = cos ( a );
MB[0][1] = -sin ( a );
MB[0][2] = 0;

MB[1][0] = sin ( a );
MB[1][1] = cos ( a );
MB[1][2] = 0;

MB[2][0] = 0;
MB[2][1] = 0;
MB[2][2] = 1;

multiply_matrix (&MA[0], &MB[0], &MC[0]);

/*————————————————rotate data with matrix MA */
/*———convert data to cartesian direction cosines*/

l = ( sin ( thetr ) * cos ( azr ) );
m = ( sin ( thetr ) * sin ( azr ) );
n = cos ( thetr );
```

```
        /*-----------------------------------perform rotation*/
        for (j = 0; j < 3; j++)
                {
                LL [ j ] = ((MA[j][0] * l ) + ( MA[j][1] * m ) + ( MA[j][2] * n ) );
                }
        /*-------------------------rotated poles from cartesian to polar*/

        razr = ( atan ( LL [1] / LL [0] ) );

        if ( LL [0] < 0 )
                razr = (razr + pi);

        temp = pow ( (1 / LL [2] ), 2 );
        temp = ( sqrt ( temp - 1 ) );
        rthetr = ( atan ( temp ) );

        if (LL[2] < 0)
                razr = (razr + pi);

        if (razr < 0)
                razr = (razr + (2 * pi));

        if (razr > (2 * pi))
                razr = (razr - (2 * pi));

        /*-----------------------------rotation complete-----------------------*/

        /*-------------------------convert to degrees*/

        *azPtr = ( ( razr * 180 ) / pi );
        *dipPtr = 90 - ( ( rthetr * 180 ) / pi );
}


/*=========================================*/
/*=========================================*/
/*=========================================*/


void multiply_matrix (float MA[3][3], float MB[3][3], float MC[3][3])

{

int i = 0;
int j = 0;

/*---------multiply matrices MC=MB*MA and assign MC to MA */
/*---------line number 4410*/


for (j = 0; j < 3; j++)
        {
        for (i = 0; i < 3; i++)
                {
                MC [i][j] = ( MB[i][0] * MA[0][j] ) + ( MB[i][1] * MA[1][j]) + ( MB[i][2] * MA[2][j] );
                }
        }

for (i = 0; i < 3; i++)
        {
        for (j = 0; j < 3; j++)
                {
                MA[i][j] = MC[i][j];
```

```
                }
        }
return;

}

/*-------------------------------------------------------------------/
/* Get a line but only return the first character entered*/
/* This makes the program more robust and removes the   */
/* need to call getchar twice (once for the desired     */
/* character and once to remove the newline             */
/*-------------------------------------------------------------------*/
char char_user()
{
 char tmp[LINE];
 gets(tmp);
 return(tmp[0]);  /* return first character entered */
}
/*-------------------------------END OF CHAR_USER FUNCTION*/

/*END OF PROGRAM*/
```

ARC MACRO LANGUAGE CODE

The following pages contain Arc Macro Language code that automate tedious processes in ArcInfo. They are mostly commented, and in some cases they are hardcoded. Keep in mind that writing these macros took the author a while, so long in fact, that it would have been faster to perform these processes by hand one time. Since the creation of the geologic database took many trial-and-error repetitions, writing these AML's actually saved a great deal of time. The process of modification can be equally long and frustrating, but remember, a hacker would rather force the computer to do his job. No matter how long it takes.

Mkcover.aml

This AML takes two input text files, one containing coordinate information, and the other containing field data, merges them to create an ArcInfo coverage. Mostly hard-coded.

```
=====================================================================
mkcover.aml

=====================================================================
/* This AML should take two input text files
/* one containing coord info, and the other
/* containing field data, and create a coverage,
```

```
/* and then create a table, and join them to
/* create a coverage with all the attributes
/* it would also be nice if it could convert
/* strike, dip, and dip direction fields into
/* Dip and dip direction in azimuth.
/* Not much user interface, it is mostly hard-coded.
/* Camilo Montes.  June 1999
/*This aml needs this file (called fields) somewhere in
/*the same directory:
/*    'Strike-Dip-DipD' 1
/*    'Strike-Dip-DipD-Spac-Thick'2
/*    'Strike-Dip-DipD-Spacing' 3
/*    'Strike-Dip-DipD-Style-Spac' 4
/*    'Trend-Plunge-Style' 5
/*    'Trend-Plunge' 6


&sv type = 1
&sv ext1 = dat
&sv ext2 = -ID
&sv ext3 = .PAT
&sv ext4 = utm
&sv codesloc = /u01/cmontes/girardotdd/fields

&terminal 9999

&type Choose file containing the ID,x,y data
&sv ttin = [getfile * -file -none]   /*user input

&type Choose file containing field data
&sv fdata = [getfile * -file -none]

&type Choose the kind of datafile to be created
&sv ttype = [getchoice -file %codesloc% -display 1 ~
 -value 2 -var type]

&if [null %ttin%] &then
  &do
    &return
  &end
&else

&sv mas = [response 'Enter a name for the cover']

&if ( [exists %mas% -cover] ) &then
&do
   &type The cover %mas% already exists,
   &sv mas = [response 'Enter another name for the cover: ']
&end

generate %mas%
points
&r %ttin%
end
quit
build %mas% point

&sv station = %mas%%ext2%

&if ( %type% = 1 ) &then
&do
tables
define %mas%%ext1%
```

```
%station%, 4, 4, i
Strike, 4, 4, i
Dip, 4, 4, i
DipD, 2, 2, c,
~
&end
&else

&if ( %type% = 2 ) &then
&do
tables
define %mas%%ext1%
%station%, 4, 4, i
Strike, 4, 4, i
Dip, 4, 4, i
DipD, 2, 2, c
Spacing, 4, 4, i
Thickness, 4, 4, i
~
&end
&else

&if ( %type% = 3 ) &then
&do
tables
define %mas%%ext1%
%station%, 4, 4, i
Strike, 4, 4, i
Dip, 4, 4, i
DipD, 2, 2, c
Spacing, 4, 4, i
~
&end
&else

&if ( %type% = 4 ) &then
&do
tables
define %mas%%ext1%
%station%, 4, 4, i
Strike, 4, 4, i
Dip, 4, 4, i
DipD, 2, 2, c
Style, 15, 15, c
Spacing, 4, 4, i
~
&end
&else

&if ( %type% = 5 ) &then
&do
tables
define %mas%%ext1%
%station%, 4, 4, i
Trend, 4, 4, i
Plunge, 4, 4, i
Style, 15, 15, c
~
&end
&else

&if ( %type% = 6 ) &then
&do
```

```
tables
define %mas%%ext1%
%station%, 4, 4, i
Trend, 4, 4, i
Plunge, 4, 4, i
~
&end

add from %fdata%
items
sel
quit
joinitem %mas%%ext3% %mas%%ext1% %mas%%ext3% %mas%%ext2% %mas%%ext2%
list %mas%%ext3%

projectcopy cover stationdd cover %mas%

project cover %mas% %mas%%ext4% /u01/cmontes/girardotdd/ddtoutm

&workspace /u01/cmontes/piedrasutm
copy /u01/cmontes/girardotdd/%mas%%ext4%
&workspace /u01/cmontes/girardotdd
kill %mas%%ext4%
tables
kill %mas%%ext1%
quit

&return
```

Mkgrid.aml

This AML takes a .txt input file out of translator, converts it to a TIN, then to a GRID, then to a DEM, and finally to an image in TIFF format.

==========

mkgrid.aml

==========

```
/*This aml takes the txt input file out of translator, and
/*converts it to a TIN, GRID, DEM, and TIF in DD and in UTM coords.
/*This partially solves the problem of the cork-model look.
createtin piedrastin 0.001
generate /u01/cmontes/txtfiles/topo/lines/contdd.txt line
end
~
~
PROJECTCOPY COVER STATIONDD TIN piedrastin
tinlattice piedrastin piedraslat quintic
~
~
6000
~
project GRID piedraslat /u01/cmontes/piedrasutm/piedutmlat /u01/cmontes/txtfiles/ddtoutm
&workspace /u01/cmontes/piedrasutm
hillshade piedutmlat piedutmsh 290 45 all 2
gridimage piedutmsh gray piedrash tiff
~
```

```
LATTICERESAMPLE PIEDUTMLAT PIEDutmsmll
~
~
2000
latticeoperate replace PIEDUTMSMLL 0 pieutmscl spot = -9999
projectdefine grid PIEUTMSCL
zunits meters
parameters
latticedem PIEUTMSCL piedrasdem 1

&return
```

Dip.aml

This AML takes the PAT file of a coverage containing planar features, creates a new field called dipdazm, and converts the existing strike and dip into dip and dip direction in azimuth.

==========

dip.aml

==========

```
/*this aml should take the PAT file of a coverage
/*containing planar features, create a new field
/*called dipdazm, and convert the existing strike and
/*dip into dip and dip direction in azimuth.


&sv modu = [show program]
    &do &while %modu% ^= ARC
    quit
    &type Going down to ARC
    &sv modu = [show program]
    &end
&terminal 9999

&sv fdata = [getcover * -none]

&sv fdata2 = [entryname %fdata%]


tables

additem %fdata2%.pat dipdaz 4 4 i
sel %fdata2%.pat
resel
asel dipd lk 'n*'
resel strike > 180
calculate dipdaz = strike + 90
resel dipdaz > 360
calculate dipdaz = dipdaz - 360
resel
asel dipd lk 'n*'
```

```
resel strike < 180
calculate dipdaz = strike - 90
resel dipdaz < 0
calculate dipdaz = dipdaz + 360
resel

asel dipd lk 's*'
resel strike > 180
calculate dipdaz = strike - 90
resel
asel dipd lk 's*'
resel strike < 180
calculate dipdaz = strike + 90
resel

asel dipd = 'e'
resel strike > 90 and strike < 270
calculate dipdaz = strike - 90
resel
asel dipd = 'e'
resel strike < 90 or strike > 270
calculate dipdaz = strike + 90
resel dipdaz > 360
calculate dipdaz = dipdaz - 360

asel dipd = 'w'
resel strike > 90 and strike < 270
calculate dipdaz = strike + 90
resel
asel dipd = 'w'
resel strike < 90 or strike > 270
calculate dipdaz = strike - 90
resel dipdaz < 0
calculate dipdaz = dipdaz + 360

sel
quit
&return
```

Idfmaker.aml

This AML reads records in a pat table (x,y,z, dip, dip direction in azimuth, surface type, and stratigraphic unit), and writes them to a text file in .idf format ready to go to Geosec2D

==========

Idfmaker.aml

==========

```
/*_____
/*This AML should read records in a pat table (x,y,z, dip,
/*dip direction in azimuth, surface type, and stratigraphic unit),
/*and write them to a text file in .idf format
/*ready to go to Geosec2D
/*
/*_____
/*Open new file to write to
```

```
&sv outfile = [open nada.idf nada -write]
&sv cero = 0
&sv blankspace = ''
&sv num_set = 1
&sv set_name = sumadre
&sv set_kind = 900
&sv set_stracol = A
&sv col_name = Default_SC

cursor dipper declare prueba points ro
cursor dipper open

&sv num_set = [quote %cero% %cero% %cero% 1 %cero% %cero% %cero%]

&sv nada = [write %outfile% IMPORT_DATA_HEADER]
&sv nada = [write %outfile% %num_set%]
&sv nada = [write %outfile% %blankspace%]
&sv nada = [write %outfile% DATA_VERSION]
&sv nada = [write %outfile% 3.1]
&sv nada = [write %outfile% %blankspace%]
&sv nada = [write %outfile% WELL_DATA_FORMAT]
&sv nada = [write %outfile% COORDINATE]
&sv nada = [write %outfile% %blankspace%]

&sv nada = [write %outfile% WELL_3D]
&sv nada = [write %outfile% %:dipper.aml$nsel%]
&sv nada = [write %outfile% %set_name%]
&sv nada = [write %outfile% 1]
&sv nada = [write %outfile% %col_name%]
&sv nada = [write %outfile% %blankspace%]


&do &while %:dipper.aml$next%
  &sv nada = [write %outfile% WELL_POINT_3D]
  &sv coord_line = [quote %:dipper.x-coord% %:dipper.y-coord% %:dipper.spot%]
  &sv nada = [write %outfile% %coord_line%]
  &sv nada = [write %outfile% %:dipper.dip%]
  &sv nada = [write %outfile% %:dipper.dipdaz%]
  &sv nada = [write %outfile% [quote %set_kind% %set_stracol%]]
  &sv nada = [write %outfile% %blankspace%]

cursor dipper next
&end

&sv nada = [write %outfile% %blankspace%]
cursor dipper close
cursor dipper remove
&sv nada = [close %outfile%]
&return
```

Tips

Georeferencing

Georeferencing and rectifying different data sets to a single projection using ArcInfo and Imagine0) Projected everything to IGAC (TM) coordinates.

1)Create an empty coverage with tics (taken straigth from the station map). I used about 15 tics (the corners, and 11 stations distributed throughout the map).

2) Created an empty coverage with the same tic marks, but this time I read the tics coordinates from the distorted station map, and coords coverages.

3) Copied the attributes and geometry of each coverage (copyfeatures) into a copy of the empty coverage with the distorted tics.

4) Used transform with the affine option to rectify the distorted coverage into a copy of the empty coverage with correct tics.

5) In Imagine, I used Rubbersheeting with about 50 GCP to rectify the radar image. Then I did image to image rectification to rubbersheet the satellite image to the radar image.

Converting to VRML

Converting .iv exported scences from geosec3D to VRML, browser-friendly models

1) in geosec simplfy the model to its barest.

2) export it as an inventor scene.

3) open it in annotator, enable editing, and save it (using .iv extension)

4) translate it to vrml using: /usr/sbin/ivToVRML

/usr/sbin/ivToVRML -o newfile.vrml oldfile.iv (this step may not be needed)

5) Open Showcase, import the vrml file, add lights, floor, and save as vrml.

Plotting strikes and dips in ArcView

In order to get ArcView (3.0 or 3.1) to correctly plot the dip symbols, I had to create a new field (only temporary) select all dipaz less than 180, and apply (180 - x), then select all dipaz greater than 180, and apply (540 - x), and then select all dipaz = 180, and subtract 180.

Bringing three-dimensional data into Geosec2D

0) Recreated a topo map of the 1:100000 map.

1) Took the contourtm coverage to Illustrator because it had been slightly distorted, and used it as a template to scale the original contours in the adobe55 file. The distotion I applied in illustrator does not exactly account for the distortion that I applied using transform in ArcInfo.

2) Used translator to create a generate file from lines.

3) Took the generate file to arcinfo where I created a TIN (following the instructions in newmakegrid.aml).

4) Created a grid in arcinfo with 50 m resolution

Arc: latticedem PIEDUTFAKE2 PIEDemfk 1 int

5) Used latticeoperate to replace the nodata values for zeroes

6) Faked a utm projection for this TM lattice

7) created a DEM from this file. I did not define zunits, and did not apply a factor of 1 for Z.

This way Geosec reads it just fine. Otherwise, geosec will apply a large VE.

8) The only problem is that merge_DEM_and_DB_sgi reads the DEM as having vertical units as feet.

9) Exported the contacts from Arcview into illustrator, and then use translator to do the conversion into Geosec 2D.

10) merge_DEM_and_DB_sgi -B piedemfk geologicmap.db

Generating topographic cross-sections from DEMs

0) I have to create a coverage that contains the lines (two end points are sufficient).

1)Then, in arcplot I select the surface (lattice):

Arcplot: surface lattice PIEDRASGRID

(For some strange reason the surface gets an ID of 3. Don't know why is there such a thing as an ID number instead of the name for the lattice. Don't know how to query its ID number either. I found out by chance.)

2) Then, I use surfacexsection to get the profiles. Since there is a 5000 point limit, I have to increase the sample_distance. Its default is .45 times the mesh point spacing. For the piedras grid, it is 50 m. If it exceeds the number of points, it won't say anything, it will simply cut off the sections.

3) I then go to tables and unload it:

4) I then edit the text file to add this line at the end: %%PageTrailer

5) Then, I run the file through translator using the u option.

6) I then create a new project in geosec2D, edit the units to meters, and import from file, making a best fit section. That creates the number of sections I need.

7) Then I export each section as a 3D section, and import it into the project.

Create a shotpointmap

1) create a line coverage that defines each individual seismic line

2) Use densifyarc (arc option) command to create as many shotpoints as needed (from seismic line paper header)

3) use nodepoint command to convert from nodes to a point coverage.

Excel Macro

Unfortunatley, this dissertation is not completely Microsoft-free. At some point I had no choice but to write an Excel Macro. The problem was that the whole database could not be brougth into ArcInfo as a single table. It seems better to create a point coverage with only the rock types and comments, and then RELATE the individual fabric elements to this table. This should be a Non-redundacy database. The problem with this is that the relate would be a "one to many" relate, which does not work.

So, I went back to excel, and separated fabric elements in different files, containing only the data and the station number (which is also in the stations coverage).

Created a macro in Excel to get the data out in individual files, (a coord file, and a data file per fabric element). And then a macro in Arcinfo to create a cover using each file, and an info file to join to the cover later. The AML also projected the cover to UTM and copied the cover to the piedrasutm folder. Most references are absolute.

==========

Excel Macro

==========

```
'
' macroprueba Macro
' Macro recorded 6/24/99 by cmontes.
' This macro extracts data from a spreadsheet  based
' on Codes defined by an outer loop (i). Inner loops
' take care of the column location of the code (j)
' and the innermost loop (k) copies, and saves to file
' the selected records
' this macro reads column by column, and stops when it
' find the keyword 9999

'Variable definition

Sub macroprueba()
Dim i As Integer: Dim stri As String
Dim j As Integer: Dim jstr As String
Dim k As Integer: Dim kstr As String
Dim trackerstr As String
Dim filename1 As String: Dim filename2 As String
Dim temp As String: Dim temp2 As String
Dim nc1 As String: Dim nc2 As String: Dim nc3 As String
Dim nc4 As String: Dim nc5 As String
Dim nxc1 As String: Dim nxc2 As String: Dim nxc3 As String
Dim nxc4 As String: Dim nxc5 As String
Dim station As String: Dim stationx As String
Dim longtd As String: Dim longtdx As String
Dim lattd As String: Dim lattdx As String

'Setting variables to useful initial values
k = 2: kstr = "2": temp = "dataf": temp2 = "statf"
station = "A": longtd = "AK": lattd = "AL"

'start of outer loop 18 times because it is the
'number of possible codes
For i = 1 To 18 Step 1

'create file names with i as criteria, and open them
'at the end there will be 38 files
stri = Str(i)
filename1 = temp + stri
filename2 = temp2 + stri
Open filename1 For Output As #1
Open filename2 For Output As #2

   'start of j loop. 5 times because it is the number
   'of columns containing codes
   For j = 1 To 5 Step 1

      'setting up column names so they change each time this loops
      If j = 1 Then
      jstr = "G": nc1 = "H": nc2 = "I": nc3 = "J": nc4 = "K": nc5 = "L"
      ElseIf j = 2 Then
      jstr = "M": nc1 = "N": nc2 = "O": nc3 = "P": nc4 = "Q": nc5 = "R"
      ElseIf j = 3 Then
      jstr = "S": nc1 = "T": nc2 = "U": nc3 = "V": nc4 = "W": nc5 = "X"
      ElseIf j = 4 Then
```

```
    jstr = "Y": nc1 = "Z": nc2 = "AA": nc3 = "AB": nc4 = "AC": nc5 = "AD"
    ElseIf j = 5 Then
    jstr = "AE": nc1 = "AF": nc2 = "AG": nc3 = "AH": nc4 = "AI": nc5 = "AJ"
    End If

    trackerstr = jstr + kstr

    'This loop evaluates each cell in a j column
    While Range(trackerstr) <> "9999"
      nxc1 = nc1 + kstr: nxc2 = nc2 + kstr: nxc3 = nc3 + kstr
      nxc4 = nc4 + kstr: nxc5 = nc5 + kstr: stationx = station + kstr
      'writes to coordinate file if any i is true
      If Range(trackerstr) = i Then
        longtdx = longtd + kstr
        lattdx = lattd + kstr
        Write #2, Range(stationx), Range(longtdx), Range(lattdx)
      End If

      'writes data to data files if i is true in this loop
      If Range(trackerstr) = i Then
        'writes to datafile with always three fields (strike, dip, dip dir), or (trend, plunge, style)
            If ((Range(trackerstr) = 1) Or (Range(trackerstr) = 11) Or (Range(trackerstr) = 13) Or
(Range(trackerstr) = 15) Or (Range(trackerstr) = 17) Or (Range(trackerstr) = 18) Or (Range(trackerstr) = 4)
Or (Range(trackerstr) = 6) Or (Range(trackerstr) = 5) Or (Range(trackerstr) = 12)) Then
          Print #1, Range(stationx); ","; Range(nxc1); ","; Range(nxc2); ","; Range(nxc3); """"
        'writes to datafile with, possibly, three fields (trend, plunge, style)
            ElseIf ((Range(trackerstr) = 4) Or (Range(trackerstr) = 5) Or (Range(trackerstr) = 6) Or
(Range(trackerstr) = 9) Or (Range(trackerstr) = 14)) Then
          Print #1, Range(stationx); ","; Range(nxc1); ","; Range(nxc2); ","; Range(nxc3); """"
        'writes data with 4 fields (spacing)
            ElseIf ((Range(trackerstr) = 3) Or (Range(trackerstr) = 7) Or (Range(trackerstr) = 8) Or
(Range(trackerstr) = 10)) Then
              Print #1, Range(stationx); ","; Range(nxc1); ","; Range(nxc2); ","; Range(nxc3); "","";
Range(nxc4)
        'writes to datafile for faults (5 fields)
        ElseIf (Range(trackerstr) = 16) Then
            Print #1, Range(stationx); ","; Range(nxc1); ","; Range(nxc2); ","; Range(nxc3); "","";
Range(nxc4); "","; Range(nxc5)
        'writes to datafile for pencleavage, and maxelong (2 fields)
        ElseIf ((Range(trackerstr) = 9) Or (Range(trackerstr) = 14)) Then
          Print #1, Range(stationx); ","; Range(nxc1); ","; Range(nxc2)
        'writes to datafile for veins (5 fields)
        Else
            Print #1, Range(stationx); ","; Range(nxc1); ","; Range(nxc2); ","; Range(nxc3); "","";
Range(nxc4); ","; Range(nxc5)
        End If
      End If

      k = k + 1
      kstr = Trim(Str(k))
      trackerstr = jstr + kstr

    Wend
    'resetting variables to start over in a new column
    k = 2
    kstr = "2"

  Next j

'Closing files, and adding an extra space at the end for arcinfo generate
Write #1,
Write #2,
Close #1
```

```
Close #2
Next i
End Sub
```

Appendix II

Field Photographs of La Tabla Fm.

DATA BY STATION AND PHOTO NUMBER.

Station number	x coordinate decimal degrees	y coordinate decimal degrees	Number of veins measured	Total cummulative length (cm)	Area measured in photo (cm^2)	Number of veins per cm^2	Length of vein per cm^2	Average vein length	Photo number
564	-74.85757366	4.43277052	225	214.64	310	0.73	0.69	0.95	11-10
564	-74.85757366	4.43277052	304	201.61	390	0.78	0.52	0.66	11-11
564	-74.85757366	4.43277052	127	73.24	362	0.35	0.20	0.58	11-16
565	-74.86330198	4.43143291	206	95.87	233	0.88	0.41	0.47	11-17
565	-74.86330198	4.43143291	258	115.28	272	0.95	0.42	0.45	11-18
566	-74.86679339	4.43291393	204	135.38	199	1.03	0.68	0.66	11-20
647	-74.8336138	4.43075388	196	178.75	350	0.56	0.51	0.91	12-25
647	-74.8336138	4.43075388	144	111.75	182	0.79	0.61	0.78	12_27
272	-74.84672994	4.53742468	60	55.41	326	0.18	0.17	0.92	6-18
345	-74.92416414	4.47221541	152	90.01	356	0.43	0.25	0.59	7-22
345	-74.92416414	4.47221541	166	87.95	260	0.64	0.34	0.53	7-24
345	-74.92416414	4.47221541	202	128.89	263	0.77	0.49	0.64	7-26
345	-74.92416414	4.47221541	101	68.21	320	0.32	0.21	0.68	7-28
345	-74.92416414	4.47221541	307	208.46	1444	0.21	0.14	0.68	7-33
648	-74.83254169	4.43127268	278	127.02	61	4.56	2.08	0.46	12_29
42-43	-74.87161218	4.50866589	59	47.55	267	0.22	0.18	0.81	II7
100	-74.84645838	4.5260733	80	65.11	1422	0.06	0.05	0.81	IV35
100	-74.84645838	4.5260733	60	54.72	441	0.14	0.12	0.91	IV36
100	-74.84645838	4.5260733	126	93.35	912	0.14	0.10	0.74	IV37
100	-74.84645838	4.5260733	56	50.69	986	0.06	0.05	0.91	IV38
77	-74.84641234	4.52726871	105	99.46	863	0.12	0.12	0.95	IV15
77	-74.84641234	4.52726871	47	45.61	984	0.05	0.05	0.97	V8
TOTAL			**3463**	**2348.96**	**11203**				
AVERAGE						**0.63**	**0.38**	**0.73**	



Photo 11-16.

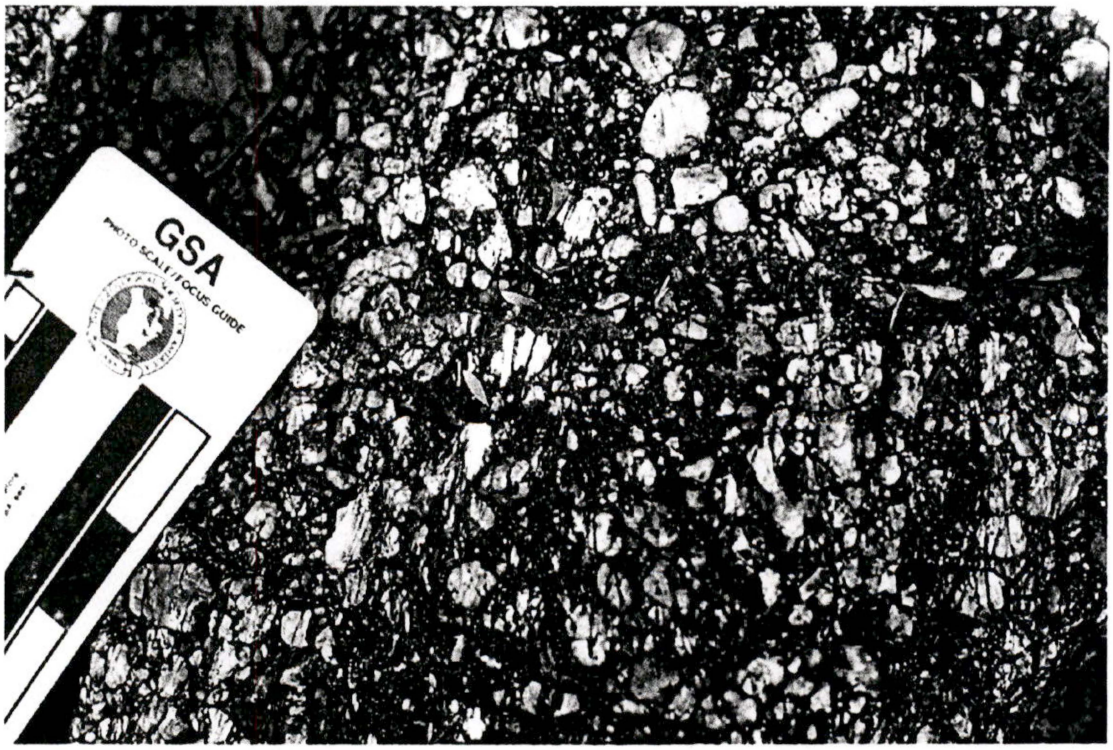


Photo 11-17

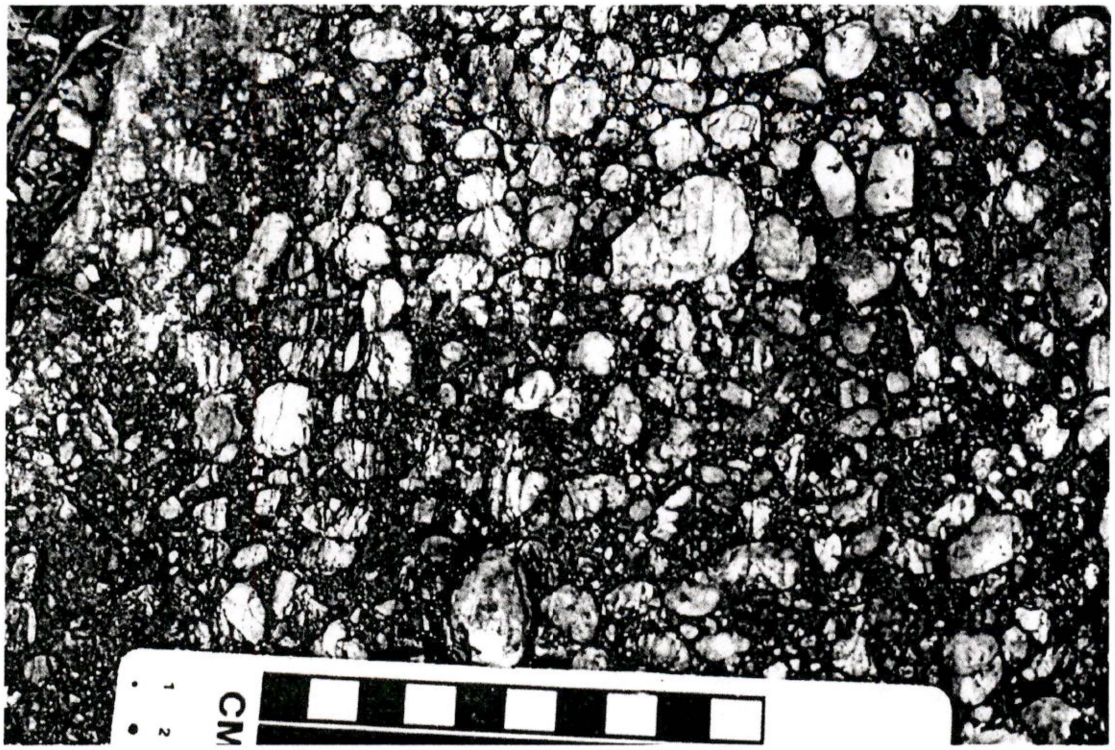


Photo 11-18.

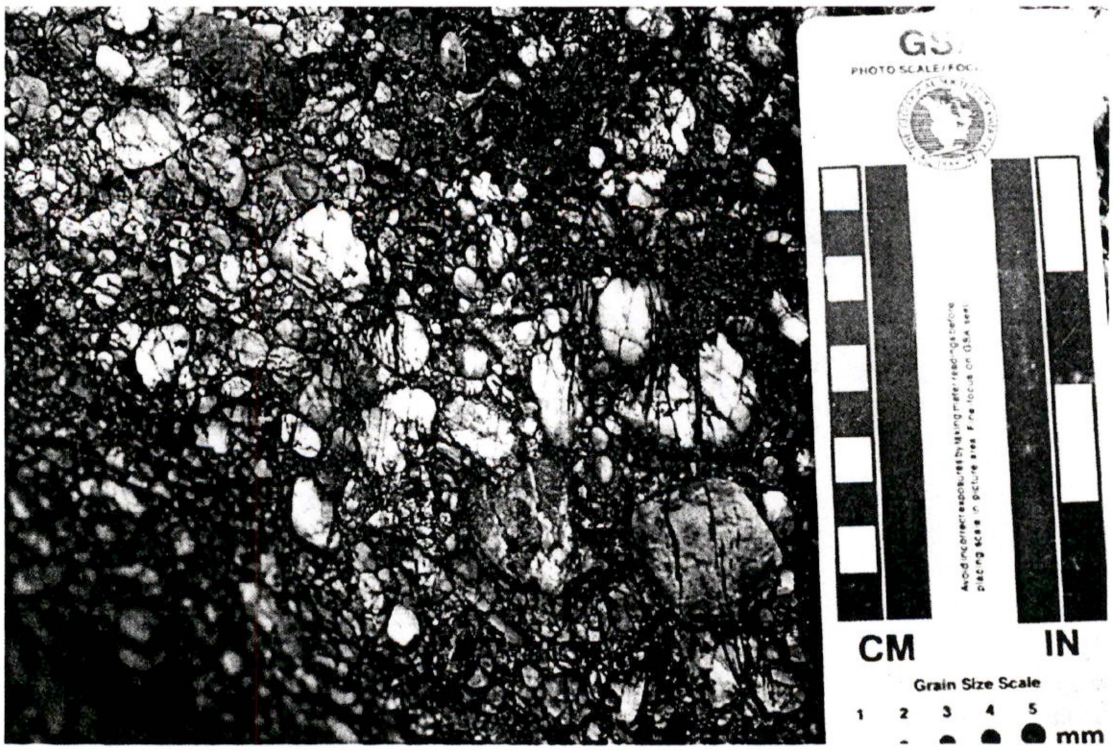


Photo 11-20.

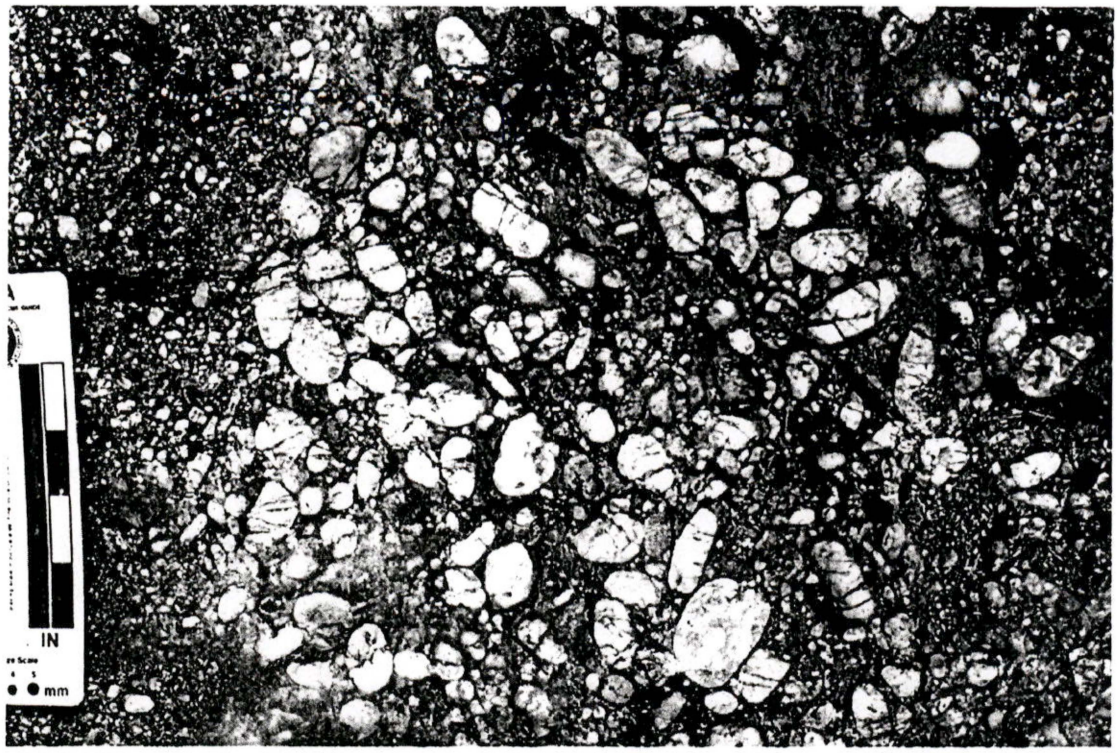


Photo 11-25.

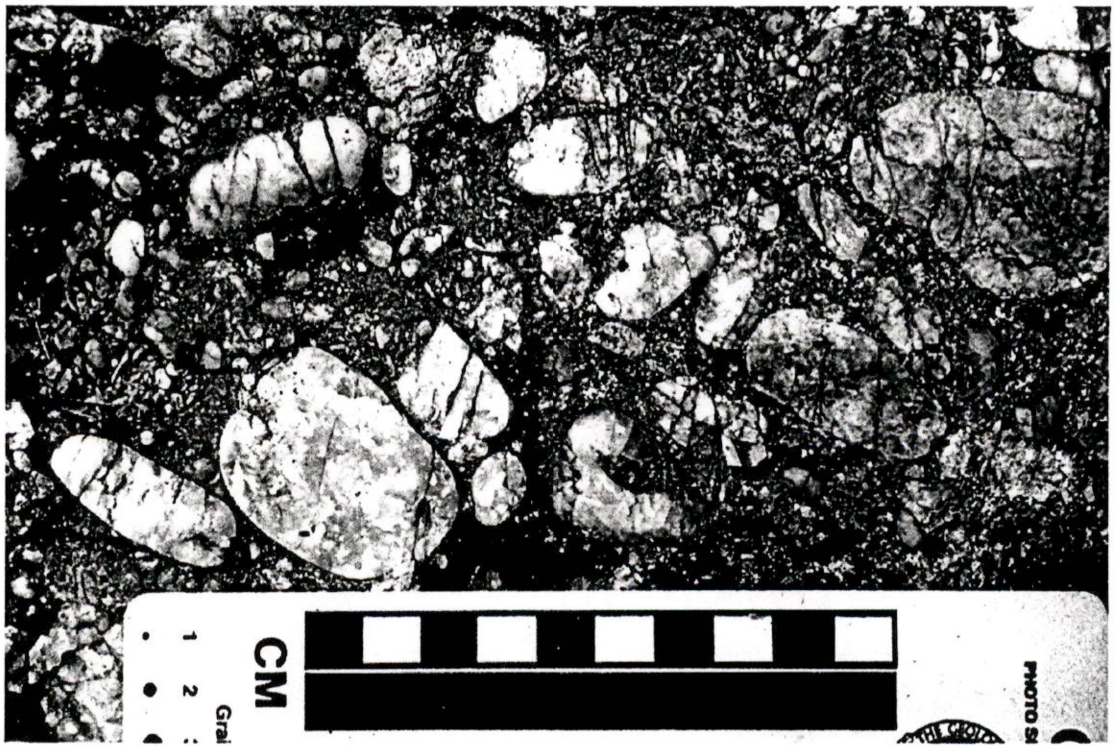


Photo 11-27.



Photo 6-18.

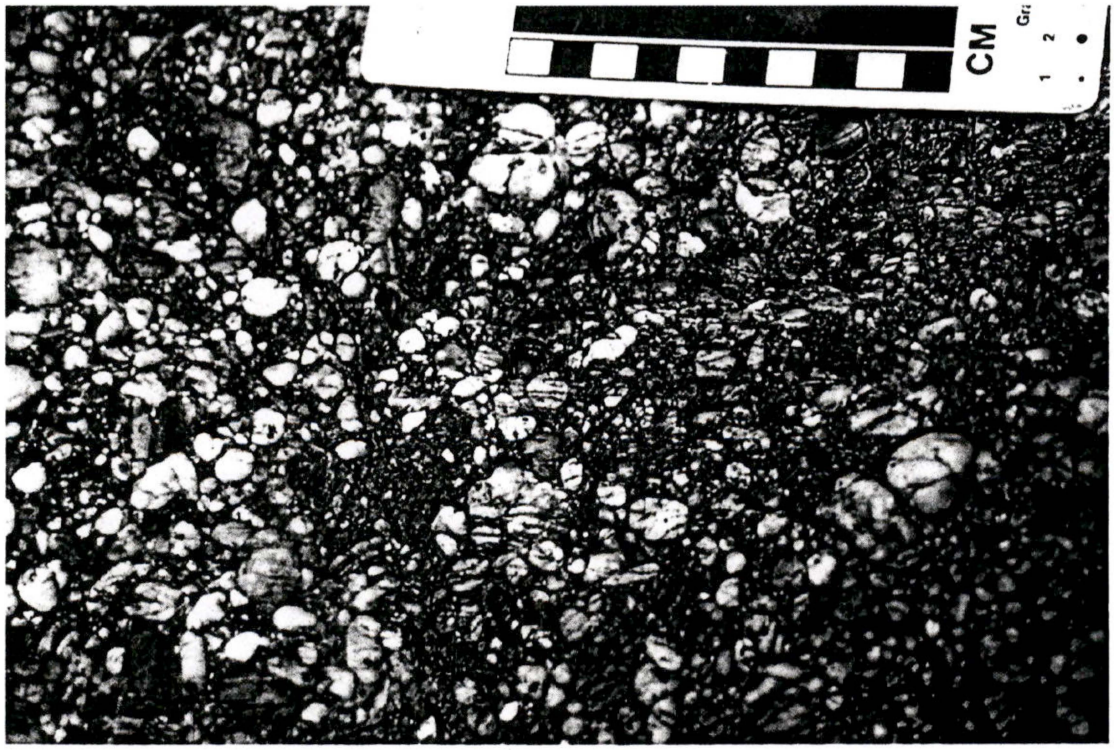


Photo 7-22.

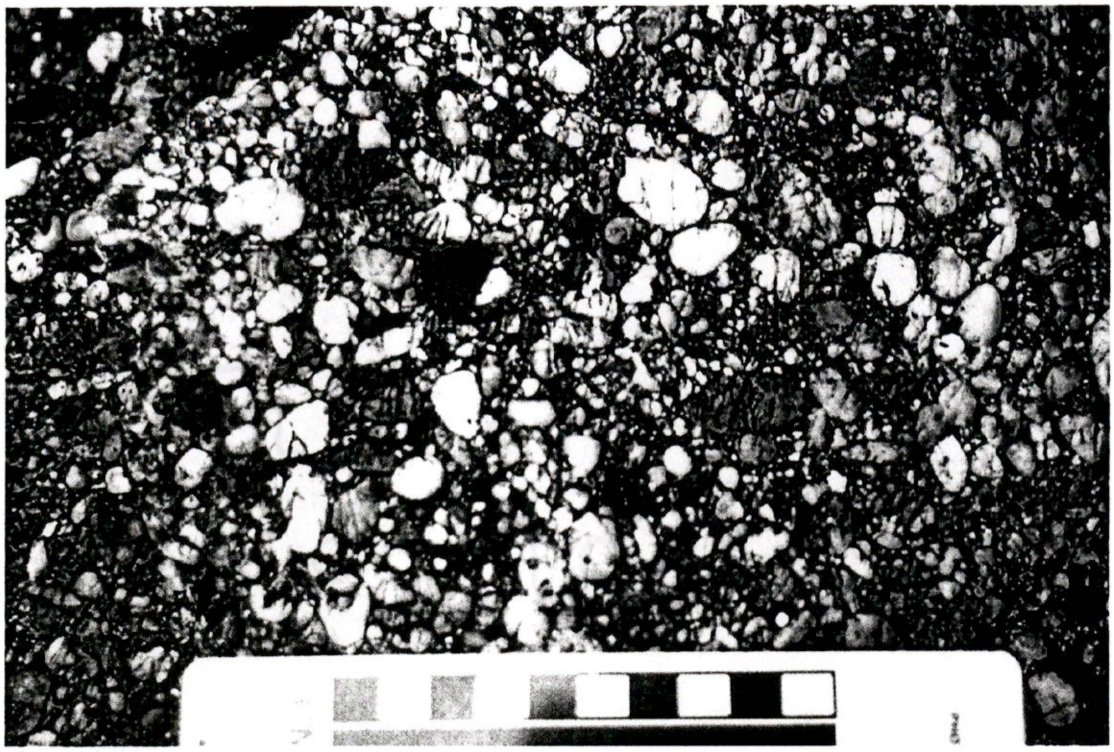


Photo 7-24.

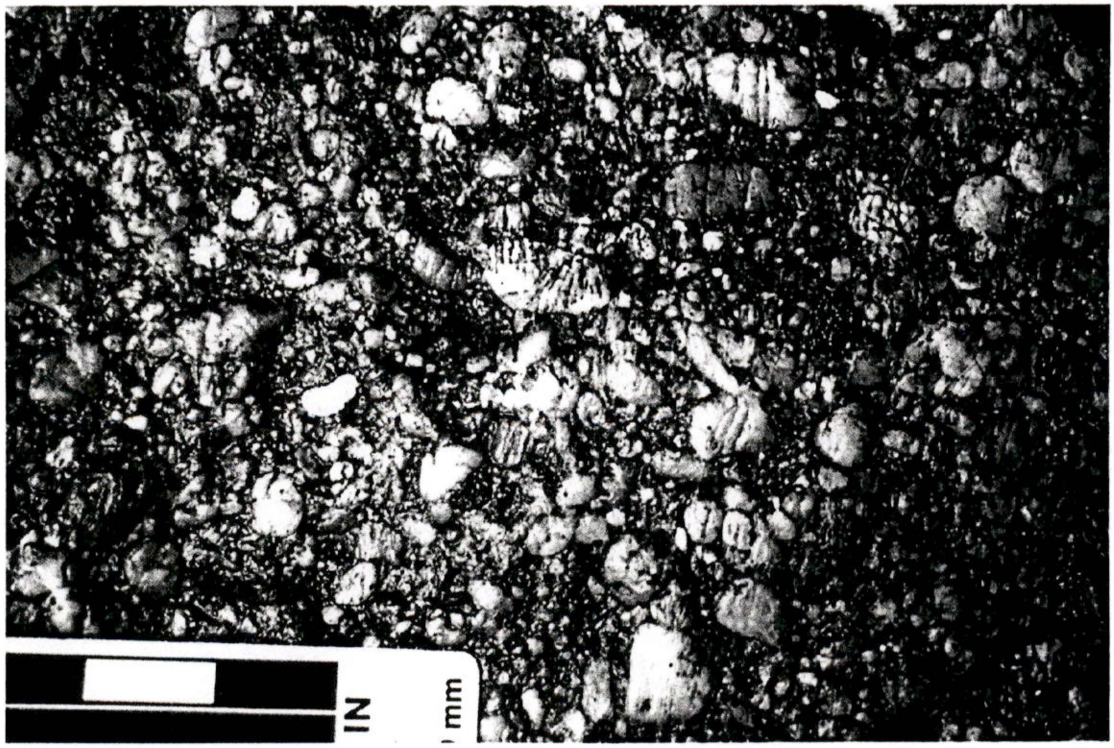


Photo 7-26

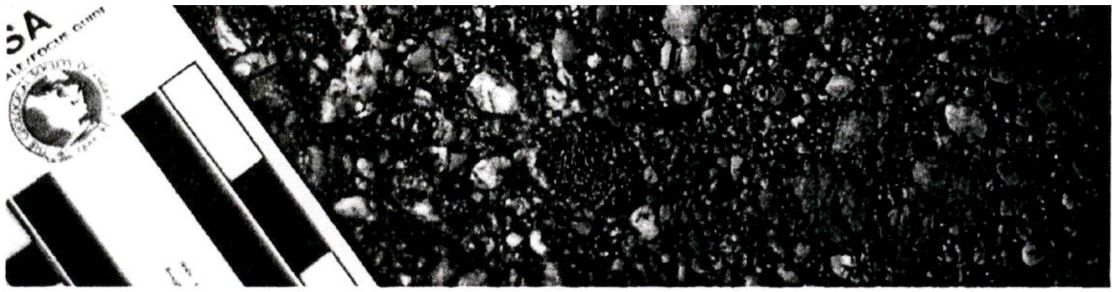


Photo 7-28

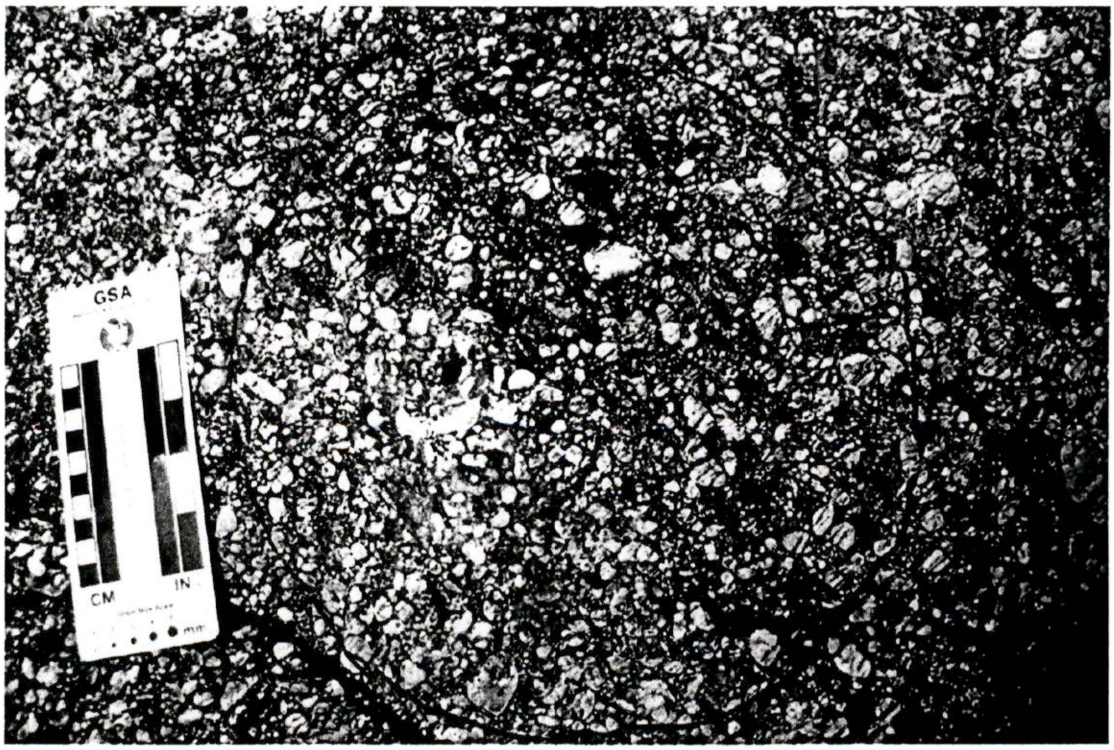


Photo 7-33



Photo new12_29



Photo II-7

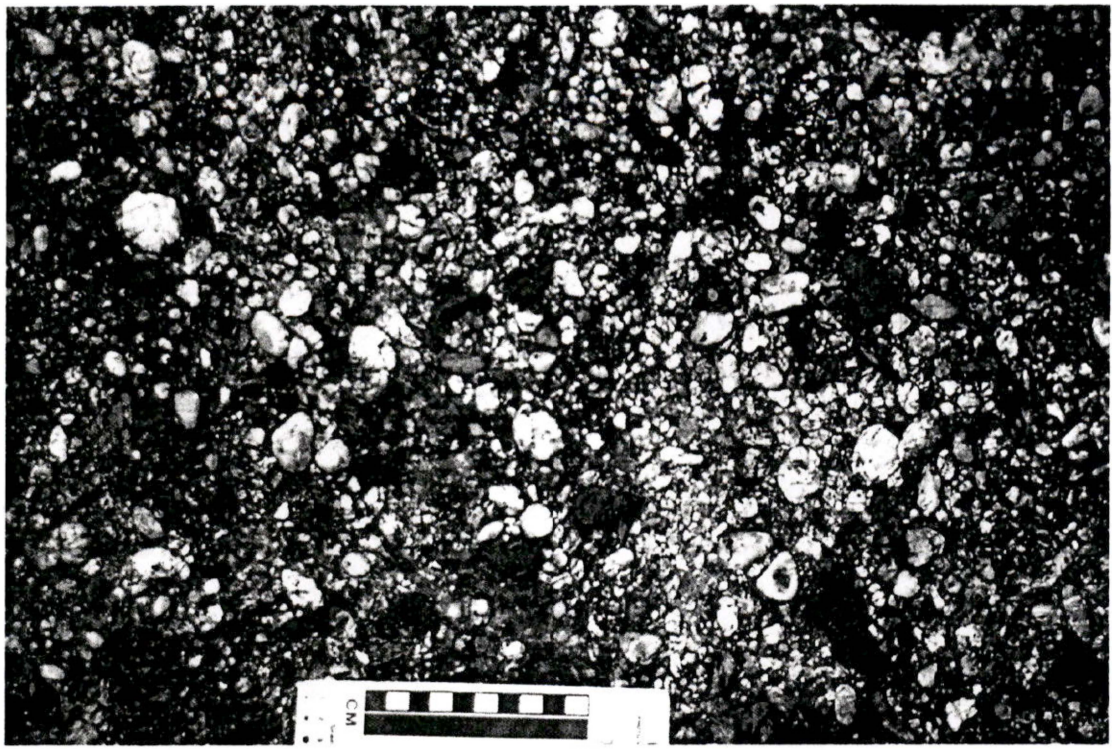


Photo IV-35



Photo IV-36

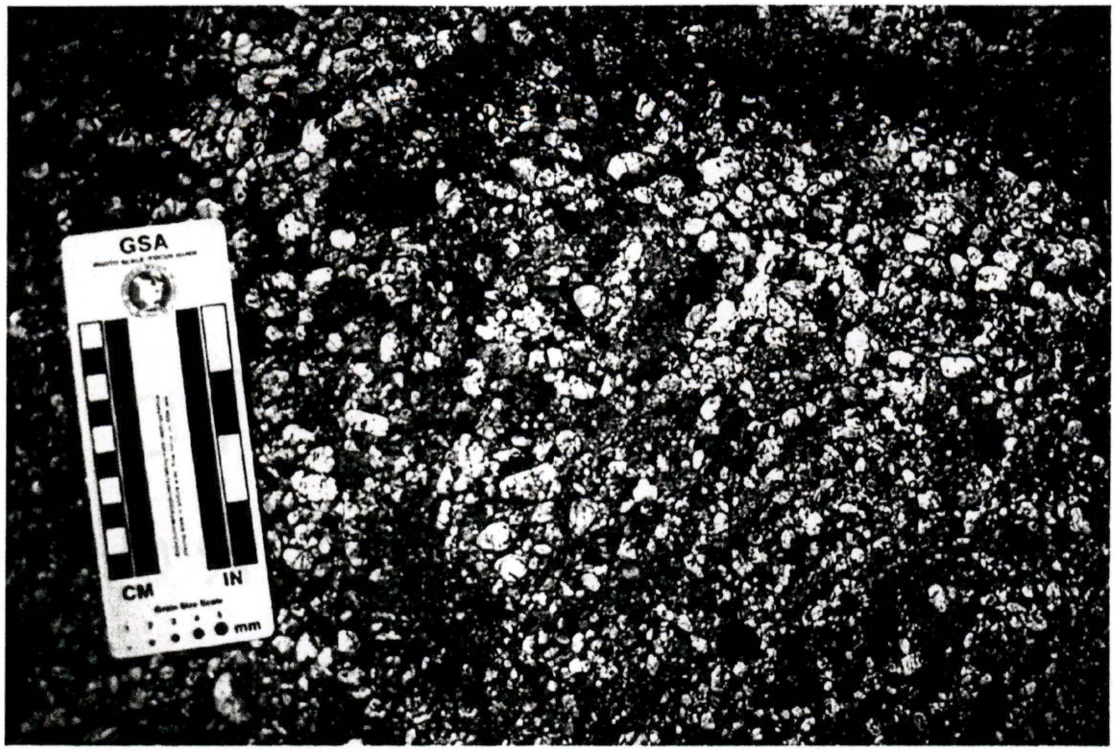


Photo IV-37

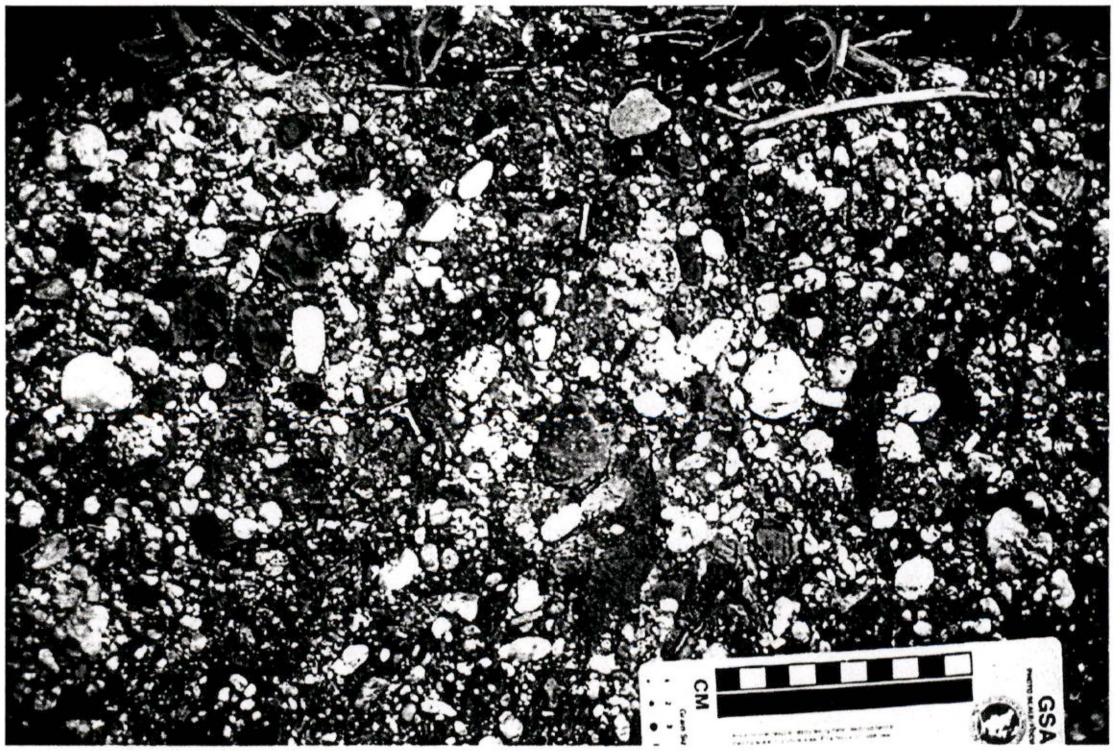


Photo IV-38



Photo I-11

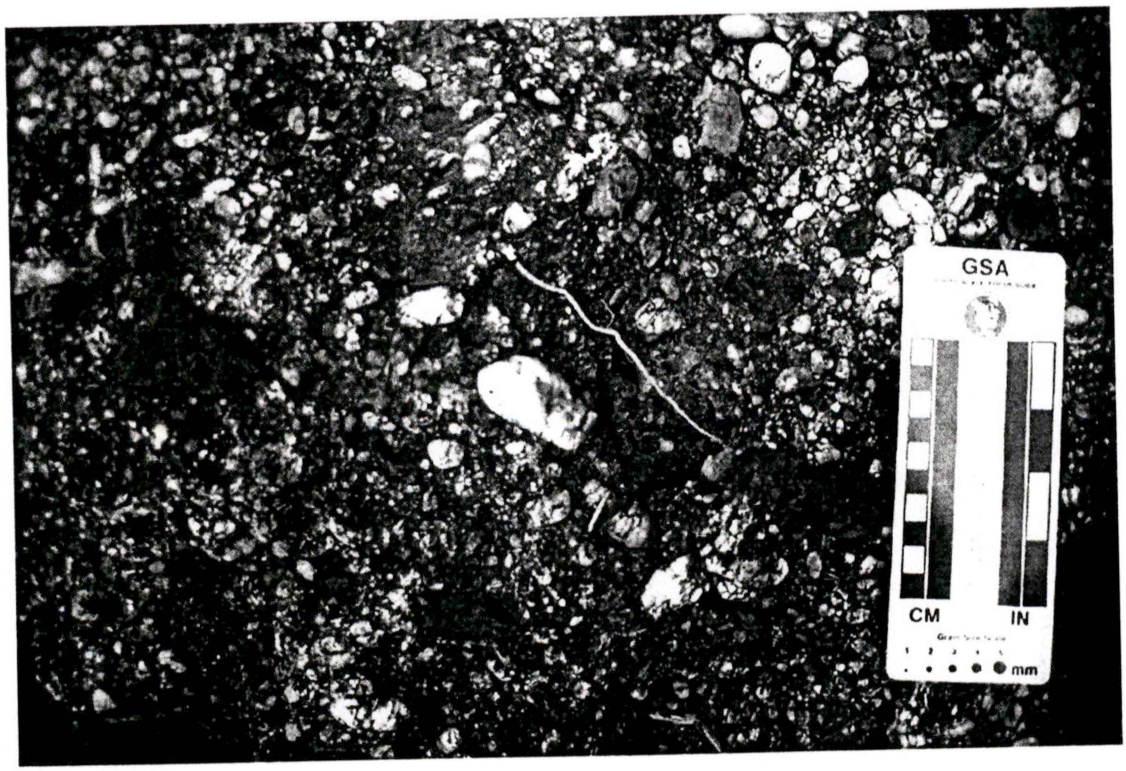


Photo IV-15



Photo V8



Photo 11-10

ADDITIONAL FIELD PHOTOGRAPHS



Photo 11-12.



Photo 11-13.



Photo 11-14.



Photo 11-15.

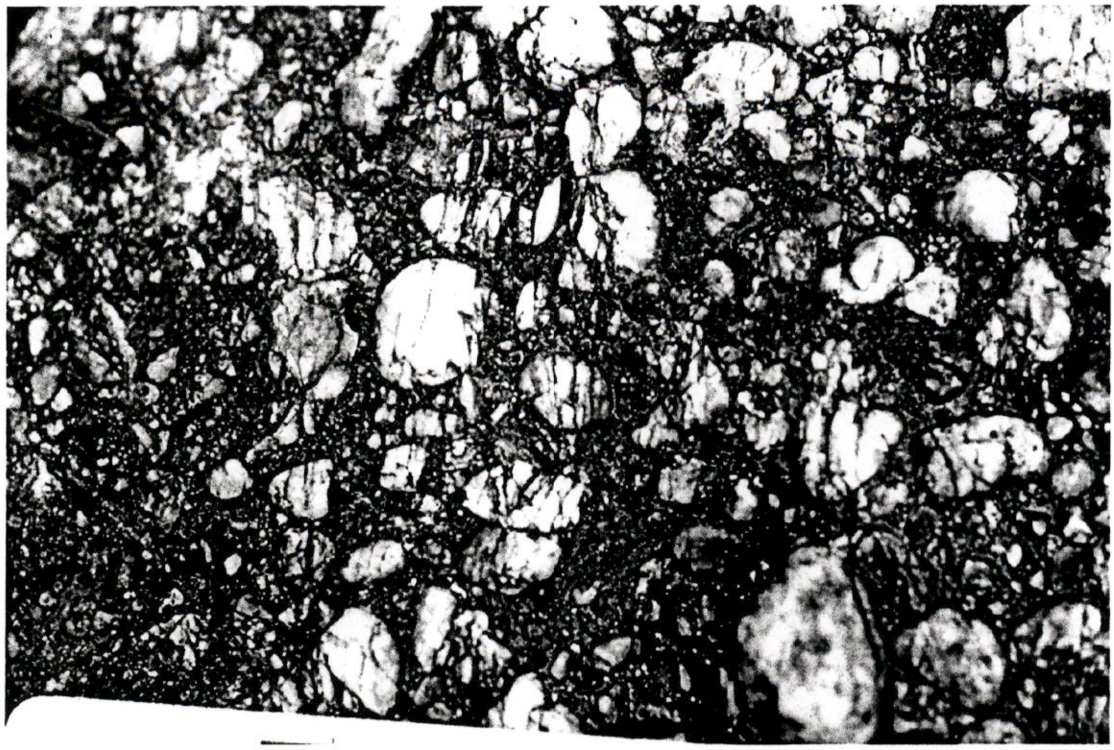


Photo 11-19.

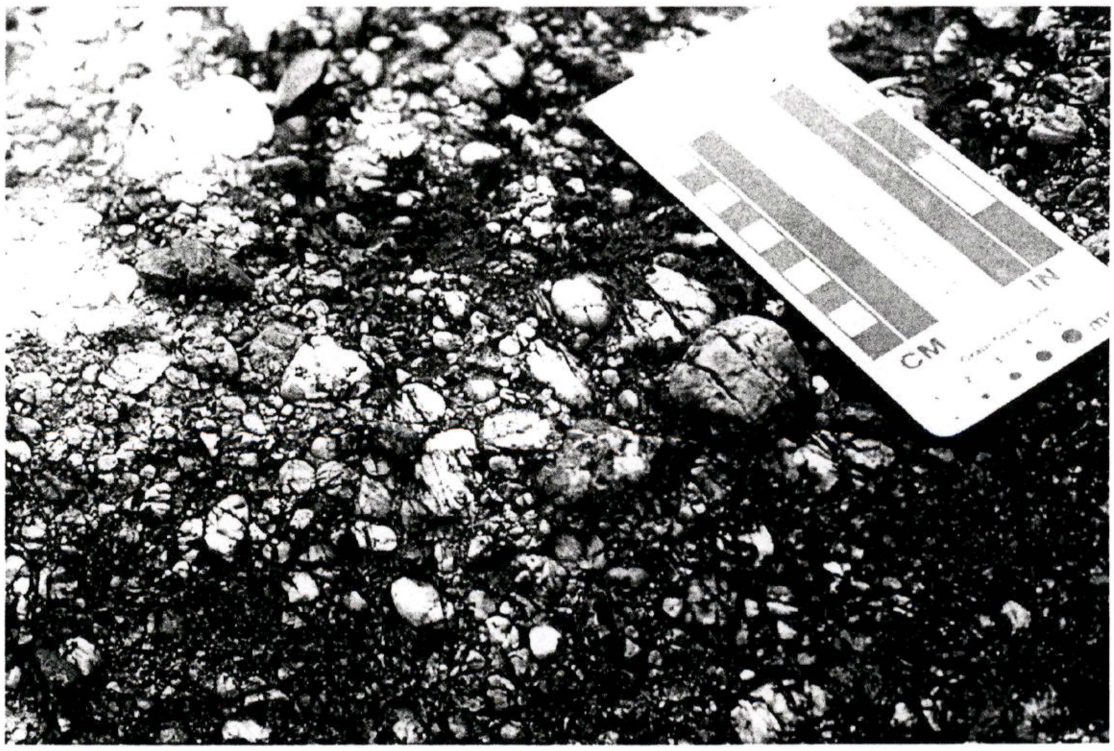


Photo 11-21.

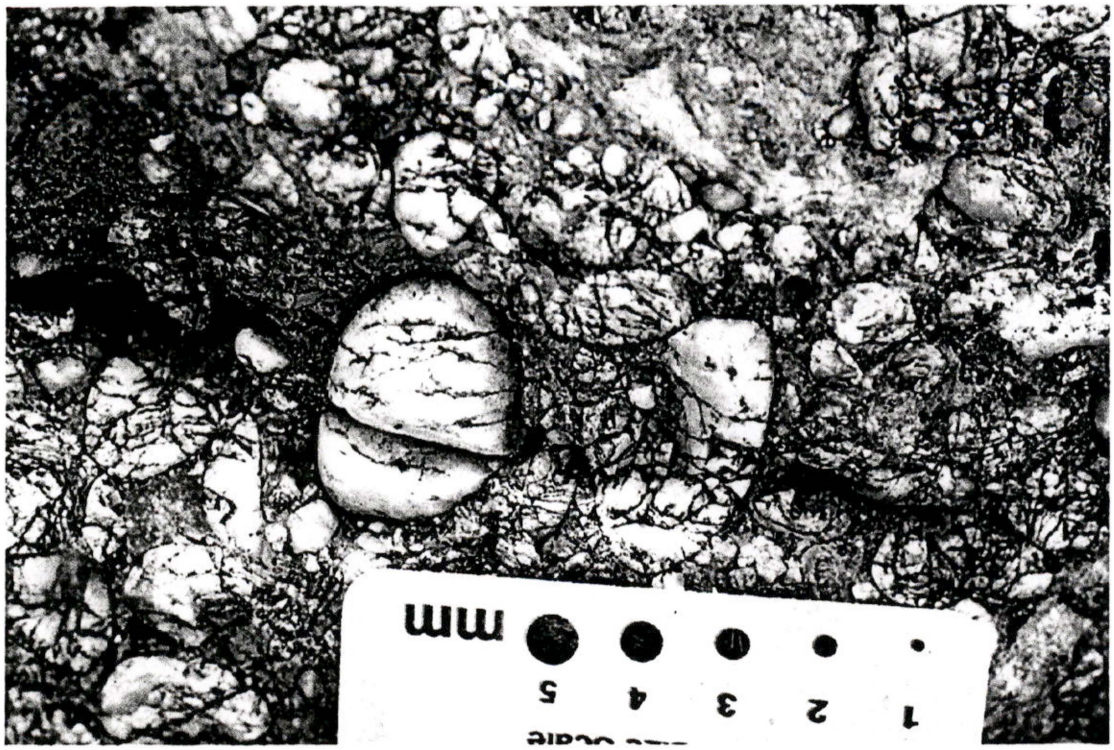


Photo 11-7.



Photo 11-8.

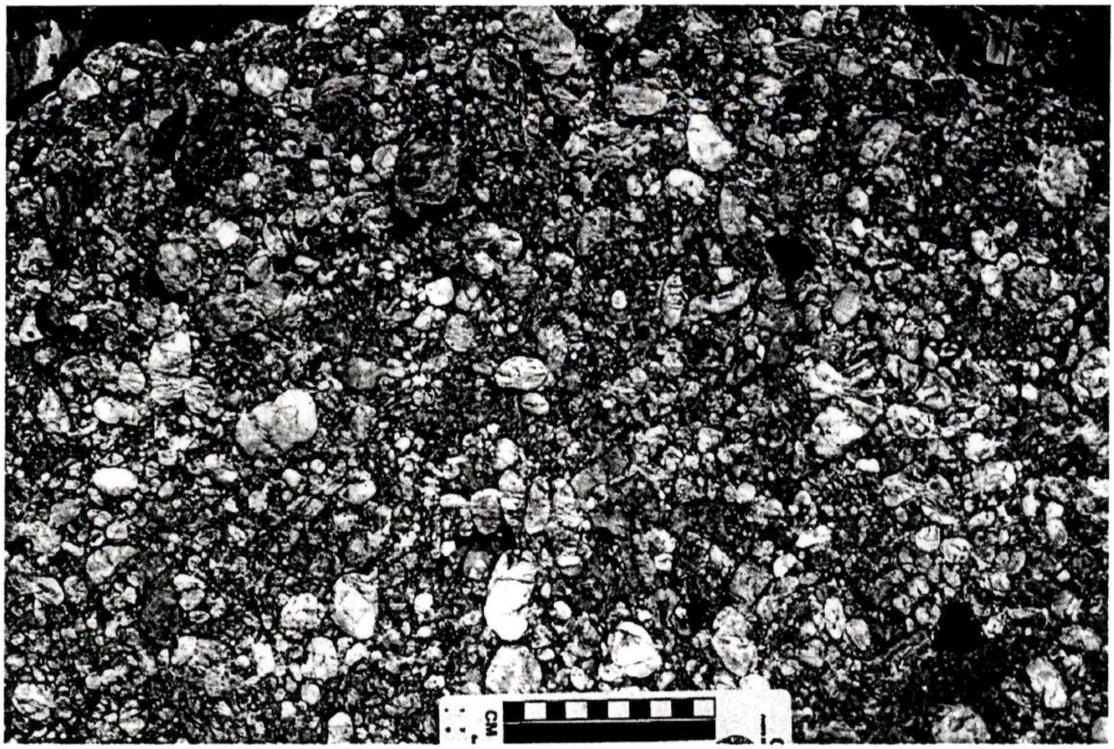


Photo 11-9.



Photo 12-26.

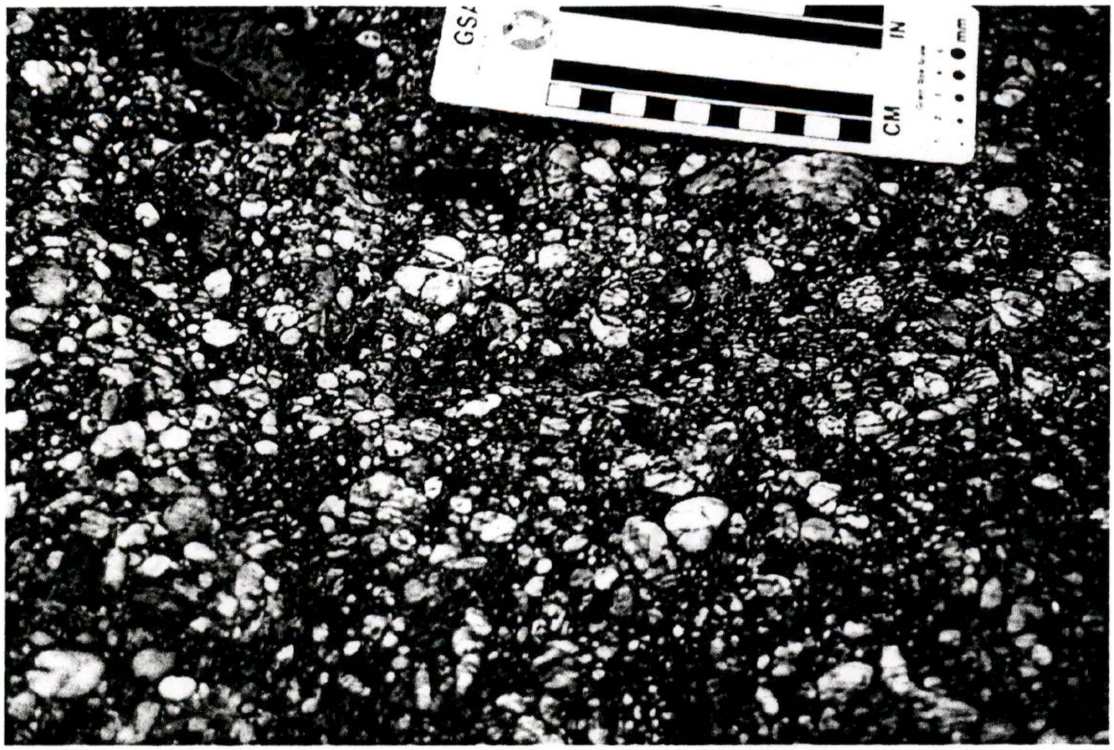


Photo 7-21.

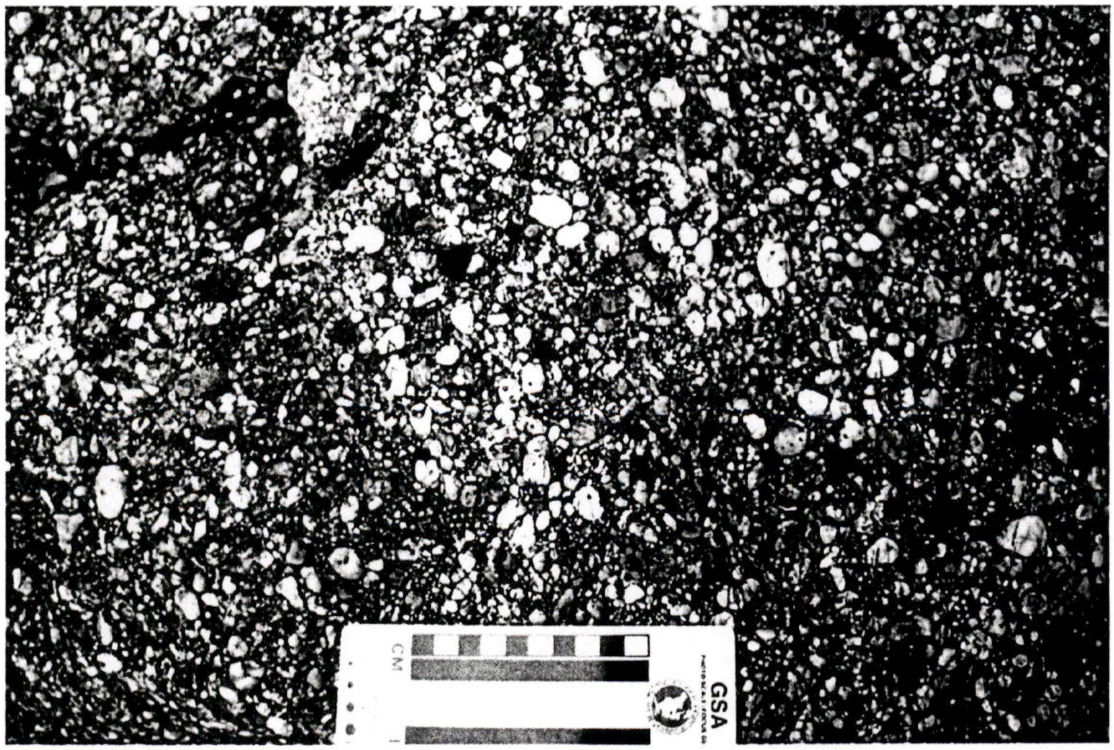


Photo 7-23.

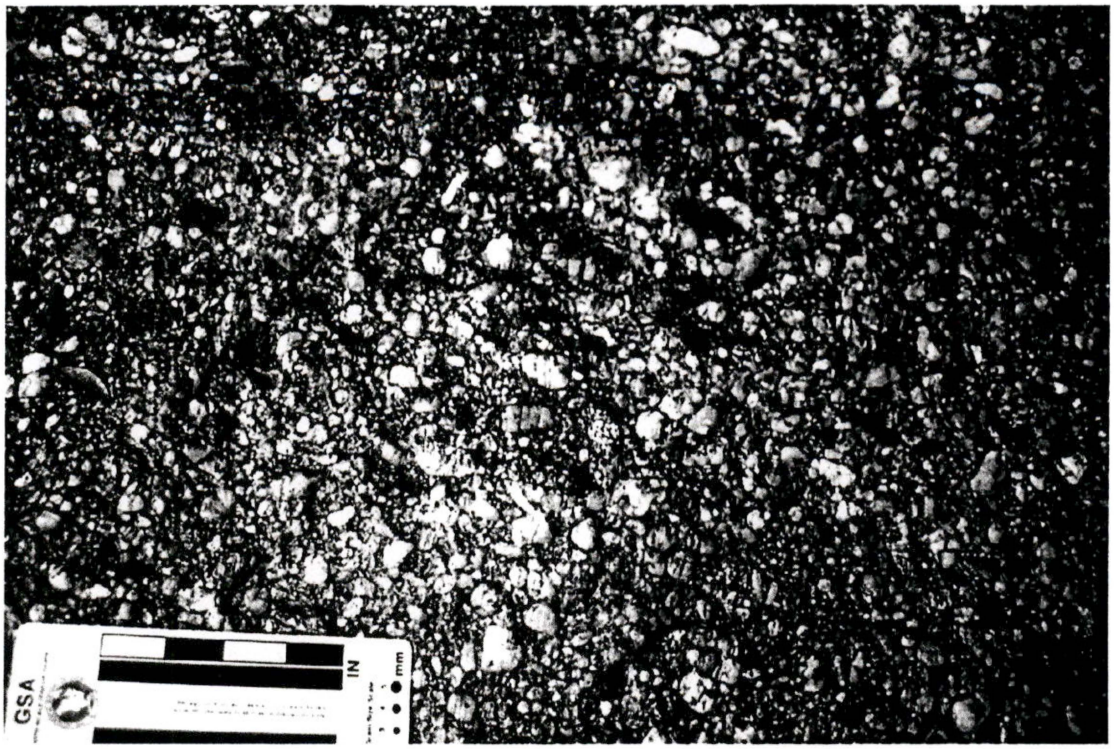


Photo 7-25.

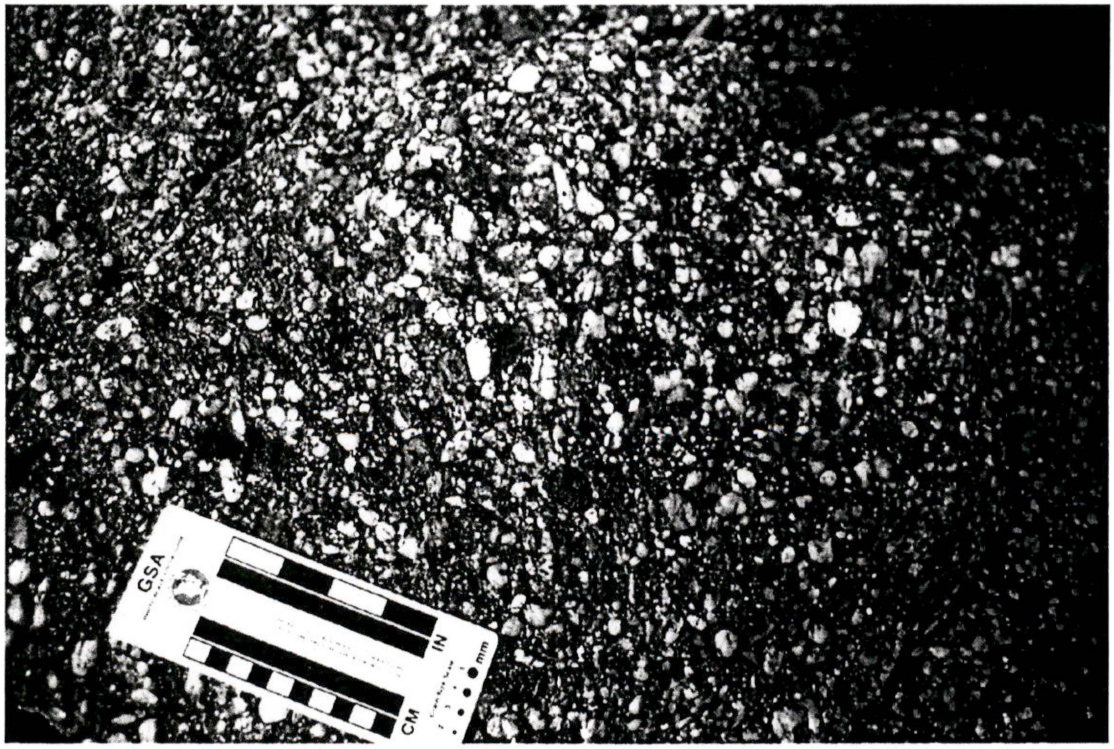
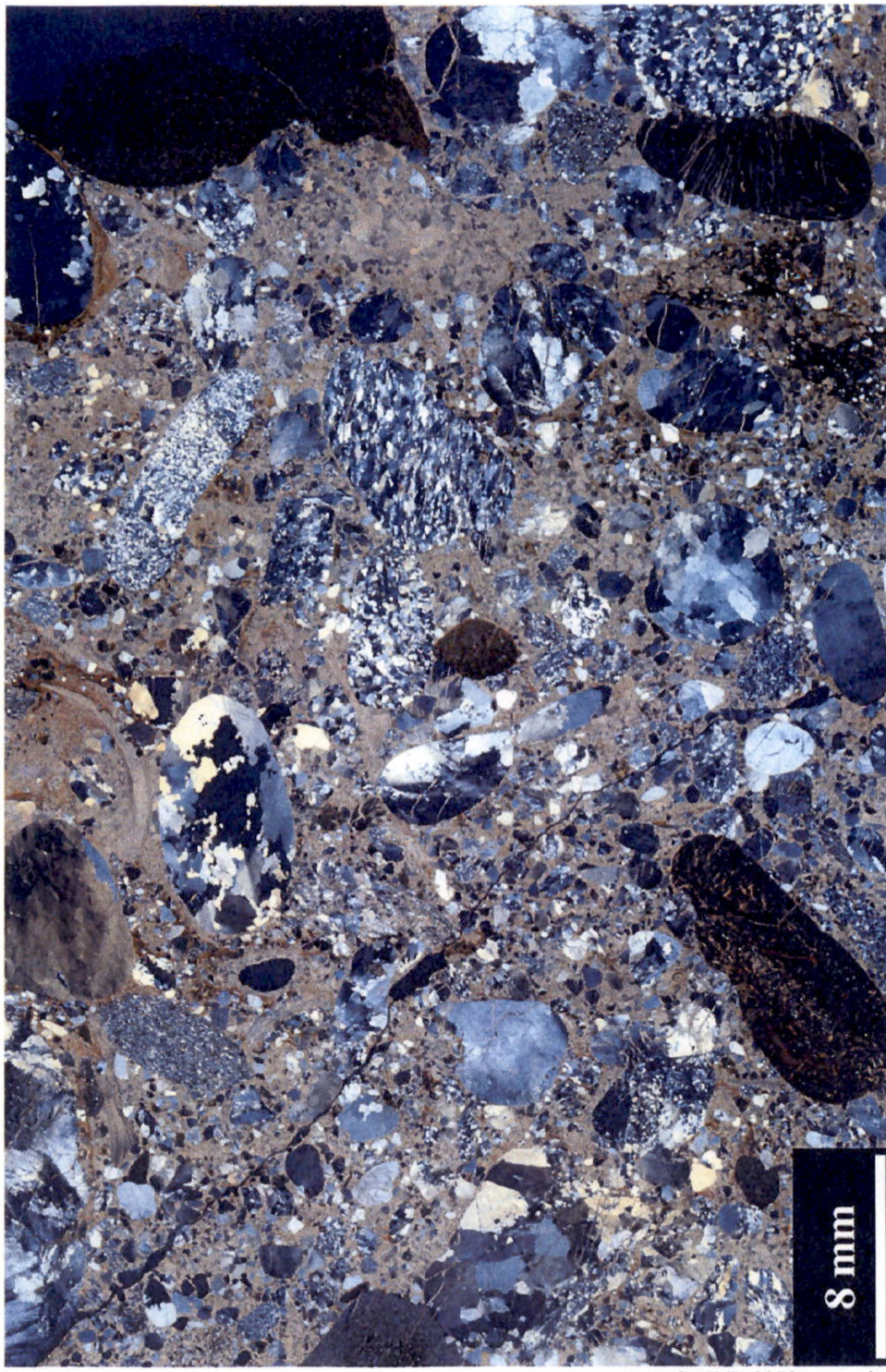


Photo 7-27.

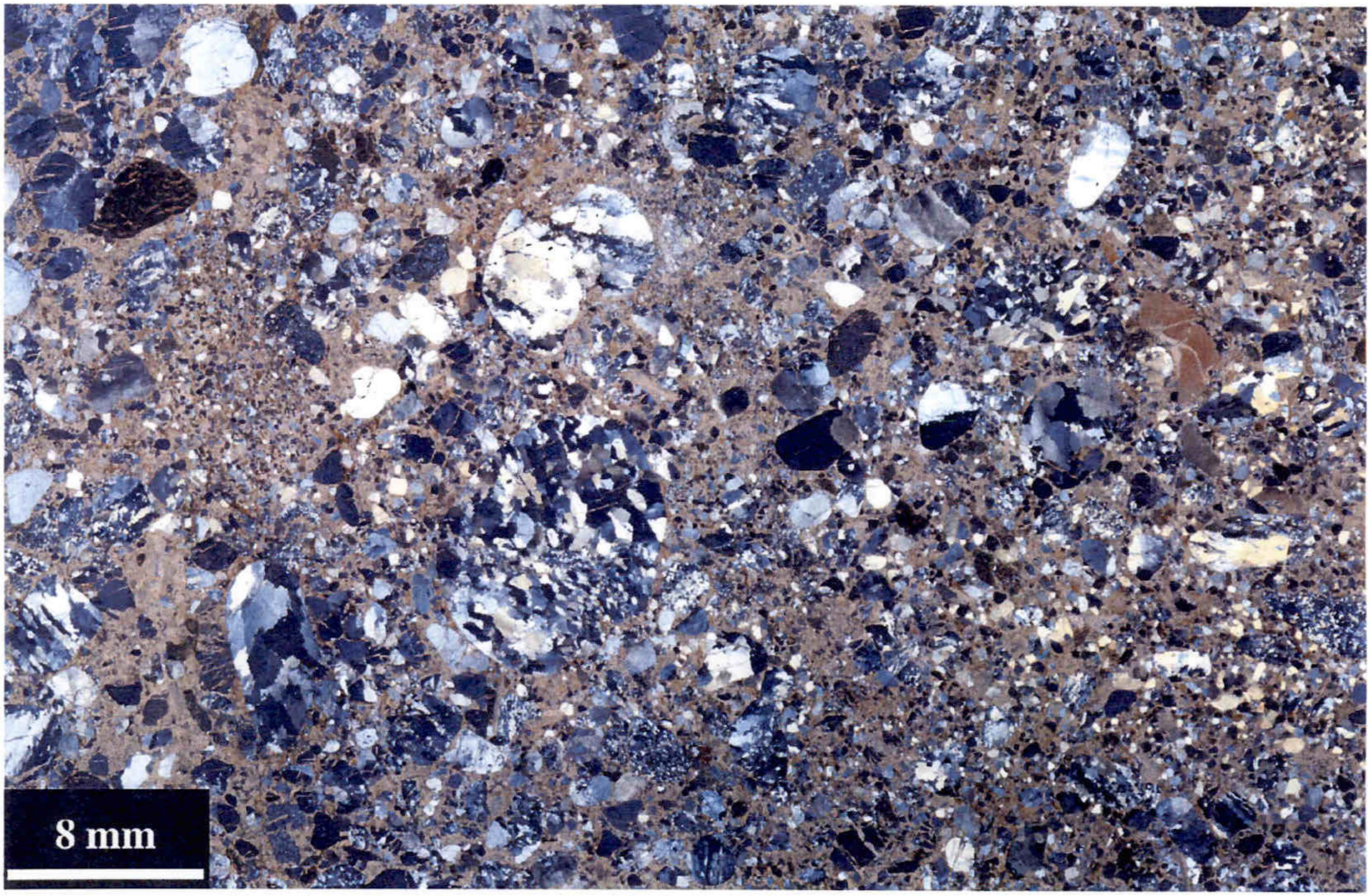


Photo II-6

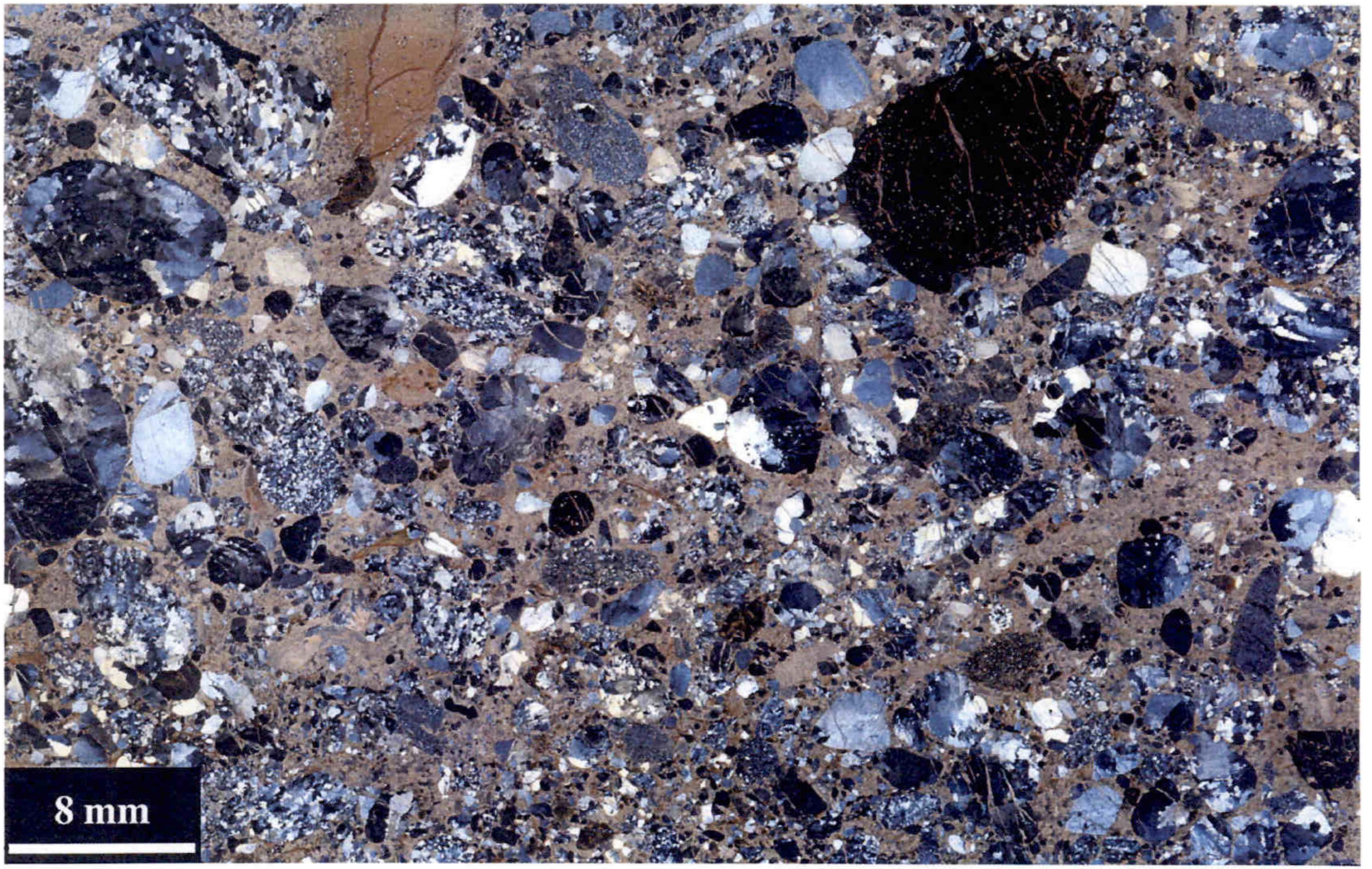
THIN SECTIONS IN STATION 345



Thin section CM-LT-2



Thin section CM-LT-3



Thin section La Tabla 345

Appendix III

Field Data

Numeric Codes to read the database

Code	Lithologic Type
1	Clastic breccia
2	Conglomerate
3	Quartz sandstone
4	Lithic sandstone
5	Calcareous sandstone
6	Feldspathic sandstone
7	Tuffaceous sandstone
8	Siltstone
9	Mudstone
10	Black shale
11	Carbonaceous shale
12	Calcareous shale
13	Limestone
14	Cherty limestone
15	Micritic limestone
16	Limestone conglomerate
17	Limestone breccia
18	Bedded chert
19	Porcelanite
20	Silicic silstone
21	Phosphorite
22	Chalk
23	Gypsum bed
24	Gypsiferous shale
25	Ash layer
26	Tuff
27	Tuff breccia
28	Lapilli tuff
29	Gabbro
30	Diorite
31	Diabase dike
32	Fault breccia
33	Silicic gneiss
34	Mafic gneiss
35	Oil seep
36	Granite
37	Lithic quartz sandstone
38	Calcareous siltstone

Code	Lithologic modifier
50	Very coarse grained
51	Coarse grained
52	Medium grained
53	Fine grained
54	Very fine grained
55	Clast supported
56	Matrix supported
57	Fe-cemented
58	Calcite-cemented
59	Unconsolidated
60	Welded
61	Conglomeratic
62	Pebbly
63	Sandy
64	Silty
65	Muddy
66	Massive
67	Laminated
68	Bedded
69	Cross-bedded
70	Concretional
71	Graded
72	Poorly sorted
73	Well sorted
74	Very well sorted
75	Angular
76	Rounded
77	Brecciated
78	Fossiliferous
79	Ammonites
80	Fish bones
81	Forams
82	Fish scales
83	Oolites
84	Inoceramus
85	Black
86	Gray
87	Yellow
88	Red
89	White
92	Green
93	Lithic
94	Feldspathic
95	Internally
96	Purple

Code	Fabric element
1	Bedding
2	Vein
3	Joint
4	Slicken slides
5	Mineral lineation
6	Stretching lineation
7	Cleavage
8	Crenulation cleavage
9	Pencil cleavage
10	Stylolitic cleavage
11	Foliation
12	Fold axes
13	Fold axial planes
14	Axis of maximum elongation
15	Preferential fracturing
16	Shear zone/fault zone
17	Intrusive contact
18	Upright bedding
19	Overturned bedding

Code	Stratigraphic unit
1	Younger Terraces
2	Older Terraces
3	Ibagué Fan
4	Tertiaty Undifferentiated
5	Honda Formation
6	T3
7	T2
8	T1
9	Sandy La Tabla Formation
10	Conglomeratic La Tabla Formation
11	Sandy Nivel de Lutitas y Arenas
12	Silty Nivel de Lutitas y Arenas
13	Lidita Superior Formation
14	Sandy Nivel Intermedio
15	Silty Nivel Intermedio
16	Lidita Inferior Formation
17	Calcareous Loma Gorda Formation
18	Siliceous Loma Gorda Formation
19	Ibagué Batholith
20	Diabase Dikes

FIELD DATA

Station Number	Lithology 1	Lithology 2	Lithology 3	Comments	Fossils ?	Photos ?	Altitude (m)	Stratigraphic Unit	Longitude (decimal degrees)	Latitude (decimal degrees)
1	52-68-4	87-88-8	0		0	0	262	10	-74.792	4.532
2	85-67-9	70-10	18	Ph. 1.1-1.4	0	1	297	15	-74.793	4.515
3	20	0	0	Ph. 1.6	0	1	252	24	-74.789	4.511
4	86-9	0	0	Gypsum filling veins	0	0	284	15	-74.788	4.507
5	20	18	0		0	0	316	16	-74.789	4.497
6	18	0	0		0	0	388	18	-74.786	4.495
7	67-53-52-6	0	0	ph. 1.7 & 1.8(looking north)	0	1	543	17	-74.787	4.493
8	10	68-3	0	Sand in 1m thick beds	0	0	279	14	-74.809	4.457
9	84-67-9	66-53-4	0		0	0	287	14	-74.813	4.45
10	67-9	53-3	0	Gypsum in veins. Ph. 1.9 (looking NNE)	0	1	322	14	-74.812	4.447
11	67-9	53-3	0		0	0	391	14	-74.811	4.446
12	67-9	53-3	0		0	0	427	14	-74.81	4.445
13	6	22	0		0	0	470	14	-74.809	4.444
14	88-76-56-63-2	0	0	Ph. 1.10-1.11. Moved?	0	1	260	12	-74.836	4.434
15	88-76-56-63-68-2	0	0		0	0	252	12	-74.836	4.436
17	18	20	0	Moved?	0	0	494	15	-74.864	4.401
18	18	0	0	ph. 1.13-1.18 (looking NW and N)	0	1	571	16	-74.863	4.4
19	2	0	0		0	0	391	12	-74.863	4.403
20	56-2	0	0	ph 1.18	0	0	264	12	-74.841	4.436
21	68-69-3	2	0	Transitional contact over 2m	0	0	295	12	-74.84	4.415
22	10	67-9	0		0	0	298	12	-74.886	4.325
25	30	0	0	Qz 20%- Fd 70%- Btt 5%	0	0	471	22	-74.906	4.523
26	30	31	0	ph. 1.21-1.25	0	1	475	22	-74.908	4.526
27	30	0	0	Qz 15%- Fds 80%- Btt 5%	0	0	425	22	-74.891	4.534
28	31	0	0		0	0	399	22	-74.891	4.536
29	51-30	31	0	ph. 1.28-1.30	0	1	418	22	-74.886	4.539
30	78-15	0	0	ph. 1.31	0	1	310	15	-74.84	4.557
31	20	0	0	ph. 1.32	0	1	428	20	-74.854	4.479
32	77-20	0	0	Moved?	0	0	448	20	-74.855	4.479
33	20	0	0	Moved?	0	0	545	19	-74.854	4.482
34	20	0	0	Drawing in field book	0	0	596	18	-74.855	4.484
35	20	0	0		0	0	611	18	-74.856	4.484
36	84-20	0	0	Ph. 1.36 & 2.1- Fossil (not in etayos hands)	1	1	679	18	-74.859	4.485
37	20	0	0		0	0	700	18	-74.861	4.488
38	20	0	0		0	0	686	18	-74.857	4.49
39	79-10	0	0		0	0	696	18	-74.856	4.492
40	70-78-10	70-78-12	0		0	0	383	20	-74.851	4.481
41	18	0	0		0	0	350	19	-74.853	4.477
42	73-76-2	0	0	Fe mineralization along fractures	0	0	800	12	-74.872	4.509
43	55-2	56-2	0		0	0	800	12	-74.873	4.508
44	89-53-73-76-3	0	0		0	0	798	12	-74.87	4.508

FIELD DATA

Station Number	Lithology 1	Lithology 2	Lithology 3	Comments	Fossils ?	Photos ?	Altitude (m)	Stratigraphic Unit	Longitude (decimal degrees)	Latitude (decimal degrees)
45	53-2	3	0		0	0	717	12	-74.871	4.503
46	53-4	0	0		0	0	747	14	-74.872	4.5
47	18	0	0	Oriented sample	0	0	750	14	-74.871	4.499
48	12	70-15	0	Slicken slides everywhere. Not in situ.	0	0	750	18	-74.871	4.499
49	10	0	0		0	0	792	18	-74.87	4.498
50	53-4	20	0		0	0	794	19	-74.869	4.497
51	12	0	0		0	0	800	20	-74.866	4.492
52	12	0	0		0	0	793	20	-74.87	4.492
53	78-80-84-79-12	0	0		0	0	785	20	-74.869	4.495
54	54-4	84-10	0		0	0	599	19	-74.879	4.518
55	20	0-78-79-12	0		0	0	600	19	-74.88	4.519
56	18	70-13	0		0	0	700	16	-74.875	4.495
57	10	6	0		0	0	700	18	-74.876	4.493
58	20	0	0		0	0	800	19	-74.876	4.491
59	84-70-12	0	0	ph. 2.8-2.15	0	1	850	20	-74.876	4.488
60	15	0	0	ph. 2.16-2.17 between stations 60 and 61- Drawing	0	1	882	20	-74.876	4.487
61	70-5	0	0		0	0	469	11	-74.881	4.529
62	61-4	0	0		0	0	452	11	-74.881	4.529
63	68-75-72-52-4	0	0		0	0	452	11	-74.883	4.528
64	86-75-53-4	0	0		0	0	425	11	-74.885	4.525
65	92-86-53-4	0	0	Drawing in Field Notebook	0	0	425	11	-74.884	4.524
66	35	0	0		0	0	425	21	-74.883	4.524
67	77-10	0	0	Ph. 2.19. Drawing	0	1	428	21	-74.882	4.523
68	0	0	0	GPS station	0	0	325	15	-74.819	4.51
69	68-72-76-81-65-3	63-9	0		0	0	337	15	-74.821	4.509
70	54-3	63-9	21	ph. 4.1-4.4- Drawing	0	1	346	15	-74.821	4.508
71	0	0	0	GPS station	0	0	410	15	-74.823	4.506
72	18	21	0	ph. 4.5-4.6- Drawing	0	1	351	15	-74.822	4.507
73	72-75-56-1	0	0		0	0	275	2	-74.807	4.514
74	55-75-72-1	0	0	ph. 4.8-4.12. Largest frags are 30cmx5cm	0	1	286	2	-74.802	4.515
75	86-76-26	67-89-7	0	ph. 4.13. GPS station	0	1	254	2	-74.819	4.535
76	0	0	0	GPS station	0	0	325	2	-74.845	4.528
77	55-76-2	0	0	ph. 4.15-4.17 and 5.7-5.8- Drawing- Strain data	0	1	325	12	-74.846	4.527
78	18	19	0		0	0	425	19	-74.845	4.503
79	70-20	0	0		0	0	450	20	-74.848	4.502
80	0	0	0	GPS station	0	0	461	20	-74.85	4.501
81	10	15	0		0	0	475	20	-74.851	4.5
82	79-84-70-10	25	0	ph. 4.18-4.19	0	1	475	20	-74.852	4.5
83	70-10	25	0	ph. 4.20-4.21	0	1	519	20	-74.852	4.499
84	86-61-63-26	25	0	Samples- weird- Drawing	0	0	500	20	-74.853	4.499
85	70-12	0	0	ph. 4.22-4.23	0	1	519	20	-74.854	4.497

FIELD DATA

Station Number	Lithology 1	Lithology 2	Lithology 3	Comments	Fossils ?	Photos ?	Altitude (m)	Stratigraphic Unit	Longitude (decimal degrees)	Latitude (decimal degrees)
86	10	0	0		0	0	448	18	-74.843	4.503
87	12	0	0		0	0	450	18	-74.842	4.497
88	70-12	0	0		0	0	501	18	-74.829	4.499
89	20	18	0	Drawing	0	0	300	19	-74.829	4.521
90	70-12	84-15	0		0	0	301	18	-74.832	4.518
91	70-12	0	0		0	0	325	18	-74.833	4.517
92	79-10	0	0	Ph 4.25-4.26. Drawing in Field Notebook	0	0	339	18	-74.833	4.517
93	10	0	0	ph. 4.27. Drawing	0	1	326	18	-74.834	4.517
94	10	12	15	ph. 4.28-4.31. Drawing	0	1	325	18	-74.835	4.517
95	12	15	25	ph. 4.32. Drawing	0	1	325	18	-74.835	4.517
96	12	0	0	No chert clasts upstream	0	0	326	18	-74.836	4.515
97	70-12	0	0		0	0	352	18	-74.836	4.513
98	86-73-52-75-4	0	0	Qz- K-Fds- Mscv- Hbl.	0	0	302	2	-74.836	4.53
99	54-73-76-69-3	0	0	ph. 4.33-4.34	0	1	325	12	-74.846	4.526
100	55-2	0	0	ph. 4.35-4.38. Milky Qz (70%)- and probably Fe Concre	0	1	325	12	-74.846	4.526
101	53-77-58-4	0	0		0	0	301	14	-74.815	4.512
102	18	0	0	Drawing- ph. 5.2-5.3	0	1	451	16	-74.828	4.506
103	0	0	0	GPS station	0	0	633	18	-74.828	4.491
104	10	0	0		0	0	635	18	-74.829	4.491
105	70-12	0	0		0	0	645	18	-74.83	4.491
106	12	0	0		0	0	643	18	-74.83	4.49
107	0	0	0	GPS station	0	0	649	18	-74.832	4.489
108	12	0	0		0	0	650	18	-74.836	4.488
109	0	0	0	Ph. 5.4- Drawing- GPS station	0	1	646	18	-74.84	4.486
110	12	0	0	folded	0	0	650	18	-74.841	4.488
111	55-2	0	0		0	0	325	12	-74.847	4.525
112	53-73-75-67-4	0	0	ph. 5.9-5.11- Drawing	0	1	325	12	-74.847	4.524
113	56-78-58-2	3	0	ph 5.12-5.13	0	0	328	12	-74.847	4.523
114	2	3	0		0	0	350	12	-74.848	4.523
115	53-4	0	0		0	0	381	12	-74.85	4.523
116	52-61-66-3	0	0		0	0	400	13	-74.85	4.523
117	66-3	0	0	Two beds each 6m thick	0	0	438	13	-74.851	4.523
118	10	63-9	0		0	0	475	14	-74.854	4.526
119	85-53-4	58-70-5	0	Discontinuous lamination and Conc 1m diam.	0	0	477	14	-74.855	4.527
120	85-53-4	0	0		0	0	499	14	-74.855	4.527
121	85-53-4	9	0		0	0	500	14	-74.856	4.528
122	66-61-4	0	0		0	0	351	12	-74.849	4.522
123	4	0	0		0	0	373	12	-74.849	4.521
124	66-58-61-4	0	0		0	0	375	12	-74.85	4.52
125	0	0	0	GPS station	0	0	375	1	-74.887	4.532
126	86-92-67-53-4	66-4	55-2	re also feldspathic with micas. Clasts in congl are upto 3	0	0	398	6	-74.887	4.531

FIELD DATA

Station Number	Lithology 1	Lithology 2	Lithology 3	Comments	Fossils ?	Photos ?	Altitude (m)	Stratigraphic Unit	Longitude (decimal degrees)	Latitude (decimal degrees)
127	52-4	0	0	Mica and Fds	0	0	400	11	-74.885	4.528
128	0	0	0	GPS station	0	0	420	11	-74.885	4.527
129	52-4	0	0	Mica & Fds	0	0	425	11	-74.885	4.527
130	52-4	0	0	Micas	0	0	425	11	-74.885	4.526
131	85-52-61-4	0	0	Drawing	0	0	425	11	-74.884	4.524
132	4	0	0	Mica	0	0	425	11	-74.883	4.524
133	70-10	0	0	GPS station	0	0	443	21	-74.882	4.523
134	85-63-67-9	79-10	0	ph. 5.14-5.17- Strain data	0	1	450	21	-74.881	4.523
135	10	0	0	Drawings- strain data	0	0	450	21	-74.881	4.523
136	10	0	0		0	0	450	21	-74.88	4.522
137	70-10	0	0		0	0	450	21	-74.88	4.522
138	12	10	0	Strain data- Drawing	0	0	450	20	-74.879	4.522
139	12	15	0	ph. 5.18- Strain data- Drawing	0	1	454	20	-74.879	4.522
140	12	10	0	Drawing	0	0	471	20	-74.878	4.521
141	12	0	0	GPS station	0	0	482	20	-74.884	4.521
142	15	12	0	GPS station- ph 5.19-5.20- Drawing	0	0	540	20	-74.882	4.521
143	12	15	0	ph 5.21- Drawing	0	0	562	20	-74.882	4.52
144	19	20	0	ph. 5.22- GPS station- strain data	0	1	575	19	-74.881	4.519
145	12	15	19	contact- GPS station	0	0	622	20	-74.878	4.516
146	12	0	0		0	0	611	20	-74.877	4.515
147	85-9	54-3	0		0	0	618	18	-74.875	4.513
148	0	0	0	GPS station- ph 5.23- Drawing	0	0	697	17	-74.874	4.512
149	52-3	18	0	Glauconite- GPS station	0	0	749	16	-74.874	4.511
150	19	0	0	GPS station	0	0	750	16	-74.874	4.51
151	52-3	9	0		0	0	772	15	-74.874	4.509
152	10	70-12	0	ph 5.24- Drawing	0	0	479	20	-74.878	4.521
153	79-84-12	0	0	Fossil- ph. 5.25	1	1	477	20	-74.878	4.52
154	70-12	0	0		0	0	481	20	-74.877	4.519
155	12	0	0		0	0	522	20	-74.877	4.518
156	12	15	0	Drawing	0	0	503	20	-74.876	4.517
157	12	15	0		0	0	505	20	-74.876	4.517
158	12	15	70-15		0	0	559	20	-74.875	4.517
159	85-20	18	0	pseudo-stylolites- ph. 5.26- Drawing	0	1	575	19	-74.874	4.516
160	70-12	0	0		0	0	429	20	-74.875	4.532
161	53-5	12	0		0	0	433	20	-74.875	4.531
162	19	0	0		0	0	556	19	-74.871	4.528
163	20	0	0		0	0	545	19	-74.87	4.528
164	84-20	12	0		0	0	525	18	-74.868	4.527
165	10	0	0		0	0	525	18	-74.867	4.526
166	10	54-5	0	contact	0	0	577	18	-74.865	4.523
167	5	0	0		0	0	596	18	-74.865	4.522

FIELD DATA

Station Number	Lithology 1	Lithology 2	Lithology 3	Comments	Fossils ?	Photos ?	Altitude (m)	Stratigraphic Unit	Longitude (decimal degrees)	Latitude (decimal degrees)
168	54-4	5	0		0	0	600	17	-74.868	4.519
169	72-52-58-4	0	0		0	0	672	17	-74.868	4.518
170	52-72-58-4	0	0		0	0	654	17	-74.867	4.517
171	85-18	58-4	0		0	0	650	17	-74.865	4.518
172	55-4	0	0		0	0	635	17	-74.864	4.519
173	58-4	0	0		0	0	592	17	-74.863	4.521
174	58-4	0	0		0	0	550	17	-74.863	4.522
175	67-53-58-4	0	0	Mica	0	0	553	17	-74.862	4.523
176	20	18	0		0	0	546	17	-74.86	4.524
177	58-4	0	0		0	0	600	17	-74.863	4.524
178	4	0	0		0	0	594	17	-74.863	4.526
179	58-37	0	0		0	0	600	17	-74.862	4.528
180	18	0	0		0	0	578	16	-74.862	4.53
181	58-4	0	0		0	0	573	17	-74.862	4.531
182	58-4	0	0		0	0	425	18	-74.866	4.537
183	20	0	0		0	0	425	18	-74.868	4.538
184	94-52-67-4	0	0		0	0	419	11	-74.87	4.54
185	58-4	61-3	0		0	0	748	14	-74.868	4.504
186	78-20	18	0		0	0	578	16	-74.863	4.507
187	58-53-4	58-53-37	61-51-3		0	0	571	17	-74.861	4.509
188	82-10	12	25	ph. 5.27	0	1	475	20	-74.86	4.507
189	82-10	0	0		0	0	447	17	-74.858	4.509
190	85-63-9	85-5	0		0	0	427	17	-74.857	4.51
191	10	13	0		0	0	497	20	-74.862	4.504
192	70-12	15	0		0	0	511	20	-74.861	4.503
193	78-79-84-80-12	0	0	ph. 5.28-5.32	0	1	612	20	-74.86	4.5
194	12	20	0		0	0	700	18	-74.859	4.496
195	20	70-12	0		0	0	686	20	-74.862	4.496
196	12	0	0	ph. 5.33- Drawing	0	1	734	20	-74.866	4.493
197	18	0	0		0	0	475	19	-74.904	4.502
198	54-4	0	0	Chert &mica clasts in ss	0	0	542	18	-74.903	4.497
199	53-58-4	0	0		0	0	545	17	-74.904	4.496
200	66-37	0	0	trace fossils	0	0	592	17	-74.904	4.496
201	67-54-3	61-80-4	0	ph. 5.35	0	1	603	17	-74.903	4.496
202	18	0	0	Drawing- ph. 5.36	0	1	626	16	-74.903	4.495
203	10	12	0	contact	0	0	661	15	-74.903	4.494
204	87-58-4	0	0		0	0	700	13	-74.903	4.493
205	56-2	8-73-75-52-	0	Ss very permeable	0	0	629	12	-74.903	4.49
206	18	5	2		0	0	565	16	-74.895	4.486
207	88-61-52-3	0	0		0	0	581	12	-74.886	4.495
208	61-3	0	0	ph. 6.2-6.4	0	1	743	12	-74.889	4.498

FIELD DATA

Station Number	Lithology 1	Lithology 2	Lithology 3	Comments	Fossils ?	Photos ?	Altitude (m)	Stratigraphic Unit	Longitude (decimal degrees)	Latitude (decimal degrees)
250	10	66-85-9	0		0	0	400	15	-74.855	4.516
251	10	85-66-9	0		0	0	414	15	-74.855	4.515
252	10	0	0		0	0	409	15	-74.856	4.515
253	18	0	0		0	0	425	16	-74.857	4.515
254	18	12	4	contact	0	0	425	17	-74.857	4.515
255	70-12	0	0		0	0	425	17	-74.859	4.514
256	85-54-5	70-12	0	Mica	0	0	457	17	-74.861	4.513
257	53-3	70-12	0	ph. 6.11-6.12	0	1	491	17	-74.862	4.512
258	10	78-5	0	ph. 6.13-6.14 Drawings	0	1	435	15	-74.856	4.517
259	18	12	0	ph. 6.15-6.16	0	1	402	16	-74.853	4.515
260	85-66-38	0	0		0	0	402	16	-74.854	4.514
261	18	0	0		0	0	400	17	-74.854	4.514
262	18	20	0	Drawing	0	0	400	16	-74.85	4.516
263	85-70-54-58-37	15	55-2	50 cm thick beds internally flaser-laminated.	0	0	400	16	-74.85	4.516
264	85-54-3	0	0	Mica	0	0	400	17	-74.85	4.515
265	10	0	0		0	0	400	17	-74.85	4.514
266	70-79-84-12	0	0	Fossil	1	0	429	0	0	-74.849
267	12	0	0		0	0	453	20	-74.849	4.511
268	12	0	0		0	0	544	18	-74.846	4.512
269	70-12	0	0		0	0	562	18	-74.845	4.511
270	12	0	0		0	0	600	18	-74.846	4.509
271	56-2	0	0		0	0	305	12	-74.846	4.537
272	67-75-73-53-37	55-2	0	ph. 6.17-6.21- strain data	0	1	315	12	-74.847	4.537
273	2	0	0		0	0	341	12	-74.847	4.538
274	85-69-53-37	0	0	ph. 6.22- Contact	0	1	350	14	-74.848	4.538
275	85-63-66-9	0	0	ph. 6.23-6.24- Drawing	0	1	352	15	-74.849	4.538
276	85-82-9	0	0		0	0	356	15	-74.85	4.538
277	85-68-63-9	0	0	contact	0	0	351	15	-74.851	4.538
278	18	0	0	37.5m thick. Ph. 6.25-6.27- Strain data	0	1	357	16	-74.852	4.539
279	54-58-37	0	0		0	0	375	17	-74.854	4.539
280	54-58-37	0	0		0	0	396	17	-74.855	4.539
281	72-75-61-3	89-53-3	0		0	0	302	3	-74.841	4.544
282	86-93-6	0	0		0	0	300	3	-74.839	4.545
283	26	0	0		0	0	250	1	-74.828	4.558
284	2	89-3	67-9		0	0	325	12	-74.84	4.557
285	0	0	0		0	0	264	1	-74.84	4.561
286	-53-62-73-68-95-69	55-2	0		0	0	582	12	-74.884	4.492
287	85-54-58-4	0	0		0	0	596	12	-74.884	4.491
288	85-66-58-63-9	0	0		0	0	601	14	-74.884	4.49
289	18	63-9	2	ph. 6.28-6.29- Strain data	0	1	623	16	-74.884	4.489
290	85-63-80-82-9	0	0		0	0	636	18	-74.884	4.489

FIELD DATA

Station Number	Lithology 1	Lithology 2	Lithology 3	Comments	Fossils ?	Photos ?	Altitude (m)	Stratigraphic Unit	Longitude (decimal degrees)	Latitude (decimal degrees)
291	18	20	0		0	0	679	19	-74.882	4.487
292	87-61-37	0	0	ph. 6.29-6.34	0	1	633	12	-74.881	4.492
293	85-66-9	0	0		0	0	650	18	-74.88	4.492
294	85-63-9	0	0		0	0	650	18	-74.879	4.491
295	85-67-63-9	0	0		0	0	700	16	-74.876	4.496
296	58-52-37	0	0		0	0	650	12	-74.876	4.497
297	18	0	0	ph. 7.4- Drawing	0	1	750	16	-74.874	4.499
298	63-78-9	0	0	ph. 7.5- Drawing	0	1	729	14	-74.872	4.501
299	63-78-93-9	0	0		0	0	745	14	-74.87	4.503
300	88-4	86-4	0		0	0	586	14	-74.888	4.49
301	85-63-66-70-9	0	0		0	0	554	18	-74.891	4.487
302	70-10	12	0		0	0	593	20	-74.89	4.485
303	70-78-12	0	0		0	0	608	20	-74.889	4.485
304	12	15	0		0	0	679	20	-74.89	4.483
305	12	0	0		0	0	700	20	-74.89	4.482
306	12	67-15	0		0	0	763	20	-74.889	4.481
307	78-70-12	0	0	Fossil	1	0	833	20	-74.888	4.481
308	0	0	0	ph. 7.6-7.8. GPS station	0	1	850	20	-74.888	4.48
309	10	0	0		0	0	855	15	-74.89	4.478
310	84-10	0	0	ph. 7.8-7.9- Drawing	0	1	864	15	-74.889	4.476
311	80-78-54-3	10	0		0	0	800	14	-74.888	4.475
312	89-68-54-3	10	0		0	0	750	14	-74.886	4.476
313	78-10	0	0		0	0	749	15	-74.882	4.478
314	18	20	78-5		0	0	745	15	-74.882	4.478
315	10	0	0		0	0	750	14	-74.884	4.478
316	78-10	0	0		0	0	757	14	-74.888	4.471
317	10	0	0		0	0	760	15	-74.89	4.467
318	12	63-9	0		0	0	750	17	-74.895	4.463
319	10	0	0		0	0	712	20	-74.9	4.456
320	10	0	0		0	0	736	20	-74.903	4.452
321	10	0	0		0	0	703	20	-74.905	4.453
322	56-57-2	0	0	ph. 7.10	0	1	575	12	-74.886	4.492
323	78-61-58-3	0	0		0	0	588	16	-74.889	4.49
324	20	18	0	GPS stations along fault	0	0	594	16	-74.889	4.489
325	51-58-78-37	0	0	ph. 7.11-7.12- Drawing	0	1	598	17	-74.89	4.489
326	18	20	0		0	0	551	16	-74.893	4.488
327	78-61-4	0	0		0	0	550	12	-74.898	4.484
328	68-54-58-37	0	0	ph. 7.13- Drawing	0	1	582	17	-74.897	4.483
329	61-50-37	0	0	ph. 7.15-7.17- Drawing	0	1	547	12	-74.9	4.483
330	18	53-58-37	65-3	Drawing- Other lithologic types:Micrite- shale	0	0	550	16	-74.902	4.48
331	18	20	70-12		0	0	565	19	-74.901	4.479

FIELD DATA

Station Number	Lithology 1	Lithology 2	Lithology 3	Comments	Fossils ?	Photos ?	Altitude (m)	Stratigraphic Unit	Longitude (decimal degrees)	Latitude (decimal degrees)
332	12	0	0		0	0	550	20	-74.899	4.475
333	70-12	0	0		0	0	575	20	-74.898	4.469
334	70-12	0	0	ph.7.19-7.20	0	1	575	20	-74.897	4.469
335	12	0	0		0	0	575	20	-74.901	4.468
336	12	0	0		0	0	575	20	-74.903	4.466
337	12	0	0		0	0	600	20	-74.907	4.462
338	70-78-12	0	0		0	0	600	20	-74.907	4.46
339	70-12	68-15	0		0	0	629	20	-74.909	4.459
340	70-12	15	0		0	0	666	20	-74.911	4.459
341	96-8	0	0		0	0	525	12	-74.908	4.481
342	87-53-4	0	0		0	0	525	12	-74.913	4.478
343	87-61-4	0	0		0	0	522	12	-74.919	4.472
344	18	20	13		0	0	566	16	-74.918	4.47
345	58-54-37	55-58-2	56-57-2	riented sample- Drawing- Column- strain data-ph 7.21-7.3	0	0	500	12	-74.924	4.472
346	85-63-38	0	0	moved?	0	0	575	17	-74.922	4.464
347	2	0	0		0	0	575	17	-74.923	4.463
348	70-58-52-37	0	0		0	0	600	17	-74.922	4.462
349	87-4	0	0	Bochorno- cleavage?- bedd?	0	0	595	17	-74.924	4.465
350	2	0	0	float?	0	0	610	12	-74.926	4.465
351	2	0	0	??- float	0	0	700	12	-74.928	4.466
355	51-36	31	0	K-Fds: 45%- Hbl+Btt: 35- Qz:20%	0	0	375	22	-74.887	4.55
356	31	0	0		0	0	400	22	-74.889	4.551
357	31	0	0	ph. 8.1-8.2	0	1	399	22	-74.89	4.552
358	52-30	0	0	Qz:20%- Plag:40%- Btt: 20%	0	0	425	22	-74.89	4.55
359	30	0	0		0	0	407	22	-74.891	4.548
360	53-30	0	0	ph. 8.3-8.4- Drawing	0	1	471	22	-74.891	4.546
361	30	0	0		0	0	474	22	-74.894	4.543
362	29	0	0	Hbl: 80%- Plag:20%	0	0	475	22	-74.894	4.542
363	34	0	0	btt schist	0	0	465	22	-74.895	4.541
364	52-30	0	0	Qz:20%- Fds: 70%- Btt: 10%	0	0	450	22	-74.897	4.538
365	0	0	0	GPS station	0	0	425	22	-74.898	4.535
366	33	0	0		0	0	425	22	-74.897	4.533
367	51-30	0	0	Fds:70%- Btt: 10%- Qz: 20%	0	0	425	22	-74.898	4.532
368	32	0	0	Fds grains in green matrix	0	0	425	22	-74.898	4.533
369	93-94-61-60-7	0	0		0	0	425	22	-74.9	4.533
370	51-30	0	0	qz: 25%- Fds:60%- Btt:15%	0	0	426	22	-74.902	4.533
371	31	0	0		0	0	473	22	-74.905	4.532
372	31	0	0		0	0	463	22	-74.906	4.531
373	56-60-2	0	0	ph. 8.5-8.7- 144 strike of abrasion marks?	0	1	456	5	-74.903	4.528
374	31	0	0		0	0	475	22	-74.906	4.529
375	31	0	0		0	0	458	22	-74.905	4.526

FIELD DATA

Station Number	Lithology 1	Lithology 2	Lithology 3	Comments	Fossils ?	Photos ?	Altitude (m)	Stratigraphic Unit	Longitude (decimal degrees)	Latitude (decimal degrees)
376	34	36	0		0	0	450	22	-74.899	4.527
377	34	0	0		0	0	432	5	-74.898	4.529
378	0	0	0	ph. 8.9-8.12	0	1	425	5	-74.891	4.535
379	59-75-61-94-4	0	0		0	0	374	5	-74.857	4.557
380	53-94-4	0	0		0	0	375	11	-74.856	4.557
381	63-55-2	0	0	Andesite- tuff- and volcanic bombs clasts	0	0	350	5	-74.845	4.571
382	70-12	15	0		0	0	575	20	-74.905	4.473
383	12	0	0		0	0	575	20	-74.906	4.472
384	12	15	0		0	0	575	20	-74.907	4.471
385	12	15	0	ph. 8.13-8.14	0	1	575	20	-74.907	4.47
386	12	15	0		0	0	576	20	-74.906	4.469
387	70-12	0	0	ph. 8.15-8.17	0	1	577	20	-74.906	4.468
388	70-12	15	0		0	0	582	20	-74.907	4.467
389	70-12	15	0	ph. 8.18-8.25- Strain data	0	1	654	20	-74.909	4.466
390	70-10	12	15		0	0	713	19	-74.91	4.465
391	70-12	0	0	ph.8.26-8.28	0	1	749	19	-74.911	4.464
392	61-7	0	0		0	0	500	1	-74.927	4.474
393	58-53-37	0	0		0	0	518	14	-74.929	4.472
394	20	0	0	ph. 8.29-8.36?	0	1	559	16	-74.931	4.471
395	18	0	0	ph. 9.1-9.11- Drawings (PAR	0	1	545	16	-74.933	4.47
396	12	10	85-66-9	ph. 9.12-9.13	0	1	502	15	-74.935	4.47
397	55-63-72-75-2	96-63-8	0		0	0	550	9	-74.941	4.458
398	57-61-37	0	0		0	0	587	13	-74.932	4.461
399	88-69-58-64-61-37	0	0		0	0	575	13	-74.932	4.46
400	70-58-54-37	63-9	0		0	0	600	14	-74.93	4.46
401	85-66-58-54-37	0	0		0	0	600	14	-74.929	4.459
402	66-70-58-54-37	0	0		0	0	602	14	-74.928	4.458
403	86-54-58-4	10	85-9		0	0	615	14	-74.928	4.458
404	12	0	0		0	0	650	15	-74.927	4.457
405	18	20	0	Drawing	0	0	650	16	-74.927	4.457
406	18	63-10	0		0	0	650	16	-74.926	4.457
407	66-50-58-3	0	0		0	0	678	17	-74.926	4.456
408	85-58-37	0	0		0	0	652	17	-74.926	4.456
409	85-63-9	0	0	Clearly- veins have been reactivated by dextral faulting	0	0	673	18	-74.925	4.456
410	0	0	0	GPS station	0	0	575	1	-74.941	4.43
411	0	0	0	GPS station	0	0	575	1	-74.937	4.424
412	12	0	0		0	0	600	20	-74.932	4.424
413	12	38	0		0	0	600	20	-74.931	4.425
414	12	38	0		0	0	600	20	-74.929	4.424
415	12	0	0		0	0	600	20	-74.927	4.424
416	84-38	0	0		0	0	602	20	-74.927	4.424

FIELD DATA

Station Number	Lithology 1	Lithology 2	Lithology 3	Comments	Fossils ?	Photos ?	Altitude (m)	Stratigraphic Unit	Longitude (decimal degrees)	Latitude (decimal degrees)
417	12	15	0		0	0	628	20	-74.926	4.424
418	12	0	0		0	0	650	20	-74.924	4.423
419	12	15	0	ph. 9.13-9.16- Drawing	0	1	650	20	-74.924	4.423
420	70-12	0	0		0	0	650	20	-74.923	4.422
421	70-12	0	0		0	0	650	20	-74.923	4.422
422	70-12	0	0		0	0	575	14	-74.936	4.44
423	70-12	0	0		0	0	575	20	-74.934	4.44
424	70-12	0	0		0	0	575	1	-74.932	4.44
425	78-12	70-15	0	Fossil	1	0	594	20	-74.931	4.44
426	12	38	0		0	0	614	20	-74.93	4.44
427	20	0	0	GPS station	0	0	644	4	-74.928	4.44
428	18	20	38		0	0	716	20	-74.924	4.439
429	66-38	12	70-15		0	0	750	20	-74.923	4.44
430	70-78-12	0	0	Fossil	1	0	775	20	-74.923	4.44
431	18	20	38		0	0	799	20	-74.922	4.44
432	18	20	0	GPS station	0	0	745	4	-74.923	4.438
433	0	0	0	ph. 9.16-9.17- GPS station	0	1	824	19	-74.92	4.44
434	18	0	0		0	0	850	19	-74.918	4.441
435	18	20	21		0	0	850	19	-74.918	4.442
436	10	12	0		0	0	359	20	-74.855	4.477
437	12	0	0	ph. 9.22-9.23- Drawing	0	1	413	20	-74.857	4.477
438	12	0	0	ph. 9.24-9.26- Drawing	0	1	427	20	-74.857	4.477
439	20	18	38		0	0	515	20	-74.859	4.478
440	70-78-15	0	0	ph. 9.27- Drawing- Fossil- GPS station	1	1	563	20	-74.862	4.477
441	70-12	0	0	moved?	0	0	520	20	-74.857	4.481
442	18	0	0		0	0	568	19	-74.856	4.482
443	10	0	0	same station 34	0	0	594	18	-74.855	4.484
444	20	0	0	Same station 35	0	0	600	18	-74.856	4.484
445	10	0	0	ph. 9.28- Drawing	0	1	678	18	-74.863	4.485
446	10	0	0		0	0	700	18	-74.863	4.488
447	10	63-9	0		0	0	700	18	-74.864	4.489
448	85-54-58-37	63-9	0		0	0	703	17	-74.865	4.489
449	20	18	0		0	0	756	16	-74.866	4.49
450	70-12	0	0		0	0	800	20	-74.868	4.491
451	0	0	0	ph. 9.29-9.32. Drawing- Station not in the map	0	1	501	20	-74.854	4.484
452	10	12	0		0	0	325	18	-74.854	4.472
453	12	0	0		0	0	376	18	-74.851	4.476
454	78-12	0	0		0	0	429	18	-74.849	4.477
455	78-12	0	0		0	0	447	18	-74.849	4.478
456	70-82-10	0	0		0	0	450	18	-74.848	4.478
457	70-78-12	10	0	ph. 10.1-10.2	0	1	475	18	-74.848	4.48

FIELD DATA

Station Number	Lithology 1	Lithology 2	Lithology 3	Comments	Fossils ?	Photos ?	Altitude (m)	Stratigraphic Unit	Longitude (decimal degrees)	Latitude (decimal degrees)
458	10	0	0		0	0	499	18	-74.846	4.48
459	10	0	0	ph. 10.3-10.4	0	1	552	18	-74.843	4.48
460	12	78-10	0		0	0	563	18	-74.844	4.481
461	18	20	38	ph. 10.5-10.6- Drawing	0	1	565	20	-74.844	4.481
462	18	0	0	ph. 10.7-10.8- Drawing	0	1	571	19	-74.845	4.482
463	18	0	0		0	0	614	19	-74.846	4.483
464	70-18	0	0		0	0	650	19	-74.844	4.483
465	10	0	0		0	0	650	18	-74.844	4.486
466	82-10	0	0		0	0	650	18	-74.846	4.488
467	84-12	0	0		0	0	650	18	-74.847	4.489
468	70-82-12	0	0		0	0	650	18	-74.85	4.489
469	10	21	0		0	0	700	18	-74.856	4.493
470	18	0	0		0	0	655	19	-74.857	4.494
471	18	0	0	ph. 10.9-10.12	0	1	650	19	-74.857	4.495
472	85-54-3	63-9	0		0	0	350	18	-74.856	4.472
473	18	15	20		0	0	350	2	-74.866	4.469
474	70-12	15	0		0	0	351	20	-74.867	4.471
475	70-12	0	0		0	0	371	20	-74.868	4.471
476	70-12	15	0	ph. 10.14-10.15	0	1	350	20	-74.869	4.472
477	70-12	0	0		0	0	375	20	-74.87	4.472
478	70-12	15	0	ph. 10.16-10.20- Drawings- Fossil- GPS station	1	1	390	20	-74.87	4.472
479	70-12	15	25		0	0	400	20	-74.873	4.471
480	78-70-12	0	0		0	0	400	20	-74.873	4.471
481	0	0	0	GPS station	0	0	400	20	-74.874	4.471
482	0	0	0	ph. 10.21-10.25- Drawing in clipboard	0	1	400	20	-74.874	4.473
483	12	25	0	ph. 10.26- sample of ashes	0	1	400	20	-74.875	4.473
484	12	15	0	ph. 10.27-10.28	0	1	407	20	-74.875	4.475
485	70-12	15	0		0	0	423	20	-74.876	4.474
486	10	0	0		0	0	350	20	-74.866	4.47
487	70-78-12	0	0		0	0	366	20	-74.866	4.471
488	12	0	0	Drawing- Guessed Lithology	0	0	411	20	-74.866	4.471
489	10	0	0	ph. 10.30	0	1	650	18	-74.862	4.483
490	10	0	0		0	0	628	18	-74.864	4.483
491	18	21	0		0	0	601	18	-74.865	4.483
492	12	84-15	0		0	0	550	18	-74.868	4.481
493	84-12	15	0		0	0	550	18	-74.867	4.481
494	18	0	0		0	0	549	19	-74.867	4.48
495	10	0	0		0	0	546	18	-74.87	4.48
496	18	0	0	GPS station	0	0	618	17	-74.874	4.478
497	85-63-9	0	0		0	0	549	18	-74.869	4.479
498	12	0	0		0	0	525	18	-74.869	4.478

FIELD DATA

Station Number	Lithology 1	Lithology 2	Lithology 3	Comments	Fossils ?	Photos ?	Altitude (m)	Stratigraphic Unit	Longitude (decimal degrees)	Latitude (decimal degrees)
499	12	0	0		0	0	525	18	-74.869	4.477
500	20	0	0	ph. 10.31-10.32	0	1	542	18	-74.869	4.477
501	58-54-37	0	0		0	0	300	2	-74.848	4.459
502	18	0	0		0	0	276	16	-74.844	4.455
503	18	20	0		0	0	275	2	-74.844	4.455
504	20	18	0		0	0	278	16	-74.809	4.489
505	12	38	18		0	0	305	18	-74.813	4.492
506	78-70-12	15	0		0	0	325	18	-74.813	4.493
507	70-12	15	0		0	0	349	18	-74.815	4.493
508	18	20	0		0	0	438	16	-74.817	4.494
509	18	20	0		0	0	494	15	-74.819	4.495
510	0	0	0	GPS station	0	0	525	15	-74.82	4.495
511	10	38	0		0	0	523	18	-74.819	4.493
512	70-10	0	0		0	0	574	17	-74.822	4.494
513	20	0	0		0	0	599	18	-74.826	4.49
514	0	0	0	ph. 10.34-10.36	0	1	585	18	-74.826	4.489
515	12	0	0		0	0	509	18	-74.824	4.487
516	82-70-10	0	0		0	0	491	18	-74.826	4.487
517	12	0	0		0	0	515	18	-74.828	4.488
518	10	18	0		0	0	524	18	-74.828	4.488
519	12	0	0		0	0	458	18	-74.823	4.488
520	12	0	0		0	0	352	18	-74.821	4.489
521	18	20	38		0	0	350	19	-74.82	4.489
522	38	0	0		0	0	300	15	-74.814	4.483
523	12	63-82-9	0		0	0	523	18	-74.842	4.481
524	12	0	0		0	0	490	18	-74.84	4.481
525	12	0	0		0	0	446	18	-74.839	4.482
526	70-10	0	0		0	0	444	18	-74.838	4.481
527	38	10	0	stinks H2S	0	0	375	18	-74.835	4.481
528	18	0	0		0	0	395	19	-74.835	4.482
529	18	21	0		0	0	419	19	-74.837	4.482
530	20	0	0		0	0	400	19	-74.835	4.483
531	12	0	0		0	0	351	18	-74.834	4.479
532	10	0	0		0	0	353	18	-74.833	4.477
533	0	0	0	GPS station	0	0	406	18	-74.836	4.48
534	86-70-54-58-37	0	0		0	0	256	24	-74.836	4.449
535	2	0	0		0	0	254	24	-74.829	4.449
536	0	0	0	ph. 11.2	0	1	275	2	-74.82	4.454
537	18	0	0		0	0	325	16	-74.829	4.469
538	20	38	0		0	0	306	16	-74.845	4.457
539	38	20	0		0	0	351	15	-74.845	4.459

FIELD DATA

Station Number	Lithology 1	Lithology 2	Lithology 3	Comments	Fossils ?	Photos ?	Altitude (m)	Stratigraphic Unit	Longitude (decimal degrees)	Latitude (decimal degrees)
540	63-20	0	0		0	0	409	15	-74.845	4.461
541	63-20	0	0	ph. 11.3- Drawing	0	1	503	15	-74.847	4.466
542	38	0	0		0	0	533	15	-74.847	4.467
543	70-12	38	0		0	0	550	15	-74.846	4.469
544	58-81-20	0	0		0	0	575	15	-74.843	4.471
545	63-81-38	0	0	Oriented sample	0	0	575	15	-74.843	4.471
546	38	0	0		0	0	580	15	-74.841	4.472
547	38	0	0		0	0	563	15	-74.84	4.473
548	20	18	0		0	0	522	15	-74.839	4.472
549	20	0	0		0	0	528	15	-74.838	4.472
550	38	12	0		0	0	528	15	-74.842	4.469
551	58-54-37	0	0		0	0	414	15	-74.839	4.457
552	89-59-63-8	0	0	Kaolin?	0	0	396	15	-74.838	4.455
553	53-4	0	0		0	0	275	14	-74.835	4.45
554	66-70-58-53-37	0	0		0	0	300	14	-74.827	4.455
555	67-70-58-65-37	0	0		0	0	350	14	-74.829	4.461
556	53-58-37	0	0		0	0	373	14	-74.829	4.458
557	70-53-58-37	0	0		0	0	401	14	-74.831	4.459
558	78-53-58-37	0	0		0	0	424	14	-74.832	4.459
559	54-58-37	0	0	Gypsum filled veins	0	0	350	14	-74.832	4.456
560	70-53-58-37	0	0	Fossil	1	0	252	14	-74.833	4.45
561	89-63-8	0	0		0	0	275	2	-74.822	4.454
562	58-4	81-3	0		0	0	332	14	-74.824	4.46
563	68-58-53-37	0	0		0	0	326	14	-74.816	4.469
564	71-63-55-2	0	0	- Samples-Clasts of milky Qz- Chert- Siltstone-silicic- G	0	1	300	12	-74.858	4.433
565	56-2	0	0	ph. 11.17-11.19	0	1	300	1	-74.863	4.431
566	2	5-72-61-37	0	ph. 11.20-11.21	0	1	354	12	-74.867	4.433
567	18	0	0		0	0	450	18	-74.872	4.436
568	12	21	0	Drawing: observation on cleavage morphology	0	0	450	18	-74.873	4.437
569	12	38	0		0	0	451	18	-74.874	4.436
570	10	0	0		0	0	473	18	-74.875	4.438
571	70-10	0	0	Drawing	0	0	501	18	-74.875	4.439
572	12	0	0		0	0	525	18	-74.875	4.44
573	12	10	0		0	0	544	18	-74.876	4.442
574	70-10	0	0		0	0	550	18	-74.877	4.442
575	20	0	0		0	0	602	20	-74.878	4.445
576	10	0	0		0	0	651	20	-74.876	4.45
577	12	10	0		0	0	575	18	-74.874	4.453
578	66-38	85-53-3	0		0	0	590	17	-74.873	4.454
579	20	38	0		0	0	553	17	-74.872	4.453
580	18	0	0		0	0	550	16	-74.871	4.453

FIELD DATA

Station Number	Lithology 1	Lithology 2	Lithology 3	Comments	Fossils ?	Photos ?	Altitude (m)	Stratigraphic Unit	Longitude (decimal degrees)	Latitude (decimal degrees)
581	89-67-8	0	0	Kaolin?	0	0	522	15	-74.869	4.453
582	2	0	0	GPS station	0	0	526	14	-74.868	4.452
583	2	0	0	GPS station	0	0	549	12	-74.865	4.448
584	64-58-53-72-37	0	0		0	0	318	14	-74.844	4.447
585	86-54-58-37	0	0		0	0	367	14	-74.847	4.449
586	58-53-37	0	0	No Fckng bdd	0	0	400	14	-74.849	4.45
587	58-53-3	0	0		0	0	450	15	-74.849	4.451
588	73-53-37	0	0		0	0	312	14	-74.844	4.45
589	85-63-9	0	0	ph. 11.22	0	1	275	2	-74.84	4.449
590	56-2	0	0		0	0	263	12	-74.839	4.437
591	86-53-68-58-37	56-2	0	samples of clasts	0	0	275	12	-74.841	4.437
592	85-9	63-9	58-53-3		0	0	278	12	-74.841	4.438
593	86-54-70-4	0	0	ph 11.23 Bioturbation	0	0	303	14	-74.842	4.439
594	86-63-9	0	0		0	0	300	14	-74.843	4.44
595	82-20	21	0		0	0	425	19	-74.891	4.44
596	70-18	0	0	ph. 11.24-11.25- Drawings- strain data	0	1	445	19	-74.891	4.441
597	18	20	0		0	0	450	19	-74.892	4.443
598	70-18	10	38	ph. 11.26-11.27	0	1	516	19	-74.894	4.447
599	18	0	0		0	0	502	18	-74.895	4.448
600	10	0	0		0	0	518	18	-74.896	4.448
601	0	0	0	GPS station- Ph. 11.28-11.29 (looking SSW)	0	1	550	18	-74.894	4.449
602	58-53-37	0	0	Gypsum veins- Ph. 11.30-11.31	0	1	700	17	-74.898	4.456
603	86-58-53-37	0	0		0	0	720	17	-74.896	4.459
604	70-10	0	0		0	0	579	18	-74.893	4.456
605	85-70-9	0	0		0	0	552	18	-74.892	4.455
606	18	63-20	15	Drawing	0	0	325	1	-74.873	4.409
607	0	0	0	Ph. 11.35- GPS station	0	1	325	1	-74.882	4.409
608	12	0	0	Drawing	0	0	358	19	-74.888	4.414
609	12	15	38		0	0	368	20	-74.889	4.416
610	0	0	0	Ph. 11.36- GPS station	0	1	376	20	-74.89	4.421
611	70-12	38	0		0	0	375	20	-74.89	4.423
612	70-12	15	0	ph. 11.37-12.1	0	1	375	20	-74.891	4.429
613	12	0	0		0	0	400	20	-74.887	4.438
614	20	0	0	ph. 12.2-12.4	0	1	425	20	-74.886	4.441
615	70-12	0	0		0	0	435	20	-74.886	4.442
616	70-12	79-15	0	Fossil	1	0	425	0	0	-74.886
617	70-12	0	0		0	0	426	20	-74.885	4.443
618	70-12	0	0		0	0	438	20	-74.884	4.443
619	61-3	56-58-2	0	moved?	0	0	328	4	-74.867	4.404
620	56-2	0	0		0	0	380	12	-74.869	4.4
621	58-53-37	0	0		0	0	393	15	-74.87	4.4

FIELD DATA

Station Number	Lithology 1	Lithology 2	Lithology 3	Comments	Fossils ?	Photos ?	Altitude (m)	Stratigraphic Unit	Longitude (decimal degrees)	Latitude (decimal degrees)
622	58-54-37	0	0		0	0	417	15	-74.87	4.399
623	81-38	0	0		0	0	500	15	-74.871	4.401
624	18	20	0		0	0	514	15	-74.872	4.401
625	38	12	0	ph. 12.5-12.8	0	1	581	15	-74.874	4.399
626	81-38	0	0		0	0	650	16	-74.872	4.393
627	18	0	0		0	0	650	16	-74.871	4.392
628	18	21	0		0	0	650	16	-74.87	4.391
629	81-63-20	70-12	0		0	0	568	17	-74.873	4.391
630	70-12	0	0	ph. 12.10-12.11- Drawing	0	1	550	17	-74.874	4.391
631	38	12	0	ph. 12.12-12.15	0	1	489	17	-74.875	4.391
632	38	0	0		0	0	461	17	-74.876	4.392
633	70-12	38	0		0	0	417	18	-74.878	4.394
634	10	0	0		0	0	375	18	-74.88	4.396
635	0	0	0	GPS station	0	0	380	18	-74.88	4.397
636	38	0	0		0	0	300	15	-74.863	4.376
637	38	0	0		0	0	300	16	-74.864	4.375
638	18	81-38	0		0	0	300	16	-74.865	4.375
639	12	0	0		0	0	325	18	-74.867	4.375
640	78-70-12	78-15	0	fossil (not originally in notes)	1	0	326	20	-74.87	4.375
641	63-9	63-70-12	0	Drawing	0	0	327	20	-74.872	4.375
642	12	0	0		0	0	350	20	-74.874	4.375
643	0	0	0	Ph. 12.16-12.18- Drawing- GPS station	0	1	351	20	-74.875	4.374
644	70-12	0	0	Sample	0	0	375	20	-74.876	4.373
645	79-70-12	0	0	fossil- ph. 12.19- strain data	0	1	440	20	-74.879	4.373
646	12	0	0	ph. 12.20-12.24	0	1	544	20	-74.884	4.374
647	89-52-75-64-3	55-56-2	61-52-75-3	ph. 12.25-12.27	0	1	274	12	-74.834	4.431
648	55-2	0	0	ph. 12.28-12.29	0	1	307	12	-74.833	4.431
649	58-54-37	0	0		0	0	351	14	-74.83	4.433
650	86-63-9	67-54-3	0		0	0	389	15	-74.826	4.434
651	58-67-70-37	0	0		0	0	448	15	-74.824	4.433
652	18	20	0	GPS station- ph. 12.30- Drawing	0	1	516	15	-74.821	4.434
653	18	0	0	ph. 12.31- Drawing- GPS station	0	1	609	15	-74.82	4.434
654	18	21	20		0	0	375	15	-74.791	4.473
655	15	38	18		0	0	375	15	-74.79	4.473
656	20	0	0		0	0	400	15	-74.789	4.473
657	12	9	0	Drawing	0	0	416	15	-74.787	4.473
658	12	0	0		0	0	465	15	-74.786	4.472
659	70-38	0	0		0	0	458	16	-74.785	4.471
660	89-8	0	0	Kaolin? mine	0	0	359	17	-74.796	4.473
661	58-53-37	0	0		0	0	275	15	-74.8	4.472
662	70-20	38	23		0	0	392	20	-74.779	4.501

FIELD DATA

Station Number	Lithology 1	Lithology 2	Lithology 3	Comments	Fossils ?	Photos ?	Altitude (m)	Stratigraphic Unit	Longitude (decimal degrees)	Latitude (decimal degrees)
663	70-12	23	0		0	0	451	20	-74.777	4.502
664	18	23	0	ph. 12.32-12.34- Same station 5- Drawing	0	1	320	16	-74.788	4.497
665	10	0	0	GPS station	0	0	750	20	-74.759	4.504
666	12	38	0		0	0	721	20	-74.76	4.503
667	70-12	15	0		0	0	362	20	-74.78	4.497
668	18	0	0	Drawing	0	0	261	16	-74.799	4.496
669	81-38	10	0		0	0	263	15	-74.8	4.495
670	58-54-37	0	0	ph. 12.35-13.1-13.3- Drawing	0	1	261	14	-74.804	4.479
671	37	0	0	Gypsum veins	0	0	280	14	-74.804	4.473
672	70-67-58-37	0	0	Same station 8	0	0	286	14	-74.809	4.457
673	85-67-70-9	0	0	Gypsum veins	0	0	259	14	-74.82	4.447
674	96-86-67-8	0	0		0	0	300	9	-74.779	4.527
675	77-18	0	0	ph. 13.6-13.12- Drawing	0	1	325	16	-74.775	4.526
676	77-18	0	0		0	0	337	16	-74.775	4.526
677	52-4	66-21	0		0	0	350	15	-74.775	4.525
678	61-37	0	0		0	0	374	12	-74.774	4.523
679	88-58-78-56-2	89-53-58-3	0		0	0	400	12	-74.772	4.521
680	66-95-67-63-58-3	15	0	ph. 13.13	0	1	428	15	-74.771	4.521
681	85-9	0	0	ph. 13.14	0	1	430	15	-74.771	4.52
682	18	53-3	0		0	0	431	16	-74.77	4.52
683	70-63-9	0	0		0	0	436	16	-74.77	4.519
684	10	9	0	ph. 13.15-13.17. Drawing	0	1	459	18	-74.769	4.518
685	10	82-8	0		0	0	500	18	-74.767	4.517
686	10	21	0		0	0	525	18	-74.767	4.516
687	38	4	0		0	0	609	18	-74.765	4.518
688	18	0	0	Drawing	0	0	712	19	-74.764	4.518
689	10	21	65-3	Drawing- almost same station 2	0	0	290	15	-74.792	4.514
690	10	0	0		0	0	251	15	-74.789	4.51
691	38	18	0	Same station ""casi me mata un palo	0	0	278	15	-74.788	4.508
692	18	0	0	sample with forams	0	0	350	16	-74.792	4.482
693	77-18	20	0	Drawing- ph. 13.18	0	1	359	17	-74.791	4.482
694	58-64-53-3	70-65-3	0	Gypsum	0	0	382	17	-74.789	4.482
695	70-82-9	54-65-3	0		0	0	417	17	-74.786	4.482
696	63-9	70-10	0	GPS station	0	0	425	17	-74.785	4.482
697	70-54-37	0	0		0	0	425	17	-74.783	4.481
698	70-4	0	0		0	0	443	17	-74.783	4.481
699	82-10	4	0		0	0	450	17	-74.782	4.48
700	20	0	0		0	0	475	18	-74.78	4.48
701	19-20	0	0		0	0	475	18	-74.78	4.479
702	18	38	0		0	0	475	19	-74.78	4.479
703	70-63-10	0	0		0	0	497	20	-74.779	4.478

FIELD DATA

Station Number	Lithology 1	Lithology 2	Lithology 3	Comments	Fossils ?	Photos ?	Altitude (m)	Stratigraphic Unit	Longitude (decimal degrees)	Latitude (decimal degrees)
704	9	21	10		0	0	516	20	-74.778	4.478
705	86-63-8	0	0		0	0	275	2	-74.835	4.54
706	61-66-64-72-52-4	0	0		0	0	275	2	-74.834	4.538
707	63-56-2	0	0		0	0	275	9	-74.834	4.536
708	55-2	0	0	moved?	0	0	276	9	-74.833	4.534
709	88-8	0	0		0	0	320	9	-74.837	4.527
710	70-57-52-94-4	1	88-8	Sample. Weird.	0	0	303	2	-74.836	4.53
712	0	0	0	ph. 13.21-13.25	0	1	275	15	-74.8	4.472
714	52-58-37	0	0	Formerly station 293a	0	0	654	12	-74.878	4.497
715	58-37	0	0	ph. 7.1-7.3- Formerly station 294a	0	1	689	14	-74.877	4.497
716	61-26	0	0	ph. 13.19. Station not in map. Formerly station 704.1	0	1	307	5	-74.846	4.563
977	0	0	0	Remote strike/dip- Doima	0	0	800	18	-74.924	4.434
978	0	0	0	Remote strike/dip- Doima	0	0	571	12	-74.906	4.486
979	0	0	0	Remote strike/dip- Doima	0	0	900	19	-74.91	4.446
986	0	0	0	Remote strike/dip- Vindi	0	0	850	17	-74.876	4.459
987	0	0	0	Remote strike/dip- Vindi	0	0	700	16	-74.824	4.496
988	0	0	0	Remote strike/dip- Vindi	0	0	766	15	-74.878	4.48
989	0	0	0	Remote strike/dip- Vindi	0	0	749	13	-74.885	4.5
994	0	0	0	Remote strike/dip- Piedras	0	0	469	8	-74.883	4.532
995	0	0	0	Remote strike/dip- Piedras	0	0	575	17	-74.862	4.536
996	0	0	0	Remote strike/dip- Piedras	0	0	617	18	-74.872	4.515
997	0	0	0	Remote strike/dip- Piedras	0	0	298	7	-74.819	4.565
998	0	0	0	Remote strike/dip- Piedras	0	0	439	15	-74.818	4.516
999	0	0	0	Remote strike/dip- Piedras	0	0	399	10	-74.782	4.531

BEDDING

Station Number	Strike	Dip	Dip Direction	Dip Direction Azimuth
1	150	25	ne	60
2	34	35	se	124
2	55	78	s	145
3	60	46	n	330
3	49	53	nw	319
4	34	35	nw	304
5	1	57	w	271
7	35	30	w	305
8	39	45	nw	309
9	84	21	n	354
10	86	69	n	356
11	30	39	nw	300
12	54	44	nw	324
13	0	0	n	270
14	156	46	e	66
15	160	31	w	250
17	100	37	s	190
18	49	56	nw	319
20	156	15	s	246
21	52	51	nw	322
22	69	46	s	159
31	114	26	s	204
33	59	50	se	149
34	0	0	n	270
35	53	44	nw	323
36	50	19	se	140
37	60	11	nw	330
38	62	15	se	152
40	122	24	s	212
41	61	15	s	151
42	82	14	s	172
43	76	36	s	166
44	107	22	s	197
45	52	56	se	142
47	52	77	sw	142
48	53	54	se	143
49	10	52	e	100
50	47	59	se	137
51	67	29	s	157
52	59	50	se	149
53	95	44	s	185
54	98	13	s	188
55	20	30	e	110
56	53	74	se	143
57	77	27	s	167
58	24	40	e	114
59	29	14	e	119
60	55	40	se	145
61	42	17	s	132
63	12	46	e	102
65	47	66	se	137
67	47	84	nw	317

BEDDING

Station Number	Strike	Dip	Dip Direction	Dip Direction Azimuth
69	297	16	n	27
70	294	16	n	24
72	75	6	n	345
75	0	0	n	270
77	14	23	e	104
78	335	25	e	65
79	43	20	se	133
81	7	11	e	97
82	42	14	se	132
82	90	17	n	0
83	50	25	se	140
83	21	5	e	111
84	0	0	n	270
85	0	0	n	270
86	10	20	e	100
87	131	21	n	41
88	175	29	e	85
89	20	75	e	110
90	64	82	n	334
91	44	27	se	134
92	94	36	n	4
93	59	75	s	149
93	16	61	e	106
94	109	43	n	19
95	9	29	e	99
96	43	47	se	133
97	58	59	se	148
98	5	47	e	95
99	4	24	e	94
100	4	24	e	94
102	153	30	e	63
104	75	27	nw	345
105	77	34	n	347
106	90	33	n	0
108	72	29	nw	342
111	10	24	e	100
112	180	25	e	90
113	354	20	e	84
114	20	14	e	110
115	4	26	e	94
116	7	15	e	97
117	178	19	e	88
118	145	15	w	235
119	24	18	e	114
120	50	12	se	140
121	21	21	e	111
122	22	35	e	112
123	169	21	e	79
124	0	63	e	90
126	43	62	s	133
127	8	49	e	98
129	5	54	e	95

BEDDING

Station Number	Strike	Dip	Dip Direction	Dip Direction Azimuth
130	10	54	e	100
131	232	68	e	142
133	26	56	e	116
134	43	28	se	133
135	0	0	n	270
136	149	48	sw	239
137	22	11	se	112
138	104	29	s	194
139	79	24	se	169
140	17	89	w	287
141	38	43	se	128
142	31	26	nw	301
142	34	42	se	124
143	105	34	s	195
144	0	31	e	90
145	94	75	s	184
145	55	28	se	145
146	103	28	s	193
147	19	19	e	109
149	115	52	n	25
150	155	30	sw	245
151	95	43	s	185
152	29	81	se	119
152	12	14	e	102
154	45	34	se	135
155	35	19	se	125
156	39	70	nw	309
157	14	31	e	104
158	66	15	n	336
159	24	10	e	114
160	17	44	e	107
161	26	26	e	116
163	344	39	e	74
164	66	21	se	156
165	28	21	se	118
166	9	12	w	279
167	142	23	w	232
168	38	19	se	128
169	25	15	e	115
170	64	17	s	154
171	83	33	s	173
172	156	12	e	66
173	32	13	se	122
175	161	26	e	71
176	135	35	ne	45
177	166	40	e	76
178	151	34	ne	61
179	159	15	e	69
181	40	27	se	130
182	30	37	se	120
183	61	45	n	331
183	49	56	se	139

BEDDING

Station Number	Strike	Dip	Dip Direction	Dip Direction Azimuth
184	30	89	se	120
185	53	52	se	143
186	39	48	nw	309
187	241	39	n	331
188	50	62	e	140
189	69	79	n	339
190	87	62	n	357
191	72	81	n	342
192	42	81	se	132
193	93	28	s	183
194	53	69	nw	323
195	77	26	n	347
196	112	27	s	202
198	57	24	se	147
199	40	39	se	130
200	50	29	se	140
201	50	29	se	140
202	42	39	se	132
203	66	27	se	156
204	76	59	s	166
205	82	26	s	172
206	14	19	e	104
207	74	24	s	164
208	80	23	s	170
209	112	29	s	202
210	52	75	nw	322
211	36	49	se	126
212	21	39	e	111
213	23	36	se	113
214	25	49	se	115
216	57	34	se	147
218	80	30	n	350
219	110	25	s	200
221	111	30	s	201
223	43	46	se	133
224	78	24	s	168
225	60	43	se	150
226	31	39	se	121
226	243	23	s	153
227	151	26	ne	61
228	98	32	n	8
229	104	38	n	14
230	9	42	e	99
231	63	48	n	333
232	118	50	n	28
233	74	61	n	344
234	38	37	se	128
235	5	39	e	95
236	35	21	se	125
237	39	32	se	129
238	33	14	se	123
239	11	18	e	101

BEDDING

Station Number	Strike	Dip	Dip Direction	Dip Direction Azimuth
240	183	13	e	93
241	51	14	se	141
242	62	44	se	152
243	130	35	se	220
244	179	36	e	89
245	66	88	se	156
246	68	76	nw	338
247	0	0	e	90
248	9	7	e	99
249	9	29	e	99
250	184	57	e	94
252	27	21	e	117
253	19	20	e	109
254	24	19	e	114
255	14	24	e	104
256	37	25	e	127
257	50	21	se	140
258	134	24	ne	44
259	66	89	s	156
259	63	64	se	153
260	126	21	ne	36
261	59	89	nw	329
262	54	59	nw	324
263	41	80	se	131
264	61	82	se	151
265	65	90	s	155
266	77	76	s	167
267	62	59	se	152
268	67	26	se	157
269	20	17	se	110
270	124	7	sw	214
271	35	22	se	125
272	0	28	e	90
272	349	27	e	79
274	48	20	se	138
276	3	21	e	93
277	357	36	e	87
278	0	36	e	90
279	20	31	se	110
280	164	4	e	74
282	177	16	e	87
283	0	0	e	90
284	35	70	se	125
285	49	45	se	139
286	43	70	se	133
286	48	46	se	138
287	80	40	se	170
288	59	61	se	149
289	70	64	se	160
290	99	62	s	189
291	61	78	se	151
292	65	68	se	155

BEDDING

Station Number	Strike	Dip	Dip Direction	Dip Direction Azimuth
293	103	40	s	193
294	80	69	s	170
295	48	42	se	138
296	51	42	se	141
297	5	47	se	95
298	51	35	se	141
299	38	44	nw	308
300	83	38	se	173
301	94	58	s	184
302	74	88	n	344
304	83	56	s	173
305	52	41	se	142
306	81	23	s	171
307	67	35	se	157
309	14	19	e	104
310	40	35	se	130
311	46	30	se	136
312	68	21	s	158
313	127	17	s	217
314	114	17	s	204
315	109	8	s	199
316	46	28	se	136
317	70	24	se	160
318	53	83	se	143
319	45	68	nw	315
320	47	81	se	137
321	157	28	e	67
322	31	44	se	121
323	139	40	sw	229
324	35	24	se	125
325	34	40	nw	304
326	36	45	se	126
327	43	11	se	133
328	62	55	se	152
329	44	65	se	134
330	65	89	s	155
331	62	68	nw	332
332	41	50	nw	311
333	46	44	se	136
334	61	32	se	151
335	14	42	w	284
336	14	30	w	284
337	35	46	nw	305
338	101	18	s	191
339	14	28	w	284
340	36	50	nw	306
342	352	40	e	82
344	65	42	se	155
345	10	20	e	100
346	16	51	nw	286
347	90	53	n	0
348	50	64	se	140

BEDDING

Station Number	Strike	Dip	Dip Direction	Dip Direction Azimuth
349	60	89	s	150
350	52	76	nw	322
351	30	50	e	120
378	72	22	s	162
379	0	0	s	90
380	21	71	e	111
381	0	0	e	90
382	66	63	n	336
383	29	27	se	119
384	64	45	nw	334
385	32	58	nw	302
386	54	10	se	144
387	24	57	nw	294
388	32	42	nw	302
389	43	45	nw	313
390	22	41	w	292
391	52	44	se	142
392	0	0	e	90
393	9	14	e	99
394	130	31	ne	40
396	149	14	w	239
396	139	21	w	229
397	57	33	nw	327
398	161	34	sw	251
400	148	52	sw	238
401	354	39	w	264
402	61	24	nw	331
403	154	64	w	244
404	15	56	w	285
405	17	86	e	107
405	116	51	n	26
406	36	89	e	126
407	36	81	nw	306
408	35	82	se	125
409	31	79	se	121
412	162	21	w	252
413	40	16	nw	310
414	86	34	n	356
415	56	12	nw	326
416	57	11	nw	327
417	10	30	w	280
418	15	18	w	285
420	63	30	se	153
421	44	5	se	134
422	20	77	e	110
423	50	54	nw	320
424	146	16	sw	236
425	40	33	nw	310
426	45	28	nw	315
428	66	24	nw	336
429	52	18	nw	322
430	46	15	nw	316

BEDDING

Station Number	Strike	Dip	Dip Direction	Dip Direction Azimuth
431	69	19	nw	339
434	151	39	w	241
435	42	9	nw	312
436	91	9	s	181
438	45	24	nw	315
439	121	14	ne	31
441	150	9	sw	240
442	87	11	n	357
443	0	0	e	90
444	49	34	nw	319
445	354	9	w	264
446	59	11	nw	329
447	58	30	nw	328
448	55	37	nw	325
449	28	15	nw	298
450	1	19	e	91
452	71	13	se	161
453	79	33	s	169
454	74	11	s	164
455	83	16	s	173
456	79	14	s	169
457	97	18	s	187
458	59	21	s	149
460	88	66	s	178
461	65	45	se	155
461	65	74	se	155
463	80	30	s	170
463	0	0	w	270
464	79	5	s	169
465	115	11	s	205
466	82	12	n	352
467	99	8	n	9
468	144	21	ne	54
469	13	12	e	103
470	0	0	e	90
471	0	0	w	270
472	158	21	w	248
473	49	41	se	139
474	44	29	se	134
475	52	54	se	142
476	53	19	se	143
477	75	18	se	165
478	42	35	se	132
479	50	25	nw	320
480	15	65	e	105
480	15	57	e	105
483	110	22	n	20
484	0	0	n	270
485	58	21	nw	328
486	20	50	e	110
487	10	9	nw	280
489	136	20	sw	226

BEDDING

Station Number	Strike	Dip	Dip Direction	Dip Direction Azimuth
490	156	10	w	246
491	158	16	w	248
492	34	20	nw	304
493	131	12	sw	221
494	34	45	nw	304
495	176	31	e	86
497	39	79	se	129
498	50	38	nw	320
499	141	6	ne	51
501	15	23	e	105
502	45	12	e	135
503	52	16	se	142
504	56	21	se	146
505	52	39	se	142
506	65	54	se	155
507	87	12	n	357
508	104	12	n	14
509	96	14	n	6
511	72	44	s	162
512	116	24	n	26
513	101	21	n	11
515	79	84	s	169
516	73	19	n	343
517	62	35	n	332
517	65	70	s	155
518	55	67	s	145
519	67	41	s	157
520	76	87	n	346
521	37	71	se	127
522	85	14	s	175
523	67	28	nw	337
524	84	21	s	174
525	87	18	s	177
526	81	32	s	171
527	48	33	se	138
528	81	22	s	171
529	84	24	s	174
530	94	55	s	184
531	51	24	se	141
534	5	19	e	95
537	44	19	se	134
538	66	17	se	156
538	68	3	s	158
539	109	25	s	199
540	40	20	se	130
541	40	19	se	130
542	45	27	se	135
543	53	28	se	143
544	89	18	s	179
545	116	11	s	206
546	7	7	e	97
547	123	24	sw	213

BEDDING

Station Number	Strike	Dip	Dip Direction	Dip Direction Azimuth
548	112	20	s	202
549	53	20	se	143
550	56	5	se	146
551	43	24	se	133
552	40	50	se	130
553	37	11	se	127
554	124	7	sw	214
555	147	14	ne	57
557	67	12	s	157
558	53	16	se	143
559	68	13	s	158
560	127	14	sw	217
560	75	10	s	165
563	141	10	ne	51
565	102	9	s	192
566	73	11	s	163
567	174	63	e	84
567	6	64	e	96
568	1	64	e	91
569	178	62	e	88
570	14	8	e	104
571	14	89	e	104
572	0	23	e	90
573	175	21	e	85
574	168	29	e	78
575	59	29	se	149
576	48	29	nw	318
577	22	72	e	112
578	16	61	e	106
579	44	43	se	134
580	12	68	e	102
581	82	4	s	172
585	125	9	s	215
587	95	4	s	185
588	49	10	se	139
589	0	0	w	270
589	90	10	s	180
591	94	8	s	184
592	66	10	se	156
593	145	5	sw	235
594	90	2	s	180
595	104	9	s	194
596	80	10	s	170
597	230	7	se	140
598	105	5	s	195
599	148	5	sw	238
600	5	6	w	275
603	65	56	se	155
604	8	15	w	278
605	168	12	w	258
606	169	60	e	79
608	18	40	e	108

BEDDING

Station Number	Strike	Dip	Dip Direction	Dip Direction Azimuth
609	4	30	e	94
611	0	31	e	90
612	131	6	sw	221
613	105	9	s	195
614	79	15	s	169
615	129	6	sw	219
616	95	11	s	185
617	102	7	s	192
618	101	18	s	191
619	72	89	n	342
620	31	63	se	121
621	26	39	e	116
622	5	89	w	275
623	23	47	e	113
624	13	39	e	103
625	19	30	e	109
626	118	47	n	28
627	24	36	e	114
628	136	39	ne	46
629	107	40	n	17
629	89	46	s	179
630	105	32	n	15
631	108	26	n	18
632	91	26	n	1
633	98	22	n	8
634	91	15	n	1
636	49	21	se	139
637	175	17	e	85
638	20	33	e	110
639	184	61	e	94
640	176	64	e	86
641	17	37	w	287
641	8	90	w	278
642	32	43	se	122
644	27	34	se	117
645	57	28	se	147
646	51	28	nw	321
647	132	21	sw	222
648	154	38	w	244
649	75	57	s	165
650	168	18	w	258
651	120	8	sw	210
654	56	24	se	146
654	84	12	se	174
655	55	18	se	145
656	52	31	nw	322
657	28	48	w	298
657	24	80	w	294
658	46	56	nw	316
659	33	61	nw	303
659	38	73	w	308
662	54	9	nw	324

BEDDING

Station Number	Strike	Dip	Dip Direction	Dip Direction Azimuth
663	31	16	nw	301
664	0	60	w	270
666	129	36	ne	39
667	56	48	nw	326
668	68	29	se	158
669	56	21	se	146
670	59	31	se	149
671	150	25	se	240
672	46	29	w	316
673	80	23	n	350
674	49	51	nw	319
675	86	42	n	356
675	48	54	se	138
676	49	62	se	139
678	76	53	n	346
681	60	59	nw	330
682	28	73	nw	298
682	36	85	nw	306
683	45	87	nw	315
684	40	51	se	130
685	78	42	se	168
686	173	31	e	83
687	21	26	se	111
688	21	29	se	111
689	58	62	se	148
689	52	52	se	142
689	48	73	nw	318
690	86	47	n	356
691	48	51	nw	318
691	62	47	nw	332
692	18	61	nw	288
692	11	56	w	281
693	118	8	sw	208
694	89	15	s	179
695	98	24	s	188
696	85	24	n	355
697	134	24	sw	224
698	177	32	w	267
699	24	53	nw	294
699	22	68	nw	292
700	38	41	nw	308
701	41	50	nw	311
702	15	70	w	285
703	348	24	w	258
704	28	12	nw	298
704	43	65	nw	313
706	194	12	w	284
708	164	32	ne	74
714	59	23	se	149
977	38	7	w	308
978	59	25	s	149
979	27	10	w	297

BEDDING

Station Number	Strike	Dip	Dip Direction	Dip Direction Azimuth
986	181	8	w	271
987	103	19	n	13
988	275	14	s	185
989	79	23	s	169
994	49	9	s	139
995	24	18	e	114
996	65	17	se	155
997	0	3	w	270
998	340	15	e	70
999	64	40	nw	334

PREFERENCIAL FRACTURING IN PEBBLES

Station Number	Strike	Dip	Dip Direction	Dip Direction Azimuth
14	126	47	ne	36
20	154	71	e	64
42	124	71	s	214
43	113	62	ne	23
77	110	38	s	200
77	154	75	w	244
100	127	89	n	37
111	115	89	s	205
111	274	86	s	184
113	96	67	n	6
126	163	76	w	253
230	177	45	w	267
272	144	65	w	234
272	147	66	sw	237
284	154	40	sw	244
327	30	59	nw	300
345	128	78	ne	38
564	155	84	e	65
564	171	81	e	81
565	159	83	e	69
566	146	79	e	56
596	104	81	n	14
620	155	58	ne	65
647	139	57	ne	49
648	130	69	ne	40
648	104	68	n	14
648	87	76	n	357

CLEAVAGE

Station Number	Strike	Dip	Dip Direction	Spacing (cm)	Dip Direction Azimuth
31	68	67	n	1	338
35	121	84	ne	0	31
36	77	73	n	0	347
37	64	71	se	2	154
38	81	64	n	2	351
47	162	57	ne	0	72
47	97	45	n	1	7
70	64	89	n	2	334
79	94	84	n	4	4
83	25	89	s	0	115
85	72	89	s	2	162
89	106	79	s	1	196
92	70	80	n	0	340
93	122	79	s	0	212
102	76	81	n	1	346
102	55	52	nw	1	325
102	43	62	e	1	133
132	44	71	nw	0	314
145	90	46	s	0	180
152	25	57	e	0	115
155	44	70	se	0	134
159	67	84	n	3	337
187	155	89	e	2	65
226	131	79	ne	1	41
235	48	68	nw	1	318
277	96	81	n	1	6
309	77	50	n	2	347
310	79	54	n	1	349
315	58	79	nw	1	328
368	145	89	n	0	55
389	83	46	s	2	173
390	72	77	s	1	162
391	57	56	ne	1	327
394	54	58	se	1	144
396	59	89	se	0	149
416	61	83	se	1	151
421	77	64	n	0	347
426	69	67	se	0	159
429	69	79	s	0	159
430	72	84	s	0	162
435	62	89	nw	0	332
436	62	79	nw	0	332
444	36	66	se	0	126
445	66	89	s	0	156
447	56	62	se	0	146
449	31	72	se	0	121
454	66	70	nw	0	336
455	51	54	nw	0	321
457	56	73	nw	3	326
465	60	81	n	0	330
466	71	78	s	0	161
467	64	79	nw	1	334

CLEAVAGE

Station Number	Strike	Dip	Dip Direction	Spacing (cm)	Dip Direction Azimuth
468	69	89	s	0	159
473	69	46	nw	0	339
486	70	45	nw	0	340
489	47	65	nw	0	317
490	59	89	s	0	149
491	69	88	s	0	159
492	58	87	se	0	148
493	57	59	nw	0	327
494	65	53	s	0	155
503	66	65	nw	0	336
517	111	23	n	0	21
525	62	75	nw	0	332
527	75	66	n	0	345
538	64	73	nw	0	334
540	37	65	nw	0	307
541	45	59	nw	0	315
542	71	56	n	0	341
544	86	54	n	0	356
545	62	74	nw	0	332
547	54	83	nw	0	324
550	68	77	nw	0	338
560	143	33	sw	0	233
567	125	39	sw	0	215
568	81	61	n	0	351
569	103	57	n	0	13
595	76	75	n	0	346
596	69	78	n	0	339
597	82	60	n	0	352
598	68	75	s	0	158
605	47	77	nw	0	317
608	94	67	n	0	4
609	79	79	n	5	349
611	70	79	n	0	340
612	77	51	n	0	347
613	74	53	n	0	344
614	87	71	n	5	357
623	92	60	n	5	2
625	105	74	n	0	15
628	92	80	n	0	2
630	55	69	n	0	325
630	91	61	s	0	181
631	83	69	s	0	173
633	72	68	s	0	162
634	81	87	n	0	351
636	15	62	w	0	285
639	80	61	n	0	350
654	55	57	nw	1	325
656	36	79	se	2	126
657	31	35	e	0	121
658	79	60	s	0	169
659	64	60	se	0	154
663	109	90	s	0	199

CLEAVAGE

Station Number	Strike	Dip	Dip Direction	Spacing (cm)	Dip Direction Azimuth
670	54	53	nw	0	324
671	67	85	s	0	157
675	27	30	se	0	117
684	241	49	n	0	331
690	148	53	w	0	238
695	65	57	n	0	335
696	126	69	sw	0	216
698	136	73	ne	0	46
700	76	72	s	0	166

FAULT ZONES

Station Number	Strike	Dip	Dip Direction	Style	Spacing (cm)	Dip Direction Azimuth
29	75	89	n	0	0	345
29	75	89	n	0	0	345
29	75	89	n	0	0	345
30	187	87	e	0	0	97
34	139	89	n	0	0	49
64	116	77	n	0	0	26
92	46	31	nw	0	0	316
94	161	40	w	0	0	251
112	145	75	sw	0	0	235
113	4	89	e	cw	0	94
131	171	60	w	normal	12	261
155	55	35	se	0	0	145
189	134	73	sw	0	400	224
190	146	44	sw	0	50	236
235	132	44	sw	0	0	222
245	16	74	e	0	0	106
259	56	44	se	0	0	146
273	118	51	n	thrust	0	28
275	44	85	se	ccw	0	134
287	15	86	e	0	0	105
289	7	55	e	1-thick	10	97
292	21	53	nw	0	0	291
292	27	42	nw	0	0	297
294	2	68	w	cw	0	272
295	58	87	se	normal	0	148
322	109	67	n	ccw	0	19
325	169	25	e	0	0	79
327	83	8	n	normal	0	353
330	38	75	nw	ccw	0	308
330	11	89	e	ccw	0	101
358	129	46	ne	cw	0	39
359	149	67	e	0	0	59
359	1	88	e	0	0	91
370	147	39	ne	0	0	57
376	102	89	s	ccw	0	192
403	104	55	n	normal	0	14
409	90	71	s	cw	0	180
478	170	35	ne	thrust	0	80
478	58	66	nw	thrust	0	328
482	51	55	se	ccw	0	141
482	43	65	se	thrust	0	133
507	69	60	n	0	0	339
675	104	24	ne	cw	0	14
681	13	40	se	inverse	0	103
689	122	47	ne	0	0	32
689	85	67	n	0	0	355
701	49	65	n	0	0	319
715	39	76	nw	thrust	0	309
715	42	48	nw	normal	0	312
716	98	58	s	0	0	188

JOINTS

Station Number	Strike	Dip	Dip Direction	Spacing (cm)	Dip Direction Azimuth
3	0	46	e	0	90
3	0	46	e	0	90
11	80	71	s	0	170
12	92	79	s	0	182
22	168	84	w	0	258
25	171	83	e	0	81
26	131	69	s	0	221
29	89	84	s	1	179
35	46	76	s	0	136
37	107	89	n	50	17
38	137	71	ne	0	47
42	142	73	ne	0	52
44	111	48	n	50	21
49	32	75	sw	0	122
61	101	84	n	0	11
65	101	70	s	0	191
67	84	60	n	0	354
67	10	56	w	0	280
67	97	70	n	0	7
69	143	66	sw	25	233
70	359	85	w	10	269
77	121	85	s	200	211
87	90	66	s	50	180
99	107	88	s	100	197
100	61	80	n	150	331
106	4	87	w	100	274
111	283	85	n	50	13
113	112	70	s	100	202
114	121	44	ne	0	31
114	140	50	e	50	50
117	152	67	s	1500	242
118	132	84	s	100	222
120	134	80	n	100	44
122	99	59	n	300	9
123	264	59	n	50	354
126	312	61	n	30	42
134	118	89	sw	20	208
135	119	63	ne	30	29
137	84	76	s	25	174
144	214	81	w	3	304
144	49	55	nw	7	319
155	163	76	w	50	253
161	31	64	w	25	301
161	113	81	s	25	203
188	149	65	w	15	239
214	102	69	n	10	12
217	136	84	ne	25	46
228	171	71	w	10	261
245	172	50	e	0	82
245	146	51	sw	5	236
265	139	84	ne	20	49
266	166	90	e	50	76

JOINTS

Station Number	Strike	Dip	Dip Direction	Spacing (cm)	Dip Direction Azimuth
272	155	60	w	50	245
276	126	66	sw	20	216
311	134	81	sw	4	224
311	102	74	n	30	12
313	173	60	e	5	83
345	95	65	n	200	5
356	325	84	e	0	55
358	74	70	s	10	164
385	136	82	ne	50	46
387	101	81	n	20	11
388	123	88	n	100	33
389	135	84	n	20	45
393	56	75	nw	5	326
396	4	79	e	15	94
396	140	72	ne	55	50
399	46	38	se	30	136
409	101	74	s	50	191
418	82	81	s	25	172
425	89	66	s	60	179
429	112	82	s	3	202
435	2	80	e	20	92
445	136	85	sw	15	226
453	46	41	nw	20	316
454	106	77	n	20	16
455	139	78	sw	60	229
469	150	76	w	0	240
473	142	85	sw	22	232
476	56	69	nw	30	326
489	7	55	e	75	97
531	112	79	n	15	22
538	149	89	n	20	59
554	147	88	w	100	237
558	104	74	n	0	14
573	15	82	w	15	285
591	141	82	ne	50	51
600	154	84	sw	10	244
613	156	65	e	20	66
614	154	86	e	50	64
615	168	88	w	60	258
618	60	89	s	40	150
625	22	55	w	9	292
630	65	61	s	100	155
634	148	77	w	20	238
642	114	81	n	5	24
644	104	64	n	60	14
654	137	87	ne	5	47
658	131	45	sw	15	221
663	157	81	e	10	67
668	157	84	ne	40	67
669	105	70	n	15	15
677	7	80	e	10	97
678	34	67	se	12	124

JOINTS

Station Number	Strike	Dip	Dip Direction	Spacing (cm)	Dip Direction Azimuth
683	141	59	sw	13	231
684	115	84	n	30	25
698	10	69	e	0	100
698	105	78	ne	10	15
703	55	88	nw	0	325
703	36	89	nw	0	306

FOLD AXIS

Station Number	Trend	Plunge	Style
32	112	10	0
67	215	10	0
72	261	5	ccw
82	60	0	0
89	231	44	0
92	24	45	cw
136	1	11	0
153	16	6	0
154	226	11	0
156	42	9	0
156	1	54	0
210	51	17	0
266	75	6	0
291	75	7	0
385	327	58	cw
395	2	14	cw
405	14	19	0
419	230	10	0
430	241	7	cw
462	59	27	0
462	24	32	ccw
471	56	0	0
482	51	49	ccw
488	104	19	cw
488	71	1	cw
608	177	11	0
628	75	44	0
638	34	8	0
641	203	5	0
664	210	62	0

SLICKEN LINES

Station Number	Trend	Plunge	Style
29	220	4	0
30	351	10	0
64	119	12	0
94	10	41	0
94	184	15	0
95	110	40	0
95	184	14	0
113	196	26	thrust
114	26	20	0
143	149	12	0
235	291	20	0
251	119	13	ccw
257	129	20	cw
259	171	38	0
273	2	24	0
275	240	4	ccw
275	81	11	0
278	186	17	0
278	190	34	0
287	200	79	0
289	170	37	0
289	290	55	0
292	308	40	normal
292	282	54	normal
294	358	15	0
295	74	79	0
322	96	36	0
325	118	17	0
327	324	3	normal
330	26	46	ccw
358	320	15	0
359	149	0	0
403	312	34	normal
409	270	7	cw
482	33	174	0
482	199	14	0
675	276	22	ccw
715	22	66	0
715	326	50	0
716	271	16	0

VEINS

Station Number	Strike	Dip	Dip Direction	Spacing (cm)	Thickness (cm)	Dip Direction Azimuth
4	155	82	e	20	4	65
26	148	34	ne	0	3	58
29	46	57	nw	0	2	316
48	75	61	n	5	0	345
70	302	82	s	40	0	212
82	310	84	n	50	1	40
83	107	84	n	65	0	17
85	156	79	ne	100	1	66
114	36	46	n	40	4	306
130	97	82	n	0	1	7
130	106	52	s	100	1	196
134	168	59	n	25	1	78
135	115	79	n	65	1	25
138	140	73	ne	21	0	50
139	91	81	s	10	2	181
140	132	42	sw	100	3	222
152	107	84	n	10	0	17
153	106	79	n	5	0	16
154	141	72	ne	4	1	51
157	139	80	nw	30	1	49
157	127	70	sw	10	1	217
158	149	82	w	20	1	239
190	146	44	sw	50	0	236
200	152	74	ne	40	0	62
200	68	69	n	50	0	338
201	69	85	n	100	1	339
221	36	74	nw	30	0	306
247	185	85	e	60	0	95
247	82	80	n	60	0	352
248	102	69	n	50	0	12
250	82	59	n	75	0	352
251	178	84	nw	30	0	88
251	79	70	s	75	1	169
258	149	50	nw	10	0	59
273	14	59	w	100	2	284
277	122	66	ne	4	0	32
295	58	87	se	30	1	148
304	15	81	w	25	0	285
323	52	59	nw	0	0	322
355	72	79	se	100	1	162
363	96	72	s	25	1	186
389	122	85	s	200	2	212
391	116	74	ne	150	0	26
493	149	71	se	15	1	239
559	132	89	ne	20	1	42
592	146	86	ne	35	0	56
598	149	89	ne	15	0	59
641	10	74	s	25	1	100
671	94	85	s	3	0	184
673	164	59	e	100	1	74
673	12	60	w	100	0	282
681	154	67	nw	5	0	64

VITA

Camilo Montes was born in Santafé de Bogotá, Colombia on April 29, 1967. His love for the great Andean outdoors, and his aversion for desk-based disciplines and for wearing ties, made him follow geology as his major in the Universidad Nacional de Colombia. He received his degree in Geology in 1992 from this institution. During this time, continued exploration of the high Andes made him realize that there was so much more to know and study beyond the Bachelor's degree. He joined the Master's program at the University of Tennessee, in fall 1993, officially receiving the Master's degree in May 1997, while working in his Ph. D. at the same institution. He continued his long academic career in Knoxville, and finished his Ph.D. in the summer of 2001.